

**MICROSTRUCTURAL BREAKDOWN AND SCALE-UP EFFECTS
IN EQUAL CHANNEL ANGULAR EXTRUSION OF CAST COPPER**

A Thesis

by

SHABIBAHMED JEHANGIR KADRI

Submitted to the Office of Graduate Studies of
Texas A&M University
in partial fulfillment of the requirements for the degree of

MASTER OF SCIENCE

August 2005

Major Subject: Mechanical Engineering

**MICROSTRUCTURAL BREAKDOWN AND SCALE-UP EFFECTS
IN EQUAL CHANNEL ANGULAR EXTRUSION OF CAST COPPER**

A Thesis

by

SHABIBAHMED JEHANGIR KADRI

Submitted to the Office of Graduate Studies of
Texas A&M University
in partial fulfillment of the requirements for the degree of

MASTER OF SCIENCE

Approved by:

Chair of Committee,
Committee Members,

K. Theodore Hartwig
T. S. Creasy
T. R. Lalk
K. L. Peddicord

Head of Department,

D. O'Neal

August 2005

Major Subject: Mechanical Engineering

ABSTRACT

Microstructural Breakdown and Scale-up Effects in Equal Channel Angular Extrusion of
Cast Copper.

(August 2005)

Shabibahmed Jehangir Kadri,

B.S., Gujarat University (India)

Chair of Advisory Committee: Dr. K. Theodore Hartwig

The primary objectives of this study were: (1) to verify the effectiveness of ECAE to induce equal amounts of strain and grain refinement in bars of different cross-sectional areas, (2) to determine the effectiveness of ECAE in breaking down the as-cast macrostructure in CDA 101 Cu and in producing a homogeneous material containing micron-scale grains upon recrystallization, and (3) to determine a thermomechanical processing (TMP) schedule (from the ones examined) that produces the best microstructure in terms of grain size and uniformity. The effects of extrusion route, levels of strain and intermediate heat treatment were investigated.

To achieve the first objective, bars having square cross-sections of three different sizes, 19 mm, 25 mm and 50 mm, were processed up to eight ECAE passes through routes A, B, C and E. To achieve the second and third objectives, bars were processed up to eight ECAE passes with and without intermediate heat treatments through routes Bc, C, E and F. ECAE processing was carried out in a 90° extrusion die with sliding walls at an extrusion speed of 2.5 mm/s. Recrystallization studies were carried out on the processed material to evaluate the recrystallization behavior and thermal stability of the material. The as-worked and recrystallized materials were characterized by Vickers microhardness, optical microscopy (OM) and transmission electron microscopy (TEM).

Results indicate that similar hardness values, sub-grain morphology and recrystallized grain size are generated in the three bars having different cross-sectional sizes processed through ECAE. ECAE is shown to induce uniform strain in all three billet sizes. ECAE is therefore shown to be effective in scale-up to a size of at least 50 mm, with larger billets giving better load efficiency.

Results from the later parts of this study indicate that eight extrusion passes via route Bc produces the best microstructure in terms of grain size and microstructural uniformity. The routes can be arranged in the sequence Bc > E, F > C for their ability to produce a uniform recrystallized microstructure with small average grain size. Macroscopic shear bands are sometimes generated during extrusion depending upon the initial grain morphology and texture of the material.

To my parents.

ACKNOWLEDGEMENTS

I take this opportunity to thank my advisor Dr. K. Ted Hartwig, for providing guidance over the last two years. Dr. Hartwig accepted me as a member of his research group. He has been very patient when I could not get something done and has always motivated me to try out new ideas. Your kind help has made this thesis possible. I extend my gratitude to the members of my advisory committee, Dr. Tom Lalk, Dr. Terry Creasy and Dr. Kenneth Lee Peddicord, for their time and effort.

Big thanks to Robert Barber, not just for his invaluable help during extrusions, but also for teaching me the intricacies of machining and ECAE. I am greatly indebted to Suveen Mathaudhu and Jae Taek Im, my friends and colleagues at the ECAE research group. Suveen has helped me out whenever I was stuck with something, be it the polishing of samples or in selecting a course. I thank my friends and roommates: Yash Shukla, Sandeep Gaudana, Ajit Ambike and Srinivas Cherla, for encouragement and friendship over the years.

Last and definitely not the least, I thank my family, Dad, Mom, Asrar and Tafwiz for their constant love, encouragement and support.

TABLE OF CONTENTS

	Page
ABSTRACT.....	iii
DEDICATION.....	v
ACKNOWLEDGEMENTS.....	vi
LIST OF FIGURES.....	ix
LIST OF TABLES.....	xviii
1. INTRODUCTION.....	1
2. LITERATURE REVIEW.....	4
2.1. Properties and applications of pure copper.....	4
2.2. Problems associated with cast structures and subsequent defects...	5
2.3. Different techniques for grain refinement.....	7
2.4. Equal channel angular extrusion.....	11
2.5. ECAE of copper.....	15
2.6. ECAE of cast alloys.....	17
2.7. Effect of intermediate heat treatments.....	19
2.8. Need for scale-up of equal channel angular extrusion.....	20
3. EXPERIMENTAL PROCEDURE.....	24
3.1. Material.....	24
3.2. Billet extraction from ingot.....	24
3.3. ECAE processing.....	29
3.3.1. ECAE processing for scale-up project.....	29
3.3.2. Selection of ECAE routes for microstructural breakdown project.....	31
3.4. Brinell hardness measurement.....	36
3.5. Heat treatments.....	36
3.6. Metallographic sample preparation.....	39
3.6.1. Sectioning.....	39
3.6.2. Engraving.....	40
3.6.3. Mounting.....	40
3.6.4. Grinding.....	43
3.6.5. Etching.....	44
3.6.6. Image analysis.....	45
3.7. Micro-hardness measurement.....	46
4. EXPERIMENTAL RESULTS.....	49
4.1. Billet extrusions.....	49
4.2. Load curves.....	50
4.2.1. Scale-up project.....	50
4.2.2. Microstructural breakdown project.....	55

	Page
4.3. Hardness.....	56
4.3.1. Brinell hardness.....	56
4.3.2. Vicker’s microhardness.....	57
4.3.2.1. Scale-up project- Vicker’s microhardness scans.....	58
4.4. Recrystallization curves.....	71
4.4.1. Scale-up project.....	72
4.4.2. Microstructural breakdown study.....	78
4.5. Recrystallization range.....	83
4.6. Transmission electron microscopy.....	88
4.6.1. Scale-up project.....	88
4.6.2. Microstructural breakdown project.....	92
4.6.3. Recrystallization TEM.....	102
4.7. Optical microscopy.....	106
4.7.1. Scale-up project.....	106
4.7.2. Microstructural breakdown project.....	122
5. DISCUSSION.....	146
5.1. Increase in load with higher extrusions.....	146
5.2. Shear localization in billet.....	146
5.3. Increase in hardness with number of extrusions.....	147
5.4. Hardness scans.....	148
5.5. Recrystallization curves.....	150
5.6. Recrystallization range.....	152
5.7. Transmission electron microscopy.....	154
5.8. Recrystallization TEM.....	161
5.9. Optical microscopy.....	162
6. CONCLUSIONS.....	169
7. RECOMMENDATIONS FOR FUTURE STUDIES.....	171
REFERENCES.....	172
VITA.....	175

LIST OF FIGURES

FIGURE	Page
1. General mechanics of equal channel angular extrusion.....	13
2. Half extruded billet of as-cast CDA 101 Cu indicating the end regions and low strain zone along the bottom edge.....	13
3. The rotation of billets between different ECAE passes for different routes.....	14
4. Values of Vickers microhardness measurements on the transverse plane taken along the Y and Z directions for the as-worked Al 1100 alloy.....	21
5. As-worked microstructure on the transverse plane for Al 1100 alloy after six passes via route Bc.....	22
6. Transverse macrostructure of cast OFHC CDA 101 Cu ingot.....	26
7. (a) View of transverse section of the ingot (b) Side section of the columnar zone (c) Side section of the chill zone.....	27
8. Image of three etched billet sizes, 50 mm x 50 mm x 250 mm, 25 mm x 25 mm x 150 mm and 19 mm x 19 mm x 160 mm (nominal) used for ECAE processing.....	27
9. Pattern of billet extraction from the ingot.....	28
10. The initial microstructure and grain orientation for billets having nominal dimensions 25 mm x 25 mm x 175 mm for microstructural breakdown study.....	28
11. Tooling arrangement for ECAE.....	31
12. Hole of 3.5 mm diameter drilled in the trailing end of a 25 mm x 25 mm cross-section billet to monitor temperature during intermediate heat treatments.....	35
13. Typical temperature profiles for intermediate heat treatments done on billets for microstructural breakdown study.....	35
14. Plane identification nomenclature.....	36
15. Dummy sample prepared to monitor temperature in the sand bath during heat treatments.....	37
16. Sand bath temperature plots showing the temperature variation for recrystallization heat treatments carried out for the scale-up study.....	38
17. Temperature plots showing the temperature history for recrystallization heat treatments carried out in vacuum for the microstructural refinement study.....	39

FIGURE	Page
18. The cutting and engraving technique used for sample labeling.....	41
19. Temperature profile for fast cure epoxy used for mounting samples.....	42
20. Temperature profile for slow cure epoxy used for mounting samples.....	42
21. Change in hardness with recrystallization temperature for CDA 101 Cu processed up to eight passes via route F without intermediate annealings.	43
22. The location of microhardness measurements on the flow, transverse and longitudinal plane of the samples for “line scans”.....	47
23. Top plane of billet # 5 (50 mm square) processed through route 4B.....	49
24. Side plane of billet # 5 (50 mm square) processed through route 4B.....	50
25. Load vs. stroke curve for billet # 5, 50 mm square cross-section billet of as-cast CDA 101 Cu, processed through route 4B in 90° die at room temperature.....	50
26. Extrusion load curves for 50 mm square billets of as-cast CDA 101 Cu extruded through 90° die at room temperature.....	51
27. Extrusion load curves for 25 mm square billets of as-cast CDA 101 Cu extruded through 90° die at room temperature.....	52
28. Load vs. stroke curve for billet # 10, 25 mm square cross-section.....	53
29. Load vs. stroke curve for billet # 2, 50 mm square cross-section.....	54
30. Punch load vs. punch displacement diagram for extrusion passes 3 to 6 for a 25 mm square billet processed for extrusion route 6C.....	55
31. Punch load vs. punch displacement diagram for passes 5 to 8 for a 25 mm square billet processed up to extrusion 8Bc.....	56
32. Average Brinell hardness values for the 25 mm and 50 mm square billets of as-cast OFHC Cu extruded up to eight passes via route E.....	57
33. Increase in Vicker’s microhardness with number of passes for 25 mm billets of as-cast OFHC Cu processed up to eight passes through a 90° die.....	58
34. Vickers microhardness scan along the flow plane for billet processed through pass 1A.....	59
35. Vickers microhardness scan along the flow plane for 25 mm and 50 mm square cross-section billets processed through pass 2C.....	60
36. Vickers microhardness scan along the flow plane for 25 mm and 50 mm square cross-section billets processed through pass 4A.....	61
37. Vickers microhardness scan along transverse plane for 25 mm and 50 mm square cross-section billets processed through pass 4A.....	61

FIGURE	Page
38. Vickers microhardness scan along longitudinal plane for 25 mm and 50 mm square cross-section billets processed through pass 4A.....	62
39. Shape of different worked regions in a square cross-section billet having an aspect ratio of five and processed up to four passes via route A.....	62
40. Vickers microhardness scan along the flow plane for 25 mm and 50 mm square cross-section billets processed through pass 4B.....	63
41. Vickers microhardness scan along transverse plane for 25 mm and 50 mm square cross-section billets processed through pass 4B.....	64
42. Vickers microhardness scan along longitudinal plane of 25 mm and 50 mm square cross-section billets processed through pass 4B.....	64
43. Shape of the fully worked region in a square cross-section billet processed up to four passes via route B.....	65
44. Vickers microhardness scan along flow plane of 19 mm, 25 mm and 50 mm square cross-section billets processed through pass 4E.....	66
45. Vickers microhardness scan along longitudinal plane of 19 mm, 25 mm and 50 mm square cross-section billets processed through pass 4E.....	66
46. Vickers microhardness scan along transverse plane of 19 mm, 25 mm and 50 mm square cross-section billets processed through pass 4E.....	67
47. Vickers microhardness scan along flow plane of 19 mm, 25 mm and 50 mm square cross-section billets processed through pass 8E.....	68
48. Comparison of as-worked hardness along flow, transverse and longitudinal planes for 25 mm and 50 mm square cross-section billets processed up to four pass via route A.....	69
49. Comparison of as-worked hardness along flow, transverse and longitudinal planes for 25 mm and 50 mm square cross-section billets processed up to four pass via route B.....	70
50. Comparison of as-worked hardness along flow, transverse and longitudinal planes for 19 mm, 25 mm and 50 mm square cross-section billets processed up to four pass via route E.....	71
51. Variation in hardness with annealing temperature for 25 mm square cross-section billet of as-cast CDA 101 Cu processed through extrusion route 1A in 90° die at room temperature.....	72
52. Variation in hardness with annealing temperature for 25 mm and 50 mm square cross-section billets of as-cast CDA 101 Cu processed through extrusion route 2C in 90° die at room temperature.....	73
53. Variation in hardness with annealing temperature for 25 mm and 50 mm square cross-section billets of as-cast CDA 101 Cu processed through extrusion route 4A in 90° die at room temperature.....	74

FIGURE	Page
54. Variation in hardness with annealing temperature for 25 mm and 50 mm square cross-section billets of as-cast CDA 101 Cu processed through extrusion route 4B in 90° die at room temperature.....	75
55. Variation in hardness with annealing temperature for 19 mm, 25 mm and 50 mm square cross-section billets of as-cast CDA 101 Cu processed through extrusion route 4E in 90° die at room temperature.....	76
56. Variation in hardness with annealing temperature for 19 mm, 25 mm and 50 mm square cross-section billets of as-cast CDA 101 Cu processed through extrusion route 8E in 90° die at room temperature.....	77
57. Recrystallization curves for CDA 101 Cu processed through 1A, 2C, 4E and 8E extrusion routes.....	78
58. Variation in hardness with annealing temperature for as-cast CDA 101 Cu processed up to eight passes via route E with and without intermediate heat treatments.....	79
59. Variation in hardness with annealing temperature for as-cast CDA 101 Cu processed up to eight passes via route E with two different intermediate heat treatment temperatures.....	80
60. Variation in hardness with annealing temperature for as-cast CDA 101 Cu processed up to eight passes via route C with and without intermediate heat treatments.....	81
61. Variation in hardness with annealing temperature for as-cast CDA 101 Cu processed up to eight passes via route Bc with and without intermediate heat treatments.....	82
62. Variation in hardness with annealing temperature for as-cast CDA 101 Cu processed up to eight passes via route F with and without intermediate heat treatments.....	83
63. Recrystallization curve showing the technique used to calculate temperature regimes for % hardness variations from a recrystallization curve.....	84
64. Temperature ranges for hardness variation for 50 mm square billets processed up to eight passes via routes A, B, C and E.....	85
65. Temperature ranges for hardness variation for 25 mm square billets processed up to eight extrusion passes through different thermo-mechanical processing schedules.....	86
66. Temperature ranges for hardness variation for 25 mm square billets processed up to eight extrusion passes via different routes and with intermediate heat treatments.....	86

FIGURE	Page
67. TEM of CDA 101 Cu in as-worked condition along the flow plane of billet having 50 mm square cross-section processed through route 4E through 90° die at room temperature.....	88
68. TEM of CDA 101 Cu in as-worked condition along the flow plane of billet having 25 mm square cross-section processed through route 4E.....	89
69. TEM of CDA 101 Cu in as-worked condition along the flow plane of billet having 19 mm square cross-section processed through route 4E.....	89
70. TEM of CDA 101 Cu in as-worked condition along the flow plane of billet having 50 mm square cross-section processed through route 8E.....	90
71. TEM of CDA 101 Cu in as-worked condition along the flow plane of billet having 25 mm square cross-section processed through route 8E.....	91
72. TEM of CDA 101 Cu in as-worked condition along the flow plane of billet having 19 mm square cross-section processed through route 8E.....	91
73. TEM of as-cast microstructure in CDA 101 copper.....	93
74. TEM of CDA 101 Cu in as-worked condition along the flow plane of billet processed through route 1A in a 90° die.....	93
75. TEM of CDA 101 Cu in as-worked condition along the flow plane of billet processed through route 1A in a 90° die.....	94
76. TEM of CDA 101 Cu in as-worked condition along the flow plane of billet processed through route 2C in a 90° die.....	94
77. TEM of CDA 101 Cu in as-worked condition along the flow plane of billet processed through route 4C in a 90° die.....	95
78. TEM of CDA 101 Cu in as-worked condition along the flow plane of billet processed through TMP schedule 2C-400°C-2C.....	95
79. TEM of CDA 101 Cu in as-worked condition along the flow plane of billet processed through route 2E-350°C-2E.....	96
80. TEM of CDA 101 Cu in as-worked condition along the flow plane of billet processed through route 4F in a 90° die.....	96
81. TEM of CDA 101 Cu in as-worked condition along the flow plane of billet processed through route 2F-400°C-2F.....	97
82. TEM of CDA 101 Cu in as-worked condition along the flow plane of billet processed through route 4Bc in a 90° die.....	97
83. TEM of CDA 101 Cu in as-worked condition along the flow plane of billet processed through route 2Bc-400°C-2Bc.....	98
84. TEM of CDA 101 Cu in as-worked condition along the flow plane of billet processed through route 8C in a 90° die.....	98

FIGURE	Page
85. TEM of CDA 101 Cu in as-worked condition along the flow plane of billet processed through route 2E-400°C-2E-300°C- 2E-200°C-2E.....	99
86. TEM of CDA 101 Cu in as-worked condition along the flow plane of billet processed through route 2E-350°C-2E-350°C- 2E-350°C-2E.....	99
87. TEM of CDA 101 Cu in as-worked condition along the flow plane of billet processed through route 8F in a 90° die.....	100
88. TEM of CDA 101 Cu in as-worked condition along the flow plane of billet processed through route 2F-400°C-2F-300°C- 2F-200°C-2F.....	100
89. TEM of CDA 101 Cu in as-worked condition along the flow plane of billet processed through route 8Bc in a 90° die.....	101
90. TEM of CDA 101 Cu in as-worked condition along the flow plane of billet processed through route 8Bc in a 90° die.....	101
91. TEM of CDA 101 Cu in as-worked condition along the flow plane of billet processed through route 2Bc-400°C-2Bc-300°C- 2Bc-200°C-2Bc.....	102
92. TEM of CDA 101 Cu processed through route 4E and heat treated at 100°C for 60 minutes.....	103
93. TEM of CDA 101 Cu processed through route 4E and heat treated at 150°C for 60 minutes.....	103
94. TEM of CDA 101 Cu processed through route 4E and heat treated at 170°C for 60 minutes.....	104
95. TEM of CDA 101 Cu processed through route 4E and heat treated at 180°C for 60 minutes.....	104
96. TEM of CDA 101 Cu processed through route 4E and heat treated at 190°C for 60 minutes.....	105
97. TEM of CDA 101 Cu processed through route 4E and heat treated at 190°C for 60 minutes.....	105
98. TEM of CDA 101 Cu processed through route 4E and heat treated at 200°C for 60 minutes.....	106
99. Optical micrograph of CDA 101 Cu processed through 1A extrusion route and annealed at 175°C for 60 min.....	107
100. (a) Optical micrograph of CDA 101 Cu processed through 1A extrusion route in fully recrystallized condition, (b) Scanned image of (a) with grain boundaries delineated, (c) trace of grain boundaries for micrograph (a), (d) grain size histogram for micrograph (a).....	107
101. (a) Optical micrograph of CDA 101 Cu processed through 2C extrusion route in fully recrystallized condition, (b) Scanned image of (a) with grain boundaries delineated, (c) Trace of grain boundaries for micrograph (a), (d) grain size histogram for micrograph (a).....	108

FIGURE	Page
102. Optical micrograph of CDA 101 Cu processed through 2C extrusion route in fully recrystallized condition, billet has 50 mm square cross-section.....	109
103. Optical micrograph of CDA 101 Cu processed through 4A extrusion route in fully recrystallized condition, billet has 25 mm square cross-section.....	110
104. Optical micrograph of CDA 101 Cu processed through 4A extrusion route in partially recrystallized condition, billet has 50 mm square cross-section.....	111
105. Optical micrograph of CDA 101 Cu processed through 4A extrusion route in fully recrystallized condition, billet has 50 mm square cross-section.....	112
106. Optical micrograph of CDA 101 Cu processed through 4B extrusion route in partially recrystallized condition, billet has 25 mm square cross-section.....	113
107. Optical micrograph of 50 mm square cross-section billet of CDA 101 Cu processed through 4B.....	114
108. Optical micrograph of CDA 101 Cu processed through 4B extrusion route in fully recrystallized condition, billet has 50 mm square cross-section.....	115
109. Optical micrograph of CDA 101 Cu processed through 4E extrusion route in fully recrystallized condition, billet has 50 mm square cross-section.....	116
110. Optical micrograph of CDA 101 Cu processed through 4E extrusion route in fully recrystallized condition, billet has 25 mm square cross-section.....	117
111. Optical micrograph of CDA 101 Cu processed through 4E extrusion route in partially recrystallized condition, billet has 19 mm square cross-section.....	118
112. Optical micrograph of CDA 101 Cu processed through 4E extrusion route in fully recrystallized condition, billet has 19 mm square cross-section.....	119
113. Optical micrograph of CDA 101 Cu processed through 8E extrusion route in fully recrystallized condition, billet has 50 mm square cross-section.....	120
114. Optical micrograph of CDA 101 Cu processed through 8E extrusion route in fully recrystallized condition, billet has 25 mm square cross-section.....	121

FIGURE	Page
115. Optical micrograph of CDA 101 Cu processed through 8E extrusion route in fully recrystallized condition, billet has 19 mm square cross-section	122
116. Optical micrograph of CDA 101 Cu processed through 2E extrusion route in fully recrystallized condition.....	123
117. Optical micrograph of CDA 101 Cu processed through 2C extrusion route in fully recrystallized condition.....	124
118. Optical micrograph of CDA 101 Cu processed through 2E-400°C-2E thermomechanical schedule in fully recrystallized condition.....	125
119. Optical micrograph of CDA 101 Cu processed through 2E-350°C-2E thermomechanical schedule in fully recrystallized condition.....	126
120. Optical micrograph of CDA 101 Cu processed through 2C-400°C-2C thermomechanical schedule in fully recrystallized condition.....	127
121. Optical micrograph of CDA 101 Cu processed through 4C extrusion route in fully recrystallized condition.....	128
122. Optical micrograph of CDA 101 Cu processed through 2F-400°C-2F thermomechanical schedule in fully recrystallized condition.....	129
123. Optical micrograph of CDA 101 Cu processed through 4F extrusion route, in fully recrystallized condition.....	130
124. Optical micrograph of CDA 101 Cu processed through 2Bc-400°C-2Bc thermomechanical schedule, in fully recrystallized condition.....	131
125. Optical micrograph of CDA 101 Cu processed through 4Bc extrusion route, in fully recrystallized condition.....	132
126. Optical micrograph of CDA 101 Cu processed through 2E-400°C-2E-300°C-2E thermomechanical schedule, in fully recrystallized condition..	133
127. Optical micrograph of CDA 101 Cu processed through 2C-400°C-2C-300°C-2C thermomechanical schedule, in fully recrystallized condition..	134
128. Optical micrograph of CDA 101 Cu processed through 2E-400°C-2E-300°C-2E-200°C-2E thermomechanical schedule, in fully recrystallized condition.....	135
129. Optical micrograph of CDA 101 Cu processed through 2E-350°C-2E-350°C-2E-350°C-2E thermomechanical schedule, in fully recrystallized condition.....	136
130. Optical micrograph of CDA 101 Cu processed through 2C-400°C-2C-300°C-2C-200°C-2C thermomechanical schedule, in fully recrystallized condition.....	137
131. Optical micrograph of CDA 101 Cu processed through 8C extrusion passes, in fully recrystallized condition.....	138

FIGURE	Page
132. Optical micrograph of CDA 101 Cu processed through 2F-400°C-2F-300°C-2F-200°C-2F thermomechanical schedule, in fully recrystallized condition.....	139
133. Optical micrograph of CDA 101 Cu processed through 8F extrusion passes in fully recrystallized condition.....	140
134. Optical micrograph of CDA 101 Cu processed through 2Bc-400°C-2Bc-300°C-2Bc-200°C-2Bc thermomechanical schedule, in fully recrystallized condition.....	140
135. Optical micrograph of CDA 101 Cu processed through 8Bc extrusion passes in fully recrystallized condition.....	141
136. Grain size as a function of thermo-mechanical processing schedule for route E.....	142
137. Grain size as a function of thermo-mechanical processing schedule for route Bc.....	142
138. Grain size as a function of thermo-mechanical processing schedule for route C.....	143
139. Grain size as a function of thermo-mechanical processing schedule for route F.....	143
140. Grain size as a function of different routes. No intermediate heat treatment was carried out.....	144
141. Grain size as a function of different thermo-mechanical processing schedules.....	144
142. (a) Percentage of low (<15%) and high (>15%) angle boundaries, as a function of strain, for commercial purity Al having an initial grain size of 1500 μm and 150 μm . (b) low and high angle boundary mean linear intercept spacing of the samples with initial grain sizes of 1500 μm or 150 μm as a function of strain.....	160

LIST OF TABLES

TABLE	Page
1. Properties and characteristics of pure copper	5
2. Comparison of conventional grain refining processes.....	8
3. Average recrystallized grain size, range and microhardness values for recrystallized tantalum processed through ECAE.....	19
4. Chemical content of as-cast CDA 10100 copper used for this research (in ppm by weight).....	25
5. Conditions of ECAE extrusion.....	29
6. Test matrix for verification of scale-up effects in ECAE of as-cast OFHC Cu 101.....	30
7. Test matrix for microstructural breakdown study.....	34
8. Successful grinding and polishing procedure for metallographic preparation of Cu sample.....	44
9. Independent and dependent variables in this study.....	49
10. Maximum load required during extrusion of 25 mm square billets.....	52
11. Maximum load required during extrusion of 50 mm (2") square billets.....	53
12. Temperature range for recrystallization for CDA 101 Cu processed through different thermomechanical schedules.....	87
13. Recrystallized grain size after processing with different thermo- mechanical processing schedules.....	145

1. INTRODUCTION

The size of the average crystal (grain) is an important structural parameter in a polycrystalline aggregate of a pure metal [1, 2]. Polycrystalline metals almost always show a strong correlation between grain size and mechanical properties like hardness, strength and workability, except at very elevated temperatures.

A typical as-cast microstructure consists of large columnar grains, growing from the outer regions of an ingot towards its center. Such as-cast microstructures suffer from many drawbacks like poor workability and low strength due to solute segregation, chemical inhomogeneities, large grain size and unwanted texture. These limitations of as-cast microstructures may lead to problems during subsequent processing. The problems of alligatoring and blistering while rolling, material rupture during forging, sausing and breakage in wire drawing have been traced back to large non-uniform grains, texture problems and other defects in the cast structure.

Grain refinement is the process where by smaller equi-axed grains are formed. The decrease in grain size leads to a drastic increase in strength, percentage elongation before breakage, toughness and workability. A fine grained material, because of its higher workability can be easily used for further processing.

Most as-cast pure metals suffer from large grain size and unwanted casting textures. These pure metals can be grain refined without affecting their chemical composition by cold working and subsequent recrystallization heat treatment. Some of the conventional cold working techniques currently used in industry are rolling, forging, swaging, wire-drawing and extrusion. These techniques have the advantage of low working temperature, chemical stability of the material, good surface finish, close tolerances and ability to impart certain texture to the finished material. But these cold working techniques suffer from some inherent draw backs including very high loads for deformation, stress-strain non-uniformity during working and unwanted texture. A material having fine equiaxed grains with little or no texture will facilitate further processing in many cases.

This thesis follows the style of *Acta Materialia*.

Copper is an important industrial metal and is widely used in both alloyed and pure form. Pure copper is renowned for its excellent electrical and thermal conductivity, good corrosion resistance, ease of fabrication, excellent ductility and good soldering and joining characteristics. As-cast oxygen free high conductivity (OFHC) copper (CDA 101 with nominal 99.99% purity) has large columnar grains having a highly textured structure. Copper is a face centered cubic (FCC) metal with medium stacking fault energy (SFE) (~ 40 erg/cm²). It is an ideal metal for a project on severe plastic deformation study because of its high ductility. The results of such a study could be generalized to other FCC metals in the medium SFE range.

The present study is motivated by the possibility of refining large grains present in the as-cast microstructure of CDA 101 Cu to a micron scale level without imparting undue texture to the material. A new processing technique, equal channel angular extrusion (ECAE), coupled with proper annealing schedules is the focus of the current study determine a suitable thermo-mechanical processing (TMP) schedule to obtain untextured recrystallized grains of small and uniform size. For this purpose, as-cast OFHC CDA 101 Cu was processed to different strain levels through a variety of ECAE extrusion routes with intermediate heat treatments at different temperatures. The effectiveness of these TMP schedules in producing a homogeneous and fine grained microstructure in fully recrystallized Cu was determined.

The processing schedules drawn out in the current study should be applicable to other pure metals with both FCC and other crystal structures. For the case of breaking down and homogenization of as-cast alloys, the results obtained in the current study may work as guidelines in the initial selection of ECAE extrusion routes and TMP schedules.

As ECAE is a new and upcoming processing technique, many questions still remain unanswered before this technique can be applied with confidence in industry. One of the major issues is whether ECAE shows any size effect. Because ECAE is a unit process still under development, processing billets with larger cross-sections will lead to greater productivity in industry, lower comparative loads, lower tooling costs and overall increased efficiency. A project to show that similar results are obtained in processing billets having different sizes was also carried out. This project shows that the

effectiveness of ECAE in inducing plastic deformation does not depend upon the size of the billets.

The next chapter provides detailed information about the inherent drawbacks of as-cast microstructures and the various techniques used to breakdown and refine such microstructures. The previous work done on grain refinement by ECAE and other thermo-mechanical processing techniques are discussed. The remaining chapters discuss the experimental procedures used to achieve the objectives of this study, the results and their discussion vis-à-vis the previous work reported in the literature.

2. LITERATURE REVIEW

In this section, a short overview of the properties and applications of pure copper will be discussed. By describing the defects in as-cast microstructures and their effects on subsequent processing, the rationale for grain refinement of these as-cast microstructures will be developed. The current techniques used for grain refinement will be discussed. The concept of equal channel angular extrusion (ECAE) will be discussed and the various routes used to plastically deform the material through different strain paths will be briefly described. The current work on ECAE of Cu and cast metals as well as the influence of intermediate annealings on the microstructures produced by various thermo-mechanical processes will be discussed. Finally the need for scaling up ECAE to larger sample sizes; and the current work done on the same will be described.

2.1. Properties and applications of pure copper

Copper is one of the oldest known metals. It has been used continuously by man for some 10,000 years; its applications changing with the changing needs of man and as more knowledge about its properties became available. The Neolithic man started using copper by 8000 BC, and as he advanced his knowledge of copper he started substituting stone with copper, heralding a new era, known as the copper age. The Romans used to obtain their copper from the island of Cyprus. They called this shiny metal “aes cyprium” which means “metal of Cyprus”. This name was shortened to cyprium which later became copper.

Copper is not the most abundant of metals found in the earth’s crust. It occurs to the extent of about seven parts per million compared to 80,000 ppm of aluminum and 60,000 ppm of iron. Table 1 lists some of the important properties of copper.

A major portion of copper produced in the world is utilized for applications in electrical engineering and for transmitting electricity. Copper; because of its excellent electrical conductivity is used in making wires and cable, bus bars, and motor and transformer windings.

Table 1. Properties and characteristics of pure copper [3].

Atomic Properties	
Atomic Number	29
Atomic Weight	63.54
Lattice Type	FCC
Lattice Constant (a)	0.3608 nm
Mass	
Density at 20° C	8.9 gm/cm ³
Thermal Properties	
Melting Point	1084°C
Boiling Point	2590°C
Electrical Properties	
Resistivity (20°C)	1.71 μΩ-cm

Oxygen free high conductivity (OFHC) copper is the purest form of copper in common use and has very low levels of residual volatile impurities, so it is used for high vacuum electronic applications such as cryogenic electrical and thermal conductors, transmitter tubes, waveguide tubes, linear accelerators and glass-to-metal seals. The extremely low amount of oxygen also reduces certain welding problems encountered in oxygen-bearing grades [3].

2.2. Problems associated with cast structures and subsequent defects

The as-cast ingot structure shows various defects such as large columnar grains, non-uniform structure, heavy texture, compositional gradients and chemical segregation. Many of these defects have effects that may persist through subsequent manufacturing processes and can be difficult to eliminate. The workability of these cast structures can be low, as the impurities and chemical inhomogeneities are segregated on the grain boundaries, and subsequent working can lead to the initiation and propagation of cracks along these grain boundaries. For example, the reduced ductility in rolled aluminum alloy 7050 plate may be caused by the solute segregation associated with the twinned columnar grains in the ingot. Once formed, this solute segregation may be difficult to homogenize even with deformation and annealing [4].

The density of solid copper is around 6% higher than the density of its liquid counterpart [1], so upon solidification, a cast ingot will have a shrinkage cavity of around 6% volume of the ingot. This central shrinkage cavity is in the shape of a cylinder or cone. In addition to primary shrinkage cavity (piping) near the top of the ingot, secondary regions of piping and centerline shrinkage may extend deeper into an ingot.

The elements in cast alloys may not be distributed uniformly. Similarly, most commercially pure metals contain various amounts of impurities in the form of tramp elements and dissolved gases which are also segregated. Segregation is a result of solute rejection at the solid/liquid interface during solidification. In large ingots, due to convection and gravity effects, variations in chemical compositions can be very high.

The presence of localized regions having chemical deviations from the nominal compositions can lead to lower corrosion resistance, unexpected responses to heat treatments resulting in hard or soft spots, quench cracks or other defects. Operations like forging, welding and other mechanical properties like fracture toughness and fatigue behavior can be severely affected.

Cast ingots having the above mentioned casting defects may lead to further problems in subsequent processing. In rolling, the initial ingot defects of pipe and gas porosity lead to alligating and blistering. A pipe, porosity or segregation of impurity in the ingot structure may lead to the generation of internal tensile stresses during forging and the material can be torn internally due to these high internal stresses. Segregation of low melting phases on the grain boundaries can also lead to material rupture during forging. Seaming can occur if there is a hole in the cast ingot [5]. In wire drawing, there can be breakage and sausaging of the wires due to the initial large size and texture of the grains. Most stamping and deep drawing processes are planned around the anisotropic behavior produced by rolling, but if the initial cast structure persists through the rolling operation, then additional anisotropy will be introduced in the drawing operations.

2.3. Different techniques for grain refinement

Macrostructure is affected by various casting factors such as level of super heat, alloying elements, addition of grain refining agents (inoculation), cooling rate, introduction of mechanical disturbance (vibrations) and ingot size. A higher degree of supercooling will lead to formation of more equiaxed structures. Table 2 lists some of the techniques used for grain refinement, and their advantages and disadvantages.

To improve the cast structure, a higher cooling rate is often employed. Microalloying and addition of grain refiners are also known methods of improving the cast structure. A lot of work on grain refinement of cast Al alloys has been reported, and different techniques, many times in combination, have been used with varied effectiveness. Grain refinement was achieved by increasing the cooling rate and lowering the superheat temperature for pure Al and Al-Cu alloy. Taha et al [6] carried out directional solidification experiments on pure Al and Al-Cu alloys with 1, 3 and 4.5 wt. % Cu, using melt superheat varying between 50 and 200 K. Alloy rods of 50 mm diameter and 200 mm length were solidified in a dry sand mould having a copper end-chill and a water cooling system to promote directional solidification. It was reported that most samples solidified with a columnar structure growing perpendicular to the chill surface. Some samples of Al-4.5% Cu exhibited fine and equiaxed grains which nucleated on the chill surface but were followed by coarse grains. By increasing the level of super heat, the columnar region in the cast structure increased. The size of columnar grain region decreased with an increase in the copper content. Easton & StJohn [7] have compiled data showing that a higher cooling rate leads to the formation of a finer cast structure. Grain refinement has been achieved by micro alloying and the addition of grain refiners such as TiB_2 and Al_3Ti_1B in the melt [8].

Some work on the use of inoculants to refine the as-cast grain size of pure copper casting has also been reported. Pure copper castings, unlike ingots and billets, cannot be plastically deformed and recrystallized to decrease their grain size. The addition of iron and cerium leads to a considerable decrease in the as-cast grain size of pure Cu. But there is considerable change in the physical and chemical properties of Cu. The electrical

Table 2. Comparison of conventional grain refining processes.

PROCESS	APPLICATIONS	PROS	CONS
Rapid Solidification	Al, Fe, Co alloys, tool steels, super alloys, complex ternary and quaternary alloys	<ul style="list-style-type: none"> -Substantial extension of solid solubility of one or more metals in another. -Extreme refinement of grain size. -Ultra fine grains (UFG) and nano sized grains. -Considerable reduction in micro-segregation in the solidified alloys. -Formation of new metastable crystalline phases. -Metallic glasses. 	<ul style="list-style-type: none"> -Extremely small size of products -Cannot be effectively applied to pure metals, as the required high cooling rates are not achievable. -Elaborate equipment and tight control over the solidification process is required.
Micro Alloying	Grain refinement of Al and Mg alloys and steels.	<ul style="list-style-type: none"> -Very small grain size compared to the un-alloyed microstructure. -Reduces the tendency for ingot cracking, thus increasing the casting speed. -Uniform and equiaxed microstructure. -Finer dispersion of porosity and second phases. 	<ul style="list-style-type: none"> -Cannot be applied to pure metals due to contamination. -Some grain refiners are prone to “fading”, the effectiveness of the refiner decreases with contact time in the melt before casting. -Very sensitive to the composition of the alloys. -Very inefficient, with a best of ~1% of added particles successfully nucleating grains
Deformation Processing + Recrystallization	Grain refinement of pure metals and cast alloys	<ul style="list-style-type: none"> -Good control over the grain size. -Can be applied to pure metals and alloys. -Ultra fine grains (UFG) and nano sized subgrains can be obtained. -Some control of texture and anisotropy. 	<ul style="list-style-type: none"> -Tight control of process parameters. -Elaborate thermo mechanical schedules. -Un wanted texture.

conductivity also decreases considerably. The increase in electrical resistivity of Cu is directly proportional to the amount of impurities in the metal. Impurities present in the form of solid solution show more negative effects on conductivity than those that are found in the form of intermetallic compounds. Bustos et al [9] determined the feasibility of as-cast grain refinement of pure copper by the addition of some intermetallic compounds. Various borides and carbides were tested for their grain refining capabilities. Electronic grade high purity Cu was melted in alumina crucibles heated to a temperature of 1200°C. A fixed quantity, 220 grams of Cu was melted in these crucibles. Boron was added in quantities varying from 0.01 to 0.16 wt% with a constant addition of 0.05 wt% of nuclear purity carbon. A pouring temperature of 1160°C was used with a holding time of 25 minutes after the addition of grain refiner. It is reported that a continuous decrease in grain size with increase in the added content occurs up to 0.085 wt% boron, giving an equiaxed region of 96% of the ingot, but above 0.085 wt% boron, there is no further decrease in grain size or increase in the fraction of equiaxed grains for the maximum of 0.16 wt% boron added. Addition of Zr, Ti, Cr, Mo, Co, Ni, Ce, Al and Ca in combination with boron as ternary master alloys was also studied. Zr-B, Cr-B, Mo-B and Ni-B actually lead to an increase in the as-cast grain size compared to pure copper. The addition of Al-B and Ca-B gave good results in terms of grain refinement, with the best results obtained for Al-B. All the intermetallic compounds added led to a decrease in electrical conductivity; a minimum decrease was reported for addition of boron and carbon. Intermetallic compounds were also added as powders compacted in a matrix of high purity Cu. The best results were obtained with the addition of MoS₂ and AlCo compounds.

Other deformation processes such as hot rolling have been used to improve the grain size and grain size uniformity for aluminum alloy 7475 [10] and plain carbon steel [11,12].

Cui and Ohori have carried out grain refinement of high purity Al by asymmetric rolling [13]. In asymmetric rolling, the peripheral speeds of the upper and lower rolls are different. In hot rolling, the high frictional forces lead to generation of severe shear

stresses and high shear deformations in the material, but in conventional hot rolling these severe shear strains do not reach the center of the rolled material, producing a non-uniform microstructure in the sheet cross-section. In case of asymmetric rolling, the additional shear strains generated by the unequal peripheral speeds lead to the formation of a refined microstructure throughout the thickness of the sheet. High purity Al sheet of ~6.9 mm thickness was annealed at 813 K for 30 minutes, giving a coarse grained microstructure having equiaxed grains of average size ~800 μm . Asymmetric rolling was carried out using a rolling mill with upper and lower roll diameter of 255 mm, and under conditions of a mismatch speed ratio of ~1.4, rolling speed of ~ 20 mmmin^{-1} at the high speed roll side, and without lubrication. Reduction per pass was ~0.2 mm and three different rolling reductions were used, ~ 65.2%, 85.5% and 91.3% for both conventional and asymmetric rolling. For the maximum reduction ratio, in case of conventionally rolled sheets, the common fibrous cold rolling microstructure has been reported; the original grains have been compressed and elongated in the rolling direction. In case of asymmetric rolling, at 65.2% rolling reduction, the rolled sheet shows the formation of fine equiaxed grains near the surface, while there are comparatively large and elongated grains in the center. But as the reduction level is increased, the shape and size of grains in the surface layer hardly changed, while the grains in the centre of the sheet decreased in size and tended to be equiaxed.

Mabuchi et al [14] investigated the effect of hot area reduction extrusion on the microstructural refinement and the subsequent improvement in mechanical properties for as-cast Mg-Si-Al alloy. The alloy had a composition of 12.6 wt% Si, 4.2 wt% Al and balance Mg, and had an as-cast grain size of ~ 69 μm , which reduced to a size of 27 μm after hot extrusion at a temperature of 753 K and a reduction ratio of 100:1. The as-cast structure also had an inhomogeneous distribution of Mg_2Si particles due to dendritic solidification in the mold. The hot extrusion led to a reduction in the mean size of these Mg_2Si particles as well as a more homogeneous distribution of the same. This led to an improvement in the mechanical properties like elongation to failure, 0.2% proof stress and the ultimate tensile strength.

Saqib et al [15] investigated the effects of hot isostatic pressing on the improvement in the microstructure of cast α_2 -base alloy showing a composition of Ti-25 Al-10 Nb-3V-1Mo, at. %. Hot isostatic pressing was done in a temperature range of 925 to 1125°C and pressures of 100-270 MPa. The effects of temperature and pressure on volume fraction of the different phases were investigated. The HIP processing done at a higher temperature and pressure, coupled with ageing led to a greater change in the volume fraction of the phases and led to an increased refinement in the structure.

Song et al [16] investigated the effects of hot rolling on grain size in a magnesium alloy. The magnesium alloy AZ31 having composition of 3 wt% Al, 1 wt% Zn with a minimum Mn content of 0.2 wt% with balance Mg was used. The starting material was in the form of as-cast billets having diameter of 100 mm and length of 300 mm. These billets were hot-extruded to a thin slab of 5 mm thickness and 80 mm width. After extrusion the slabs were rolled into thin sheets of 1 mm thickness after 10 passes. The rolling was carried out at a temperature of 623 K. Starting grain size in the as-cast material was 91.2 μm . In the cross-sectional plane of the cast ingot, the grains appear to be reasonably equiaxed and homogeneously distributed. After extrusion with a ratio of 20:1, the grain size reduced to 28.2 μm . The grain size after final rolling was 8.8 μm . Tensile testing indicated that there is significant increase in the strength and ductility of AZ31 alloy after plastic working.

2.4. Equal channel angular extrusion

Equal channel angular extrusion (ECAE) is a new technique that permits the application large amounts of strain to the work piece. This severe plastic deformation processing method was invented by Vladimir M. Segal in the former Soviet Union [17] and studied extensively in 1970s and 1980s. Dr. Segal transferred some aspects of the process to the Texas A&M University in the early 1990's while working as a research scientist.

The principle of ECAE is shown in Fig. 1. ECAE works by pushing a well lubricated billet through two intersecting channels of identical cross section. The

dimensions of the billet are nearly identical to the channel cross-section. The billet moves within the channel as a rigid body and the deformation is imparted through simple shear at the crossing plane of the channels. This crossing plane, ideally should be a plane of infinitesimal thickness, but due to geometrical and physical constraints, it is a zone having a thickness of around 0.10 – 0.20 of the width of the channel section [18]. As shown in Fig. 1 a square material element (abcd) is deformed by simple shear into a new material element (a'b'c'd') at a certain angle (ϕ) measured from the vertical axis. As the work piece dimensions are nearly identical before and after processing, multiple extrusions can be done. Segal has shown that for a 90° ($\phi = 45^\circ$) die, the true strain induced in each pass is ~ 1.16 . For multiple extrusions, the total strain intensity has been theoretically calculated to be [17]:

$$e = N * 1.16 \quad (2)$$

The strain induced in the billet is relatively uniform throughout the cross-section of the billet, but as can be seen from Fig. 2, the two ends of the billet are not subjected to the shearing process, and there is a low strain zone along the bottom surface of the billet for the tooling geometry used in this research (sliding side walls in the inlet channel and a sliding bottom wall in the exit channel). The thickness of this reduced strain zone is around 0.10 – 0.20 of the thickness of the billet for a die having sliding bottom wall in the exit channel [18].

It is possible to induce different types of textures and to control the as-worked and recrystallized microstructures by altering the orientation of the billet between each extrusion pass. There are four primary processing routes that are commonly used by the research community: A, B, C and Bc. Route A involves no rotation of the billet between two extrusion passes. In route B, the billet is rotated 90° counterclockwise, along its long axis (looking from the trailing end of the billet), after the even numbered passes, and 90° clockwise after the odd numbered passes. Route C involves a billet rotation of 180° between passes. Route Bc involves a 90° billet rotation in the same direction between

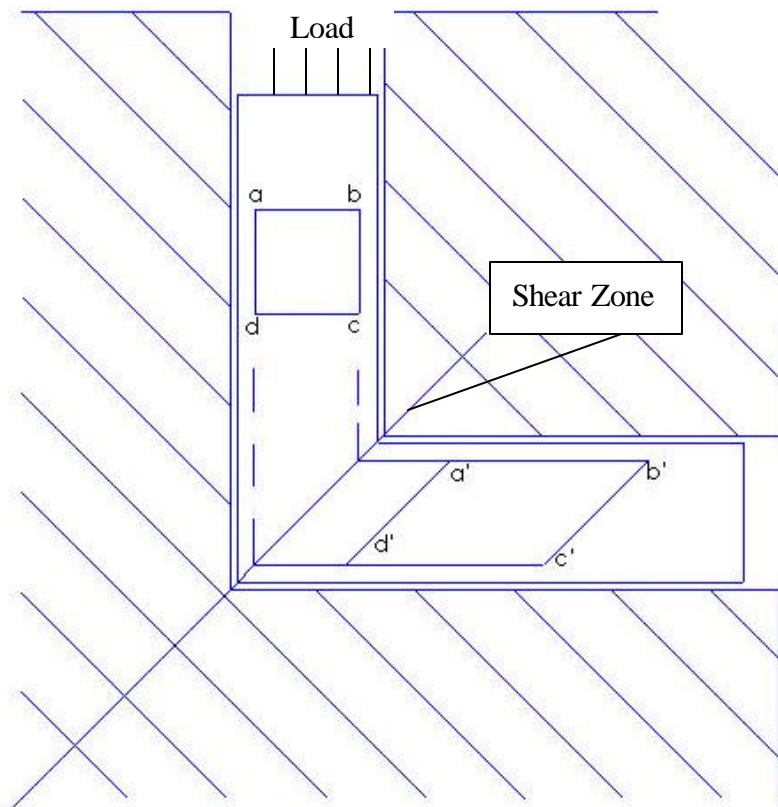


Fig. 1. General mechanics of equal channel angular extrusion.

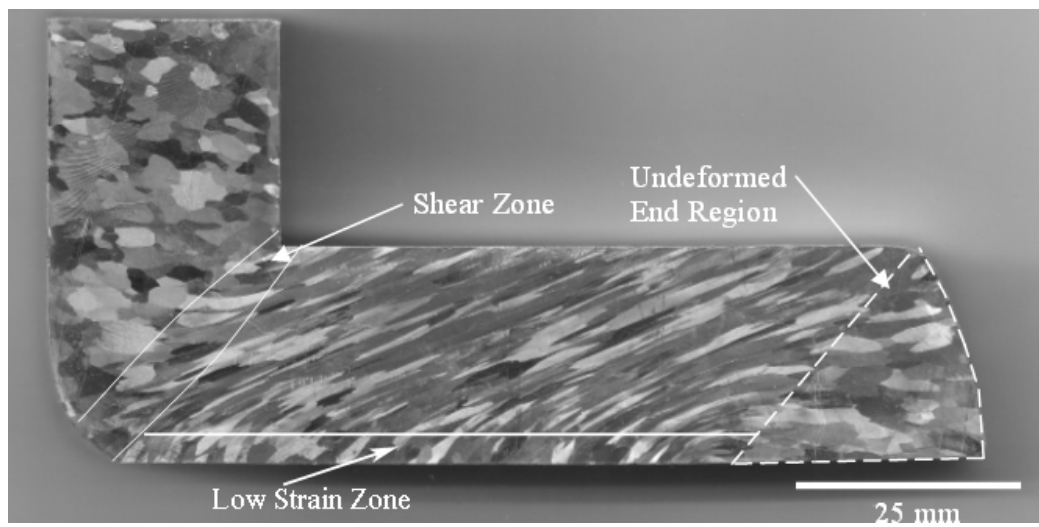


Fig. 2. Half extruded billet of as-cast CDA 101 Cu indicating the end regions and low strain zone along the bottom edge.

every pass and is a route where each pass provides deformation on a plane that intersects the previous plane of deformation. Route A leads to the formation of an elongated and laminar as-worked microstructure. Route B produces a fibrous structure, while route C leads to the formation of fairly equiaxed structure after each even numbered pass.

Routes E and F are relatively new processing routes. Route E is similar to route C, with the addition of a 90° rotation (counter clockwise-looking from the trailing end of billet) before the third pass of processing. It requires four passes to complete. After the first pass, rotate the billet 180° , process the second pass. Rotate 90° , counter clockwise and process the third pass. Rotate 180° , and process the fourth pass. This processing route produces a more equiaxed grain structure compared to the conventional routes, having applied simple shear in two intersecting planes. Route F is a hybrid route of Bc and C, which involves a 90° counter clockwise billet rotation between first and second pass, followed by a 180° rotation between the second and third pass, and a counter clockwise rotation of 270° between the third and fourth pass. Thus it also requires four passes to complete. The simple shear occurs along two intersecting planes, just like routes Bc and E. Fig. 3 shows the rotation of billets between different ECAE passes for different routes.

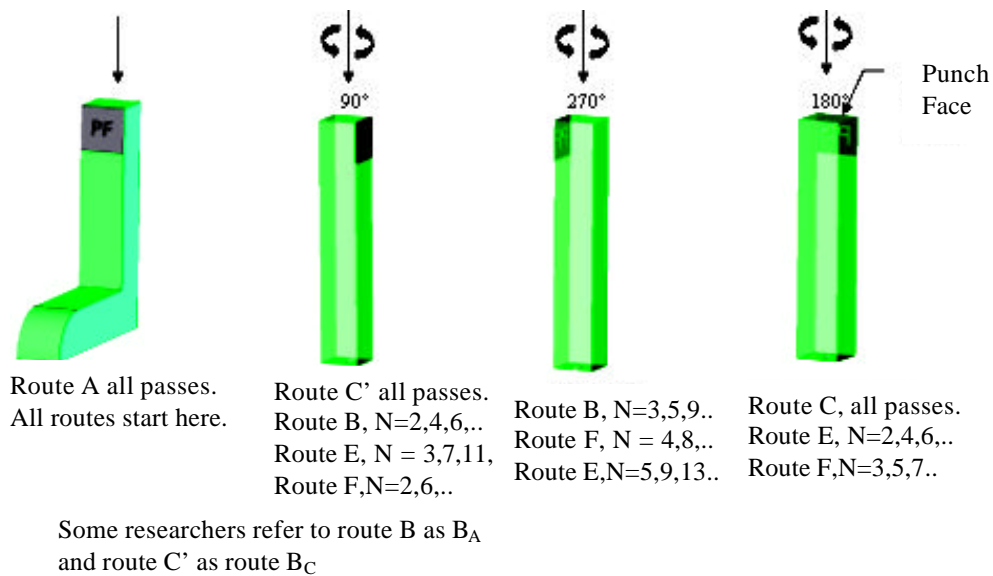


Fig. 3. The rotation of billets between different ECAE passes for different routes.

The following are some of the benefits of ECAE compared to the conventional processing techniques:

1. The induced plastic strain (1.16) in the billet is large compared to conventional techniques.
2. There is negligible change in the work-piece geometry.
3. The large plastic strain is quite uniform throughout the billet cross-section, resulting in uniform structure and properties throughout the billet.
4. By rotating the billet between extrusions, new microstructures and textures can be developed.
5. It is an effective technique for eliminating internal metallurgical defects such as pores, voids and cavities produced during casting [4].
6. A simple and elegant tooling design ensures that the required punch pressure for extrusion remains relatively low.
7. Large cross section bulk materials can be easily processed.

Accompanying the above mentioned advantages are the following limitations of ECAE:

1. ECAE in its current form is a unit process.
2. Billet end losses and dead zones can exist.
3. Only simple cross-sections (round and square) can be easily processed currently.

The recent years have seen a great increase in research done in the field of ECAE and many publications are available that deal with the deformation mechanisms, development of different textures and other microstructural behavior [19,20].

2.5. ECAE of copper

Extensive work has been done on the microstructural refinement of wrought and wrought-annealed copper. Ferrasse et al [21] studied the effect of ECAE on annealed copper. The starting material used for this research was wrought and annealed CDA 101 copper. Wrought copper bars were annealed at 600°C in an argon atmosphere for one hour resulting in an average grain size of 200 µm. This annealed copper was used as the

starting material for ECAE processing. Billets were extruded up to eight passes using routes A, B and C. The extrusions were performed at room temperature at a strain rate of 0.5 sec^{-1} . The recrystallized grain size obtained by performing post-extrusion annealing was in the range of 5 – 10 microns.

Huang et al processed annealed CDA 101 Cu for up to eight passes via routes C and Bc [22]. The objective of this study was to determine the effect of the level of strain, the deformation route and the deformation temperature on the evolution of the as-worked microstructure. The starting material was annealed copper having a grain size of $150 \text{ }\mu\text{m}$. The billets had nominal dimensions of $12 \text{ mm} \times 12 \text{ mm} \times 100 \text{ mm}$. The extrusions were carried out in a 90° angle die, and at various deformation temperatures starting from room temperature to 200°C . The punch speed used was 30 mm/min . Huang reported the generation of equi-axed sub-grains along the transverse plane of the billets, and the generation of equi-axed and elongated sub-grains along the flow plane of the billet. The sub-grain morphology obtained for routes Bc and C was similar, though the sub-grains obtained through route C were reported to be more equi-axed along the flow plane compared to those obtained through route Bc. Route Bc also led to the formation of some sub-grains free from dislocations and having a large size. These sub-grains had a size of 500 nm compared to other sub-grains that had a size of $200\text{-}250 \text{ nm}$. These sub-grains were separated from the rest of the microstructure by high angle boundaries (HABs). Huang concluded that these sub-grains are formed by dynamic recrystallization.

Dalla Torre et al [23] processed commercially available annealed copper for up to 16 passes via route Bc, and have reported extensive results on microstructural evolution and its influence on the mechanical properties of copper. The copper was annealed at 600°C for two hours under an inert atmosphere. This annealing led to an average grain size of $10 \text{ }\mu\text{m}$. ECAE was performed on square bars having a cross section of $20 \text{ mm} \times 20 \text{ mm}$. The die used for extrusions had an angle of 90° , resulting in a strain of ~ 1.15 per pass. A backpressure of 25 MPa was applied and a punch speed of 2 mm/s was used. The generation of lamellar sub-grains on the transverse plane, which evolve into equi-axed structures with increasing number of passes is reported. After 12 passes,

the sub-grains appear equi-axed on the transverse plane. The yield stress and ultimate tensile stress reach a maximum after four passes. From 4 to 16 passes, the strength of the material decreases and the uniform elongation increases, suggesting the operation of recovery mechanisms which decrease the boundary volume and the total dislocation density, thus causing an increase in the mean free path of the dislocations.

Haouaoui [24] did extensive work on characterization of CDA 101 Cu processed through ECAE. The starting material for this research was wrought copper processed through two extrusions via route C and annealed at 600°C for 90 minutes. This annealing gave a uniform grain size of 50 μm . This Cu was used as the starting material for further processing for up to four passes via route A, B, C and E. Texture and recrystallization studies were carried out. Haouaoui reported that the nucleation of new grains from the heavily deformed material occurs along shear bands with subsequent growth in the direction of slip lines. The processing route that causes intersection of shear planes creates more sites for nucleation and leads to a shifting of the recrystallization curve to lower temperatures. The formation of grains having an average grain size of 5 μm after a heat treatment at 400°C for one hour was reported.

2.6. ECAE of cast alloys

Luo et al [25] reported the effectiveness of ECAE in breaking down the as-cast structure of AM60 magnesium alloy. Luo processed billets having nominal dimensions of 8 mm x 8 mm x 50 mm cut from a cast ingot. Extrusions were performed at a temperature of 573 K (300°C) and at strain rates of 0.2 mm/min and 2 mm/min; in some extrusions back pressure was employed. Up to five extrusions were performed. Luo reported using a route in which the billet is rotated 180° axially and then rotated 90° counter-clockwise “radially”. On understanding this route, it becomes clear that it is route Bc. It is reported that during the first pass, there is some cracking due to low workability of the material, even with the application of back pressure. On further extrusions, this cracking disappears, and there is reduction in the load required for extrusion, indicating an increase in workability. It is reported that a fine grained and

homogeneous structure is obtained after five extrusion passes and a well dispersed $Mg_{17}Al_{12}$ phase is obtained in a magnesium matrix.

Goloborodko et al [26] carried out a detailed investigation to determine the effectiveness of ECAE in breaking down the as-cast microstructure of Al 7475 alloy. The alloy was direct chill cast and homogenized at 495°C for 20 hours. The as-cast microstructure is made up of dendrite lamellas that lie parallel to the ingot axis. Average sizes of these lamellas are in the range of 1 to 10 mm in longitudinal direction and 100 to 200 μm in the transverse directions. Billets having nominal dimensions of 20 mm diameter and 100 mm length were cut with their long axis parallel to the axis of the ingot and extruded for up to 12 passes using route A. Extrusions were carried out in a 90° die and at a temperature of 400°C (0.7T_m). After six passes, a fine grained microstructure with an average crystallite size of about 1.7 μm is reported to have developed.

Mathaudhu et al [27] studied the ability of ECAE in breaking down the as-cast microstructure of tantalum. As-cast vacuum arc remelted (VAR) tantalum of commercial purity was processed for up to four passes via route E and for eight passes via route C. The as-cast tantalum has columnar grains of > 5 mm diameter and ~ 20 mm length, having their long axis parallel to the long axis of the ingot. Billets having nominal dimensions of 25 mm x 25 mm x 150 mm and having their long axis parallel to the axis of the ingot were extracted. Extrusions were performed in a die having a die angle of 90°. Isochronal annealing was performed on the samples extracted from these billets, and the flow plane was examined through optical metallography. The results reported by Mathaudhu are given in Table 3.

As-cast Nb was processed by Mathaudhu et al [28] up to four passes via routes C and E. Billets having nominal dimensions of 25 mm x 25 mm x 150 mm and 50 mm x 50 mm x 250 mm were cut from a cast ingot. The long axes of these billets were parallel to the axis of the cast ingot. The billets were extruded using the same tooling as mentioned in the previous case of as-cast VAR Ta. Mathaudhu reported the formation of shear bands in the as-worked and recrystallized billets. Shear banding was more pronounced in the case of route 4C than for route 4E. The fully recrystallized

microstructure obtained after processing the billets through route 4E was uniform in terms of grain size compared to route 4C. The average grain size for route 4E was reported as $18 \pm 10 \mu\text{m}$.

Table 3. Average recrystallized grain size, range and microhardness values for recrystallized tantalum processed through ECAE [27].

Extrusion Route	Average Grain Size (μm)	Range (μm)	Vickers Microhardness (HV_{300})
1A	38 ± 25	<250	85 ± 2
2C	31 ± 25	<195	83 ± 3
4C	16 ± 11	<90	96 ± 4
4E	8 ± 5	<27	91 ± 3

2.7. Effect of intermediate heat treatments

Intermediate heat treatments are an effective way of altering the microstructure during plastic working of metals. During conventional processing like rolling and forging, intermediate anneals are employed to improve the workability of the material.

Jahazi and Goudarzi [29] carried out intermediate heat treatments on aluminum alloy 1050 and 1100 to improve the earing behavior during forming. AA 1050 and AA 1100 are used for the production of cooking vessels and depending upon the texture in the sheet, earing problems are created during forming. 300 mm slabs of the above materials were homogenized and then rolled down to a reduction of 97-98%. Intermediate heat treatments and final annealings led to the development of favorable texture and grain size, leading to a reduction in the earing behavior in the sheets.

Jin and Saimoto [30] investigated the effects of Fe impurity in commercially pure aluminum and aluminum-magnesium alloys like AA 5182 and AA 5754. A thermomechanical schedule for obtaining an ultrafine grained structure in the final sheet was also devised. It was concluded that a pre-strain rolling of 20% reduction followed by an intermediate heat treatment at 230-320°C, a continued cold rolling to a total reduction

of about 85-95% followed by a recrystallization anneal at a temperature of 320°C lead to the formation of ultra-fine grains having a size of 1-2 μm .

Chang and Shan carried out intermediate heat treatments during ECAE of pure Al [31]. Pure Al bars having a square cross section of 12 mm x 12 mm were processed through route A through a 90° tooling. Upto four extrusions were done with intermediate heat treatments of 200°C for two hours. It was observed that IHT lead to a decrease in the sub-grain size but increased the aspect ratio of these sub-grains. A final anneal at a temperature of 200°C for one hour after four passes led to the cleaning up of the microstructure and formation of high angle grain boundaries. The sub-grain shape changed from an elongated one to an equiaxed one.

Current research at Texas A&M University on ECAE of commercial purity Ta and Na has shown that the homogeneity of recrystallized microstructure is greatly improved by the incorporation of anneals between extrusion passes. During ECAE of as-cast Cu, intermediate anneals may lead to an improved homogeneity in the final processed material.

2.8. Need for scale-up of equal channel angular extrusion

Although extensive research has been done on ECAE, most work has been reported on the material characterization and microstructural refinement obtained through ECAE. Questions remain regarding the engineering aspects of the process; the issues of material yield, scale-up to larger sizes, the shear zone size, friction effects and round billet rotation to name a few. These issues and others have to be effectively addressed before ECAE can be applied with confidence in industry.

One of the major issues is whether ECAE shows any size effect. Because ECAE is a unit process still under development, processing billets with larger cross sections will lead to greater productivity in industry, lower comparative loads, lower tooling costs and overall increased efficiency.

The fact that ECAE shows uniform shear throughout the billet cross section has been effectively verified through experiments for billets having square cross section of

25 mm x 25 mm [18]. But this study has not been extended to larger sizes. Billets having round cross sections having diameters ranging from 4 mm [32] to 60 mm [33] have been processed using ECAE, but not many experiments have been reported showing that the same results are obtained for different sized billets.

Horita et al [34] verified scale-up during ECAE of commercial 1100 aluminum alloy. The billets used were of circular cross section having diameters of 6, 10 and 40 mm. These billets were extruded to eight passes via route Bc. To check the homogeneity of the induced plastic strain, Vickers microhardness measurements were taken along the transverse plane for the largest sample (40 mm diameter). These hardness measurements were taken as scans along the Y and Z axes of the transverse plane (Fig. 4). The distance between each microhardness indentation and between the last indentation and the edges was 5 mm. Hardness values obtained on the transverse plane are shown in Fig. 4. The as-worked microstructure was observed along the transverse plane using transmission electron microscopy. The micrographs obtained and their locations in the billet cross-section are indicated in Fig. 5. A is at the center of the billet, while the other points are at a distance of 5 mm from the billet edge.

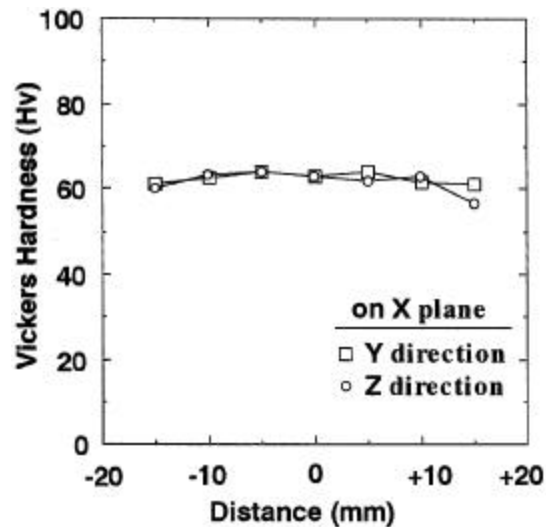


Fig. 4. Values of Vickers microhardness measurements on the transverse plane taken along the Y and Z directions for the as-worked Al 1100 alloy. These measurements were taken along the Y and Z directions [34].

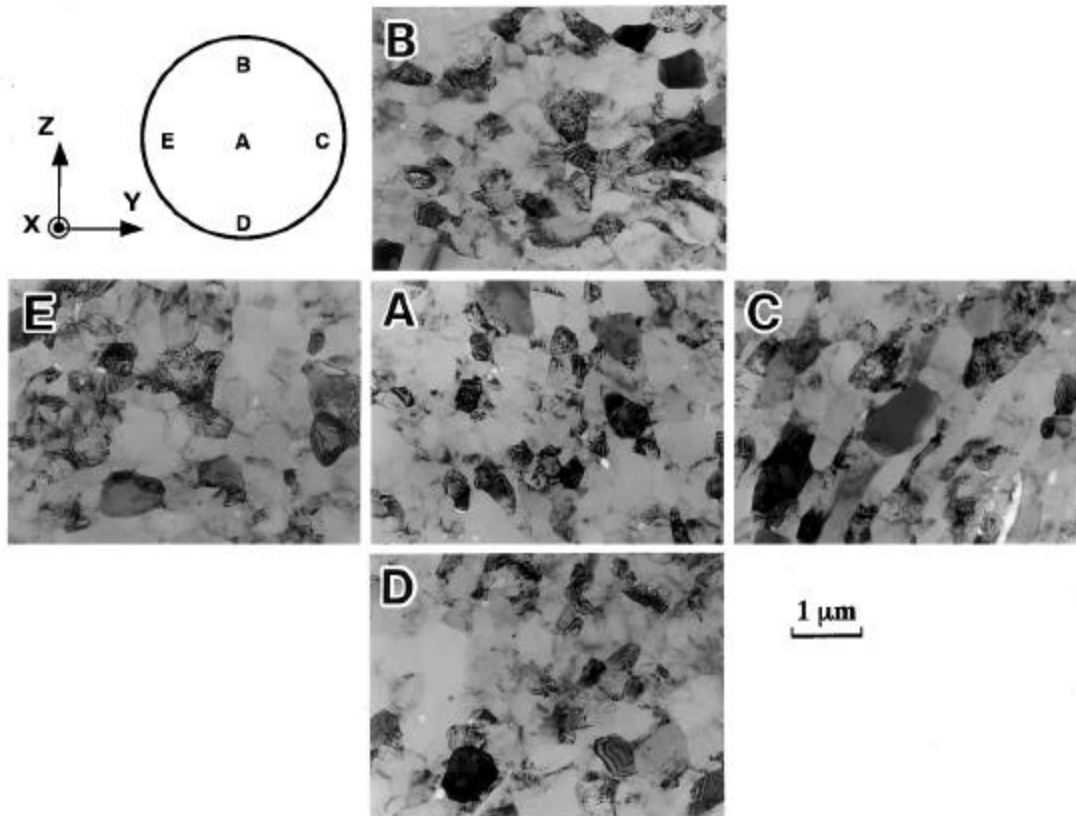


Fig. 5. As-worked microstructure on the transverse plane for Al 1100 alloy after six passes via route Bc. Note the elongated sub-grains obtained at point C [34].

Observe that sub-grains formed on the transverse plane of the billet show identical size and morphology for all locations in the billet except location C. The sub-grains at location C are elongated instead of being equiaxed. This suggests that there can be a change in the magnitude and pattern of induced plastic strain somewhere between the locations A and C, or an initial texture condition that lead to this outcome.

Horita concluded that the plastic deformation induced in the billet is independent of the size of the billet. But while extruding a round billet, the billet may rotate, bringing a texture favorable for easy shear into proper orientation. After extrusion, a round billet will have a rhomboidal shape, and during subsequent extrusions it may be difficult to

determine the size and shape of the end zone. It may also be difficult to determine the size and shape of the fully worked region for a round billet. Due to these reasons, the study of scale-up effects for billets having square cross section may lead to different results from the one done for billets having round cross sections.

The work done at Texas A&M University for grain refinement of as-cast Niobium incorporated the verification of the scale-up issue [35]. Billets having square cross-sections of 25 mm and 50 mm dimensions were processed for four passes via route 4C. The analysis of as-worked and recrystallized conditions suggested that the strain induced in the material and the subsequent grain refinement is independent of the billet size.

The as-worked microstructure was characterized by Rockwell hardness measurements. The Rockwell B hardness measurements taken on the transverse plane of the 25 mm and 50 mm billets show the same as-worked hardness in the range of 70- 85 HRB. The uniformity of the as-worked microstructure is concluded from the relative uniformity of these hardness values on the transverse plane.

The recrystallization behavior of as-worked material was analyzed by performing isochronal annealing for a range of temperatures from 300°C to 1100°C; the recrystallization curves indicate near identical behavior of the as-worked material independent of the billet size. Small differences between the two recrystallization curves were attributed to the starting microstructure and texture of the large as-cast grains. The recrystallized microstructure was characterized using optical metallography. It was concluded that for Niobium, ECAE can be successfully scaled-up to a size of at least two inches.

3. EXPERIMENTAL PROCEDURES

As mentioned earlier, this thesis comprises of two research projects; the objective of the first one is to show independence of ECAE processing from billet size. The objectives of second research project were to determine whether ECAE processing leads to grain refinement of as-cast copper and to determine the most effective thermo-mechanical processing schedule to obtain a uniform recrystallized microstructure with a small recrystallized grain size. To attain these objectives, ECAE extrusions were carried out and various characterization techniques used to determine the effectiveness of each thermomechanical processing.

This section describes in detail the various processing and characterization techniques used to achieve the research objectives. The advantages of each technique used and reasons behind choosing the same will be given.

3.1. Material

The material for this research was produced by the Mitsubishi Materials Corporation. The chemical composition, as reported by the manufacturer is given in Table 4. The as-cast CDA 10100 copper was received in the form of a cylindrical ingot having a nominal diameter of 319 mm and a length of approximately 300 mm.

3.2. Billet extraction from ingot

All billets for ECAE were cut from the above mentioned ingot. A sample of the cross-section was first taken and macro-etched to reveal the starting grain structure. This slice was used to determine the best method for sectioning the ingot into appropriate size samples.

Large columnar grains of as-cast macrostructure can be observed by carrying out a macro-etch on the surface. The chill zone is approximately 35 mm thick around the perimeter. The nominal grain size in the center region is fairly uniform, measuring 1-4 mm x 10-20mm. In the chill zone, the grains were smaller, 1mm x 5-10mm. Figs. 6 and 7 show the ingot slice and chill zone.

Table 4. Chemical content of as-cast CDA 10100 copper used for this research (in ppm by weight).

Chemical Composition	Specified Value		Measured Value
	MIN.	MAX.	
Cu	99.99		99.99
As		5	1
Sb		4	<1
P		3	2
Te		2	<1
Bi		1	<1
Cd		1	<1
Fe		10	1
Pb		5	1
Mn		0.5	0.1
Hg		1	<1
Ni		10	1
O		5	1
Se		3	<1
Ag		25	18
S		15	4
Sn		2	<1

The first project was undertaken to verify the scale-up effectiveness of ECAE. For this purpose, seven billets of each cross-sectional size (19 mm x 19 mm, 25 mm x 25 mm and 50 mm x 50 mm) were cut from the ingot using a band saw. A constant flow of cutting fluid was maintained on the band saw blade to avoid overheating of the ingot during cutting and to remove the chips generated during the cutting procedure. All billets were machined on a vertical milling machine to their final dimensions, and then stamped at the ends for identification. Selected billets were macro-etched to reveal the grain structure. A typical result of the etching is shown in Fig. 8. All billets had aspect ratios greater than five, thereby assuring good amounts of fully worked materials in the central region of the ingots. Billets were chosen from locations in the ingot that varied the grain shape and size with respect to the extrusion direction. See Fig. 9 for the extrusion directions. The purpose of choosing the extrusion direction/billet location combinations was a) to vary the initial grain structure so that a variety of initial conditions can be compared to the final worked conditions, and b) to gather empirical data on the effect of initial grain structure on extrusion loads.

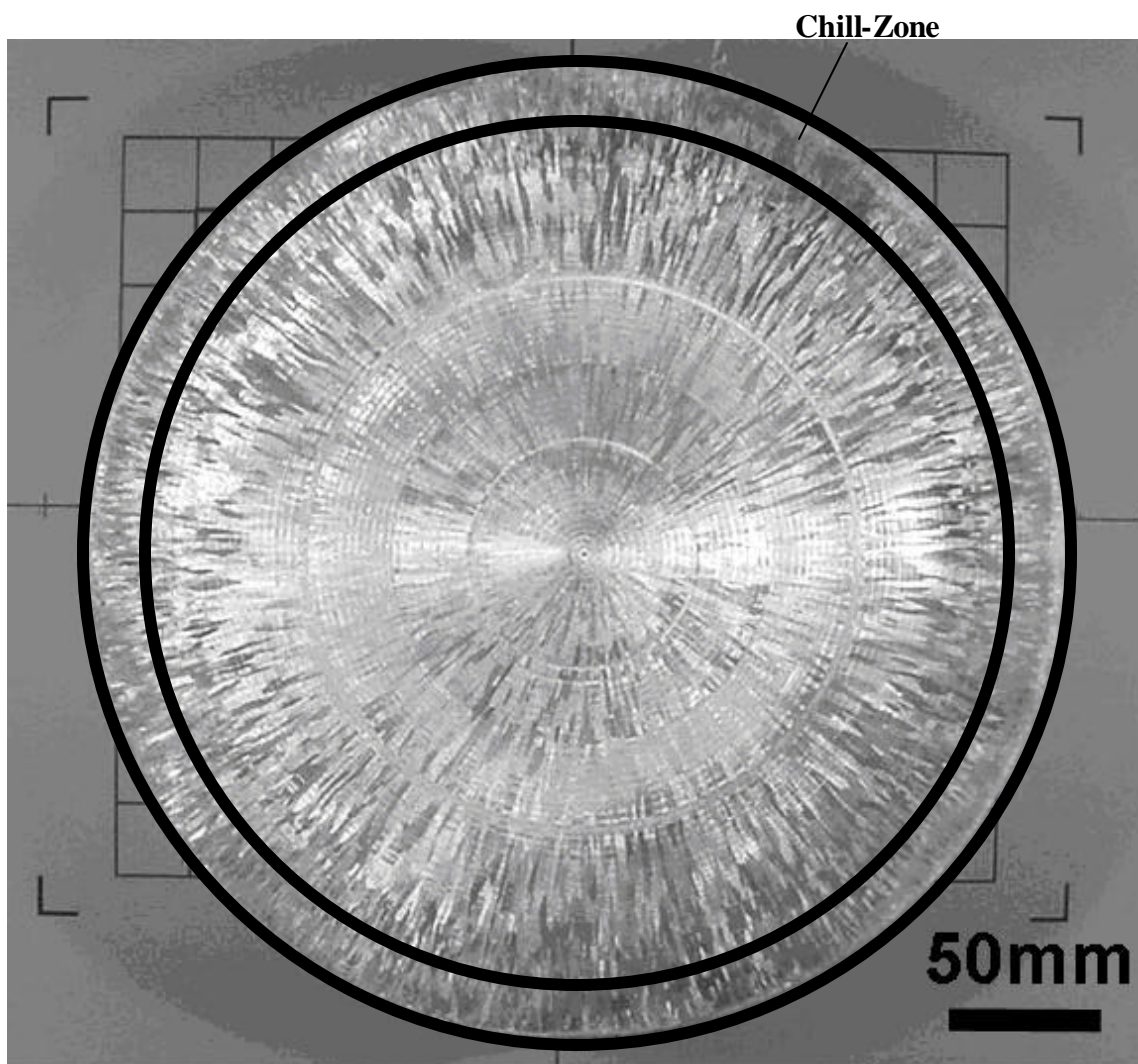


Fig. 6. Transverse macrostructure of cast OFHC CDA 101 Cu ingot.

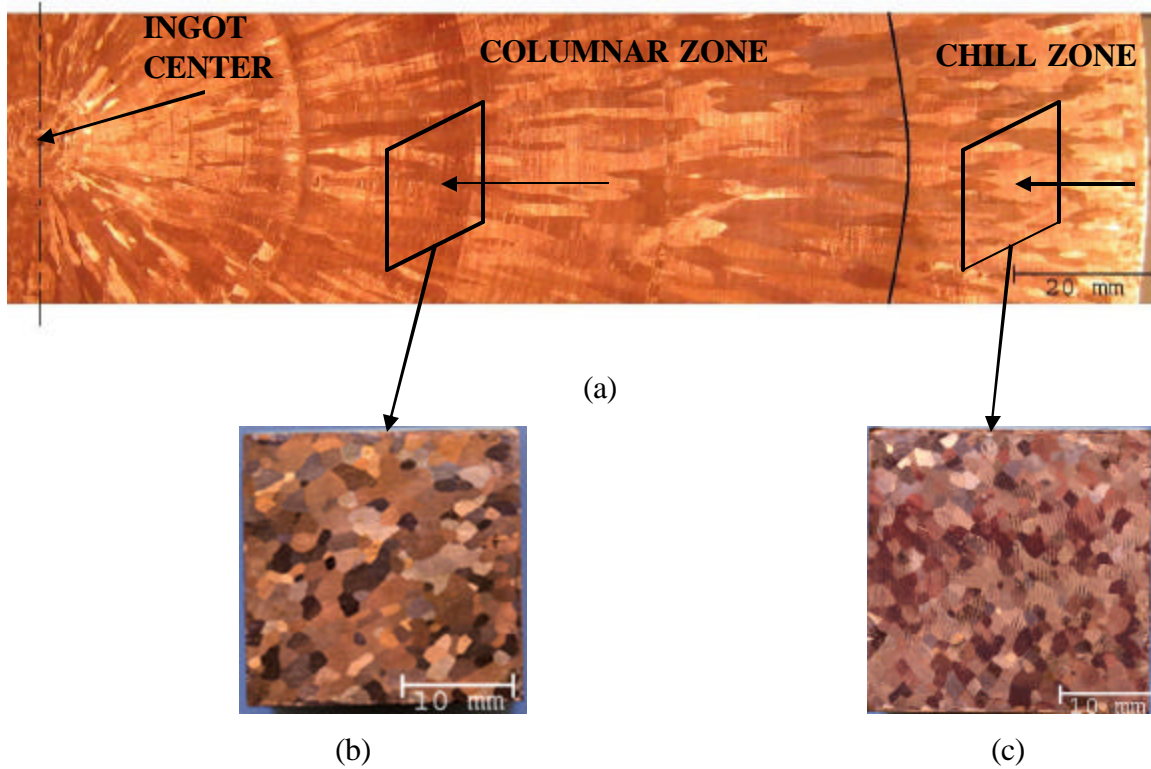


Fig. 7. (a) View of transverse section of the ingot (b) Side section of the columnar zone (c) Side section of the chill zone. Note the variation in macrostructure with location in the ingot.

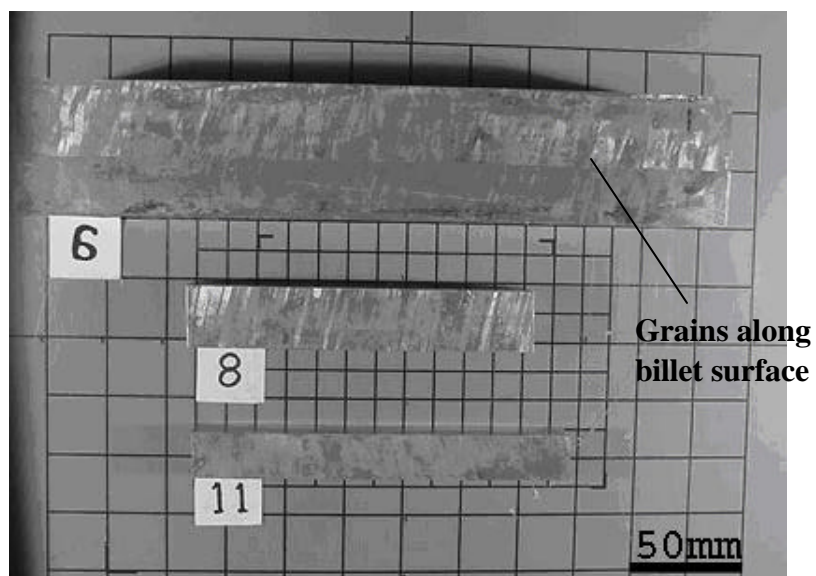


Fig. 8. Image of three etched billet sizes, 50 mm x 50 mm x 250 mm, 25 mm x 25 mm x 150 mm and 19 mm x 19 mm x 160 mm (nominal) used for ECAE processing.

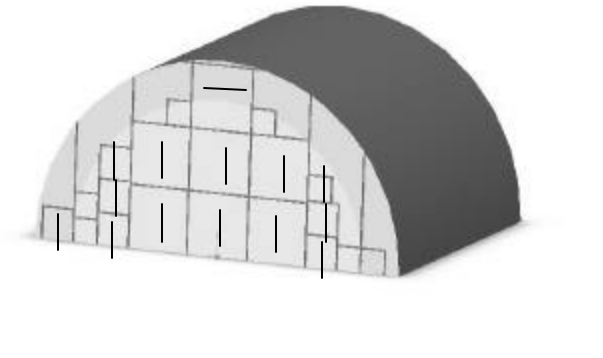


Fig. 9. Pattern of billet extraction from the ingot. Extrusion exit channel directions are illustrated by arrows.

For the second phase of this research project, the project to determine the effectiveness of ECAE in refining the as-cast microstructure of OFHC Cu, the billets with a nominal size of 25 mm x 25 mm x 175 mm were saw cut from the columnar region of the ingot. The billets had their long axes parallel to the ingot axis, thus ensuring uniformity of grain size and orientation throughout the length of each billet (Fig. 10).

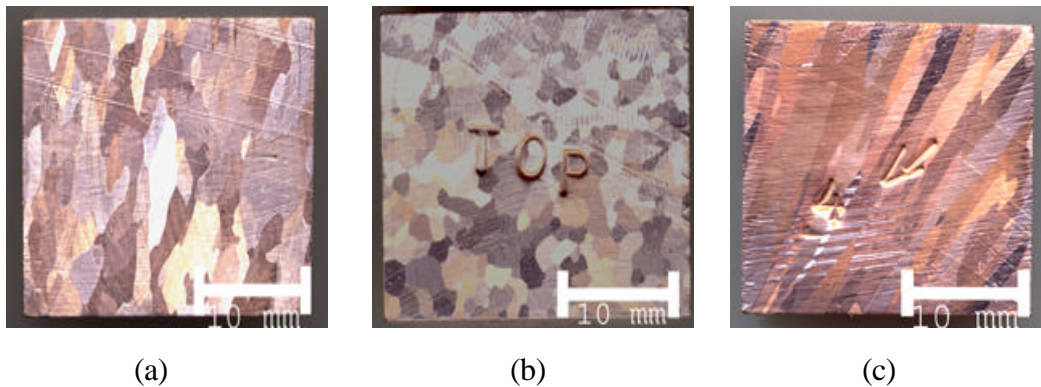


Fig. 10. The initial microstructure and grain orientation for billets having nominal dimensions 25 mm x 25 mm x 175 mm for microstructural breakdown study. (a) Flow plane (b) Top (Longitudinal) plane (c) Transverse plane.

3.3. ECAE processing

This section describes the various parameters like punch speed and extrusion temperature selected for ECAE processing. The rationale for selecting routes for the two projects will be given. The reasons behind selecting particular temperatures for intermediate heat treatments will also be discussed.

3.3.1. ECAE processing for scale-up project. Each of the billet size group was processed in the same fashion, according to Table 5. Prior to extrusion, the extrusion tool components and the billets were lubricated by anti-seize lubricant to reduce the friction during extrusion.

Table 5. Conditions of ECAE extrusion

Lubricant	Anti-seize lubricant (Pergamex Co.)
Punch Speed (V)	2.5 mm/sec (0.1 inch/sec)
Approximate Strain Rate	1.16 sec ⁻¹
Extrusion Temperature	Room temperature (23 ±2°C)

The tooling used to process the billets consisted of three different custom designed sliding wall ECAE dies in use at TAMU. One such tooling configuration is shown in Fig. 11. All die systems incorporate square channels. The design of the 19 mm square die is different from the other two in that it does not require any billet reshaping, therefore the billet length does not degrade with successive passes, and the work applied by the simple shearing action of the process remains more accurately represented in successive passes. This is accomplished by having the inlet channel slightly larger (approximately 1%, in this case) than the exit channel. All three tools are made from H13 tool steel. All ECAE processing was completed at room temperature. The tooling and billets were lubricated with a common anti-seize lubricant.

The press used for the extrusions consisted of a 2446 kN load frame controlled with a MTS TestStar© control system. The control system also records load and displacement in real time. The press is equipped with a 2446 kN load cell. Punch speed was set at 2.5 mm/s.

The test matrix for this study is shown in Table. 6. The billet size indicates the size of side in the square cross-section of the billet. The columns containing pass number and routes indicate the ECAE processing carried out on the billet. For example, billet 2 was processed through route E for eight passes. The testing and characterization columns list the various techniques used to characterize the material. Tick marks (✓) under a sub-heading indicate the use of that particular characterization technique.

Table 6. Test matrix for verification of scale-up effects in ECAE of as-cast OFHC Cu 101.

Billet ID	Billet Size (mm)	Pass No, Route								Testing and Characterization		
		1	2	3	4	5	6	7	8	Vickers Microhardness	Optical Microscopy (OM)	TEM
1A	50	0								✓	✓	
1B	50	A								✓		
3	50	A	C							✓	✓	
5	50	A	B	B	B					✓	✓	
4	50	A	E	E	E					✓	✓	
7	50	A	E	E	E					✓	✓	✓
6	50	A	A	A	A					✓	✓	
2	50	A	E	E	E	E	E	E	E	✓	✓	✓
8A	25	0								.	.	
8	25	A								✓	✓	
18	25	A	C							✓	✓	
12	25	A	B	B	B					✓	✓	
13	25	A	E	E	E					✓	✓	✓
8B	25	A	E	E	E					✓	✓	
9	25	A	A	A	A					✓	✓	
10	25	A	E	E	E	E	E	E	E	✓	✓	✓
14A	19	0								.	.	
14B	19	A								✓	✓	
16A	19	A	C							✓	✓	
16B	19	A	E	E	E					✓	✓	
17	19	A	E	E	E					✓	✓	✓
15B	19	A	A	A	A					.	.	
11	19	B	B	B	B					.	.	
19	19	A	E	E	E	E	E	E	E	✓	✓	✓

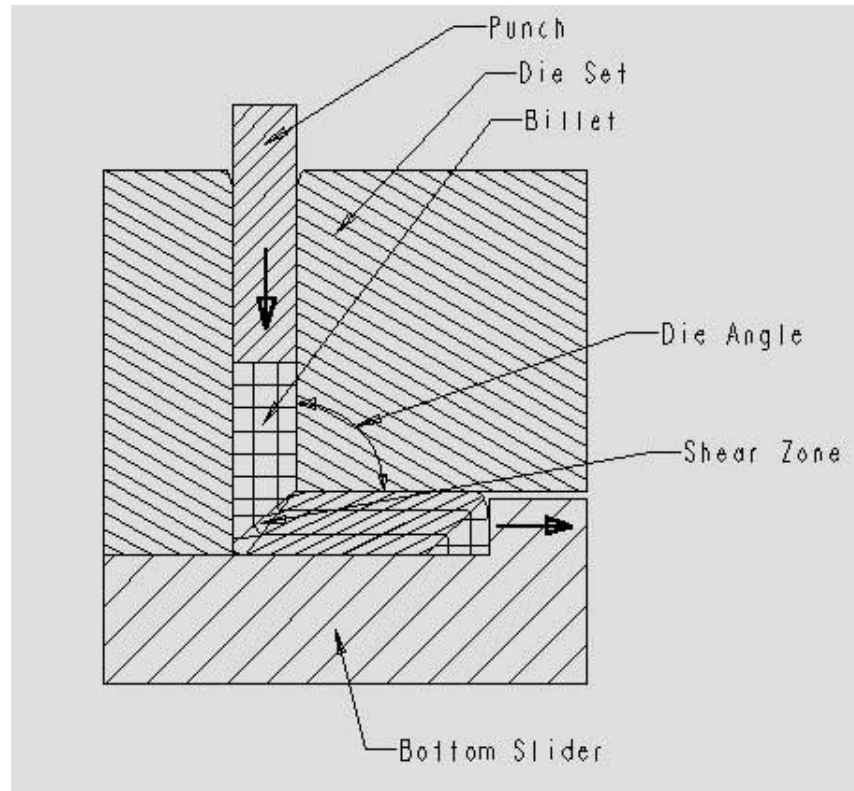


Fig. 11. Tooling arrangement for ECAE.

The extrusions led to generation of some flash along the edges of the billets. The billets also had minor bowing along the flow plane. The nominal dimensions of the billets after extrusion were 25.6 mm x 24.1 mm. This required that the billets be first rolled in a two roll rolling mill. The rolling flattened the billets into proper dimensions in one of the sides. But to remove the bow along the length of the billet and to remove the flash, billets were machined on a vertical milling machine. The rolling and milling operations have little effect on the induced strain in the material.

3.3.2. Selection of ECAE routes for microstructural breakdown project. To study the effectiveness of different routes in breaking down the as-cast microstructure in OFHC CDA 101 Cu, routes E, C, F and Bc were selected. The conventional routes such as A and B show heavy texture in the processed material. These routes suffer from the disadvantages of low process yield (lower volume of fully worked material compared to

the billet volume) [36] and complicated geometry of the worked and un-worked regions, etc. Routes C, E, Bc and F show maximum product yield and seem to have potential for industrial application.

Previous work on ECAE of Cu guided the selection of the number of ECAE passes to be employed. Ferrasse et al [21] showed that for wrought and annealed pure Cu, the sub-grain size stabilizes after four passes through route C and the sub-grains become equiaxed developing high angle misorientations as the number of passes increases from four to eight. Dalla Torre et al [23] also showed that the cell size decreases until four passes via route Bc, reaches a value of 200 nm and does not substantially change thereafter. Due to these reasons the billets were processed up to eight passes.

Kalidindi et al [37] carried out compression deformation of pure (99.9%) Al and determined the effect of initial orientations of grains upon the final orientation and breaking up upon deformation. A cast sample having columnar grains with a grain diameter of 0.75 mm was compressed to a total reduction of 40% in four stages. Different grains, depending upon their different starting orientations, developed different final orientations. Some grains preserved their orientations and did not break-up while some grains broke up easily and developed large misorientations. Sandim et al [38] have proved that in the case of tantalum, the amount of deformation undergone by a grain depends upon whether it has a favorable slip system or not. Although Sandim's research focused on tantalum, a BCC refractory metal, the conclusion holds true for FCC metals as well. Grains having favorable orientations with respect to the shear plane in ECAE will deform to a greater extent and will contain a higher dislocation density leading to a greater degree of work hardening compared to other grains. But as the number of passes increases and as the billets are rotated between passes, the slip systems activated by these extrusions start interacting and lead to the breakdown and homogenization of the microstructure. It is contended that by incorporation of heat treatments between extrusions, the homogeneity of the microstructure could be increased. Intermediate heat treatments (IHTs) lead to recrystallization of the as-worked microstructure and possible grain growth, giving a relatively uniform microstructure compared to the as-cast condition. This "better" starting microstructure can lead to a greater degree of subsequent

refinement (by further ECAE processing) and homogeneity in the fully recrystallized condition.

For the heat treatments between extrusion passes, the billets were first reshaped by the same procedure as mentioned before. In order to monitor the exact temperature obtained in the interior of the billets, a hole having a diameter of 3.5 mm and depth of 20 mm was drilled on the trailing end of the billet. As shown in Fig. 12, the thermocouple tube was inserted into this hole to measure the temperature inside the billet. CDA 101 copper has a very high thermal conductivity, so it is not expected that significant temperature gradients will exist within the billet. The billets were then cleaned by using Alconox®, an industrial grade detergent and acetone. To remove any surface oxide film that might have formed; the billets were etched using a pickling solution of nitric acid (70%): distilled water in a ration of 3:7.

Annealing at different temperatures was done in a Thermcraft radiation tube vacuum furnace under a minimum vacuum of 5×10^{-6} torr. The radiation tube has an inner diameter of 56 mm (2.25”) and a length of 500 mm (20”). The billet was placed in the central region of the furnace insuring that there was little temperature fluctuation along the length of the billet. Any temperature fluctuation, if present, would have been negligible due to the high thermal conductivity of copper. The temperatures used for annealing were different for different inter-pass heat treatments; the test matrix for this study is given in Table 7. The temperature profiles for typical intermediate heat treatments are given in Fig. 13.

Table 7. Test matrix for microstructural breakdown study (Billet size: 25 mm x 25 mm x 175 mm).

#	BILLET ID	EXTRUSION AND ANNEALING SCHEDULE (1)									ANALYSIS AND CHARACTERIZATION(2)		
											VHN	OM	RECRYSTALLIZATION HEAT TREATMENT
1	113	2E	HTR	A1	2E	A2	2E	HTR			✓	✓	✓
2	114	2E	A1	2E	HTR	A2	2E	A3	2E	HTR	✓	✓	✓
3	115	2E	A	2E	HTR	2E	A	2E	HTR		✓	✓	✓
4	116	2C	HTR	A1	2C	A2	2C	HTR			✓	✓	✓
5	121	2C	A1	2C	HTR	A2	2C	A3	2C	HTR	✓	✓	✓
6	118	4C	HTR	4C	HTR						✓	✓	✓
7	111	2F	A1	2F	HTR	A2	2F	A3	2F	HTR	✓	✓	✓
8	112	4F	HTR	4F	HTR						✓	✓	✓
9	119	2Bc	A1	2Bc	HTR	A2	2Bc	A3	2Bc	HTR	✓	✓	✓
10	120	4Bc	HTR	4Bc	HTR						✓	✓	✓

(1) A1 = 400°C, A2 = 300°C, A3 = 200°C and A = 350°C. The intermediate heat treatments were carried out at these temperatures.

(2) VHN and OM refer to Vickers microhardness and optical metallography.

The furnace and billet temperatures were measured by a K-type thermocouple and a hand held thermocouple reader.

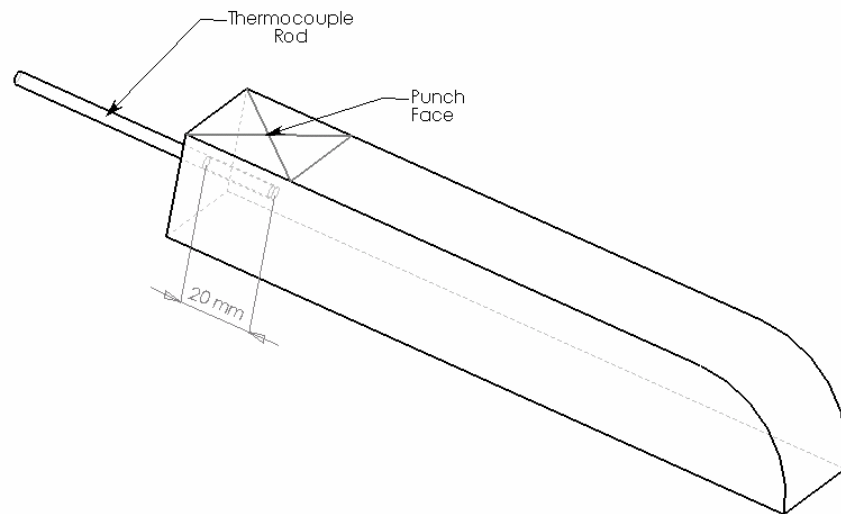


Fig. 12. Hole of 3.5 mm diameter drilled in the trailing end of a 25 mm x 25 mm cross-section billet to monitor temperature during intermediate heat treatments.

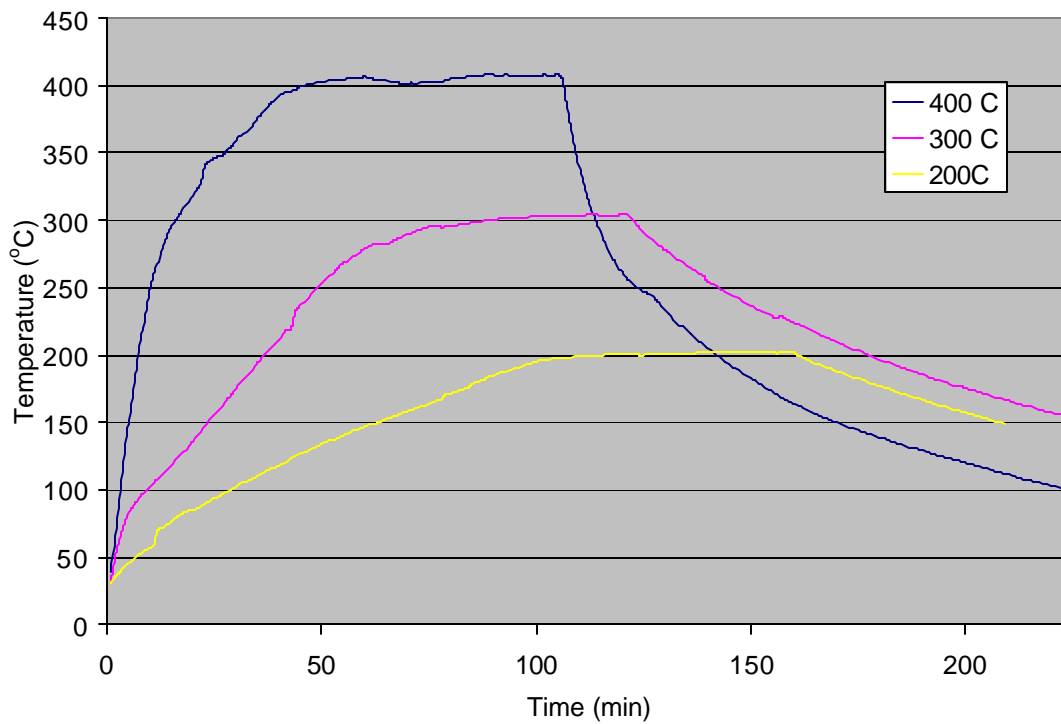


Fig. 13. Typical temperature profiles for intermediate heat treatments done on billets for microstructural breakdown study.

3.4. Brinell hardness measurement

For the scale-up project, all billets were subjected to a Brinell hardness test between two successive pass. These Brinell test were taken directly on the flow plane (Y plane, see Fig. 14) side of the billet, approximately at the center of the billet. Four measurements were taken and the average determined. The surface of the billet was cleaned, first with WD-40® and then with acetone, and since it was smooth as ejected from the die, it was not specially prepared for the Brinell test. The applied load for Brinell hardness was 1000 kgf for a duration of 10 seconds.

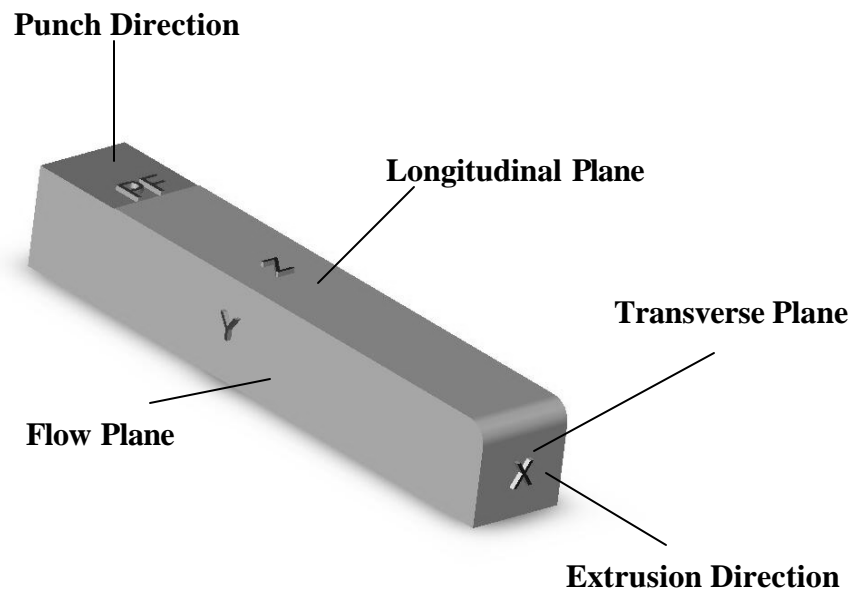


Fig. 14. Plane identification nomenclature. PF = Punch Face, X = Transverse plane, Y = Flow plane, Z = Longitudinal plane.

3.5. Heat treatments

Isochronal heat treatments were done in order to determine the recrystallization temperature of the as-worked material. These heat treatments also gave an indication about the thermal stability of the microstructure. For the scale-up project, all heat treatments were done in a sand bath. Two “dummy” specimens were made to record the temperature reached during the heat treatments. As shown in Fig. 15 the dummy specimens were drilled with small holes. The thermocouples were inserted into the specimens and tightened so that the thermocouple junction was in intimate contact with

the internal region of the specimens. Heat treatment temperatures were selected as 50°C, 100°C, 125°C, 140°C, 150°C, 160°C, 170°C, 180°C, 200°C, 250°C and 300°C. Heat treatments at two other temperatures 175°C and 190°C were performed at a later stage of research to obtain more continuity between measurements showing the largest change in hardness values.

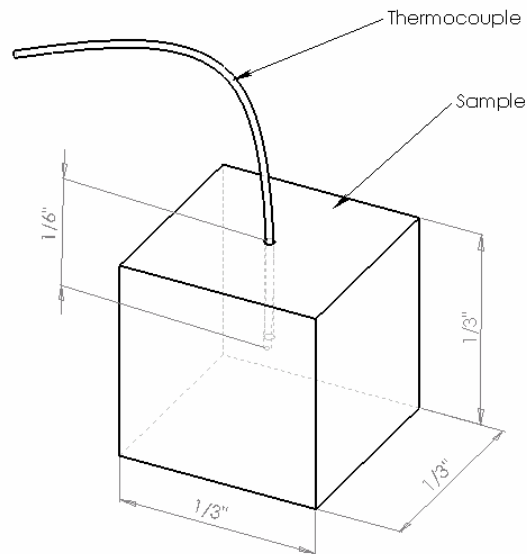


Fig. 15. Dummy sample prepared to monitor temperature in the sand bath during heat treatments.

The specimens for heat treatment were first cleaned with Alconox®, an industrial strength detergent and then washed in acetone to remove any dirt or grease sticking to the surface. This helped in decreasing any damage to the specimens through diffusion of contaminants. Copper does not show any drastic diffusion of oxygen, carbon or other elements; hence for heat treatments up to 300°C, air was used to agitate the sand in the sand bath. The temperature profiles for these heat treatments are shown in the Fig. 16. After the heat treatment the samples were immediately quenched in water. The samples were then split in the middle along the flow plane. The surface thus exposed was used for hardness measurements and optical microscopy.

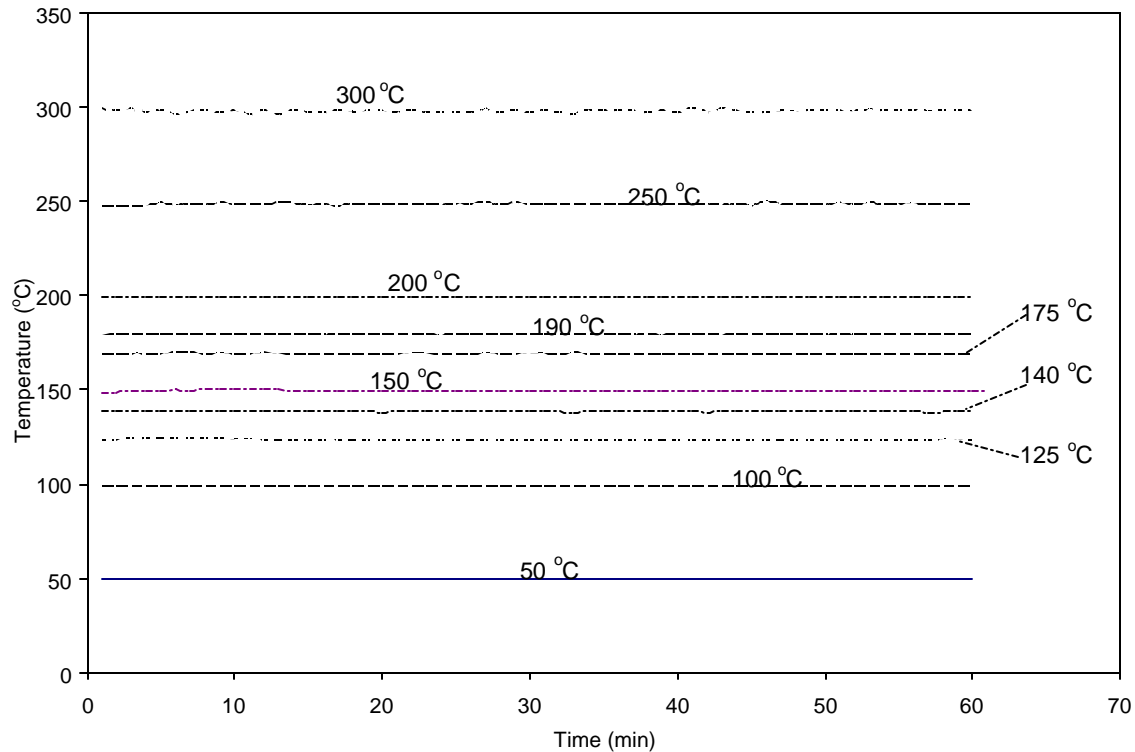


Fig. 16. Sand bath temperature plots showing the temperature variation for recrystallization heat treatments carried out for the scale-up study.

For the microstructural breakdown project, recrystallization heat treatments were done under vacuum of 5×10^{-6} torr. These heat treatments were done at 100°C, 125°C, 150°C, 175°C, 200°C, 250°C and 300°C. These heat treatments were done for a time period of 60 minutes. The specimens were allowed to cool down to room temperature in vacuum. Temperature profiles for these heat treatments are shown in Fig .17. The specimens were then split open as mentioned above and the exposed flow plane surface was used for analysis.

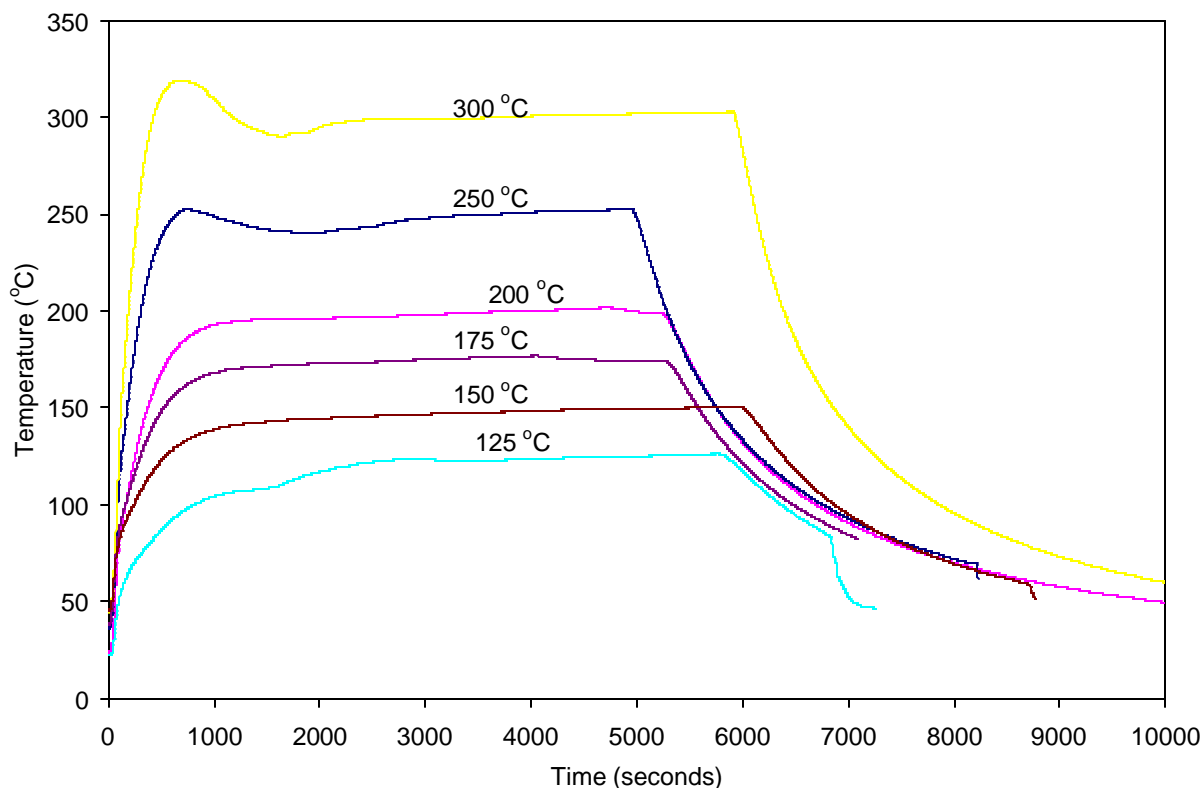


Fig. 17. Temperature plots showing the temperature history for recrystallization heat treatments carried out in vacuum for the microstructural refinement study.

3.6. Metallographic sample preparation

For the study of scale-up effects and microstructural breakdown of as-cast Cu by ECAE, it was necessary to do micro-hardness measurements along the flow, transverse and longitudinal planes of the billets. To carry out the micro-hardness measurements, the samples were prepared using the following steps: sectioning, mounting and polishing.

3.6.1. Sectioning. Copper is ductile and easy to cut with a diamond saw. The cutting of specimens from the billet was done carefully. It is important that the cuts made into the billets be straight, proper orientation of the samples is maintained and there be no effect due to cutting on the microstructure of the samples. For this purpose the billets were cut using a Buehler Isomet 1000 diamond saw, the lubricant used during cutting was Buehler Isocut Plus; a water based cutting fluid. It was not possible to cut the 50 mm (2") square

billets using the diamond saw. For these large billets, the band saw was used to cut the billets. Precaution was taken to avoid heating of the samples and a constant flow of cutting fluid was maintained over the saw and the sample to reduce heating. After cutting on the band saw, the sections obtained were ground to remove any deformities generated during cutting. Depending upon the size of the section, each sectioned slab was cut to give a different number of samples. In the case of the 19 mm square billets, four square samples were obtained from each slab. For the 25 mm square billets, nine samples were obtained from each slab while in the case of the 50 mm billets, 25 samples were obtained from each slab.

Due to the design of the extrusion die, the bottom region of the billet does not undergo the same amount of shear as the rest of the section. This region is approximately 0.10 to 0.20 times the channel width from the bottom surface of the billet [18]. For this reason, 3 mm material was removed and discarded from both the top and bottom surfaces of the 25 mm square billet. The material was not removed from the sides of the billets, just because all the measurements were taken away from this region.

3.6.2. Engraving. The samples after being cut from the billets were engraved using an electric engraver. Look at Fig 18. for details. Each sample was engraved with its identification number on its flow plane. The topmost number is the billet number from which the sample was extracted. The bottom number shows the sample number.

3.6.3. Mounting. After extracting the samples from the billets, the samples were mounted in epoxy. Mounting in bakelite was avoided because during curing, temperatures as high as 250°C are reached. Initially the samples were mounted in regular epoxy, which took approximately five hours to cure. Later, some of the samples were mounted in a fast cure epoxy, which takes approximately one hour to cure. The temperature profiles for the two epoxies are given in Figs. 19 and 20. During mounting in the fast cure epoxy, the maximum temperature reached is around 193°C for ~ 1 minute. This high temperature may lead to changes in the microstructure of the samples. As a result, samples were mounted in both fast cure and slow cure epoxy and the

recrystallization curves obtained. Fig. 21 indicates that no change is observed in the recrystallization curves obtained for samples mounted in these two different epoxies.

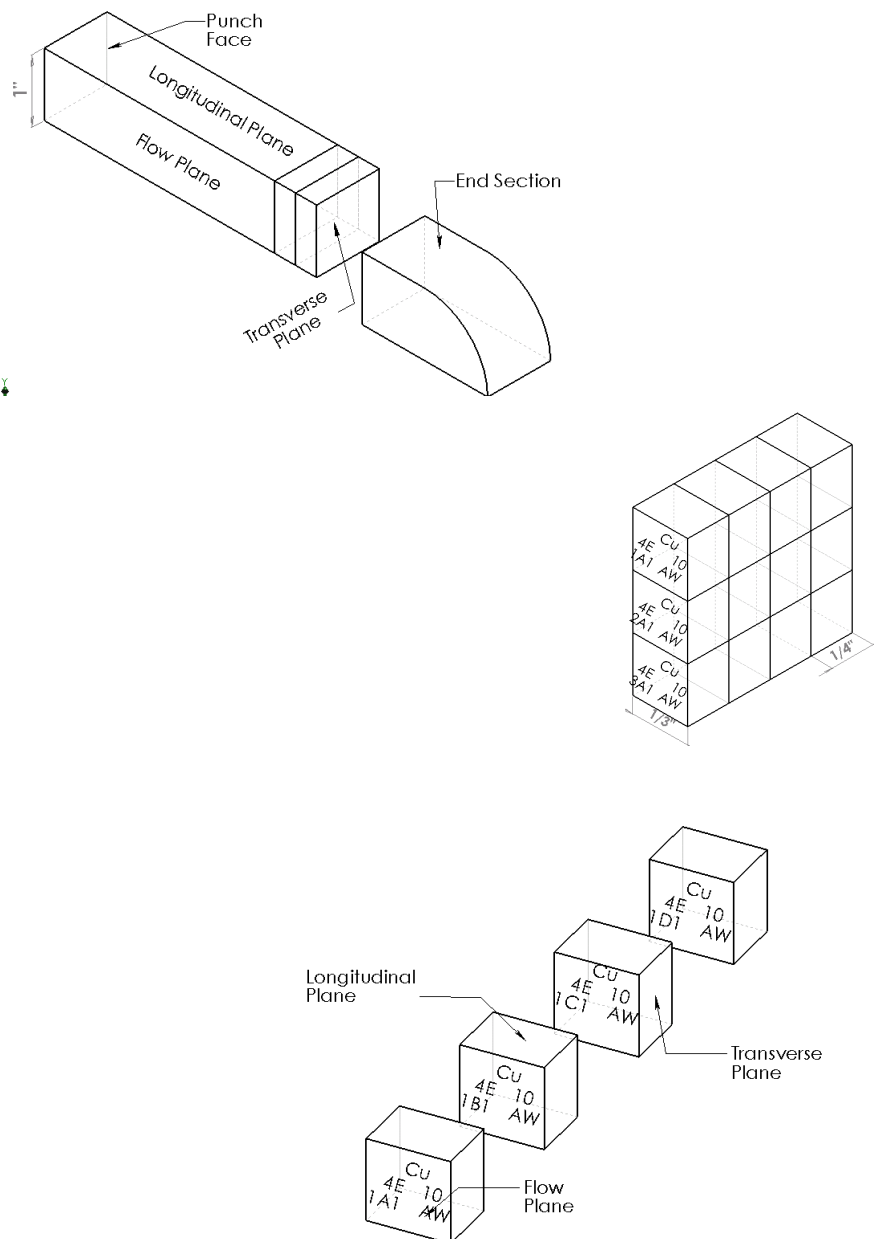


Fig. 18. The cutting and engraving technique used for sample labeling.

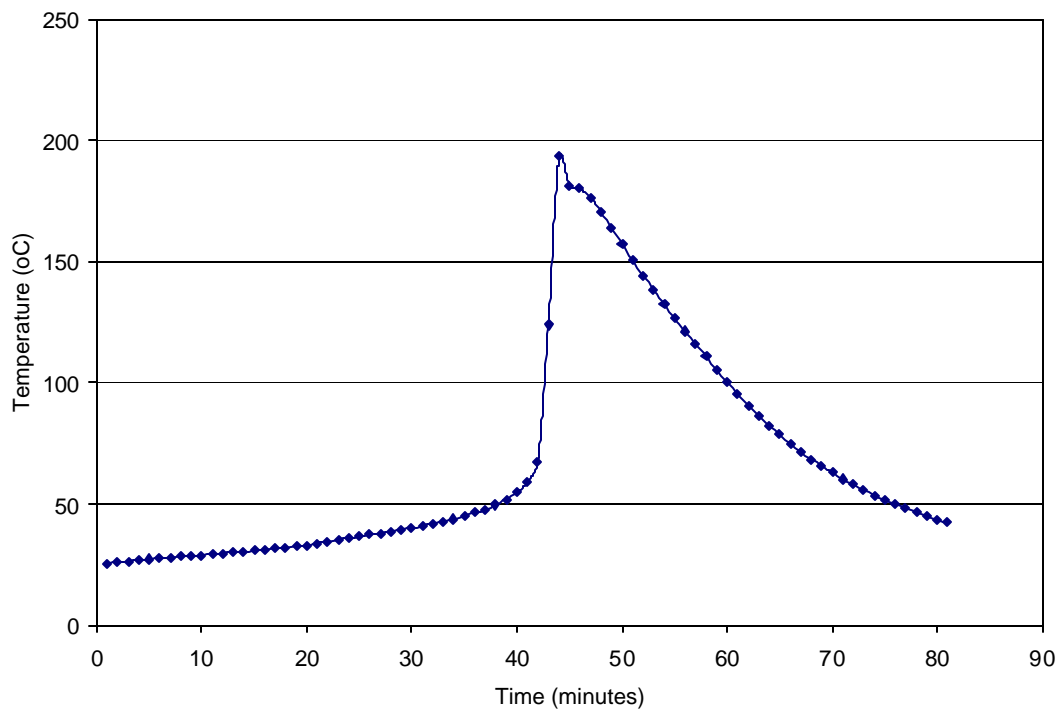


Fig. 19. Temperature profile for fast cure epoxy used for mounting samples.

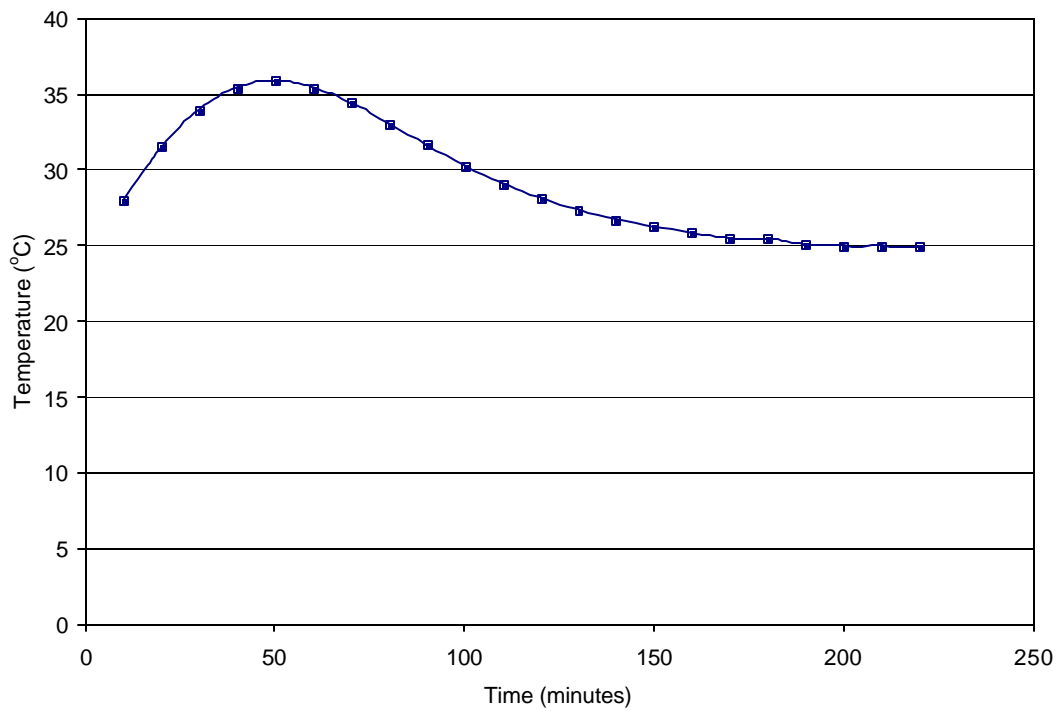


Fig. 20. Temperature profile for slow cure epoxy used for mounting samples.

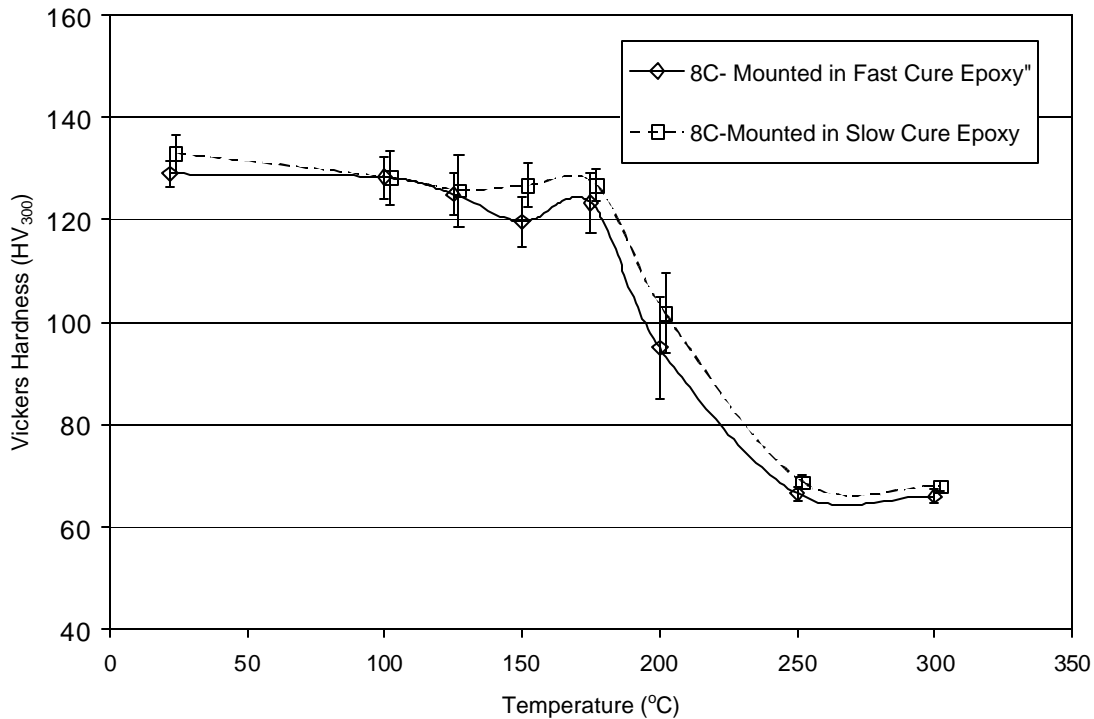


Fig. 21. Change in hardness with recrystallization temperature for CDA 101 Cu processed up to eight passes via route F without intermediate annealings. Two different epoxies were used for mounting the two sets of specimens.

3.6.4. Grinding. Grinding of the samples proved to be the first major challenge in this research. The grinding was initially done manually using abrasive paper followed by fine grinding using diamond paste. Copper proved to be extremely soft and ductile and hard to prepare by this conventional technique. By this technique one sample would take approximately one hour to prepare. A technique was devised using Buehler Automet II automatic polishing machine. Six samples could be polished simultaneously using this machine. Table 8 shows the steps used in polishing the copper samples. The time required for polishing was now reduced from one hour per sample to around 10 minutes per sample. The surface obtained was free of any scratches and pits.

Table 8. Successful grinding and polishing procedure for metallographic preparation of Cu samples.

Surface	Abrasive Size	Load (Lb./Specimen)	Base Speed (rpm)	Direction	Time (min:sec)
SiC Waterproof paper	P 320 grit	5-6	220	Complementary	Until Plane
SiC Waterproof paper	P 600 grit	5-6	220	Complementary	10:00
SiC Waterproof paper	P 800 grit	5-6	220	Complementary	10:00
Pellon Cloth	3 um diamond suspension	4-5	150	Complementary	5:00
Billiard Cloth	~0.05 um colloidal silica	4-5	150	Reverse	5:00-10:00

Cleanliness is very important during polishing. The whole platen along with the six specimens was repeatedly washed under running water after each polishing step. Cross contamination is a big problem while polishing with an automatic polishing machine. The samples once attached in the platen are not removed until the final polishing step is over. This is necessary to maintain the alignment of the specimens in the mounting platen. But because of the shape of the platen, diamond grinding particles can easily get lodged in the crevices between the specimens and the platen, leading to cross-contamination which will ruin the specimens as well as the polishing cloth. After grinding with the diamond suspension, the platen was immersed in an ultra-sonic water bath and cleaned for ~ 2 minutes. This effectively cleaned any diamond particles lodged in the platen.

3.6.5. Etching. The large columnar grains of the as-cast macrostructure can be observed by carrying out a macro-etch on the surface. For macro-etching, the surface finish is not very critical. A machined surface or one coarsely ground to a grit size of 600 is enough to give a good macro-etch. A solution of nitric acid (70%):distilled water in a ratio of 1:1 was used to obtain the macro-etch.

After etching the samples were washed under distilled water and wiped using paper towels. It was found that rinsing with methanol and then blow drying the sample

lead to formation of water marks due to the large size of the samples, hence the samples were just wiped with paper towels which gave a good finish free of any stains.

For examination of micron-scale recrystallized microstructure using optical microscopy, the samples were etched using a micro etching solution of 10 ml H₂O, 1 gm FeCl₃ and 0.5 ml HCl. Etching was done by immersion of the sample in the solution for 1 – seconds. A satisfactory micro-etching solution proved very difficult to find, and after trying numerous etching solutions, the above mentioned solution was found to be the most suitable.

After etching, the samples were quickly rinsed in distilled water and then rinsed again with methanol/acetone and dried in hot air. It is very important to rinse the sample with methanol or acetone and then blow dry them, otherwise water spots will form on the specimens, leading to unwanted etching artifacts.

The optical micrographs were obtained by using a Leica M4FM stereo wide field metallograph equipped with a Leica DC200 digital camera and a polarized light filter.

3.6.6. Image analysis. Images were stored in a .TIFF and .JPEG format and Image Processing Tool Kit (IPTK) plug-in for Adobe Photoshop was used to do the image analysis. These images were first printed in gray scale. The following steps were taken to prepare the acquired image for data acquisition and analysis.

1. Print the image on an A4 (8.5" x 11") size sheet.
2. Mark the grain boundaries of the microstructure on a tracing paper.
3. Scan the image containing only the grain boundaries.
4. Threshold the image using the automatic threshold option.
5. Skeletonize the image. This converts the grain boundaries from random thicknesses to a thickness of one pixel.
6. Increase the thickness of the grain boundaries to two pixels.
7. Invert the image. Initially the grain boundaries are black in a white background. But IPTK software is not able to recognize the grains if they are white and the grain boundaries are black. The image conversion makes the grains black and the grain boundaries white.

8. Next, calibrate the magnification using a standard scale bar. This determines the size of a pixel in the given image.
9. Run the IPTK software to measure the various dimensions of the grains.

Data was obtained regarding the average grain size, the distribution and uniformity of the grains.

3.7. Micro-hardness measurement

Hardness is a general term having different meanings for different people. It is resistance to penetration to a metallurgist, resistance to wear to a lubrication engineer, a measure of flow stress to a design engineer, resistance to scratching to a mineralogist and resistance to cutting to a machinist. The Vickers microhardness provided a means of evaluating the level of plastic strain induced in the material and was also used in finding out the recrystallization temperature of the material. The Vickers microhardness test uses a square based diamond indenter with an angle of 136° between opposite faces.

For the scale-up project, micro-hardness measurements were taken in order to determine the homogeneity of the as-worked microstructure obtained for different billet sizes. Microhardness measurements were taken using a Buehler Micromet II digital microhardness tester using a load of 0.3 kgf applied for 13 seconds. These microhardness measurements were taken in the form of line scans, starting from one end of the billet to another. For the flow plane, thin slices of ~3 mm were removed from the top and bottom surfaces of the billets, and then a line scan was taken from the top of the remaining billet section to the bottom. This ensured that all the measurements were taken in material which was free from any “end effects”. For the transverse plane, the line scan was taken from the left edge of the billet section to the right edge, and for the longitudinal plane, the line scan was taken for 25 mm (1”) in the fully worked region. In case of the longitudinal plane, a thin strip of ~ 3 mm (1/8”) was first removed from the top surface; this ensured that all the measurements were taken in material which was free from any “end effects”. On an average, 10 microhardness measurements were taken per sample, giving a total of 20 measurements for 19 mm sample, 30 for 25 mm and 50 for 50 mm samples. The sample positions with respect to the billet are shown in Fig. 22. It is necessary to maintain

a minimum distance of three times the indentation diagonal between two indentations, and between an indentation and the edge of the specimen so as to avoid overlapping of the deformation zones of these indentations and get accurate readings.

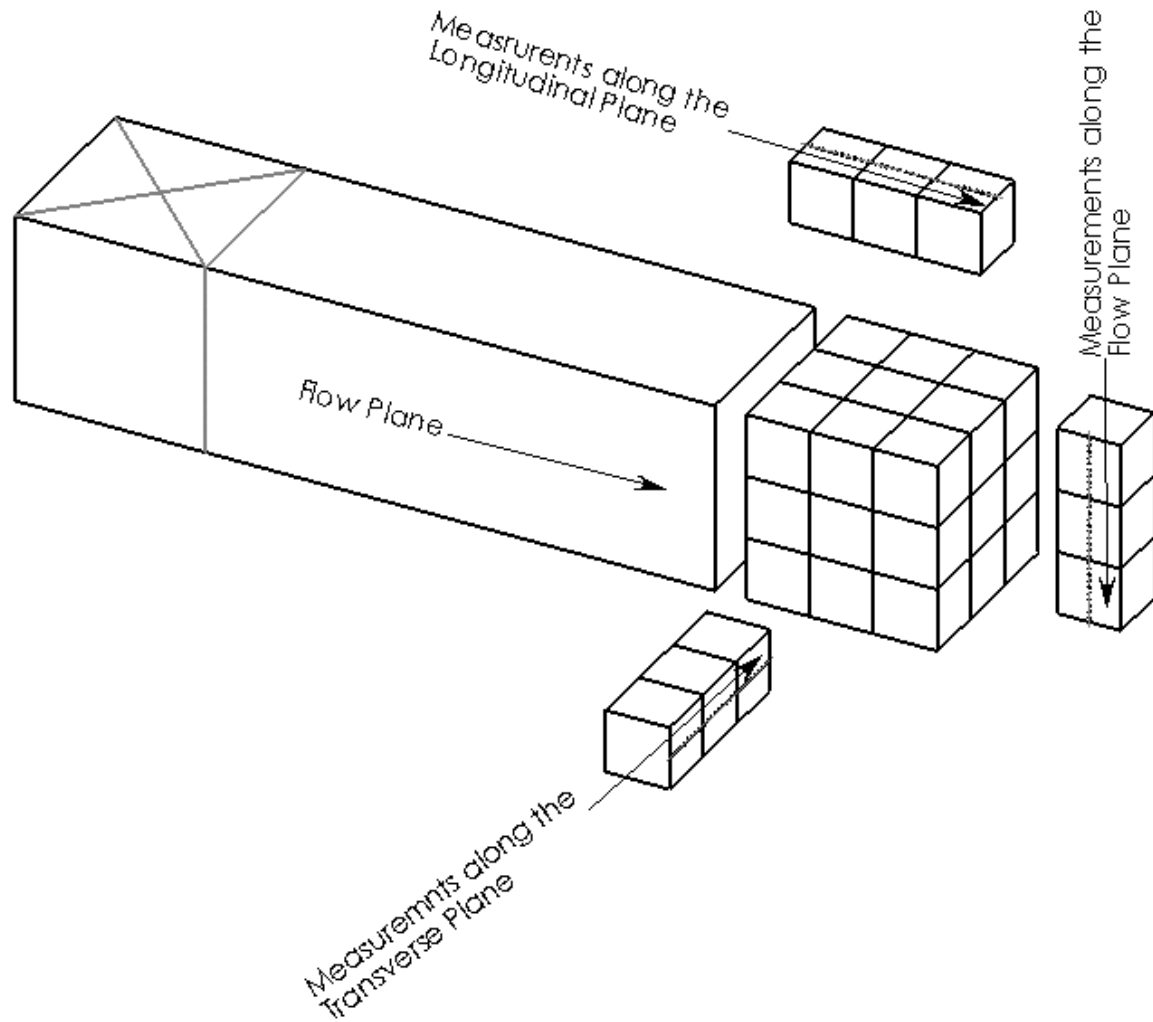


Fig. 22. The location of microhardness measurements on the flow, transverse and longitudinal plane of the samples for “line scans”.

3.8. Transmission electron microscopy

Transmission electron microscopy was carried on different specimens to study the as-worked and recrystallized microstructures. For transmission electron microscopy, slices of 1 mm thickness were cut from the flow plane. This cutting was done using a

Buehler Isomet 1000 diamond saw and “isocut fluid”, an oil based lubricant. These slices were ground and polished to a final thickness of 50-100 microns. To carry out this grinding and polishing, the thin slices of copper were mounted on an aluminum stub using a heat sensitive glue called crystal bond. It was noted that the temperature required to melt this bond was around 80°C, which is well below the onset of recrystallization or even recovery as determined by microhardness measurements. Fixing of these slices using Loctite®, an instant adhesive glue did not prove feasible because of the long time need to remove the slices from the mounting stub. The examination of the samples thus polished did not show any sign of recovery or heat damage.

Discs of 3 mm diameter were punched out from these thin slices and electro-polished using a Struers Tenupol twin-jet electro polisher; the composition of the electrolyte solution is 250 ml phosphoric acid, 500 ml distilled water, 250 ml ethanol, 50 ml iso-propanol, 5 gm urea. Temperature was at 10° F (-12.22°c) with the voltage at 6 V.

The TEM was done using a JEOL JSM 2010 electron microscope, with a lanthanum hexaboride (LaB6) filament gun operating at an accelerating voltage of 200 KV. Bright field images and selected area diffraction patterns were obtained.

4. EXPERIMENTAL RESULTS

As mentioned earlier, this research project has been divided into two separate parts. The aim of the first one is the verification of scale-up effects of ECAE for square billets having a cross-section up to 50 mm x 50 mm in size. The aim of the second sub-project is to determine the best thermo-mechanical schedule (TMP) in breaking down the as-cast microstructure of CDA 101 OFHC Cu.

The independent and dependent variables involved in this research are shown in Table 9.

Table 9. Independent and dependent variables in this study.

Independent Variables	Dependent Variables
Billet Size	Punch Load
Level of strain	Brinell hardness and Vicker's microhardness
Strain rate	Recrystallization behavior
Thermomechanical processing	Recrystallized grain size
	Microstructural Uniformity

4.1. Billet extrusions

All billets were extruded completely without any problem, with one exception. Billet 5 (size 50 mm, extruded for extrusion route 4B) exhibited signs of shear localization on the last pass (Figs. 23-24). Note that the shape of the shear localized region is consistent with the shape of the material volume which has undergone plastic strain equivalent to 4B passes. The less worked material (3B, 2B, etc) did not shear localize. The shear localization is also visible in the Punch Load vs. Displacement curve shown in Fig. 25.

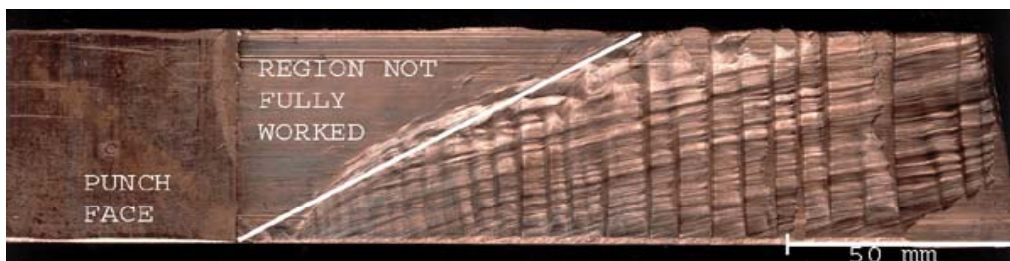


Fig. 23. Top plane of billet # 5 (50 mm square) processed through route 4B.

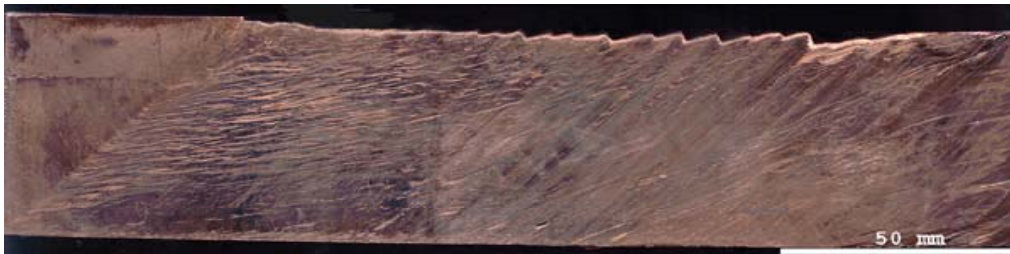


Fig. 24. Side plane of billet # 5 (50 mm square) processed through route 4B.

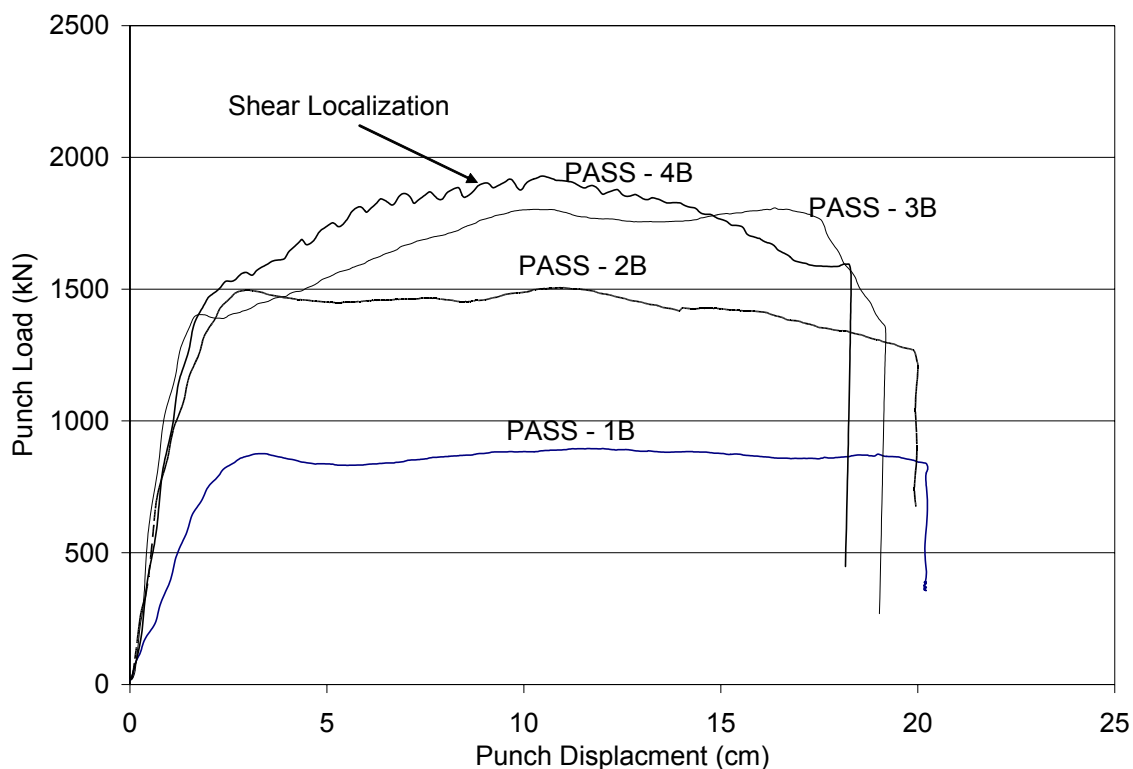


Fig. 25. Load vs. stroke curve for billet # 5, 50 mm square cross-section billet of as-cast CDA 101 Cu, processed through route 4B in 90° die at room temperature. Note the indication of shear localization in the load curve for the fourth pass.

4.2. Load curves

4.2.1. *Scale-up project.* One factor that affects the punch load is the billet's original location in the ingot (Fig. 9.). This can be clearly seen in the first pass load curves for all 25 mm and 50 mm square cross section billets (Figs. 26-27). The highest loads were obtained for billets having the direction of extrusion largely perpendicular to the long

axis of the general grain shape in the billet. Another load affecting factor can be the orientation to the previous extrusion. Fig. 28 and Table 10 gives the maximum load required for the extrusions of the 25 mm (1") square billets. In this case, also note that the maximum loads are required during the extrusions passes 3E, 5E and 7E. Fig. 29 shows the load curves for a 50 mm (2") square cross section billet extruded up to eight passes via route E, which requires the billet to be rotated 90° around the long axis at every odd pass. Table 11 shows that the three highest extrusion loads are required during these three odd passes.

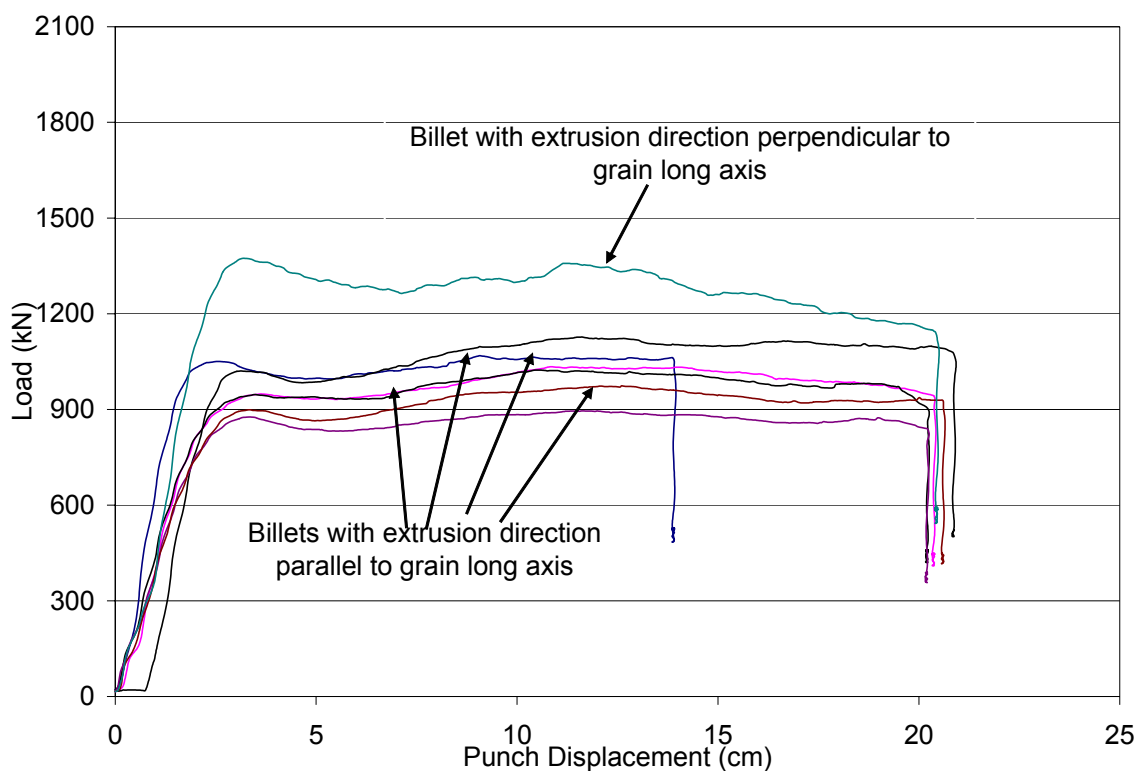


Fig. 26. Extrusion load curves for 50 mm square billets of as-cast CDA 101 Cu extruded through 90° die at room temperature. Note that the highest loads occur in the extrusions where the billets are extruded perpendicular to the long axis of the average grain.

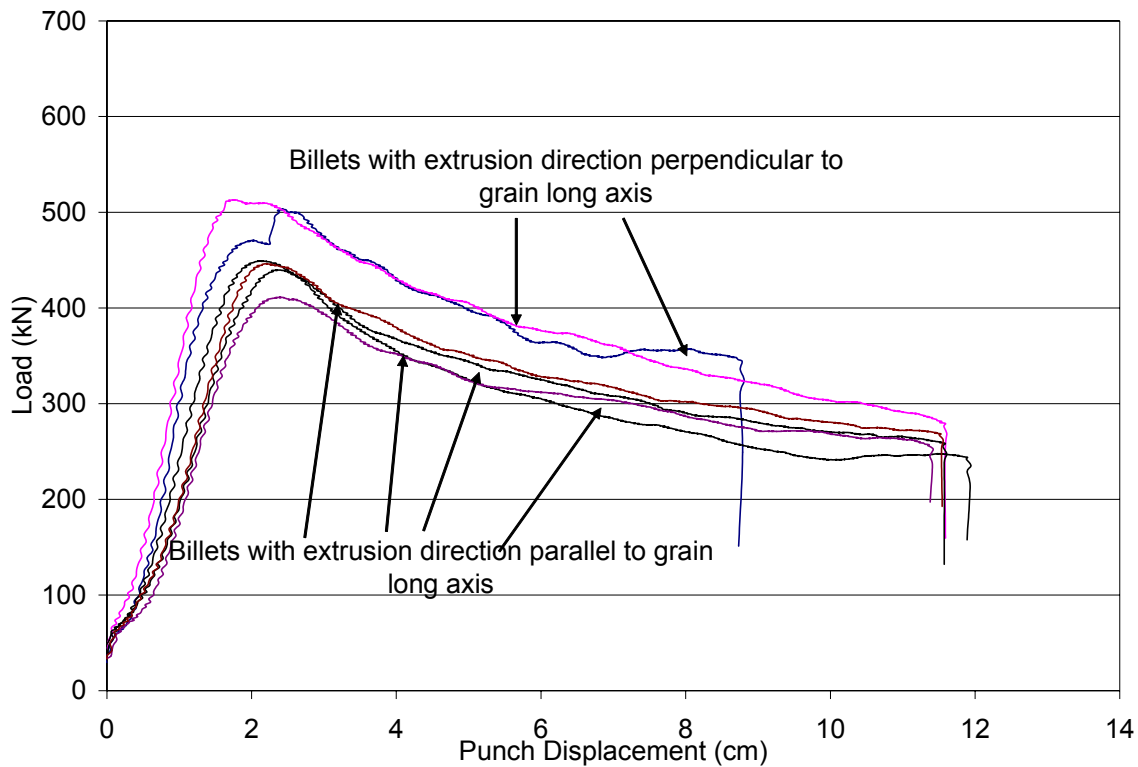


Fig. 27. Extrusion load curves for 25 mm square billets of as-cast CDA 101 Cu extruded through 90° die at room temperature. Note that the highest loads occur in the extrusions where the billets are extruded perpendicular to the long axis of the average grain.

Table 10. Maximum load required during extrusion of 25 mm square billets.

Route	Number of Passes							
	1	2	3	4	5	6	7	8
A	503.03							
A	512.84	465.8	527.4	476.6				
B	439.67	521.96	545.4	527.4				
C	446.1	466.94						
E	411.09	461.73	523.49	456.6				
E	449.09	465.41	538.59	464.88	545.02	471.08	574.29	453.91
Average	460.303	476.368	533.72	481.37	545.02	471.08	574.29	453.91
Std. Dev.	39.3975	25.5614	10.0786	31.7647				

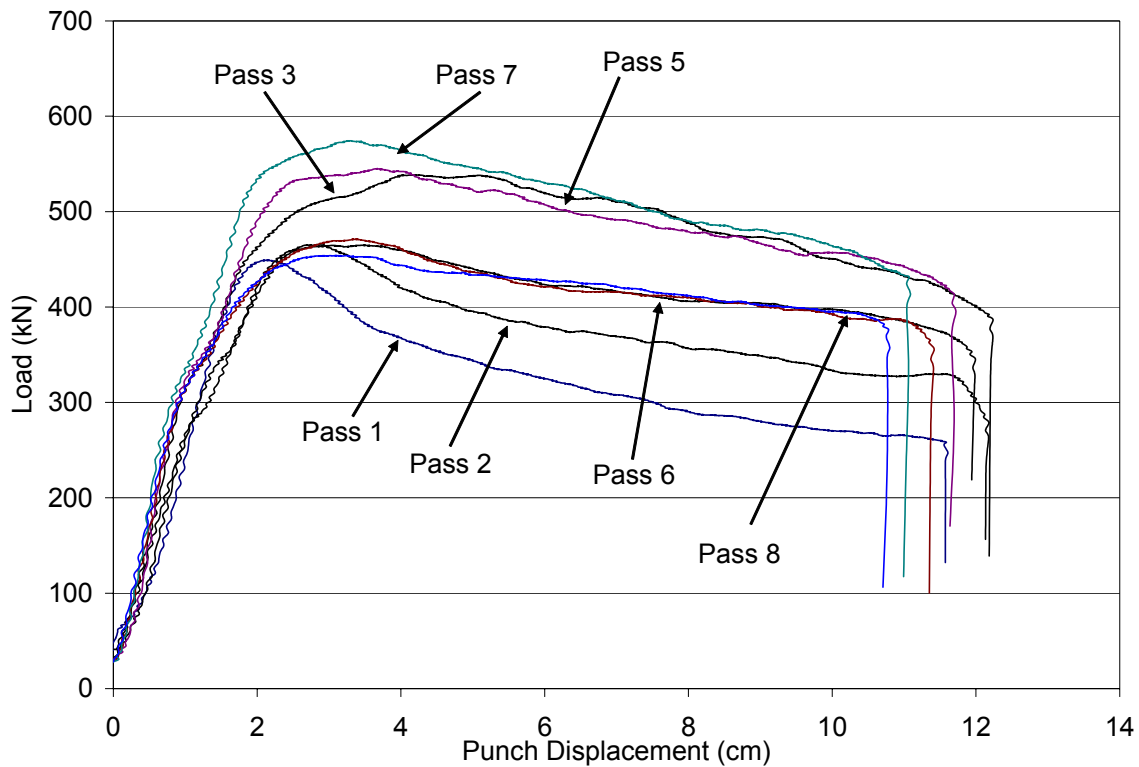


Fig. 28. Load vs. stroke curve for billet # 10, 25 mm square cross-section. Note that highest loads are achieved during passes 3, 5 and 7. These passes are perpendicular (90° rotated) to the previous extrusions.

Table 11. Maximum load required during extrusion of 50 mm (2") square billets.

Route	Number of Passes							
	1	2	3	4	5	6	7	8
A	973.6	1631.16	1465.89	1383.13				
B	895.12	1505.89	1808.55	1929.15				
E	1373.79	1545.65	1434.47	1363.21				
E	1033.73	1376.7	1991.37	1518	1630.2	1366.05	1743.11	1390.72
Average	1033.73	1376.7	1991.37	1518	1630.2	1366.05	1743.11	1390.72
Std. Dev.	210.932	105.897	270.498	262.998				

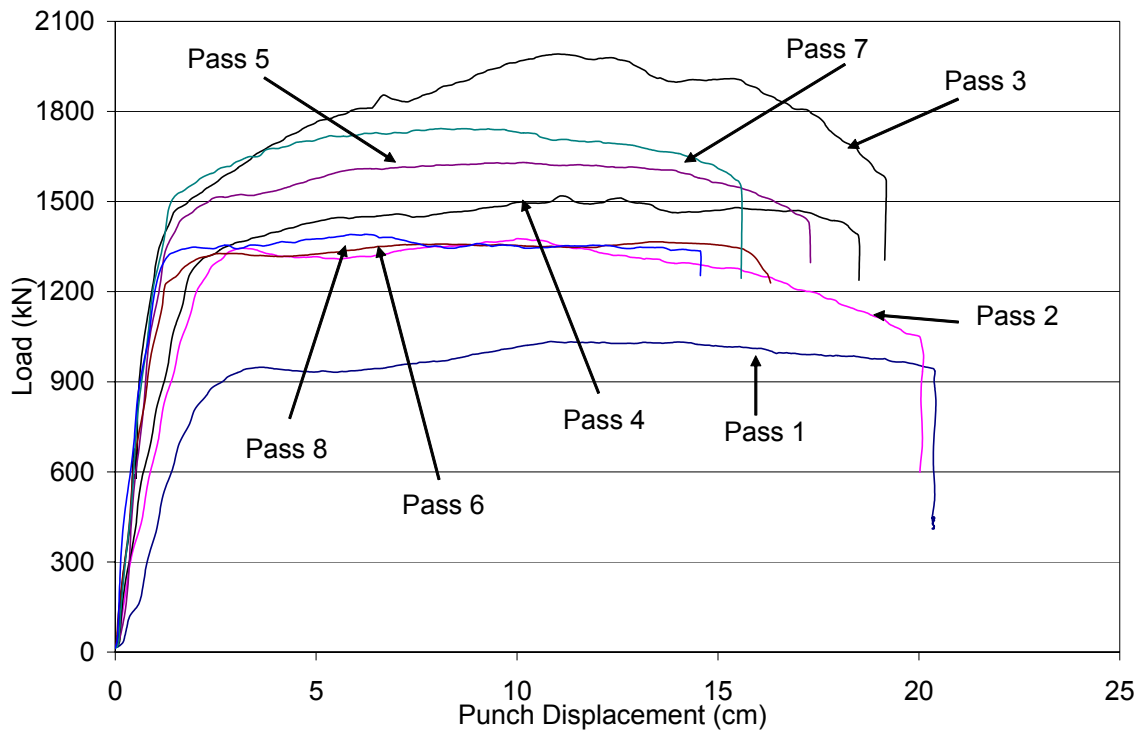


Fig. 29. Load vs. stroke curve for billet # 2, 50 mm square cross-section. Note that highest loads are achieved during passes 3, 5 and 7. These passes are perpendicular (90° rotated) to the previous extrusions.

The maximum load required during the extrusion for the 50 mm square billets is shown in Fig. 29. We note that the highest loads are achieved during the passes 3E, 5E and 7E. These passes are perpendicular to the previous extrusions. Table 11 lists the maximum loads required for each pass.

Note that the loads required for extruding the 50 mm square billets are less than three times the load required for extruding the 25 mm square billets. This indicates that various factors contribute to the load requirements during extrusion. The required load will depend not just upon the size of the billet (surface area to volume ratio) and the billet material, but it will also strongly depend upon the grain orientation and texture in the billet and on the tooling conditions. For a ductile and workable material like copper, larger billets give lower loads per cross-sectional area mainly due to the lower surface area to volume ratio, making large billet extrusion a more load efficient process compared to small billet extrusion.

4.2.2. *Microstructural breakdown project.* In case of load curves for the scale-up project, it may be contended that the initial grain orientation and texture along with the large as-cast grain size may have led to unpredictable behavior of the billets in terms of loads required for extrusions. The increase in extrusion load observed in odd numbered extrusion in case of route E may be attributed to this unpredictable behavior. But in the case of extrusions done for the microstructural breakdown project, the billets were annealed at high temperatures (400°C), leading to recrystallization and some grain growth. It is expected that the original grain structure and orientation is completely destroyed after four passes followed by this annealing. But Figs. 30-31 clearly show that higher loads are required during extrusions at 90° orientations to the previous ones even in grains having a fairly uniform and untextured starting structure.

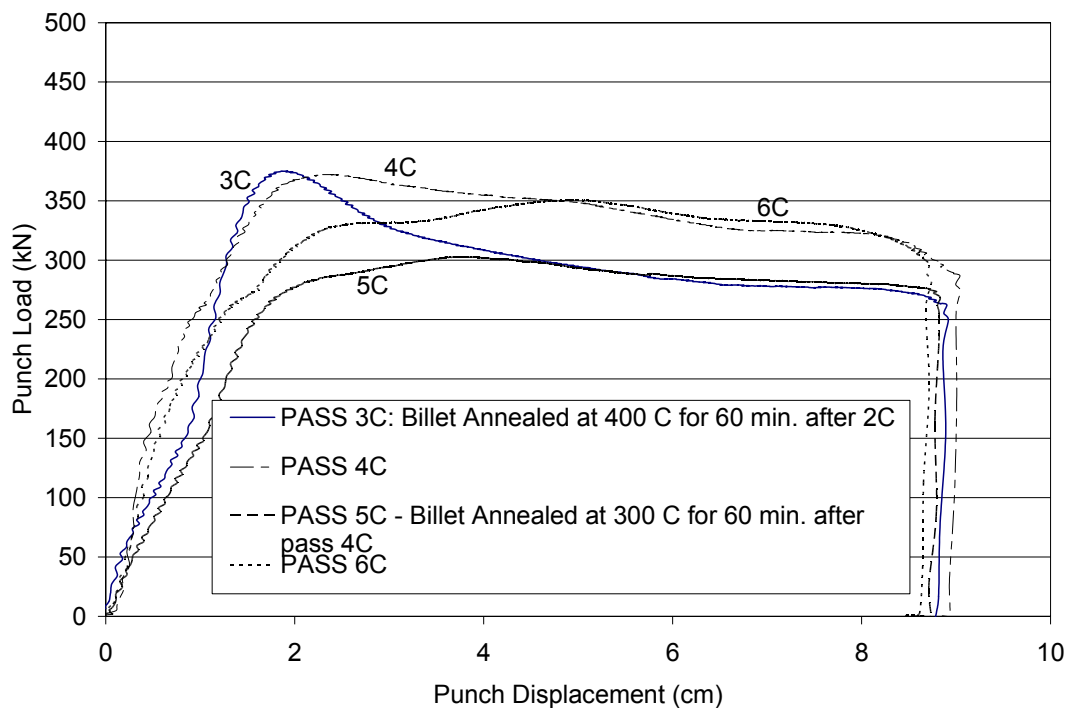


Fig. 30. Punch load vs. punch displacement diagram for extrusion passes 3 to 6 for a 25 mm square billet processed for extrusion route 6C.

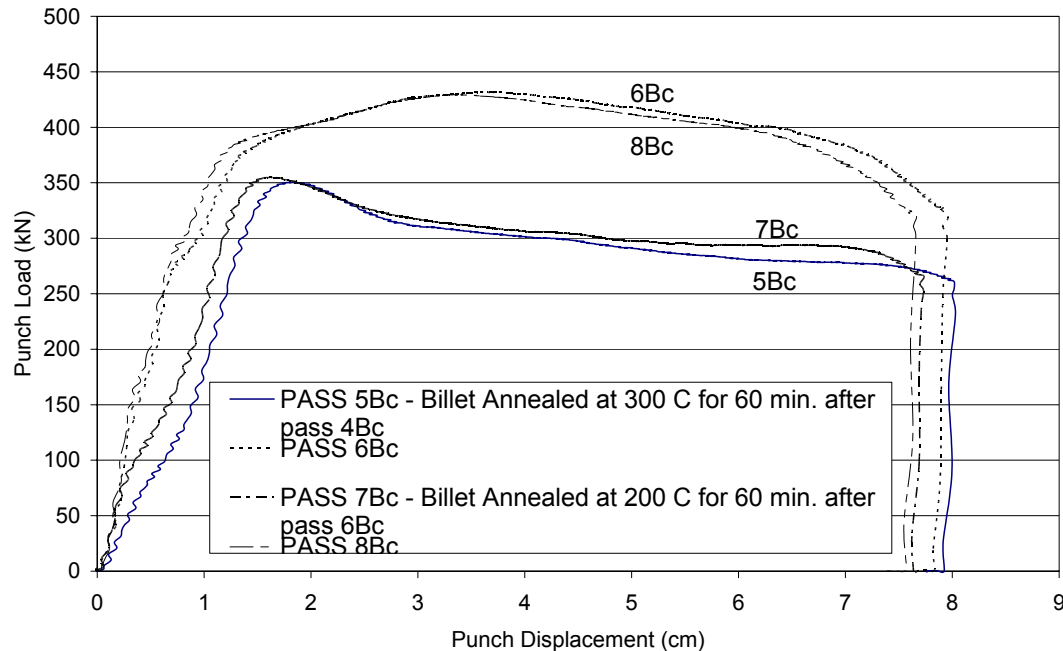


Fig. 31. Punch load vs. punch displacement diagram for passes 5 to 8 for a 25 mm square billet processed up to extrusion 8Bc.

4.3. Hardness

As mentioned previously, the hardness values provide a convenient way to measure the amount of strain hardening undergone by the worked material. Brinell hardness and Vicker's microhardness measurements were extensively taken to characterize the material.

4.3.1. Brinell hardness. Brinell hardness values were taken to determine the increase in the hardness of the material with increasing plastic shear strain. Measurements were taken on billets before extrusions to determine the hardness of the material in the as-cast condition. After each extrusion, four measurements were taken on the flow plane of the as-extruded billets. Fig. 32 shows the results of these hardness measurements.

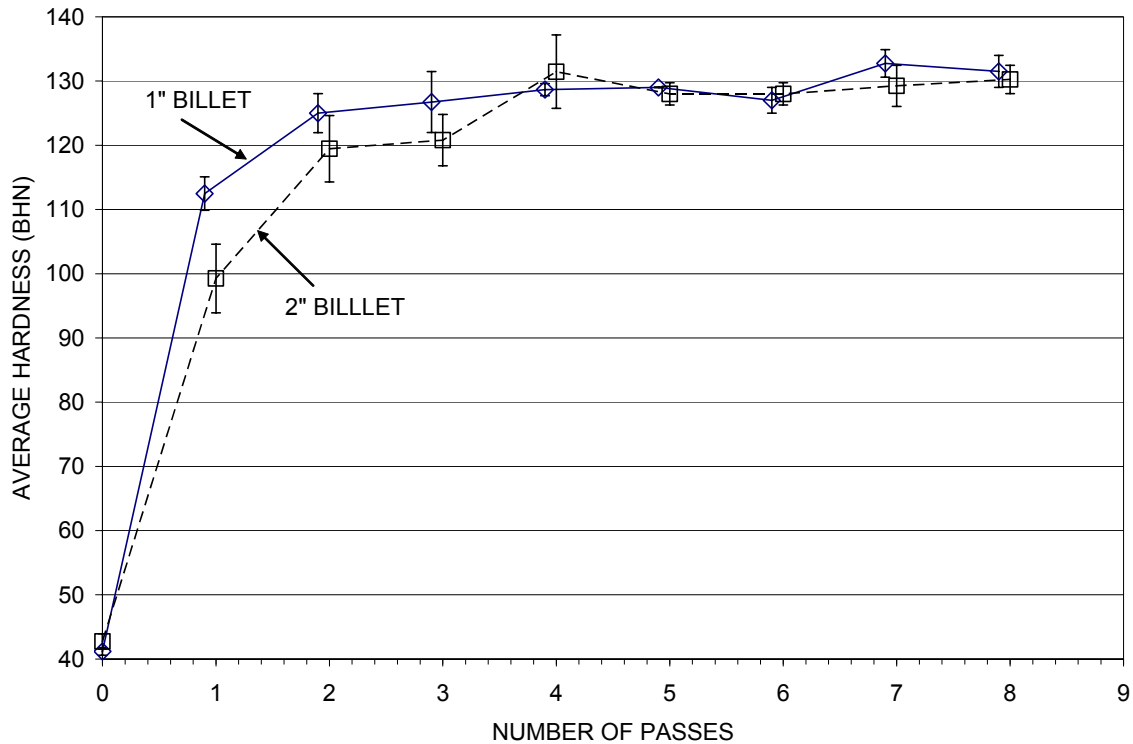


Fig. 32. Average Brinell hardness values for the 25 mm and 50 mm square billets of as-cast OFHC Cu extruded up to eight passes via route E.

Observe that the standard deviation values for the hardness measurements decrease with increasing number of passes; this happens due to the breaking up and homogenization of the cast microstructure with increasing number of extrusion passes. No Brinell hardness measurements were taken for the 19 mm billets because of the small cross-section of these billets.

4.3.2. Vicker's microhardness. The increase in the microhardness values with increasing number of extrusion passes is shown in Fig. 33. The as-worked Vicker's microhardness increases drastically for the first two passes, but plateaus after four passes to an average value of 129 HV₃₀₀ for route C and 132 HV₃₀₀ for route E. It is interesting to observe the trends in hardness increase for routes C and E. For route C the as-worked hardness plateaus after two passes, increasing from 125±5 HV₃₀₀ to 126±3 HV₃₀₀ after two and four passes respectively. Route E processing, on the other hand, leads to an average as-worked hardness of 121±3 HV₃₀₀ after two passes which increases

appreciably to 132 ± 2 HV₃₀₀ after four passes. Although the hardness difference between 2C and 2E can be statistical, a higher increase in hardness for 4E compared to 4C is consistently observed.

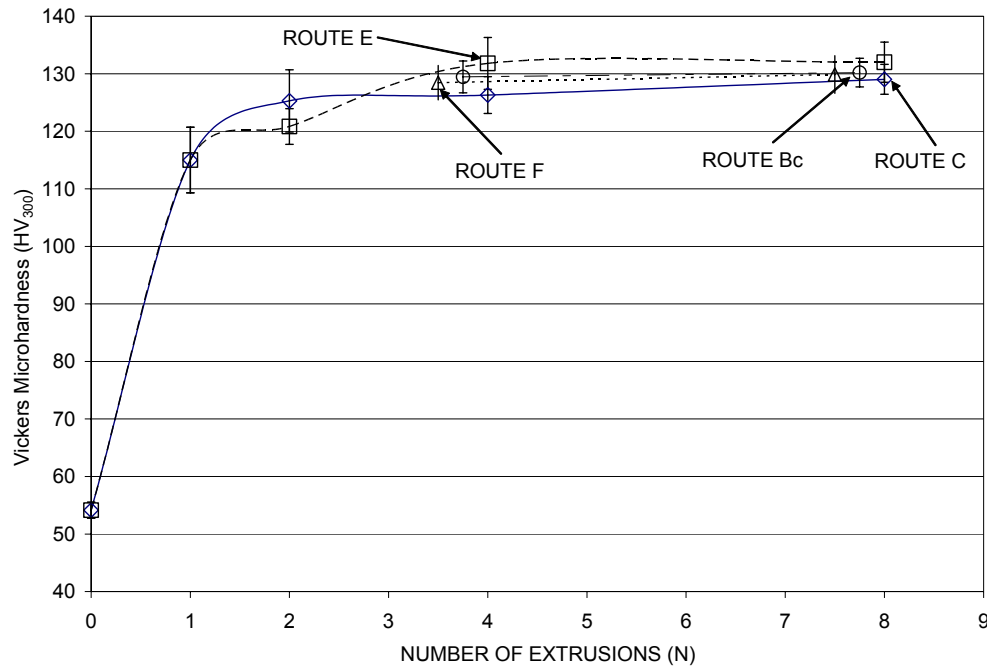


Fig. 33. Increase in Vicker's microhardness with number of passes for 25 mm billets of as-cast OFHC Cu processed up to eight passes through a 90° die.

4.3.2.1. Scale-up project- Vicker's microhardness scans. Hardness scans were done on the flow, transverse and longitudinal planes of billets to determine the homogeneity of as-worked microstructure obtained for different billet sizes. Microhardness measurement is a very convenient way of characterizing the amount of strain induced in the material.

A microhardness scan done on the flow plane for as-cast OFHC Cu processed for one pass is shown in Fig. 34. Note the variation in hardness values while going from the top of the billet to the bottom. These hardness variations can be attributed to the large grains in the initial as-cast condition.

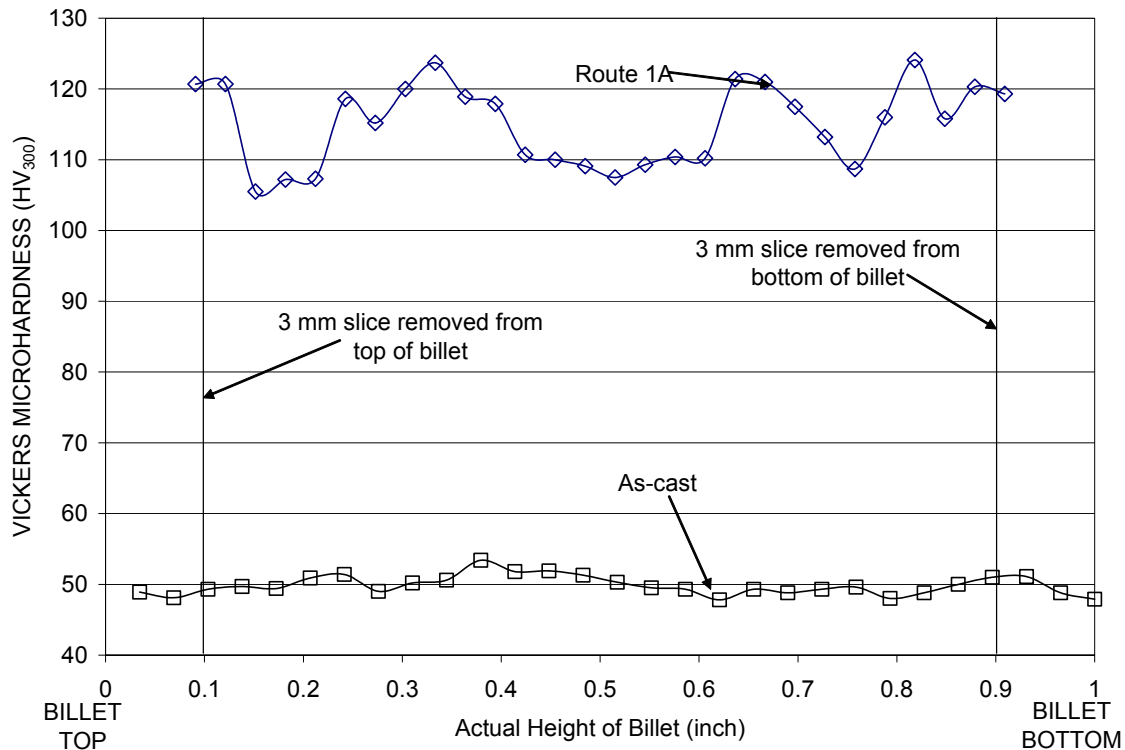


Fig. 34. Vickers microhardness scan along the flow plane for billet processed through pass 1A. Billet section is 25 mm square.

Hardness scans along the flow plane for 25 mm and 50 mm square cross-section billets processed for 2C extrusion passes are shown in Fig. 35. It is interesting to note a general increase in hardness in going from the top of the billets to the bottom.

The hardness scans along flow, transverse and longitudinal planes for billets having 25 mm and 50 mm square cross-sections processed through route 4A are given in Figs. 36-38. Note the transition zone in Fig. 36. This is the zone where the material changes from being in a fully worked condition to a partially worked condition. As shown in Fig. 39 the shape of the fully worked material obtained after four passes via route A is rather complex. For billets having an aspect ratio of five it is not possible to obtain a complete slice of fully worked material in the transverse section of the billet; each transverse section from the billet will contain portions of partially worked material. Ideally the region where the material changes from being fully worked to being partially worked should be a narrow zone, but this would only happen if the shear zone is also narrow. In this case, the size of the shear zone is ~ 0.10 times the width of the extrusion

die. Thus the transition zone will have a width of approximately 0.10 times the width of the extrusion die. In the case of the 25 mm square billets, the transition zone comes out to be 2.5 mm (0.1") wide and in the case of the 50 mm square billets, it comes out to be 5 mm (0.2") wide. Also note the relative position of these transition zones with respect to the height of the billets. If the sections used for microhardness measurements came from corresponding locations along the length of the billets, then the transition zones should coincide with each other; but this is not the case for these measurements as the sections used for these microhardness scans came from different locations along the lengths of the respective billets.

Also note that all the microhardness scans for the transverse plane were taken in the fully worked region. The hardness scans for the longitudinal plane were taken in the partially worked region. After examining the geometry of the billet, it was concluded that these hardness measurements were taken in a region that has been worked to three passes via route A.

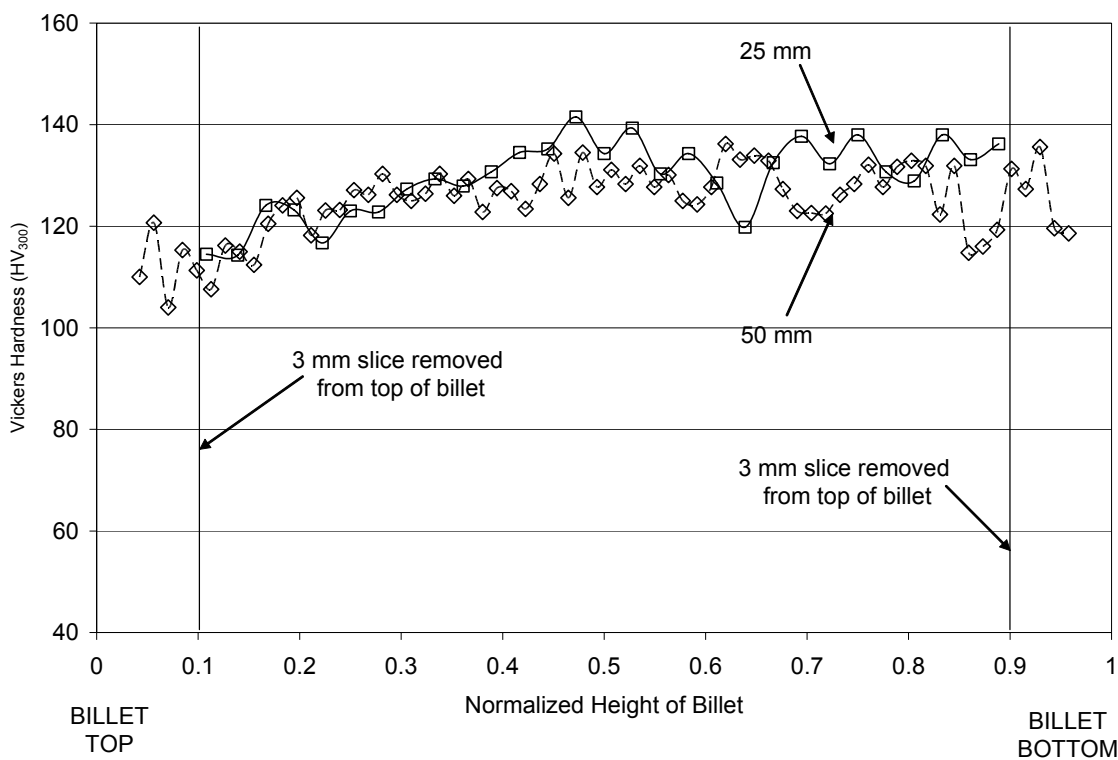


Fig. 35. Vickers microhardness scan along the flow plane for 25 mm and 50 mm square cross-section billets processed through pass 2C.

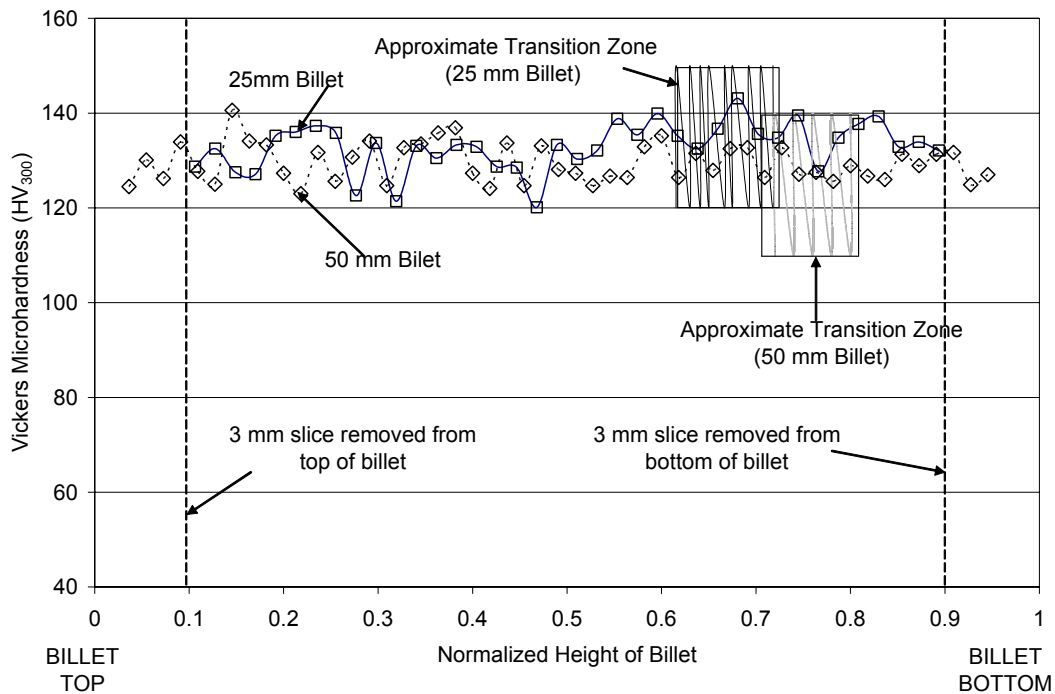


Fig. 36. Vickers microhardness scan along the flow plane for 25 mm and 50 mm square cross-section billets processed through pass 4A.

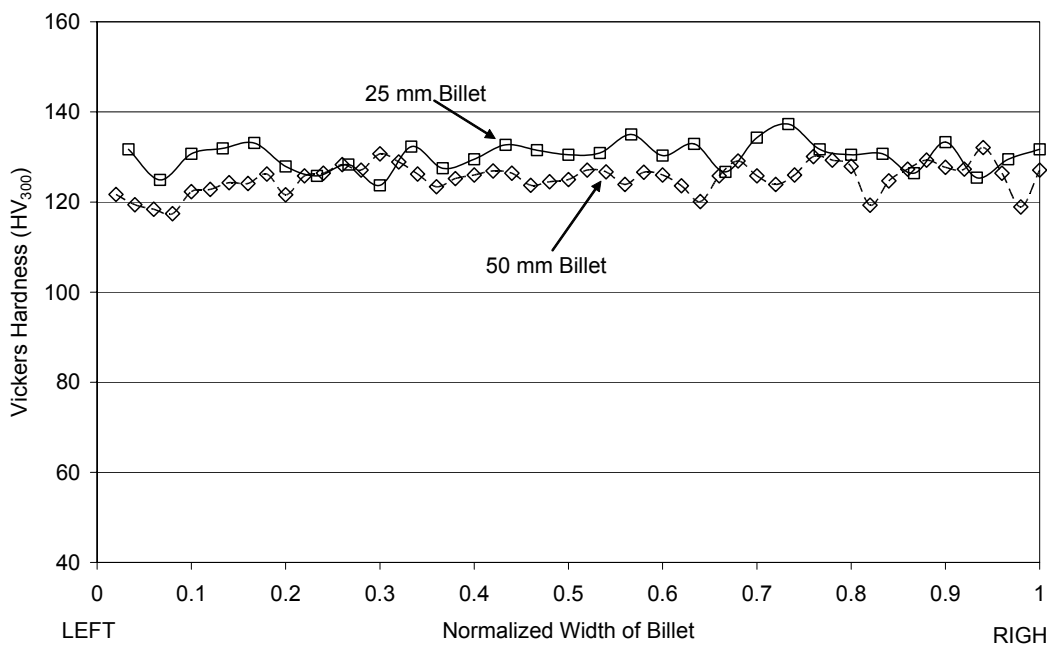


Fig. 37. Vickers microhardness scan along transverse plane for 25 mm and 50 mm square cross-section billets processed through pass 4A.

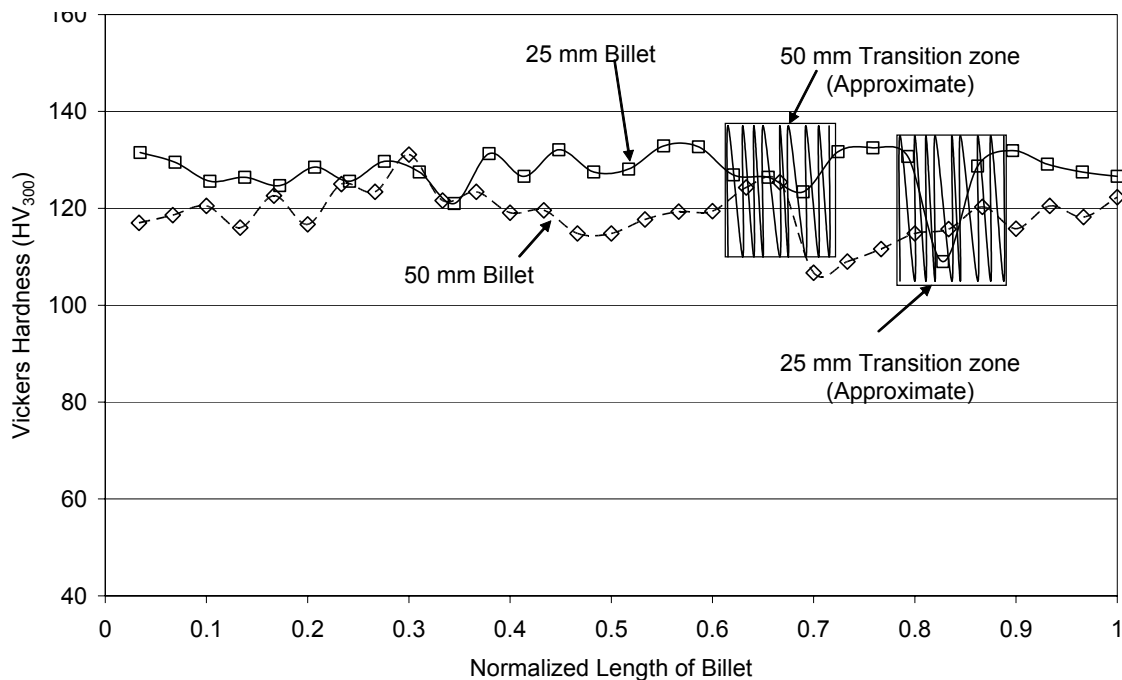


Fig. 38. Vickers microhardness scan along longitudinal plane for 25 mm and 50 mm square cross-section billets processed through pass 4A. Note that these scans were in material processed up to three passes.

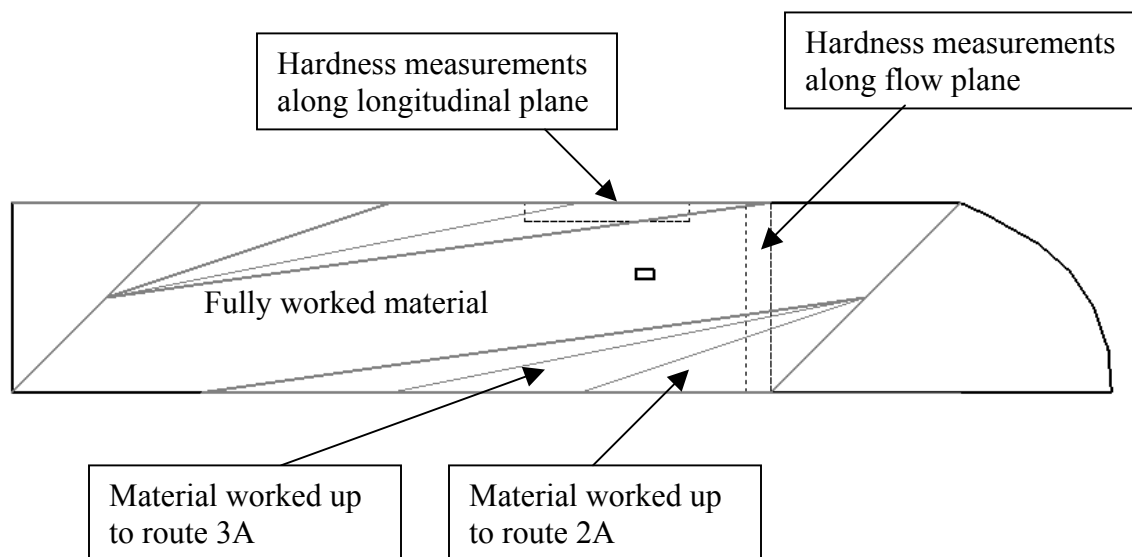


Fig. 39. Shape of different worked regions in a square cross-section billet having an aspect ratio of five and processed up to four passes via route A. Regions used for taking measurements are also shown in the figure.

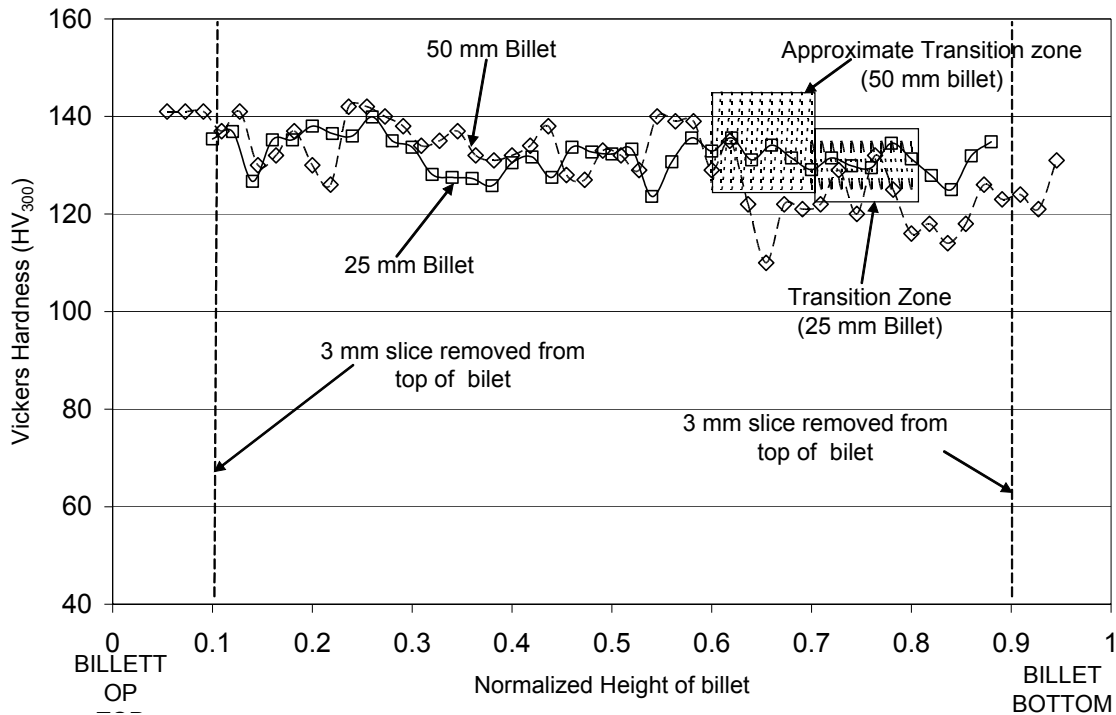


Fig. 40. Vickers microhardness scan along the flow plane for 25 mm and 50 mm square cross-section billets processed through pass 4B.

The hardness scans done for billets having 25 mm and 50 mm square cross-sections processed up to four passes via route B are shown in Figs. 40-42. The same problem was encountered during the microhardness scans done on the flow plane of the billets processed via route B. The geometry of the fully worked region for route 4B is much more complex compared to the geometry for route 4A. The transition zone between the fully worked and partially worked material for route 4B has a width of approximately 0.10 times the extrusion die width. Fig. 43 shows the “fuzzy” transition zone. In this case a clear drop in hardness is seen while going from the fully worked region to a partially worked region.

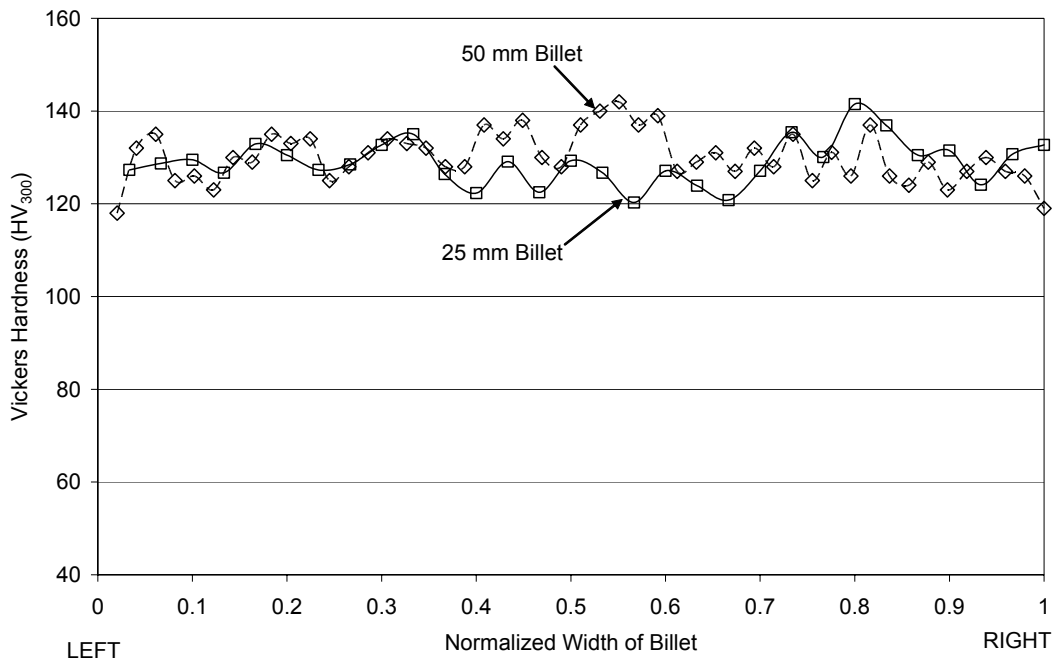


Fig. 41. Vickers microhardness scan along transverse plane for 25 mm and 50 mm square cross-section billets processed through pass 4B.

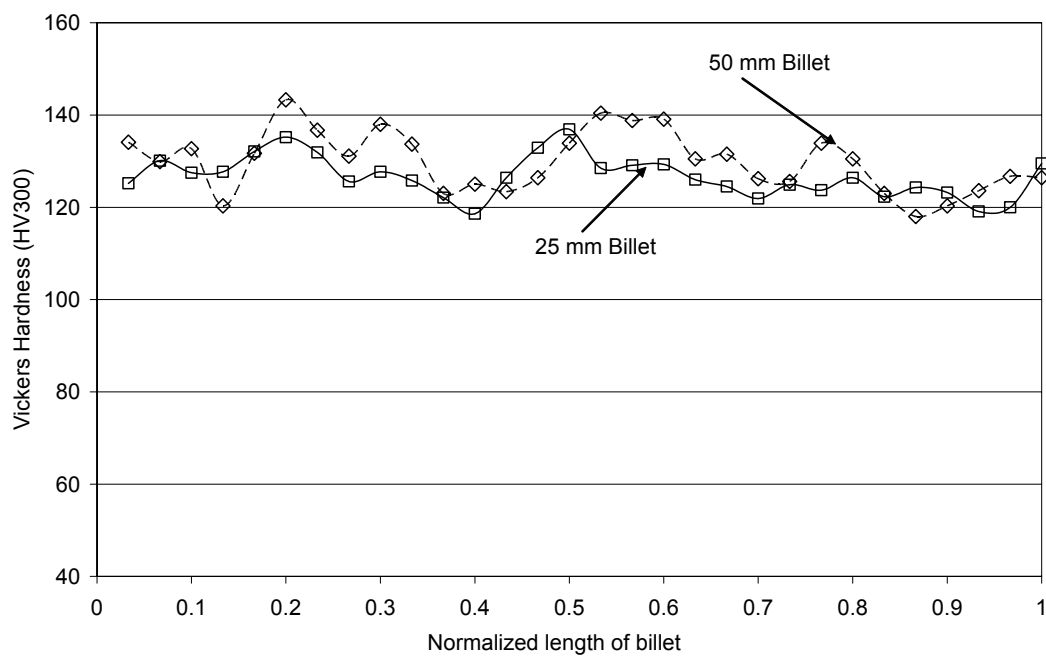


Fig. 42. Vickers microhardness scan along longitudinal plane of 25 mm and 50 mm square cross-section billets processed through pass 4B.

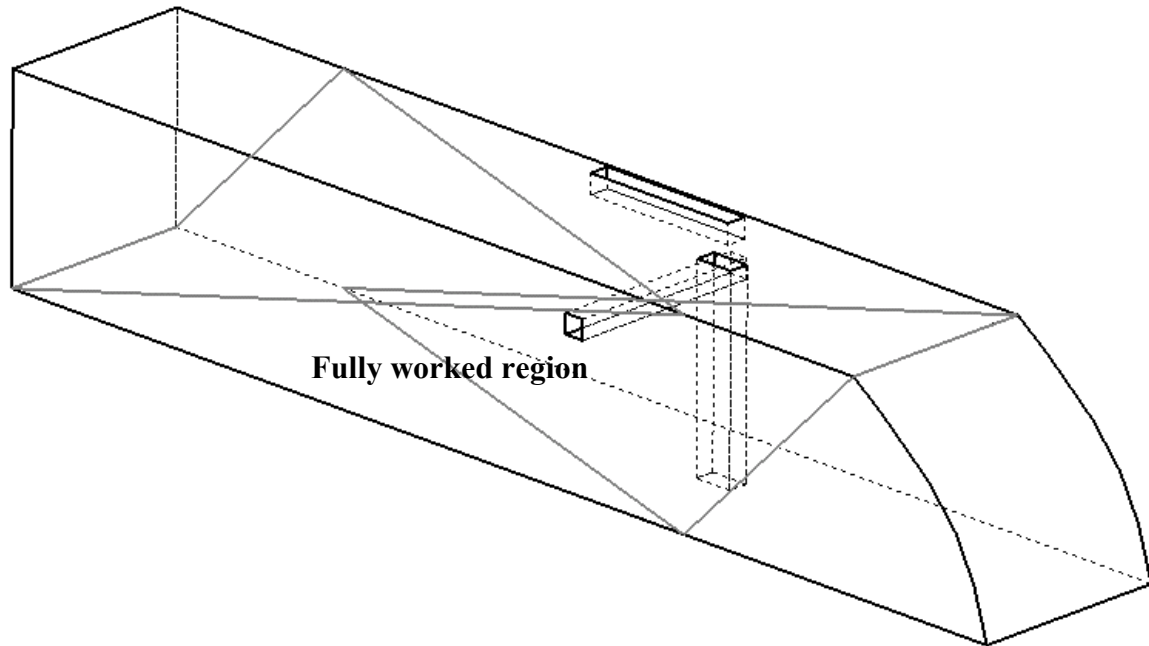


Fig. 43. Shape of the fully worked region in a square cross-section billet processed up to four passes via route B.

Hardness scans for billets having three different sizes; 19 mm, 25 mm and 50 mm processed for four passes through route E are shown in Figs. 44-46.

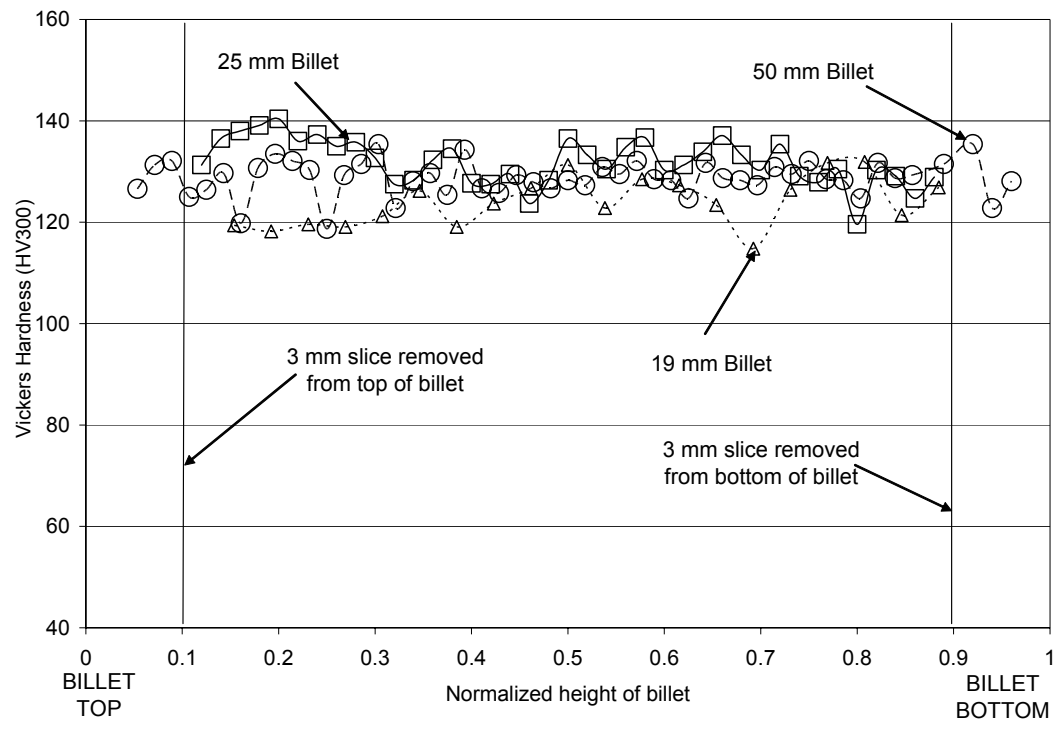


Fig. 44. Vickers microhardness scan along flow plane of 19 mm, 25 mm and 50 mm square cross-section billets processed through pass 4E.

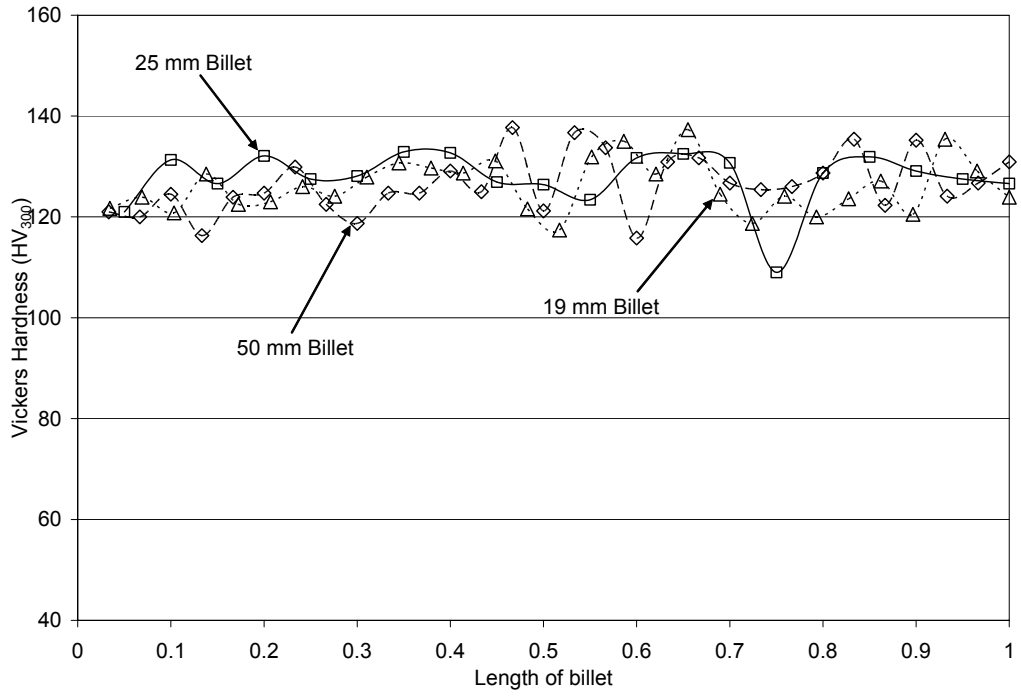


Fig. 45. Vickers microhardness scan along longitudinal plane of 19 mm, 25 mm and 50 mm square cross-section billets processed through pass 4E.

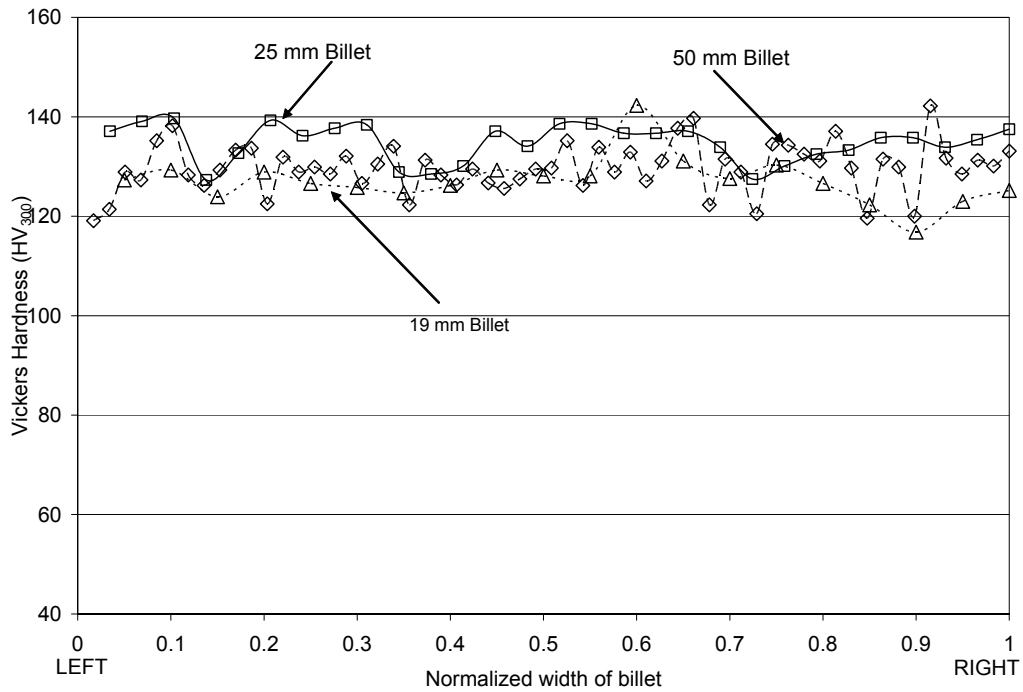


Fig. 46. Vickers microhardness scan along transverse plane of 19 mm, 25 mm and 50 mm square cross-section billets processed through pass 4E.

Vickers microhardness scans along the flow plane were also carried out for the 19 mm, 25 mm and 50 mm square cross-section billets processed through pass 8E. The scans are shown in Fig. 47.

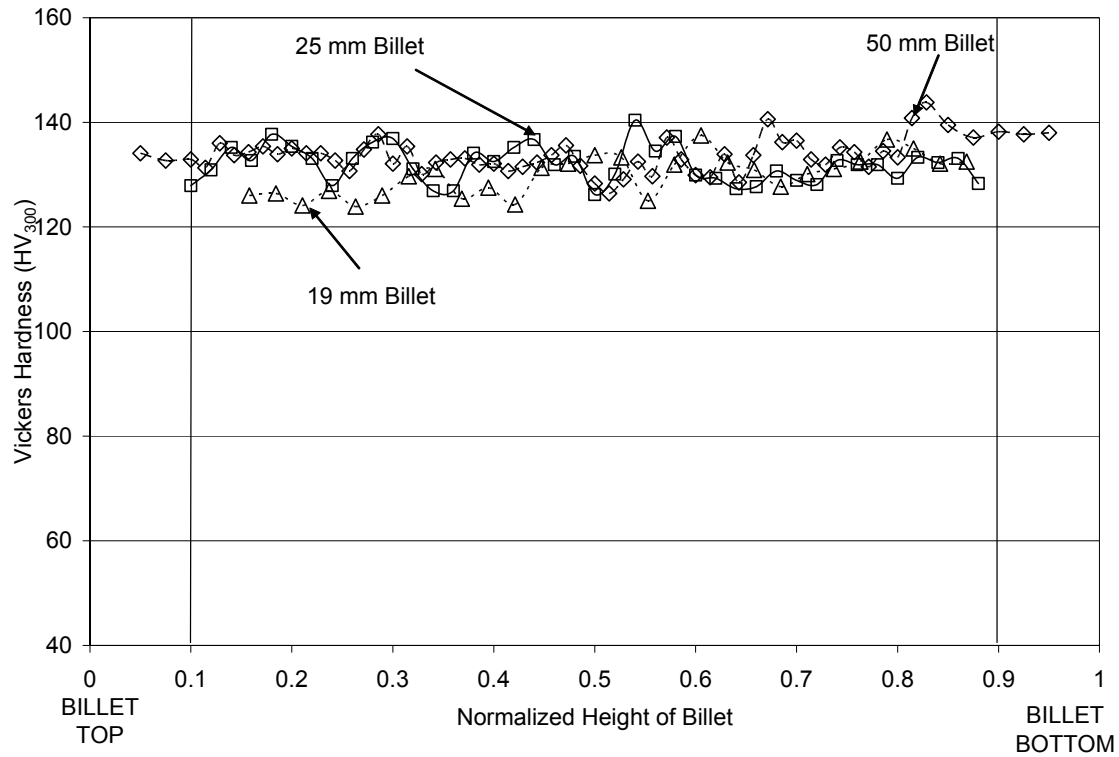


Fig. 47. Vickers microhardness scan along flow plane of 19 mm, 25 mm and 50 mm square cross-section billets processed through pass 8E.

The comparison of the as-worked microhardness values obtained for the three different sizes is shown in Figs. 48-50.

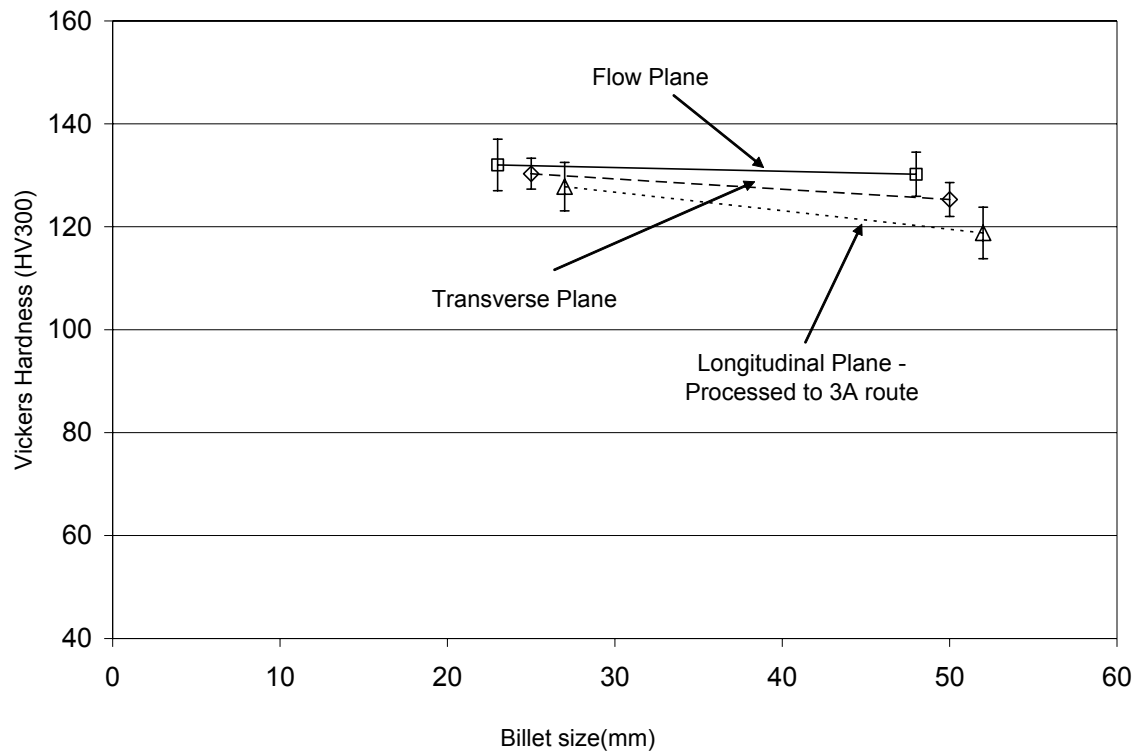


Fig. 48. Comparison of as-worked hardness along flow, transverse and longitudinal planes for 25 mm and 50 mm square cross-section billets processed up to four pass via route A.

Note that compared to the two other planes, there is a larger difference in the hardness values obtained in the longitudinal plane. One reason for this can be that these hardness readings we take in a partially worked region. This amount of work was not able to eliminate the initial hardness difference in the billets due to the differences in the starting texture or grain orientation.

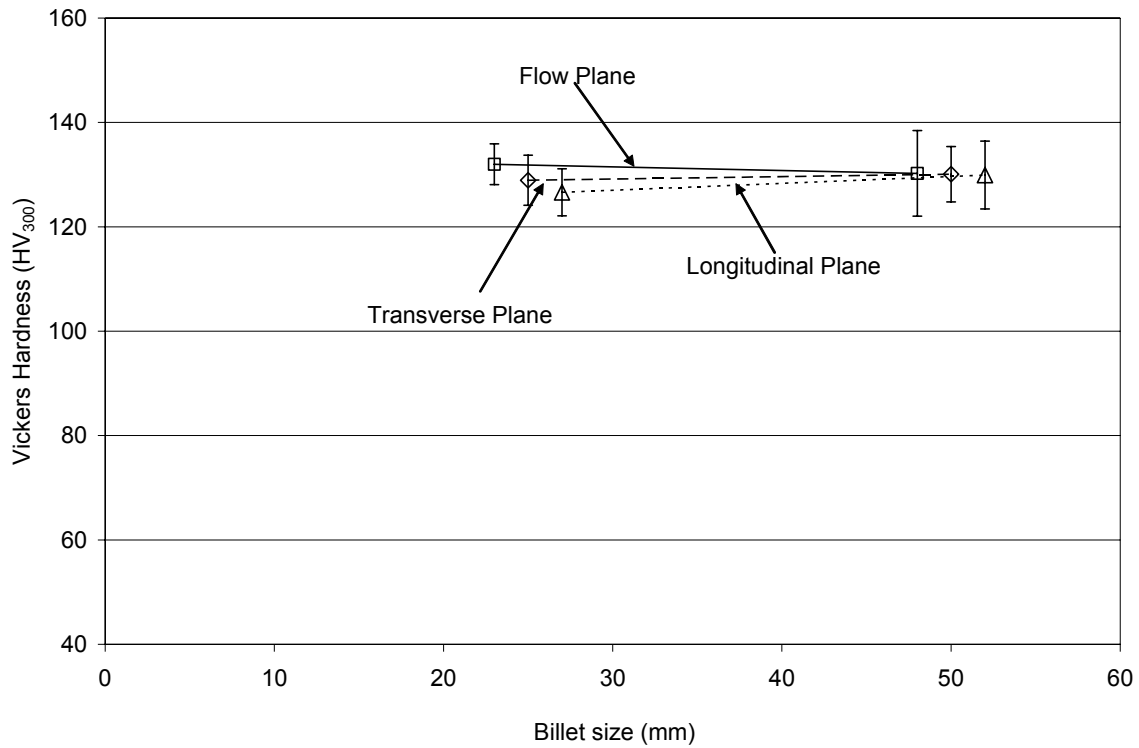


Fig. 49. Comparison of as-worked hardness along flow, transverse and longitudinal planes for 25 mm and 50 mm square cross-section billets processed up to four pass via route B.

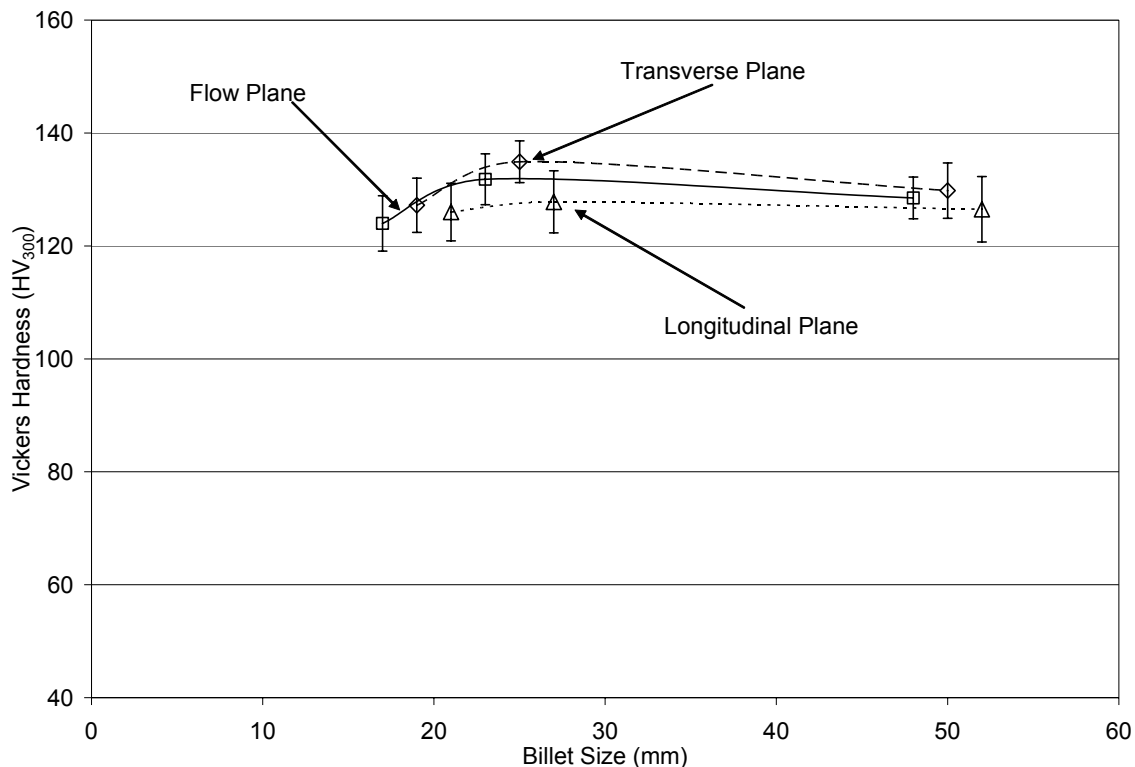


Fig. 50. Comparison of as-worked hardness along flow, transverse and longitudinal planes for 19 mm, 25 mm and 50 mm square cross-section billets processed up to four pass via route E.

It is observed that there is little variation in the as-worked hardness values obtained for the different sizes of the billets.

4.4. Recrystallization curves

Vicker's microhardness is a very effective way of determining the recrystallization temperature of as-worked copper. The recrystallization curves for billets of different cross-sections having undergone different levels of strains were obtained through Vicker's microhardness measurements.

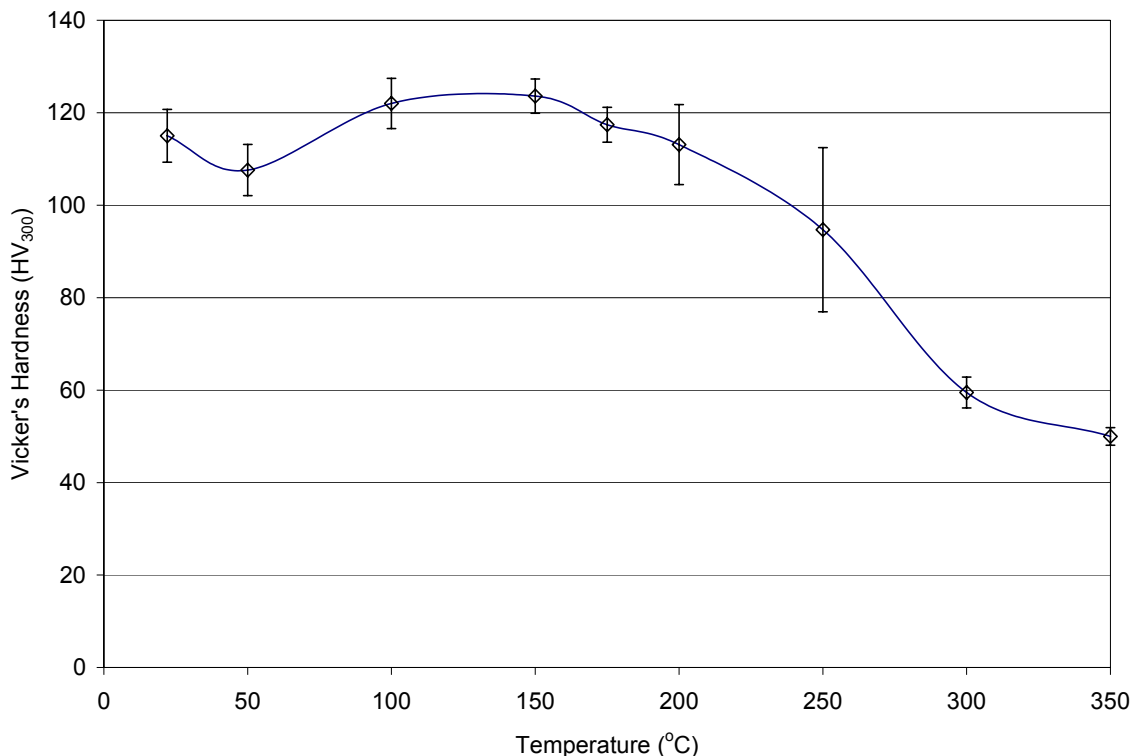


Fig. 51. Variation in hardness with annealing temperature for 25 mm square cross-section billet of as-cast CDA 101 Cu processed through extrusion route 1A in 90° die at room temperature.

4.4.1. Scale-up project. The recrystallization curve for as-cast CDA 101 Cu processed for one extrusion pass is shown in Fig. 51. Observe the large drop in average hardness value for the sample heat treated at 50°C. Also observe an increasing trend in the hardness values up to a temperature of 150°C. After 150°C, recrystallization commences in the material, giving a general hardness drop, and at 350°C complete recrystallization is achieved.

Recrystallization curves for 25 mm and 50 mm square billets processed for 2C extrusion passes are given in Fig. 52. Observe that both the materials behave in an identical manner. The recrystallization begins at a temperature of 150~175°C range and finishes off at a temperature of 250°C. It is interesting to observe the “undulations” observed in the unrecrystallized material up to a temperature of 175°C.

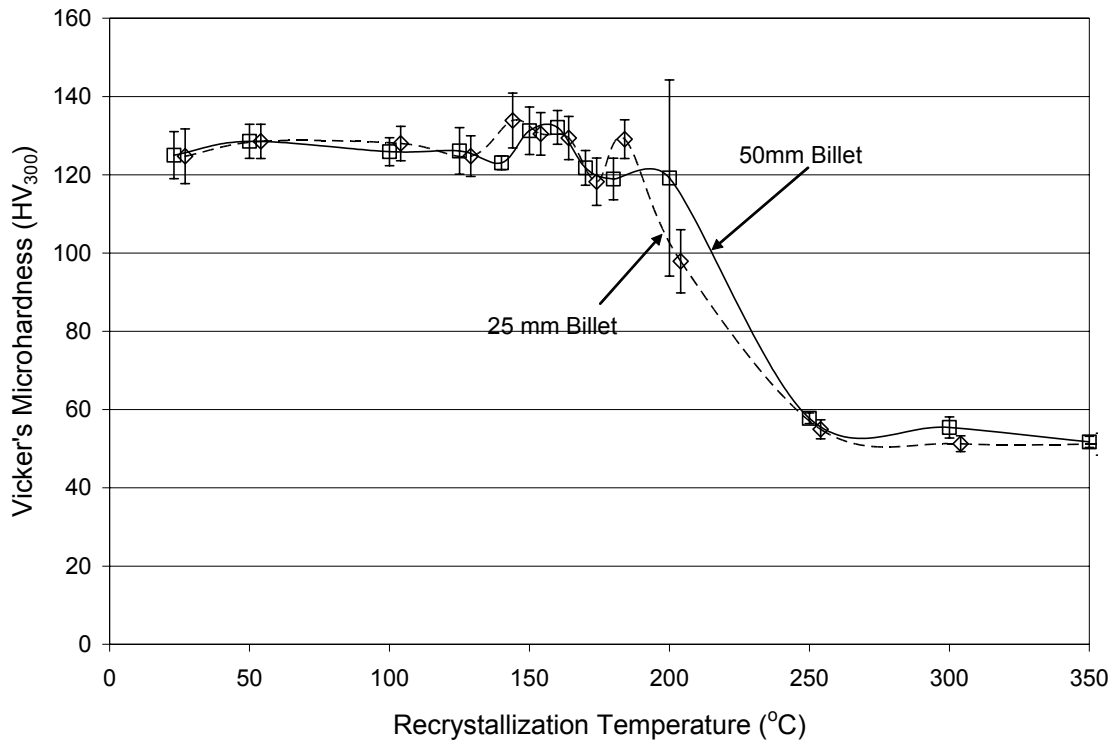


Fig. 52. Variation in hardness with annealing temperature for 25 mm and 50 mm square cross-section billets of as-cast CDA 101 Cu processed through extrusion route 2C in 90° die at room temperature.

Recrystallization curves for 25 mm and 50 mm billets processed through 4A and 4B extrusion routes are given in Figs. 53-54. It is interesting to observe that although both materials have undergone equal amounts of strain, the material processed through route B begins to recrystallize at a lower temperature ($\sim 140^{\circ}\text{C}$) compared to that processed through route A, which starts to recrystallized at a temperature of $\sim 170^{\circ}\text{C}$.

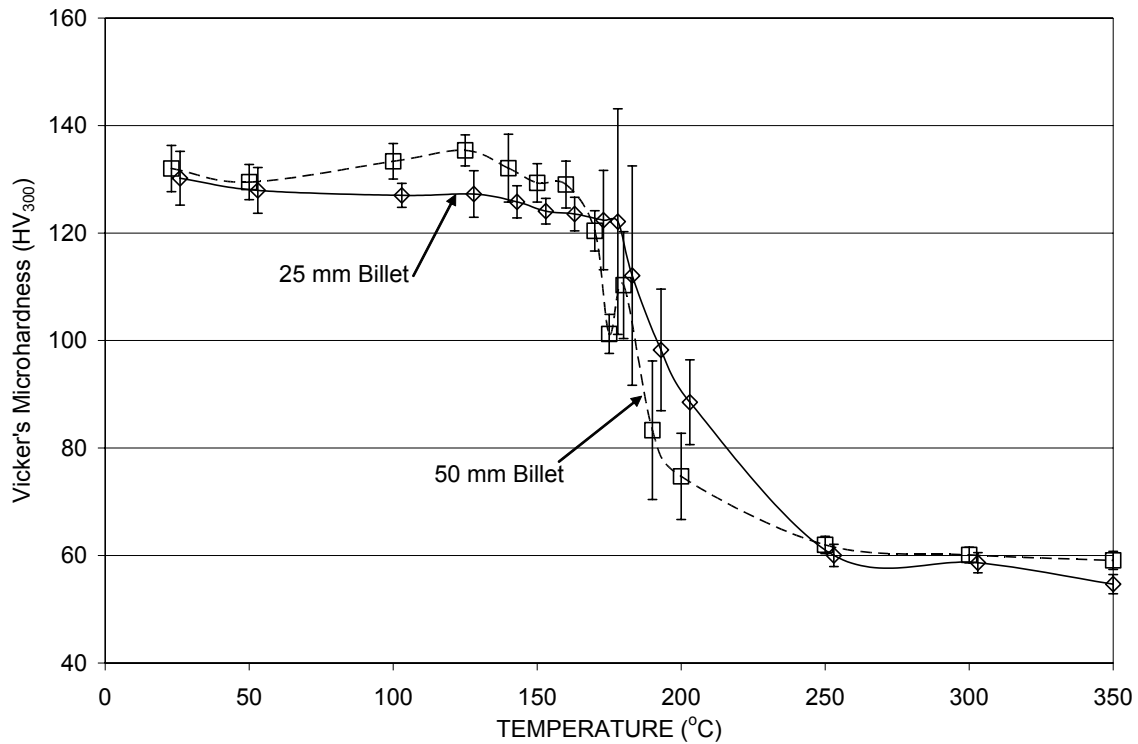


Fig. 53. Variation in hardness with annealing temperature for 25 mm and 50 mm square cross-section billets of as-cast CDA 101 Cu processed through extrusion route 4A in 90° die at room temperature.

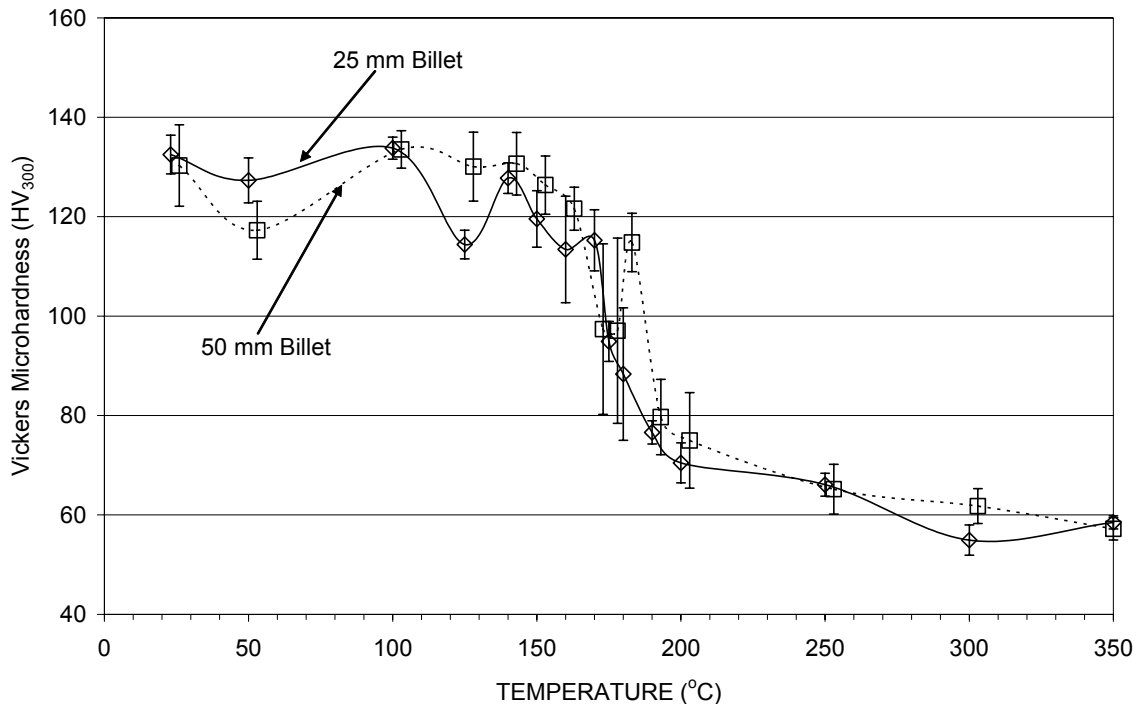


Fig. 54. Variation in hardness with annealing temperature for 25 mm and 50 mm square cross-section billets of as-cast CDA 101 Cu processed through extrusion route 4B in 90° die at room temperature.

Observe the changes in hardness values for the as-worked material up to a temperature of 140°C (Fig. 54). These drastic changes could be attributed to shear banding. Billet of 50 mm square cross-section shear localized during the final extrusion pass. This shear localization may lead to the generation of large alternating bands of high and low plastic shear deformation, leading to the variations in hardness values in the temperature range of 22 – 140°C.

The recrystallization curves for the 19 mm, 25 mm and 50 mm square billets processed through route 4E are shown in Fig. 55. Again, there is very little difference in the thermal response of the materials from these billets.

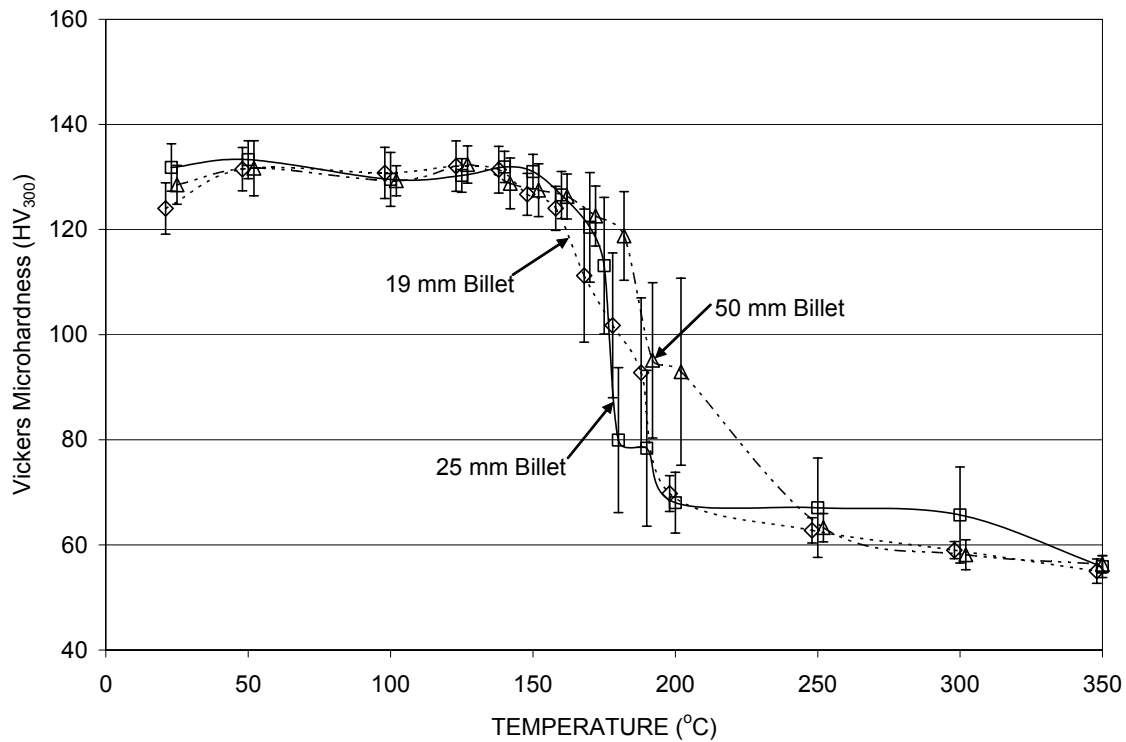


Fig. 55. Variation in hardness with annealing temperature for 19 mm, 25 mm and 50 mm square cross-section billets of as-cast CDA 101 Cu processed through extrusion route 4E in 90° die at room temperature.

The recrystallization curves for 19 mm, 25 mm and 50 mm square billets processed through route 8E are shown in Fig. 56.

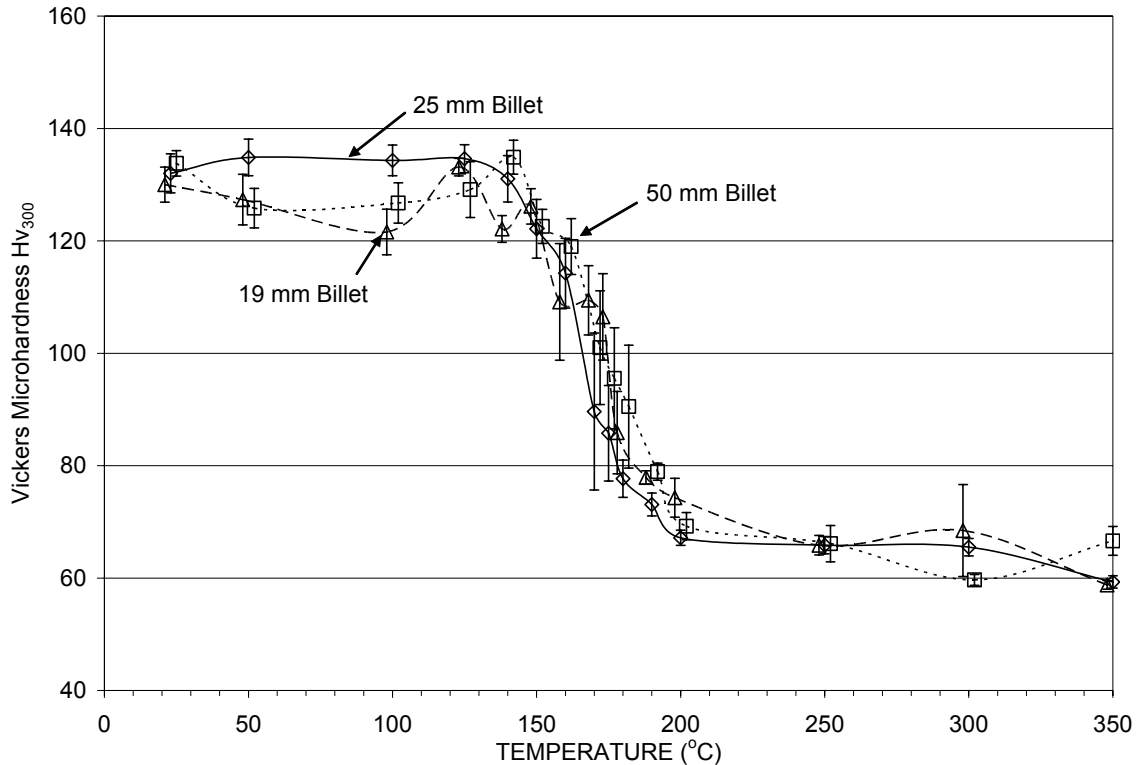


Fig. 56. Variation in hardness with annealing temperature for 19 mm, 25 mm and 50 mm square cross-section billets of as-cast CDA 101 Cu processed through extrusion route 8E in 90° die at room temperature.

The recrystallization curves for as-cast CDA 101 Cu processed through 1A, 2C, 4E and 8E extrusion routes are given in Fig. 57. Observe that not only is the as-worked hardness higher for the higher strain induced in the material, but even the fully recrystallized hardness values are higher for higher extrusion passes. This clearly indicates that the fully recrystallized grain size is smaller for higher extrusions passes.

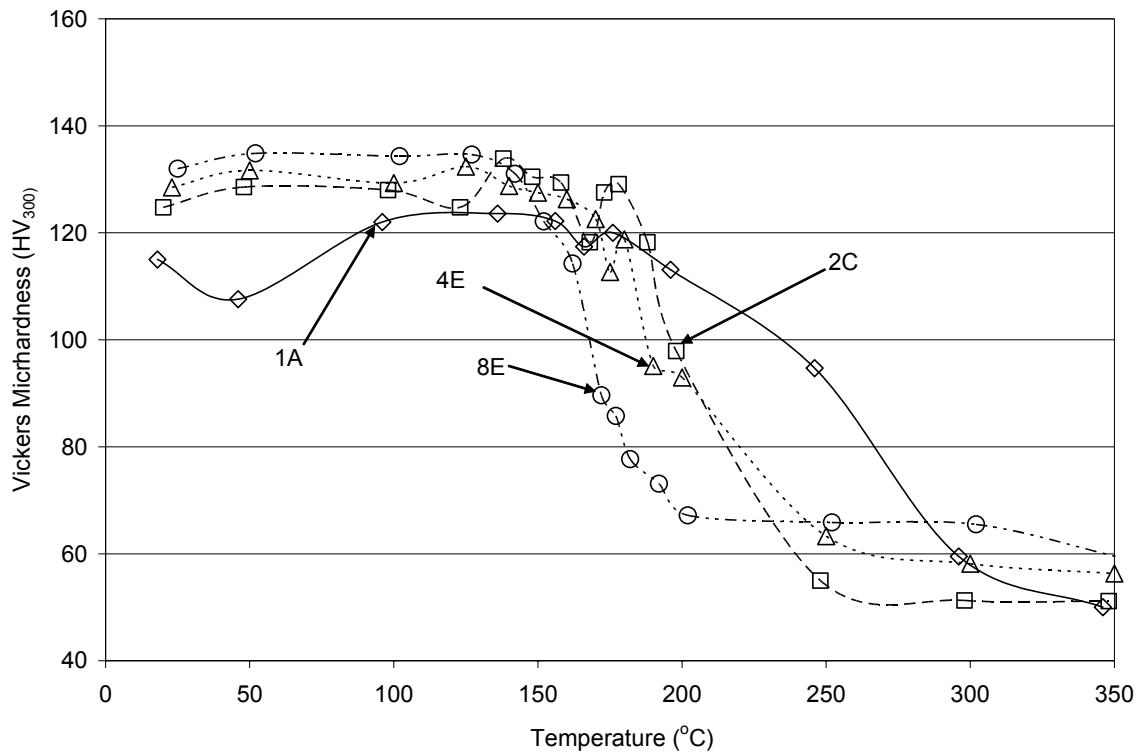


Fig. 57. Recrystallization curves for CDA 101 Cu processed through 1A, 2C, 4E and 8E extrusion routes.

4.4.2. *Microstructural breakdown study.* The heat treatments for the microstructural breakdown study were carried out in a vacuum furnace instead of a sand bath. The main reason behind choosing a vacuum furnace over sand bath was to check if oxidation occurs during heat treatments. Note that some unexpected variations in hardness values were observed for the annealing curves in the scale-up project. By carrying out heat treatments in a vacuum furnace, it will be possible to note any differences between the hardness values or annealing trends for the two different heat treatments.

The recrystallization curves for processing route E are shown in Fig. 58. Cu processed through two thermomechanical schedules is characterized in these curves. Notice that the Cu processed through eight passes with and without intermediate heat treatments shows the highest as-worked and recrystallized hardness, again indicating a smaller recrystallized grain size. The recrystallization curves for 8E extrusion routes and two different thermo-mechanical schedules are shown in Fig. 59. Notice that material processed through 8E extrusions starts to recrystallize early compared to that processed

through 4E extrusions, but the recrystallization process is completed at approximately the same temperature for both the cases.

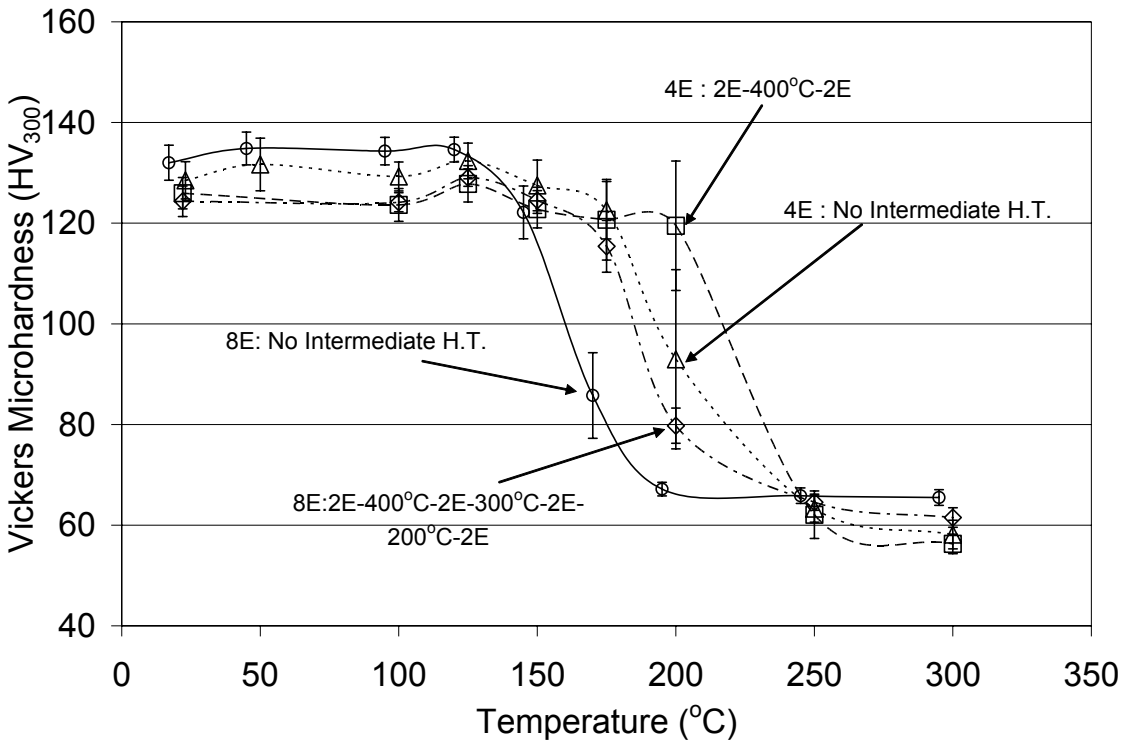


Fig 58. Variation in hardness with annealing temperature for as-cast CDA 101 Cu processed up to eight passes via route E with and without intermediate heat treatments.

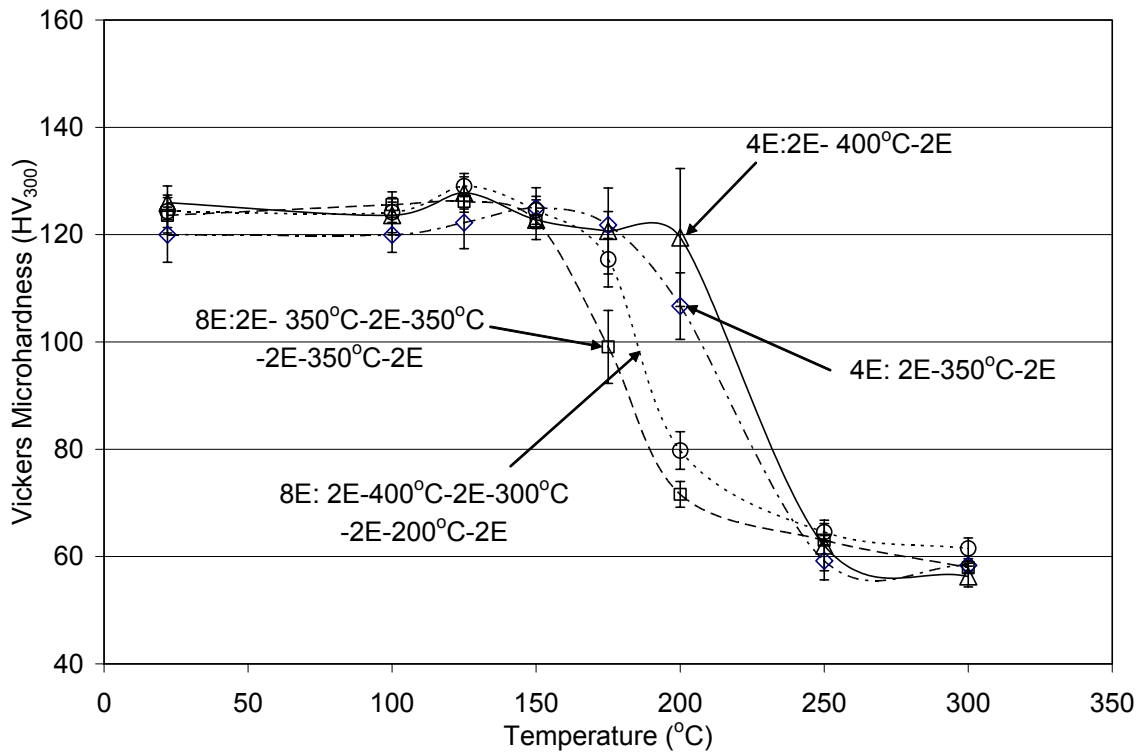


Fig 59. Variation in hardness with annealing temperature for as-cast CDA 101 Cu processed up to eight passes via route E with two different intermediate heat treatment temperatures.

Fig. 60 shows recrystallization curves for route C with two different TMP schedules. In a few cases there is some variation in the hardness values prior to the commencement of recrystallization.

The recrystallization curves for Cu processed up to eight passes via route Bc with and without intermediate heat treatments are given in Fig. 61. It is observed that for billets processed to higher strains, the recrystallization curve shifts towards the left. Also observe the decrease in the error bar values in the recrystallization curves for material given intermediate heat treatment.

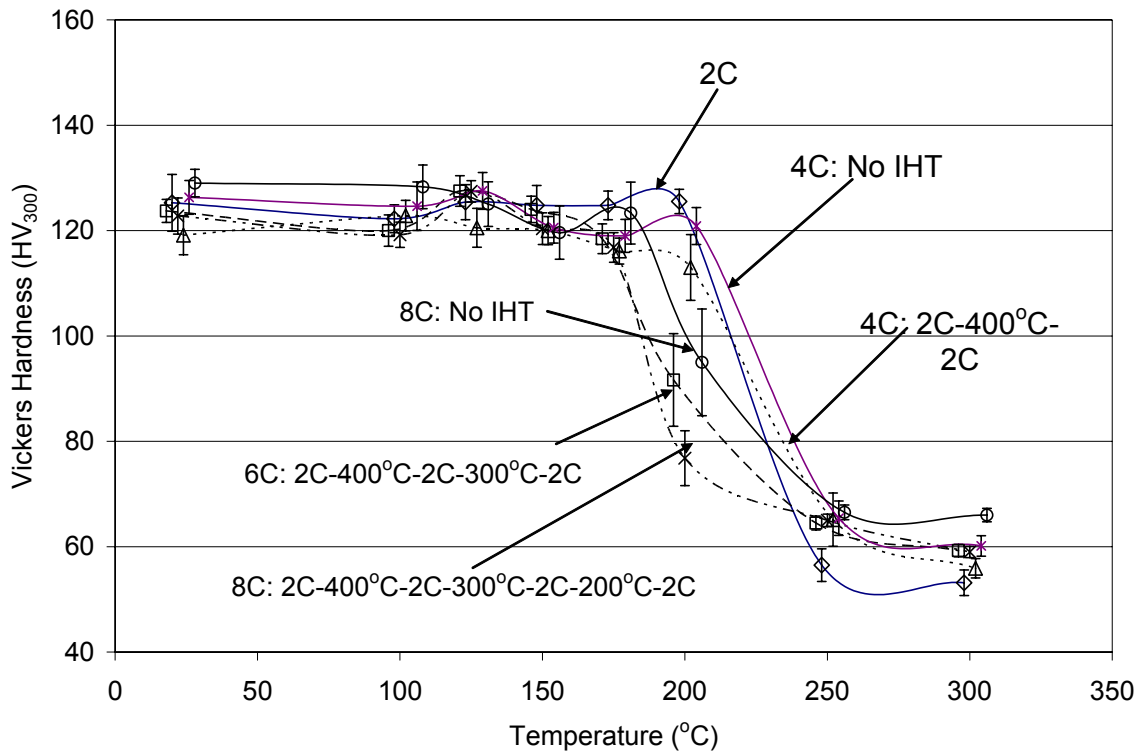


Fig. 60. Variation in hardness with annealing temperature for as-cast CDA 101 Cu processed up to eight passes via route C with and without intermediate heat treatments.

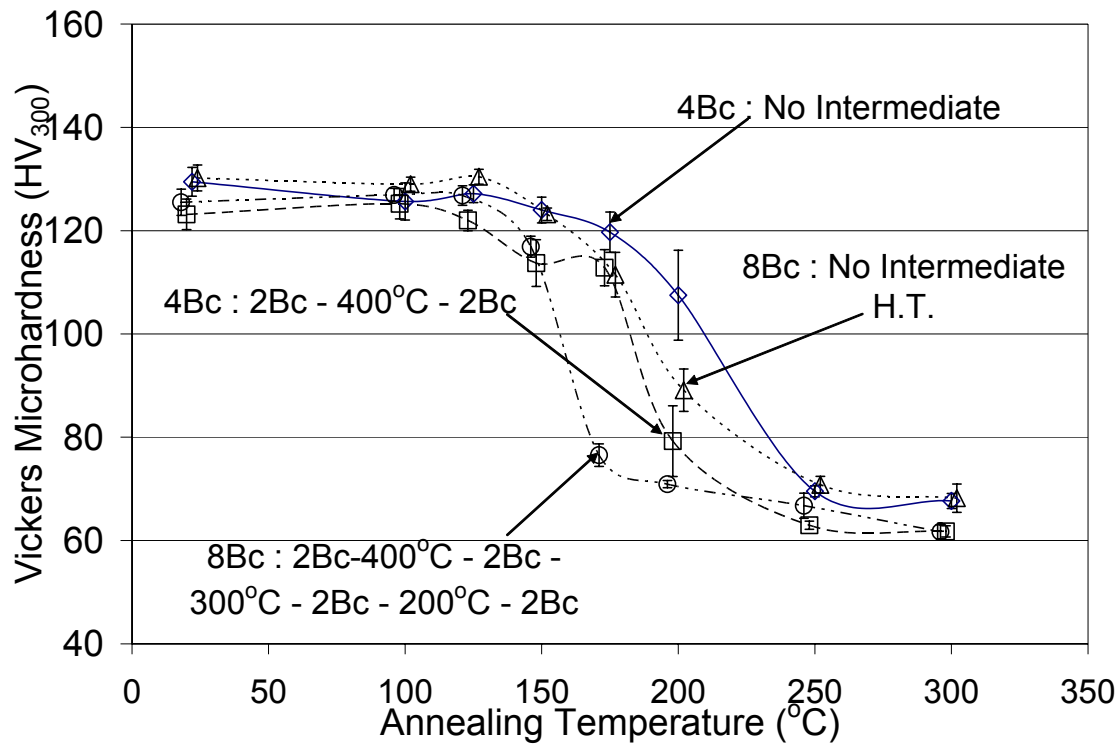


Fig. 61. Variation in hardness with annealing temperature for as-cast CDA 101 Cu processed up to eight passes via route Bc with and without intermediate heat treatments.

The recrystallization curves for Cu processed through route F with and without intermediate heat treatments are given in Fig. 62. It is again observed that the error bar values for material given intermediate heat treatments are lower compared to those for material not given intermediate heat treatments.

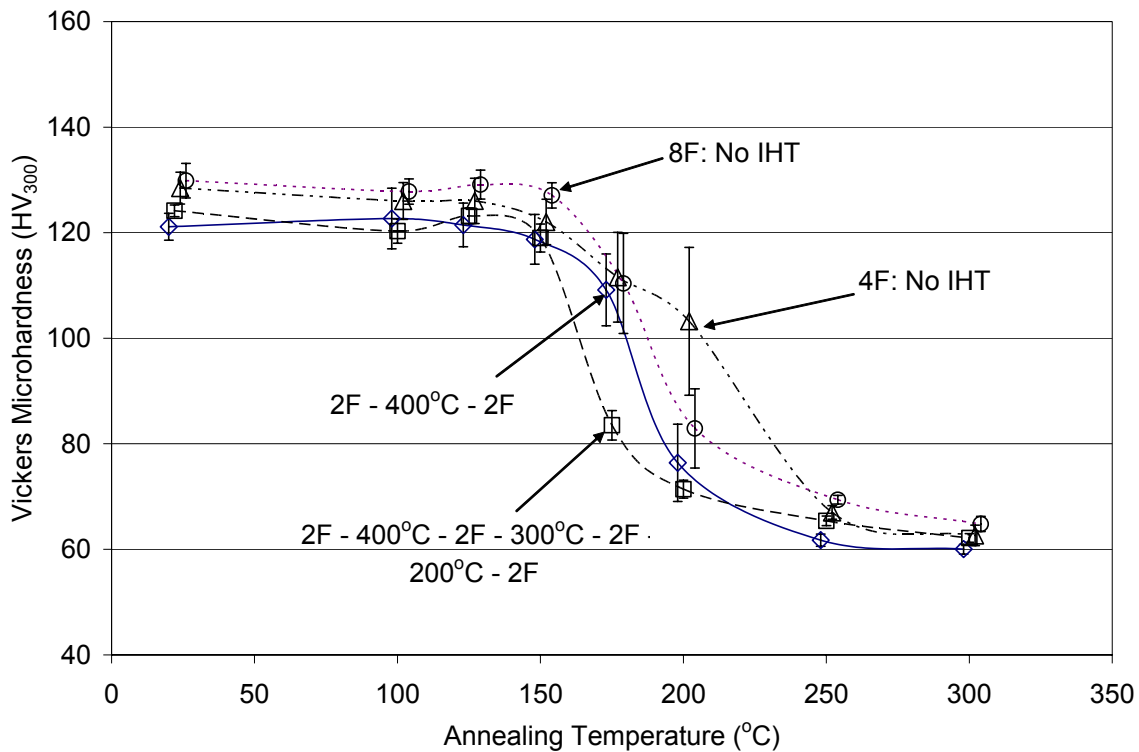


Fig. 62. Variation in hardness with annealing temperature for as-cast CDA 101 Cu processed up to eight passes via route F with and without intermediate heat treatments.

4.5. Recrystallization range

The method used for calculation of temperature range for percentage recrystallization is described in Fig. 63. For calculation purpose, the difference between average as-worked hardness and average recrystallized hardness values was obtained. 10% of this hardness difference was subtracted from the average as-worked hardness value to give the hardness value corresponding to 10% recrystallization. To obtain 10% recrystallization temperature, temperature range corresponding to this hardness value was obtained by drawing tie-lines on the recrystallization chart. Such a technique, although simple will give accurate results based on the recrystallization curves.

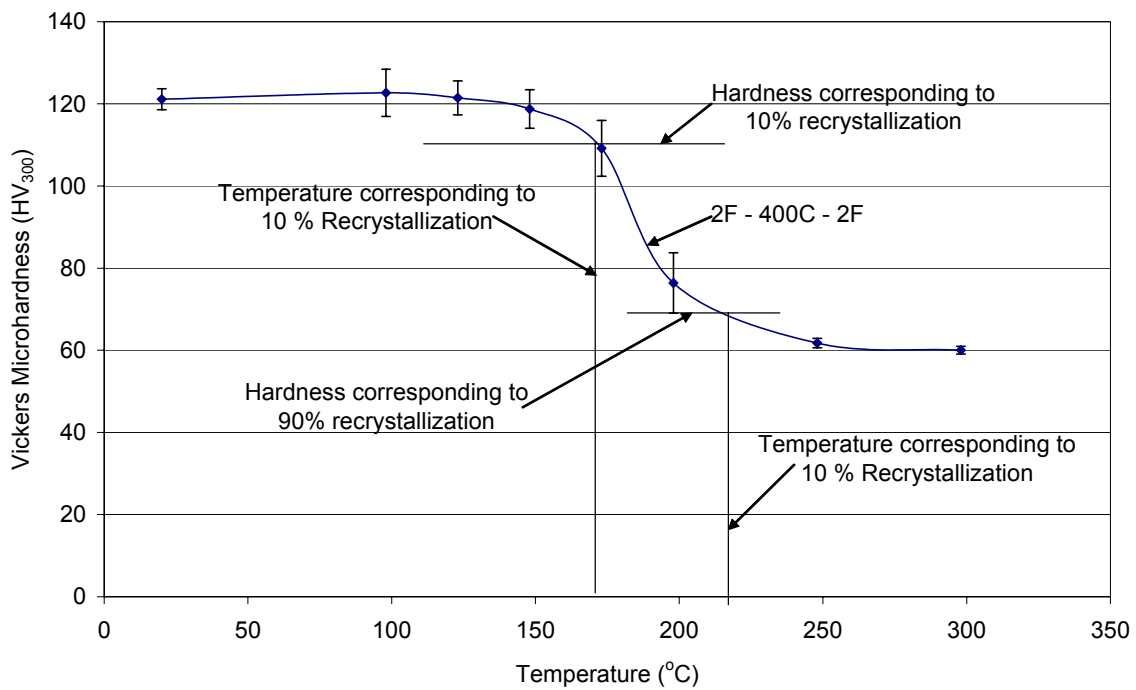


Fig. 63. Recrystallization curve showing the technique used to calculate temperature regimes for % hardness variations from a recrystallization curve.

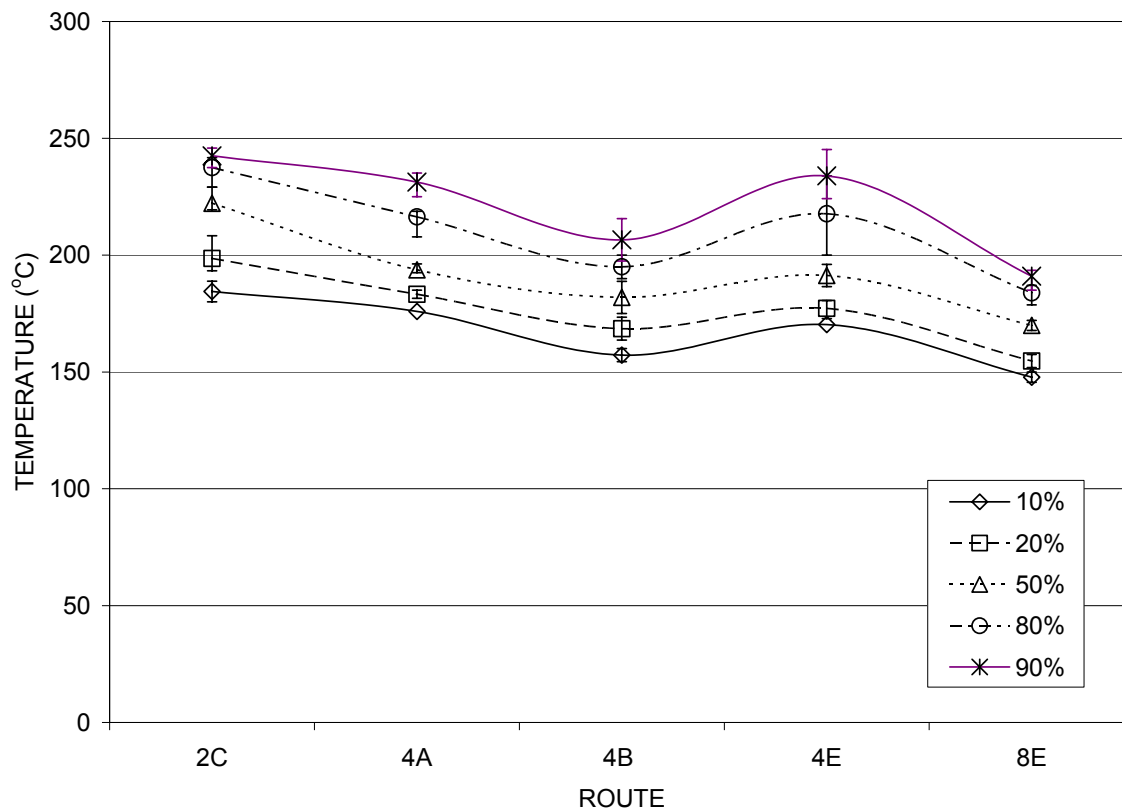


Fig. 64. Temperature ranges for hardness variation for 50 mm square billets processed up to eight passes via routes A, B, C and E.

The recrystallization temperature range for Cu processed through different TMP schedules is given in Figs. 64-66 and in Table 12. Observe that the routes which involve a rotation of 90° between passes show early commencement of recrystallization, but the completion of recrystallization process is in the same temperature range for all extrusion passes. It is observed in many cases, that the temperature range for 10% to 90% recrystallization is narrow but at higher temperature for material extruded up to two extrusions compared to material extruded for four or higher extrusions.

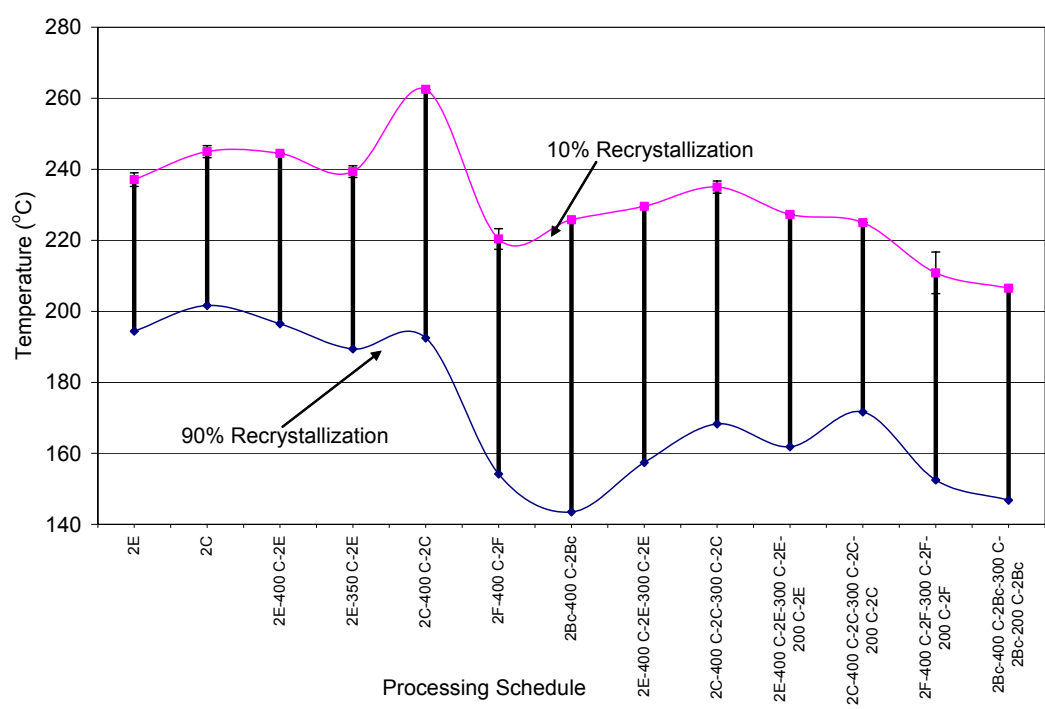


Fig. 65. Temperature ranges for hardness variation for 25 mm square billets processed up to eight extrusion passes through different thermo-mechanical processing schedules.

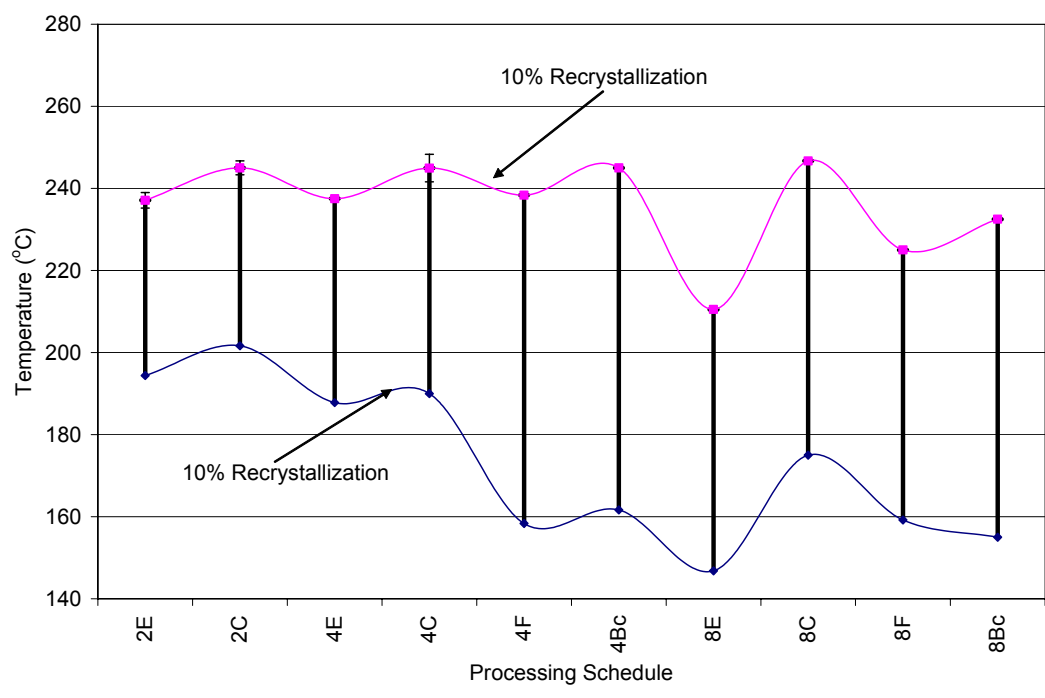


Fig. 66. Temperature ranges for hardness variation for 25 mm square billets processed up to eight extrusion passes via different routes and with intermediate heat treatments

Table 12. Temperature range for recrystallization for CDA 101 Cu processed through different thermomechanical schedules.

ROUTE	TMP SCHEDULE	Temp. for 10% Recrystallization	Temp. for 90% Recrystallization	TEMPERATURE DIFFERENCE
2E	2E	194.4	237.1	42.7
2C	2C	201.7	245	43.3
4C	4C	190	245	55
4E	4E	187.8	237.5	49.7
4F	4F	158	238	80
4Bc	4Bc	161.7	245	83.3
4C	2C-400°C-2C	192.5	262.5	70
4E	2E-400°C-2E	196.5	244.5	48
4E	2E-350°C-2E	189.4	239.3	49.9
4F	2F-400°C-2F	154.2	220.4	66.2
4Bc	2Bc-400°C-2Bc	143.5	225.8	82.3
6C	2C-400°C-2C-300°C-2C	168.3	235	66.7
6E	2E-400°C-2E-300°C-2E	157.4	229.6	72.2
8C	4C-4C	175	246.7	71.7
8E	4E-4E	146.8	210.5	63.7
8F	4F - 4F	159.2	225	65.8
8Bc	4Bc - 4Bc	155	232.5	77.5
8C	2C-400°C-2C-300°C-2C-200°C-2C	171.7	225	53.3
8E	2E-400°C-2E-300°C-2E-200°C-2E	161.9	227.3	65.4
8E	2E-350°C-2E-350°C-2E-350°C-2E	156.7	214.2	57.5
8F	2F-400°C-2F-300°C-2F-200°C-2F	152.5	210	57.5
8Bc	2Bc-400°C-2Bc-300°C-2Bc-200°C-2Bc	146.8	206.5	59.7

4.6. Transmission electron microscopy

4.6.1. *Scale-up project.* Transmission electron microscopy (TEM) was done on the flow plane of the as-worked and recrystallized specimens. The images show typical micro-structures obtained for these specimen.

Figs. 67-69 show the TEM micrographs obtained for the 50 mm, 25 mm and 19 mm square billets processed through route 4E. There is little variation in the sub-grain size and morphology amongst these micrographs indicating the independence of the sub-microstructures obtained from different billet sizes. Observe the formation of arcs in the selected area diffraction (SAD) patterns. These arcs indicate that the grain boundaries observed in the microstructure are mainly low angle grain boundaries. These arcs also give an indication of the amount of lattice distortion present in the microstructure.

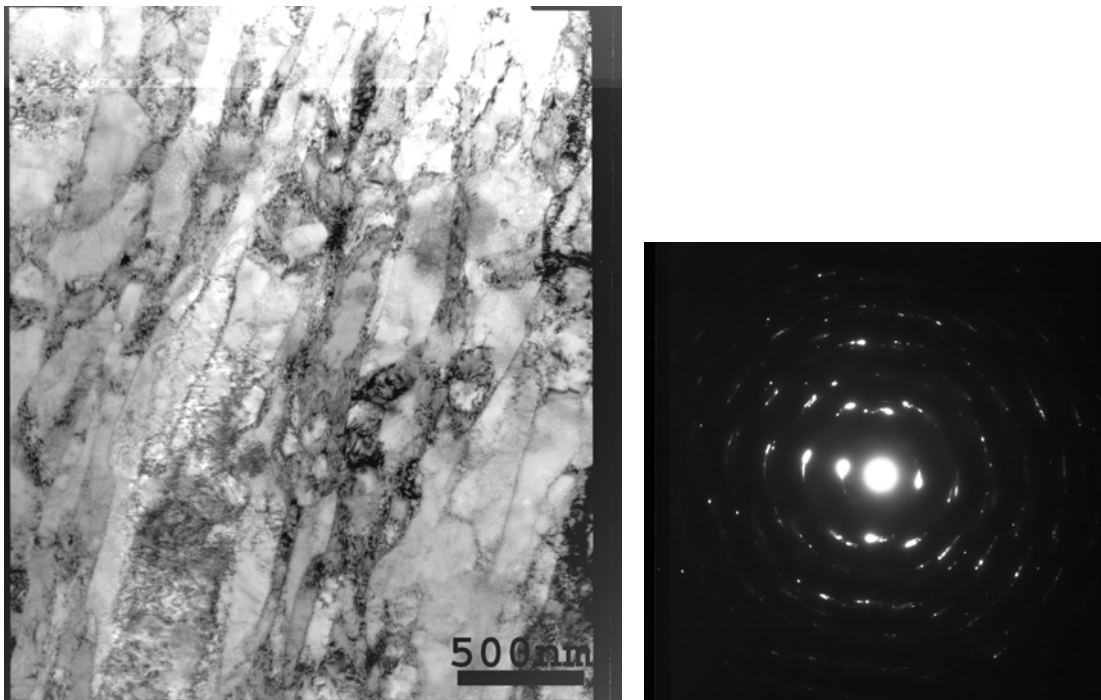


Fig. 67. TEM of CDA 101 Cu in as-worked condition along the flow plane of billet having 50 mm square cross-section processed through route 4E through 90° die at room temperature.

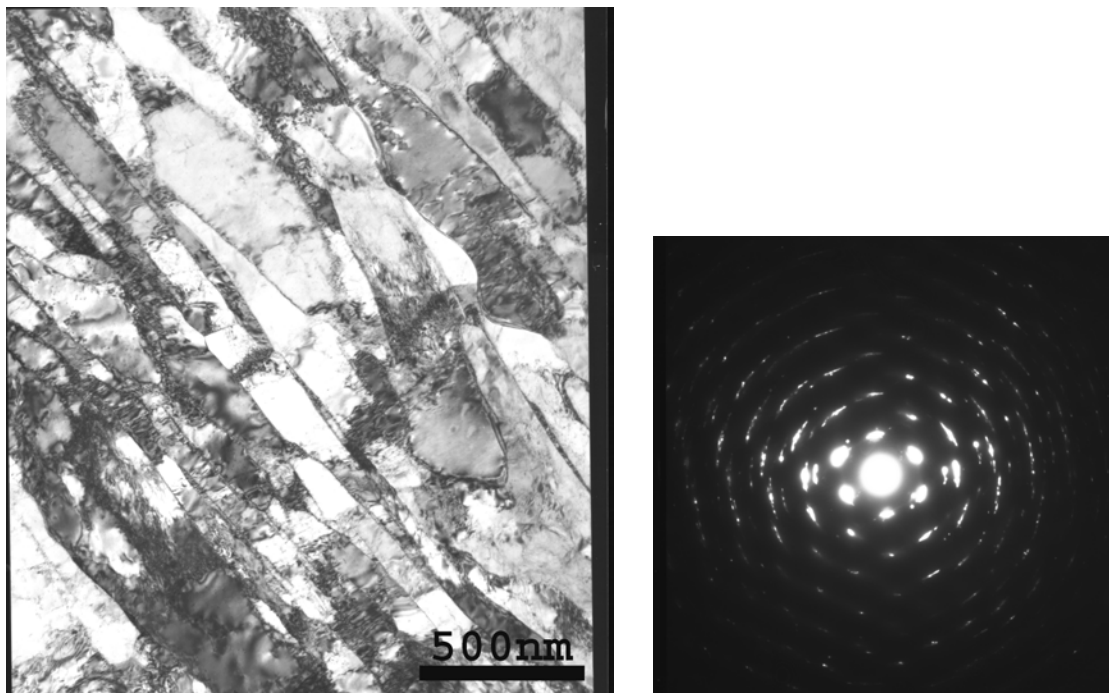


Fig. 68. TEM of CDA 101 Cu in as-worked condition along the flow plane of billet having 25 mm square cross-section processed through route 4E.

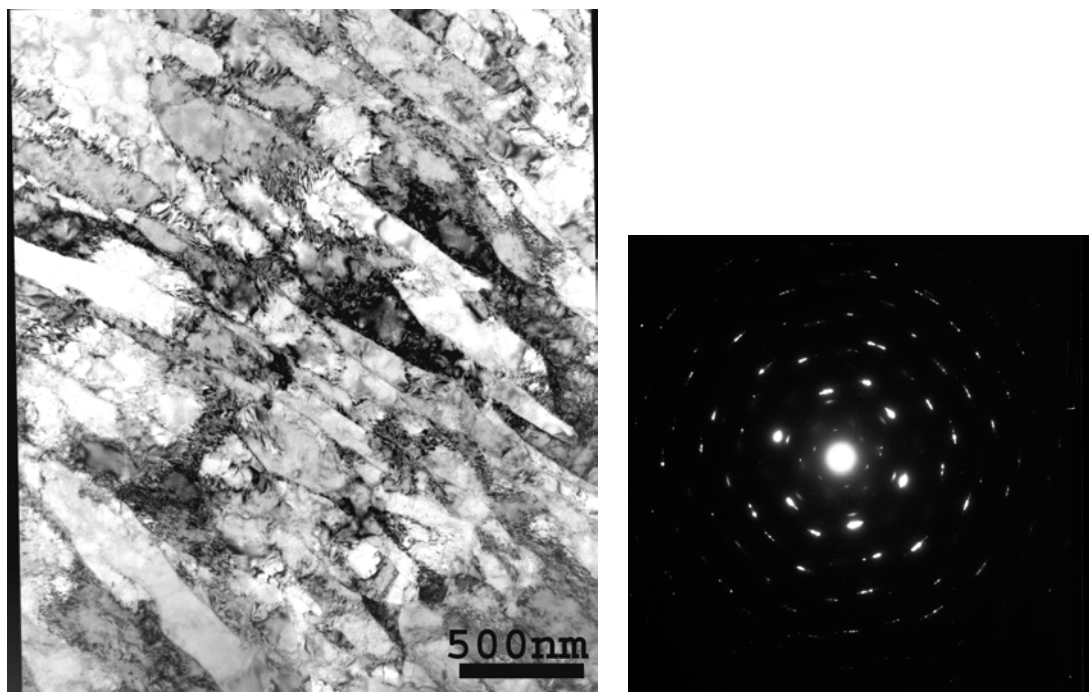


Fig. 69. TEM of CDA 101 Cu in as-worked condition along the flow plane of billet having 19 mm square cross-section processed through route 4E.

Figs. 70-72 show the TEM micrographs obtained for the 50 mm, 25 mm and 19 mm square billets processed through route 8E. Observe that, compared to route 4E, the material shows more refined subgrains. The sub-grain interior has become dislocation free in many cases and the sub-grain walls have become thin. The SAD patterns show a series of fine dots instead of arcs, which indicates that the sub-grains are more misoriented compared to route 4E. The sub-grain boundaries approach misorientation angles comparable to high angle grain boundaries.

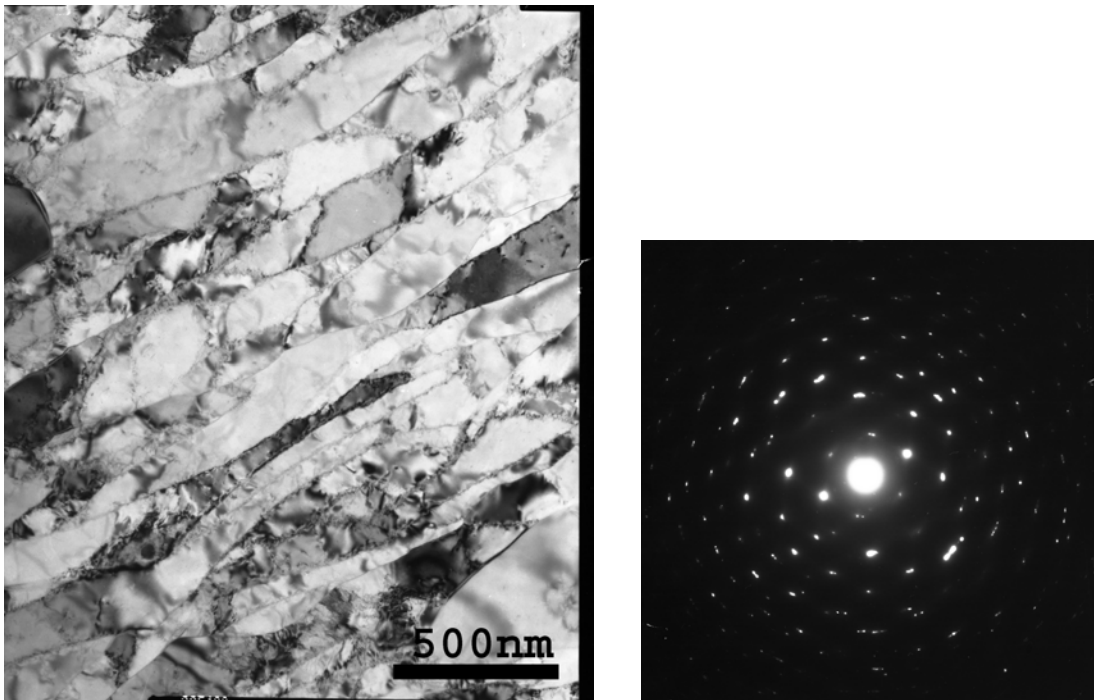


Fig. 70. TEM of CDA 101 Cu in as-worked condition along the flow plane of billet having 50 mm square cross-section processed through route 8E.

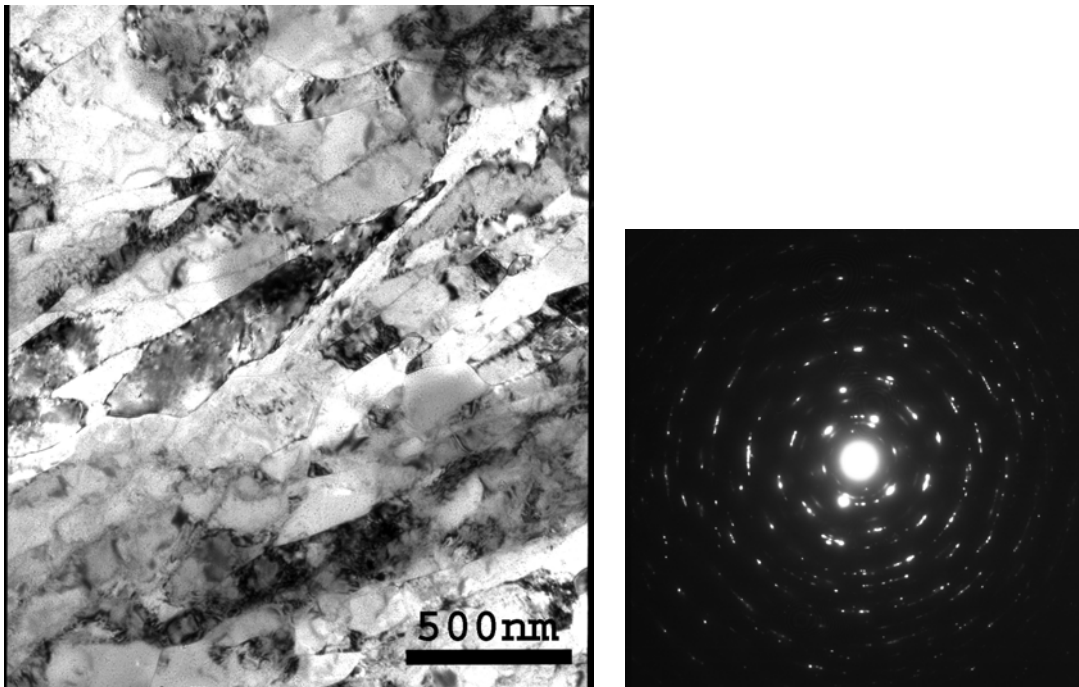


Fig. 71. TEM of CDA 101 Cu in as-worked condition along the flow plane of billet having 25 mm square cross-section processed through route 8E.

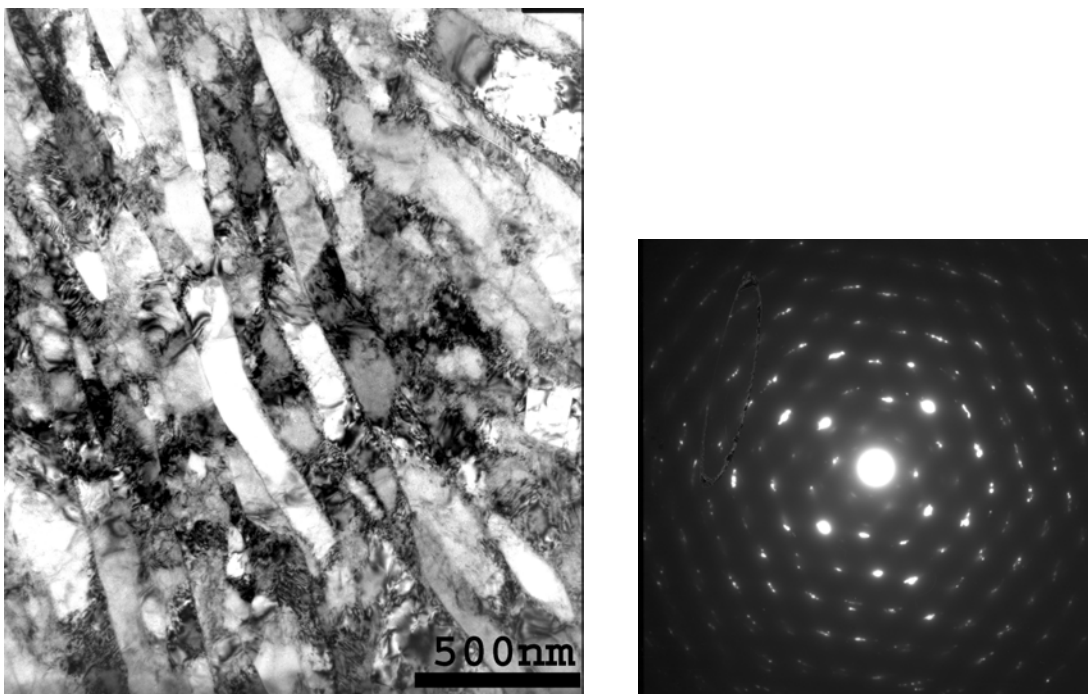


Fig. 72. TEM of CDA 101 Cu in as-worked condition along the flow plane of billet having 19 mm square cross-section processed through route 8E.

4.6.2. Microstructural breakdown project. The TEM micrograph of as-cast CDA 101 Cu is shown in Fig. 73. Unlike the as-worked microstructure, this microstructure is free from dense dislocation structures. It is interesting to observe some dislocations; these dislocations could be either solidification dislocations or could be formed during sample preparation.

The micrographs for Cu processed through routes 1A and 2C are shown in Figs. 74-76. Notice the different sub-microstructures obtained for route 1A. These microstructures were obtained within the same TEM disc, and are very interesting. Some factors that could have played a major role in the creation of such microstructures are discussed in the next chapter.

The sub-microstructure obtained after route 2C is also interesting. It was expected that route 2C will lead to generation of equiaxed subgrains as reversible strain is imparted to the billet. But such was not the case, and elongated subgrains were consistently observed in all the micrographs. Fig. 77 indicates the formation of some equi-axed subgrains after a processing through route 4C. The additional shear strain, and the strain path involving redundant shear may lead to the formation of equi-axed sub-grains in the microstructure.

Figs. 78-91 show TEM micrographs on the flow plane for different processing schedules. One can observe that routes involving IHTs lead to formation of elongated sub-grains with broad and diffuse sub-grain boundaries. Processing without any IHT leads to narrow and sharp boundaries, indicative of their high angle of misorientation. The sub-grain interiors also appear cleaner and free of dislocations with increasing strain and with processing without IHTs. Observe that route 8C without IHT leads to the formation of a microstructure containing equi-axed sub-grains with sharp and well defined boundaries. Similarly route 8Bc without IHT leads to the formation of some equi-axed sub-grains in a matrix of elongated sub-grains.

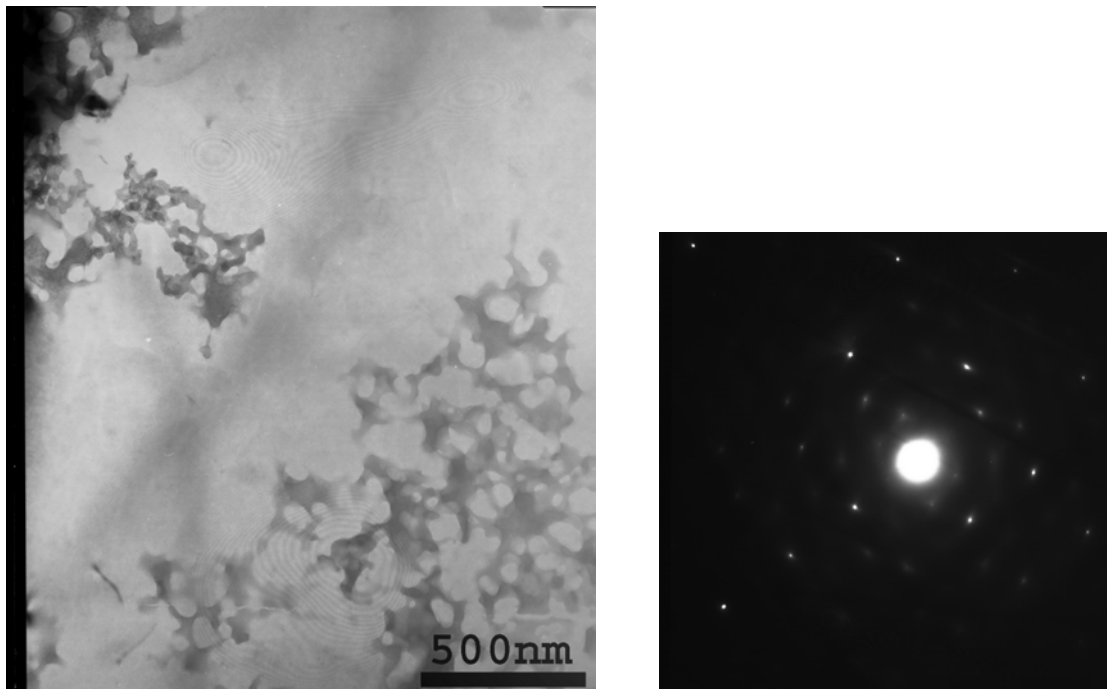


Fig. 73. TEM of as-cast microstructure in CDA 101 copper.

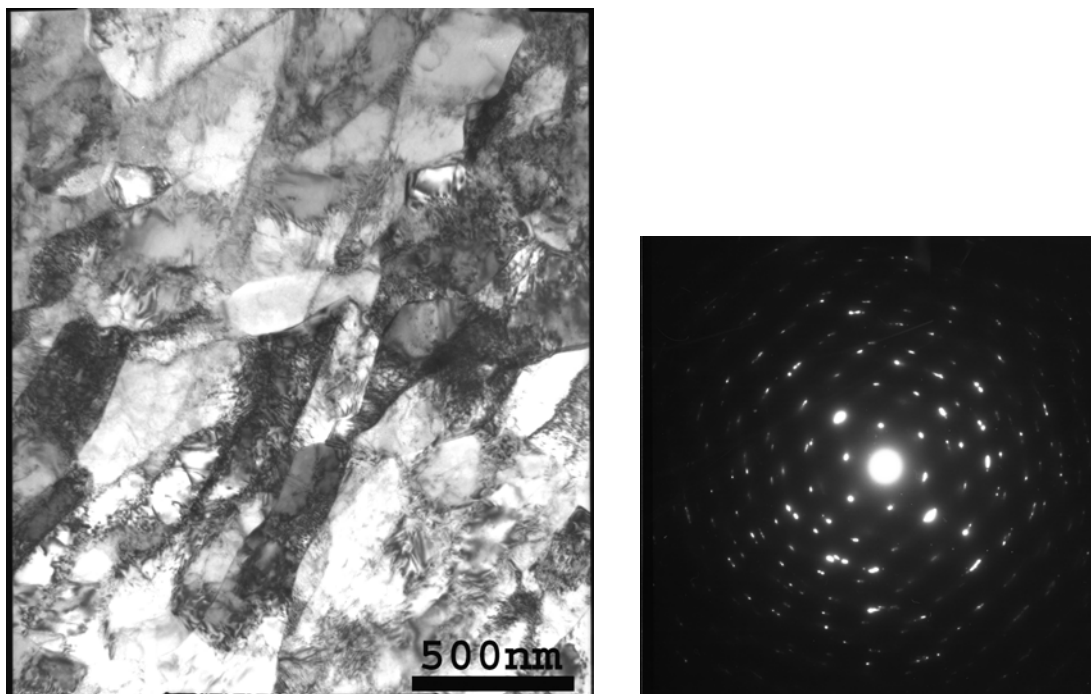


Fig. 74. TEM of CDA 101 Cu in as-worked condition along the flow plane of billet processed through route 1A in a 90° die.

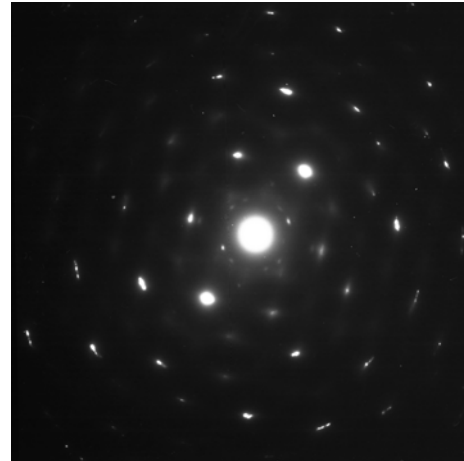
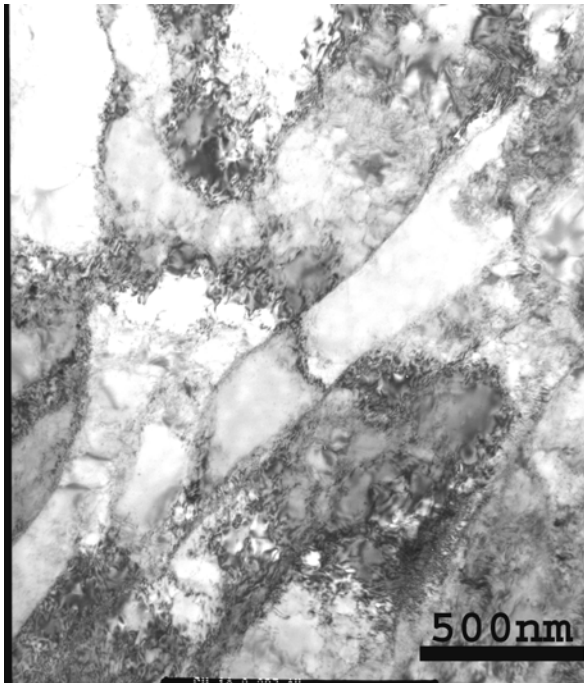


Fig. 75. TEM of CDA 101 Cu in as-worked condition along the flow plane of billet processed through route 1A in a 90° die.

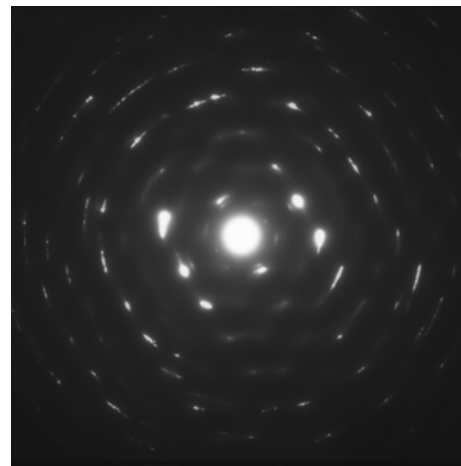


Fig. 76. TEM of CDA 101 Cu in as-worked condition along the flow plane of billet processed through route 2C in a 90° die.

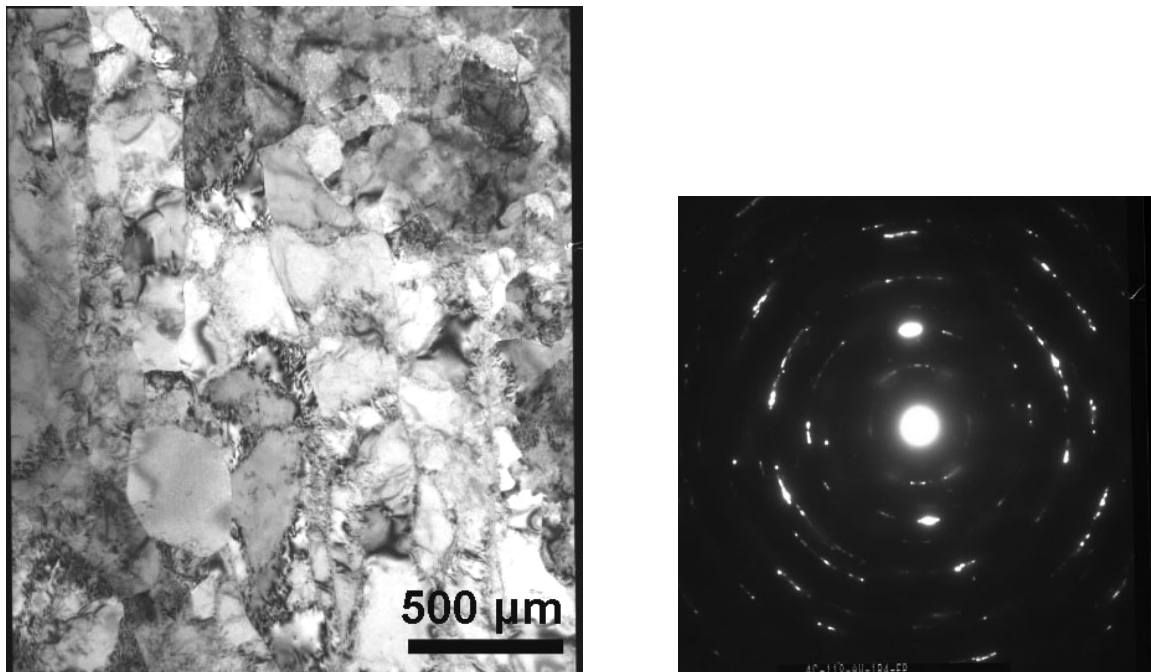


Fig. 77. TEM of CDA 101 Cu in as-worked condition along the flow plane of billet processed through route 4C in a 90° die.

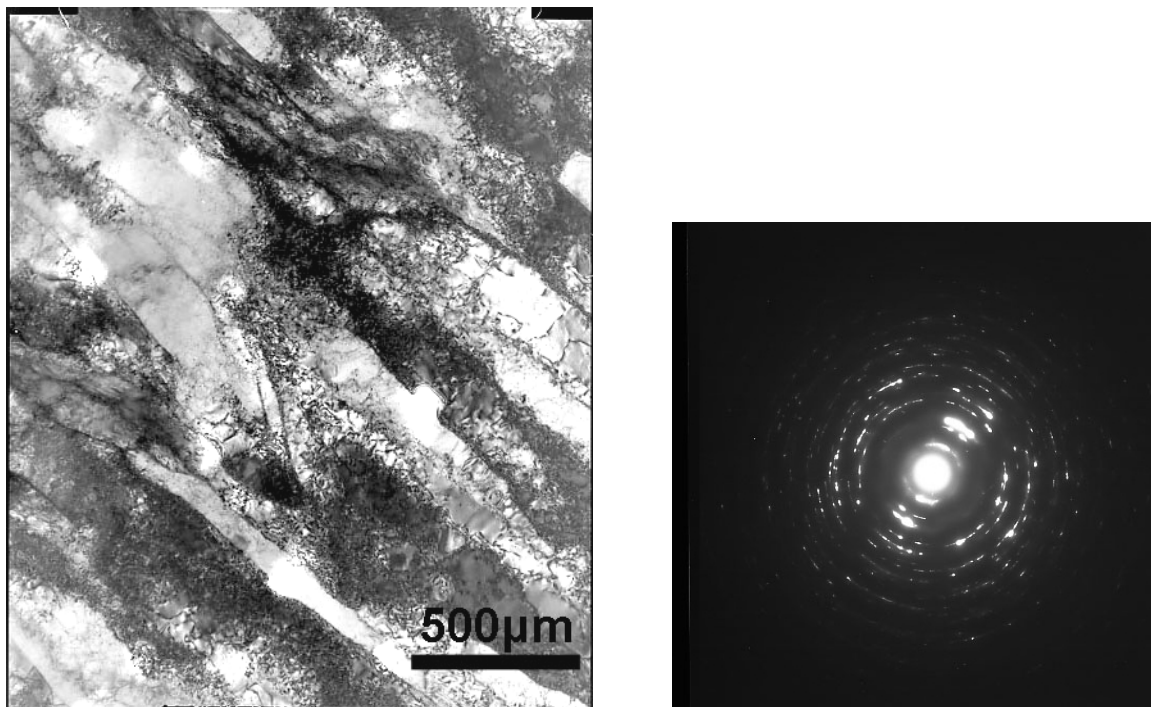


Fig. 78. TEM of CDA 101 Cu in as-worked condition along the flow plane of billet processed through TMP schedule 2C-400°C-2C.

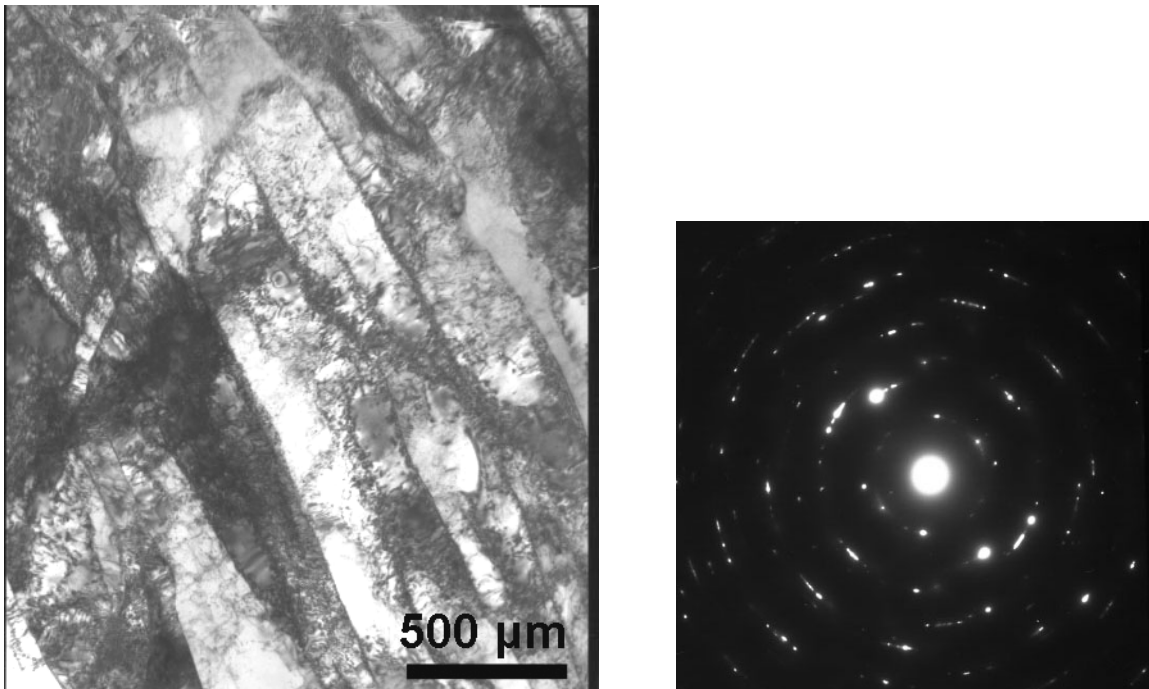


Fig. 79. TEM of CDA 101 Cu in as-worked condition along the flow plane of billet processed through route 2E-350°C-2E.

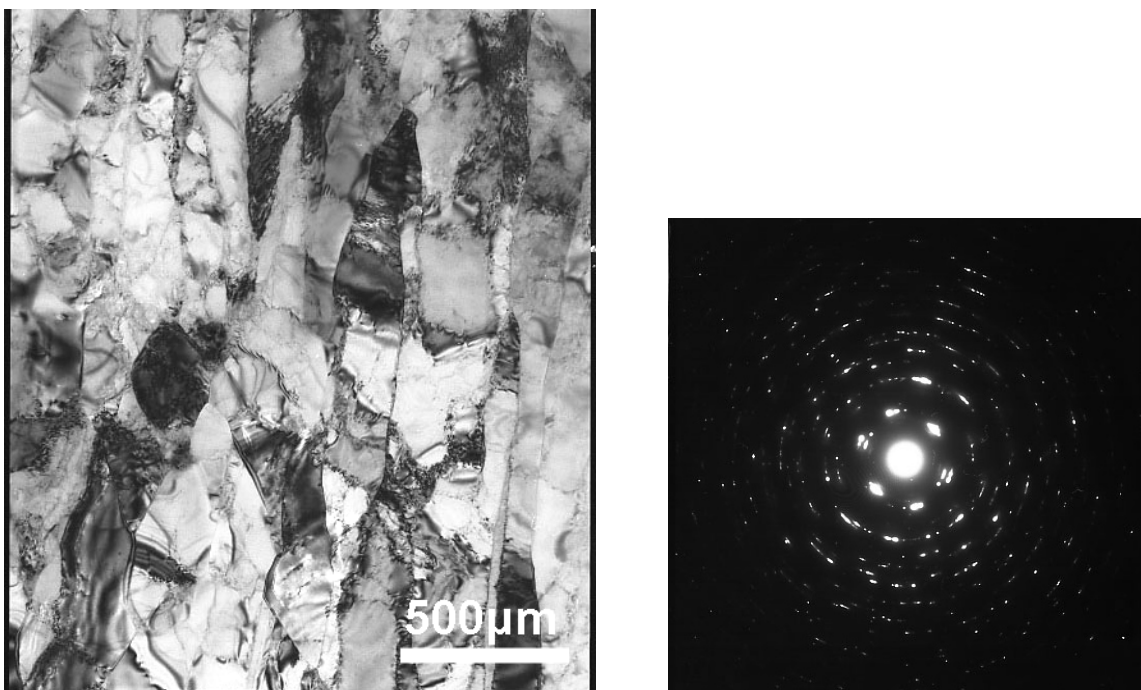


Fig. 80. TEM of CDA 101 Cu in as-worked condition along the flow plane of billet processed through route 4F in a 90° die.

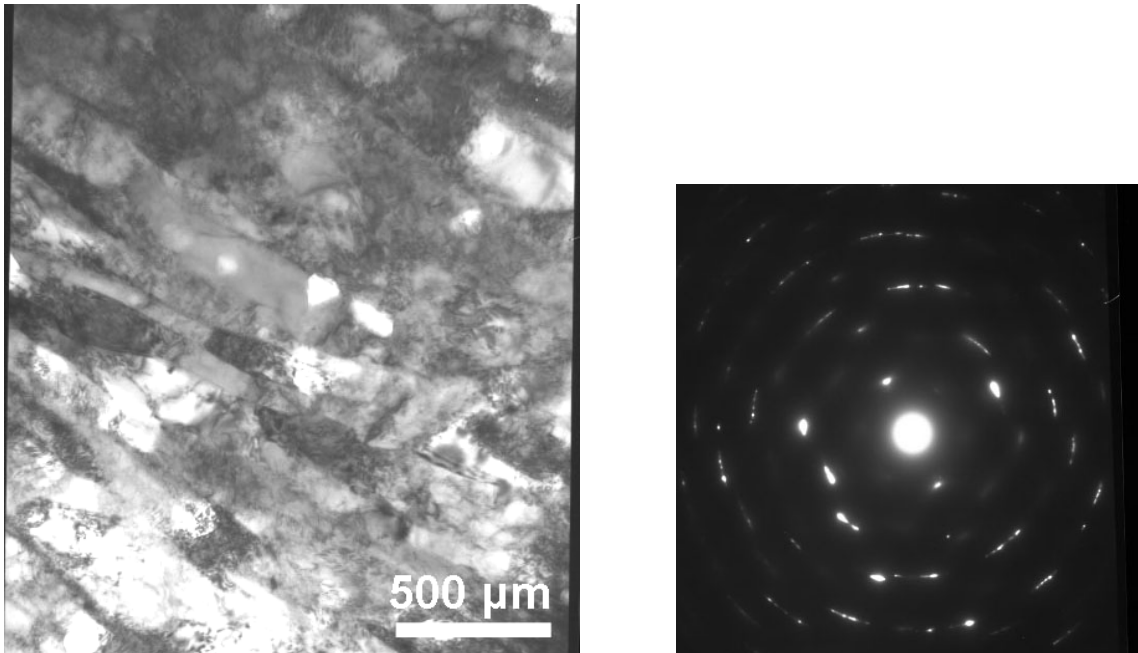


Fig. 81. TEM of CDA 101 Cu in as-worked condition along the flow plane of billet processed through route 2F-400°C-2F.

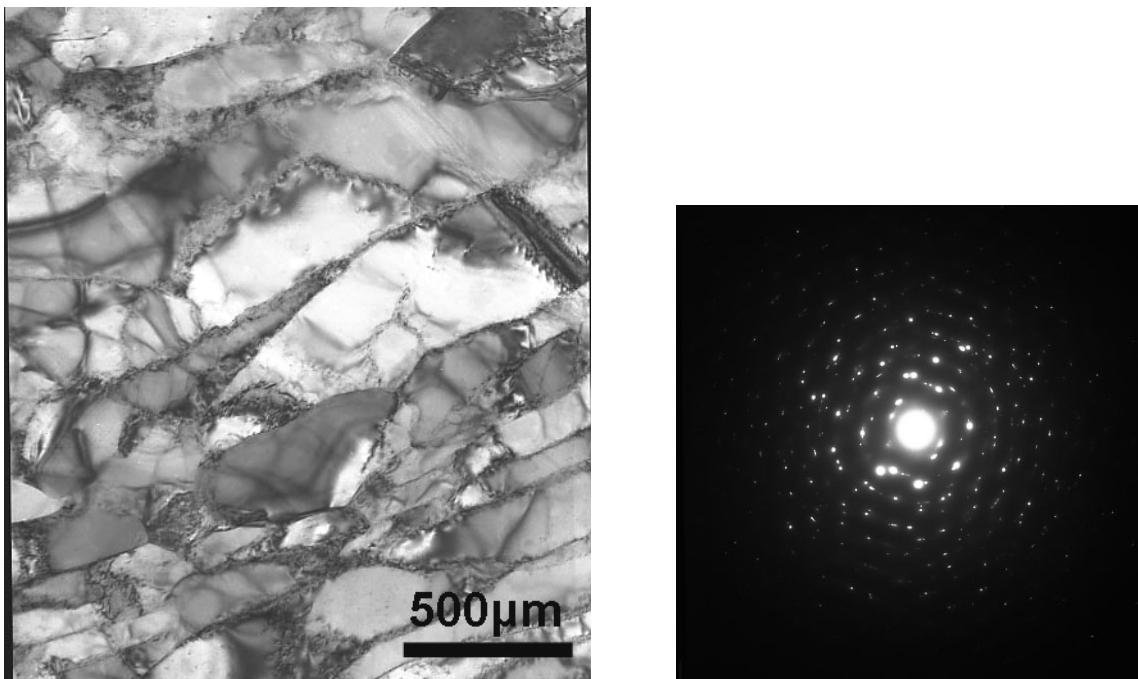


Fig. 82. TEM of CDA 101 Cu in as-worked condition along the flow plane of billet processed through route 4Bc in a 90° die.

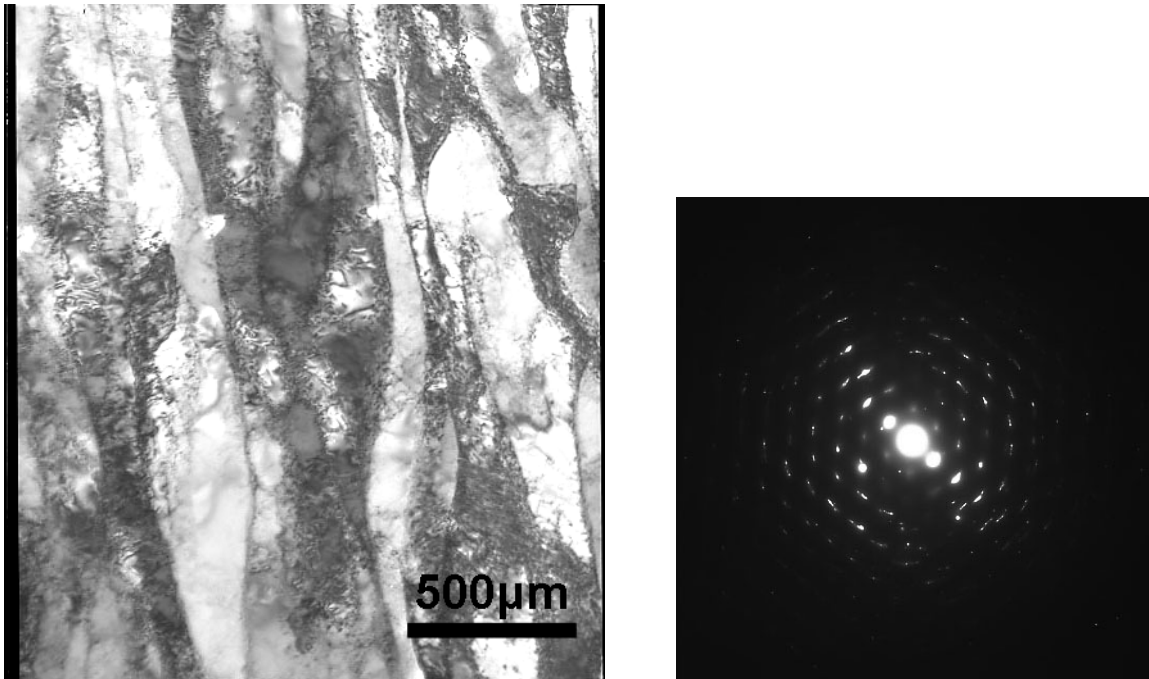


Fig. 83. TEM of CDA 101 Cu in as-worked condition along the flow plane of billet processed through route 2Bc-400°C-2Bc.

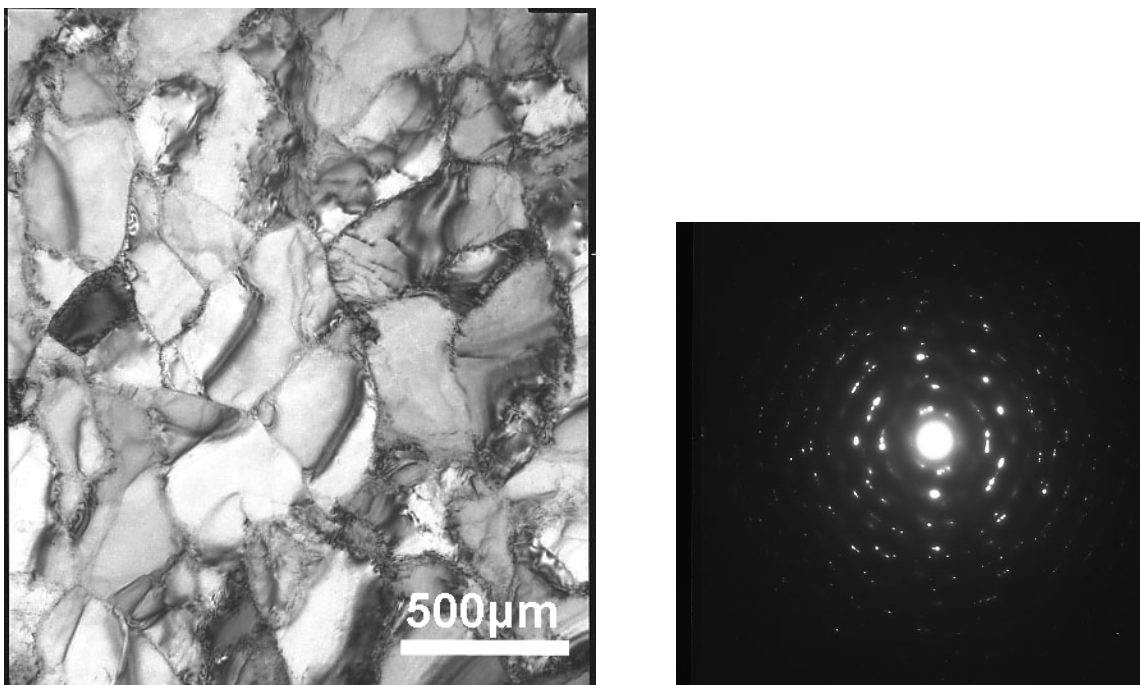


Fig. 84. TEM of CDA 101 Cu in as-worked condition along the flow plane of billet processed through route 8C in a 90° die.

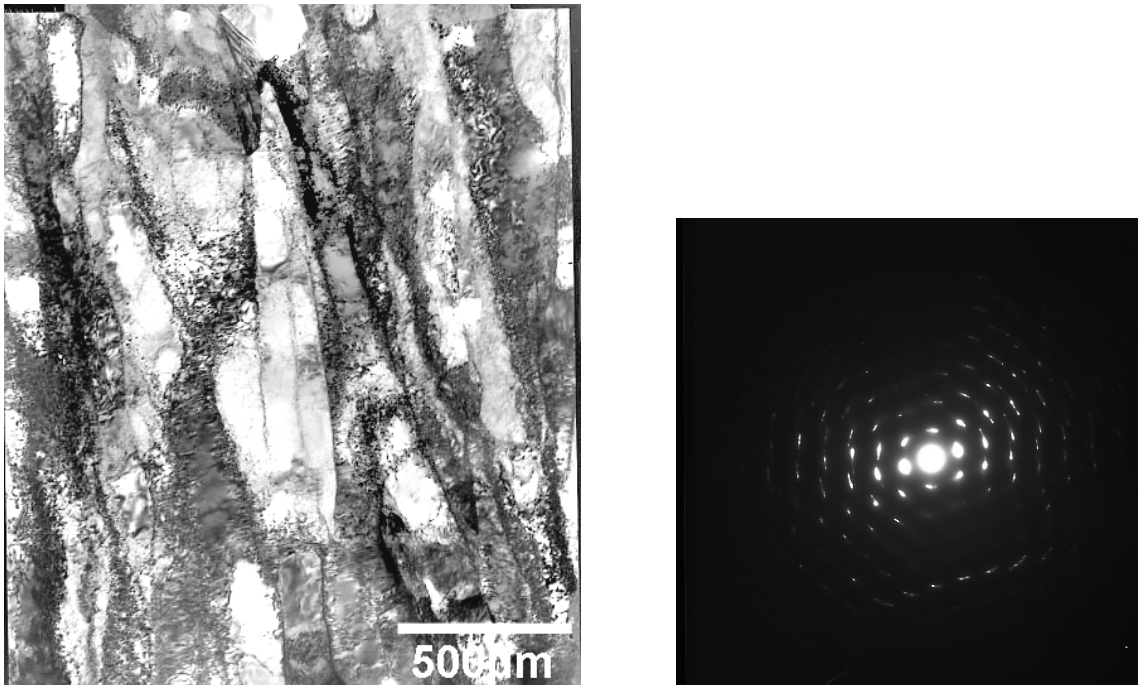


Fig. 85. TEM of CDA 101 Cu in as-worked condition along the flow plane of billet processed through route 2E-400°C-2E-300°C-2E-200°C-2E.

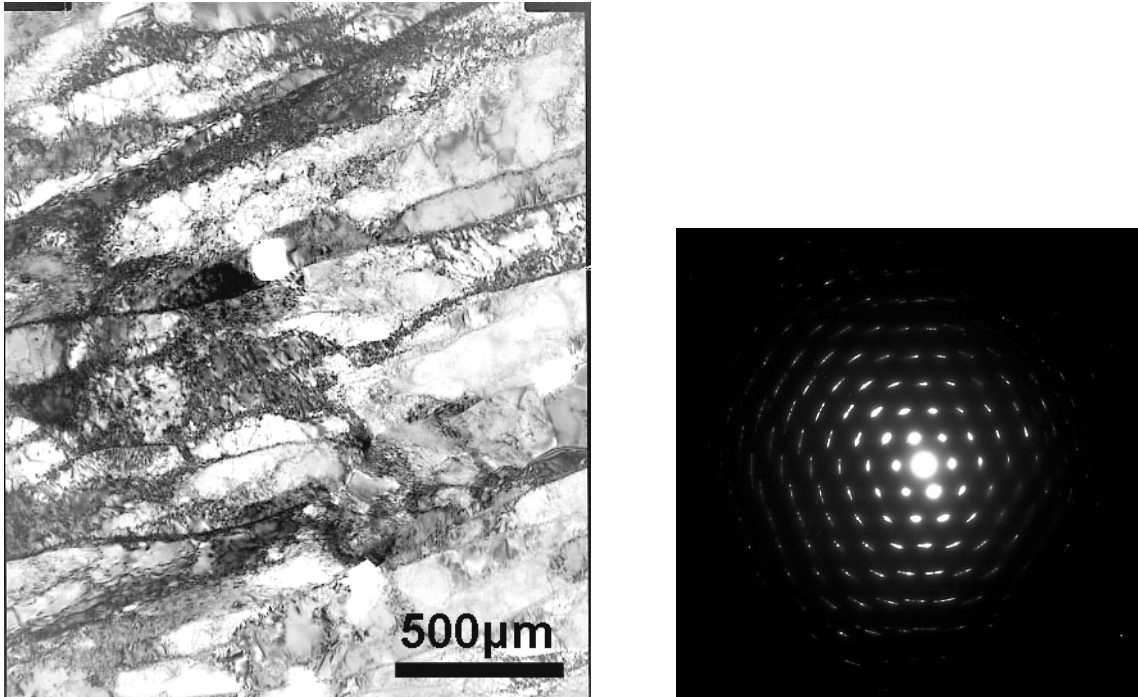


Fig. 86. TEM of CDA 101 Cu in as-worked condition along the flow plane of billet processed through route 2E-350°C-2E-350°C-2E-350°C-2E.

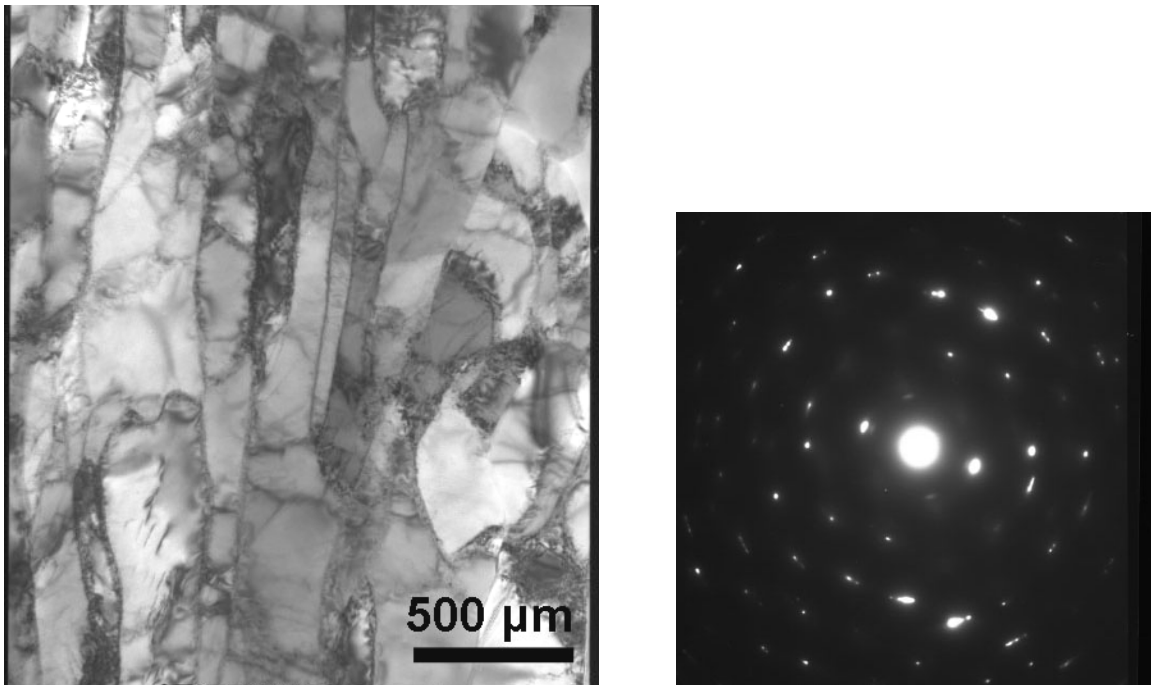


Fig. 87. TEM of CDA 101 Cu in as-worked condition along the flow plane of billet processed through route 8F in a 90° die.

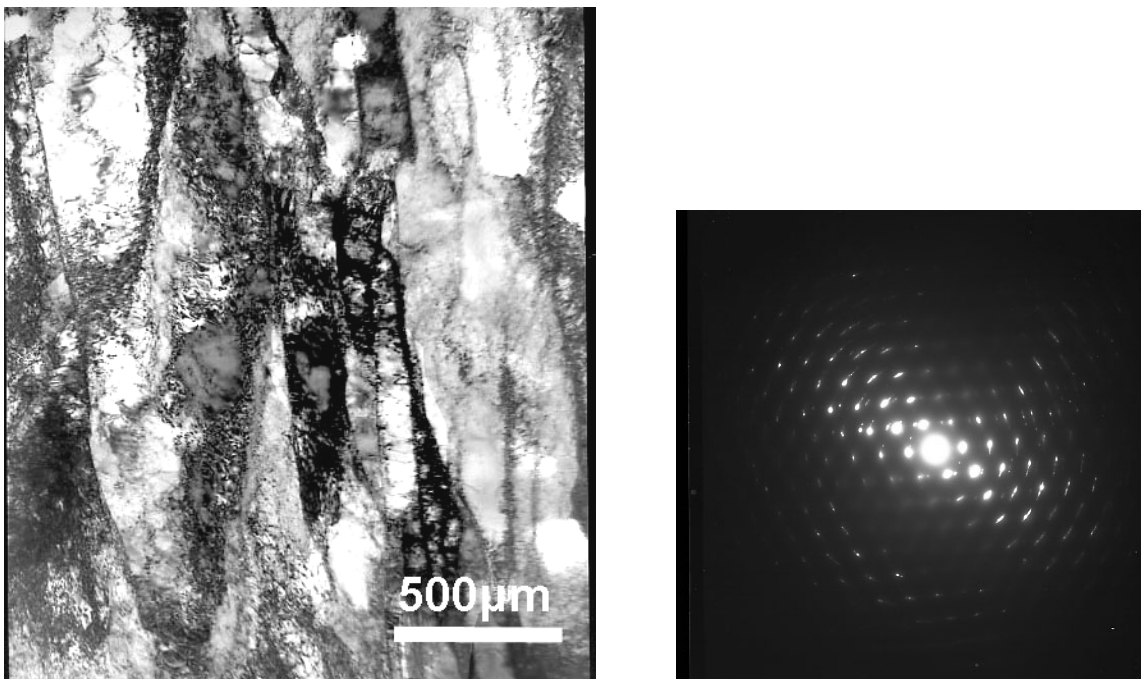


Fig. 88. TEM of CDA 101 Cu in as-worked condition along the flow plane of billet processed through route 2F-400°C-2F-300°C- 2F-200°C-2F.

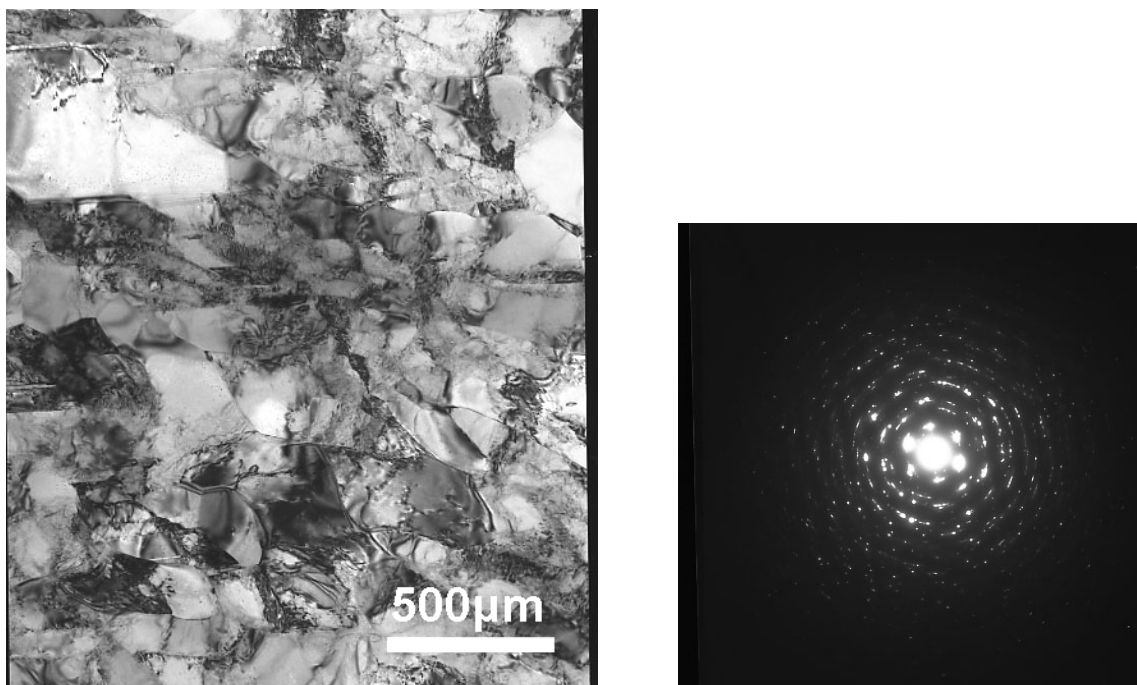


Fig. 89. TEM of CDA 101 Cu in as-worked condition along the flow plane of billet processed through route 8Bc in a 90° die.

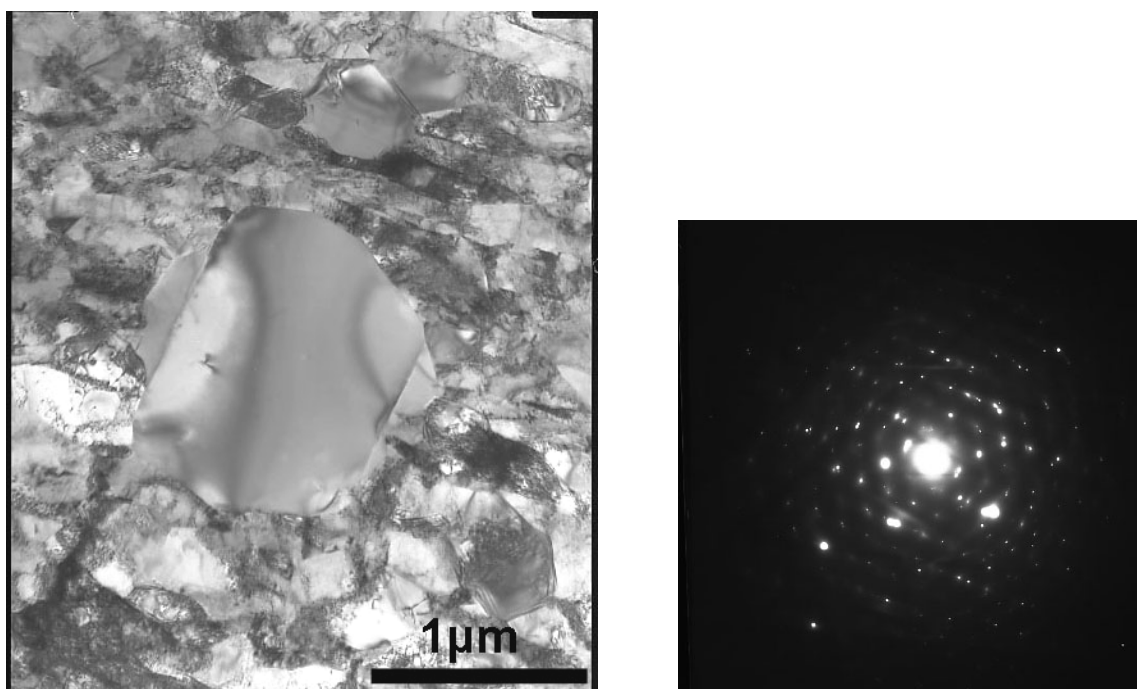


Fig. 90. TEM of CDA 101 Cu in as-worked condition along the flow plane of billet processed through route 8Bc in a 90° die.

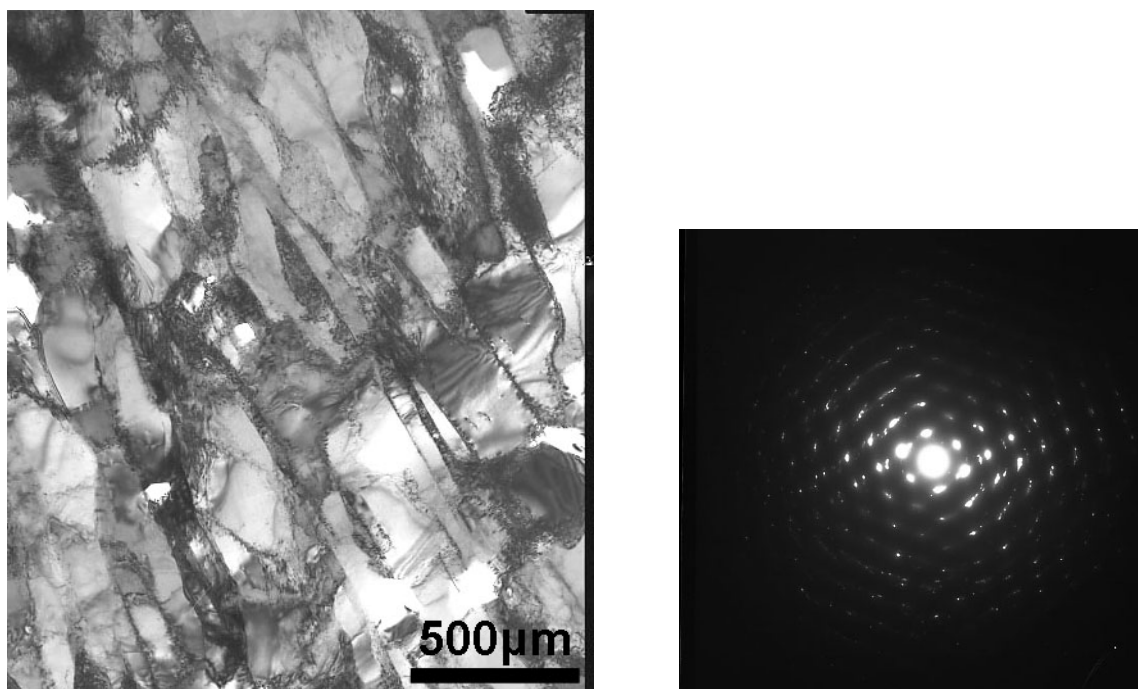


Fig. 91. TEM of CDA 101 Cu in as-worked condition along the flow plane of billet processed through route 2Bc-400°C-2Bc-300°C-2Bc-200°C-2Bc.

4.6.3. Recrystallization TEM. Transmission electron microscopy of recrystallizing microstructures was done in order to understand the changes occurring at a sub-grain level during this process. Some interesting results were obtained, Figs. 92-98 indicate the evolution of microstructure during recrystallization. The material selected for this study was processed through route 4E without intermediate heat treatments, and the flow plane was examined for all the samples. It is interesting to notice that little change is observed in the microstructures even after a heat treatment of 170°C for one hour. But upon annealing at 180°C, the microstructure starts to evolve abruptly and large strain free subgrains begin to grow in the strained matrix. Some recrystallization (annealing) twins are also observed in the recrystallized grains. With further increase in temperature, these recrystallized grains grow in size. The SAD patterns also indicate the evolution of the microstructure, as the arcs in the patterns are replaced by bright dots which indicate the formation of high angle boundaries.

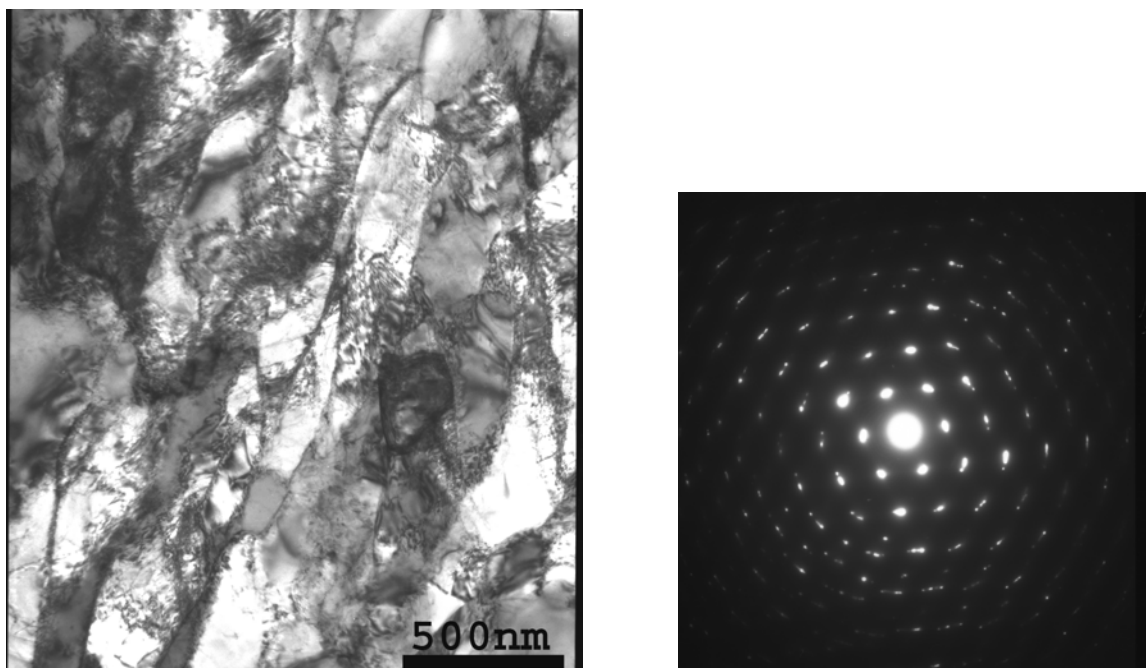


Fig. 92. TEM of CDA 101 Cu processed through route 4E and heat treated at 100°C for 60 minutes.

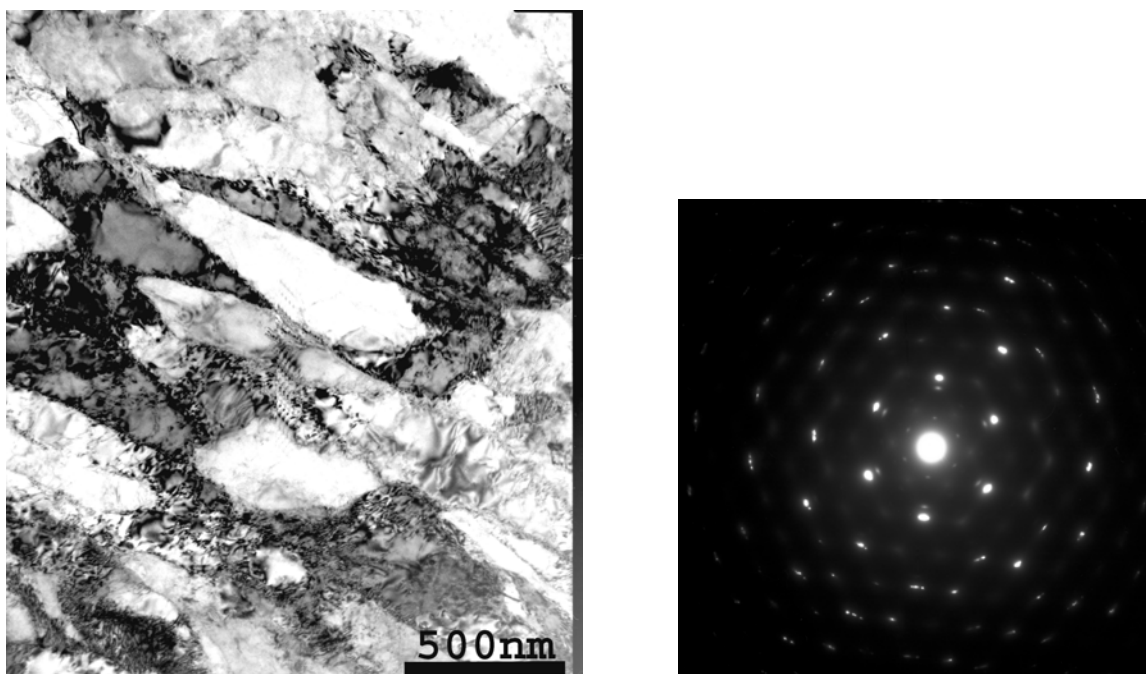


Fig. 93. TEM of CDA 101 Cu processed through route 4E and heat treated at 150°C for 60 minutes.

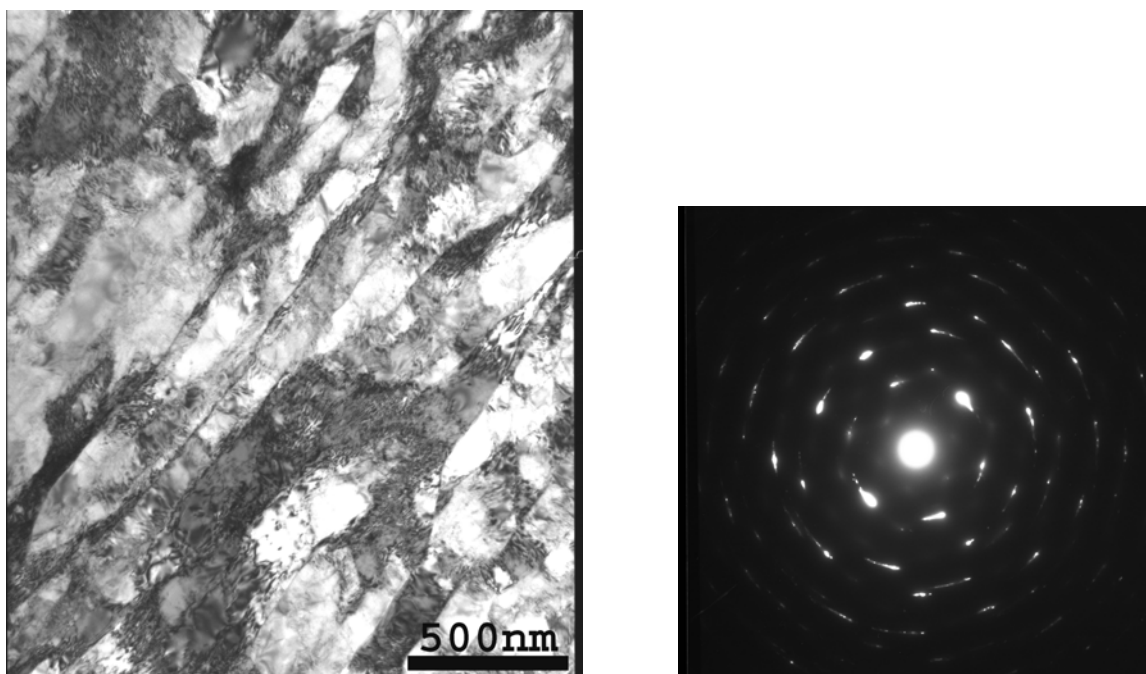


Fig. 94. TEM of CDA 101 Cu processed through route 4E and heat treated at 170°C for 60 minutes.

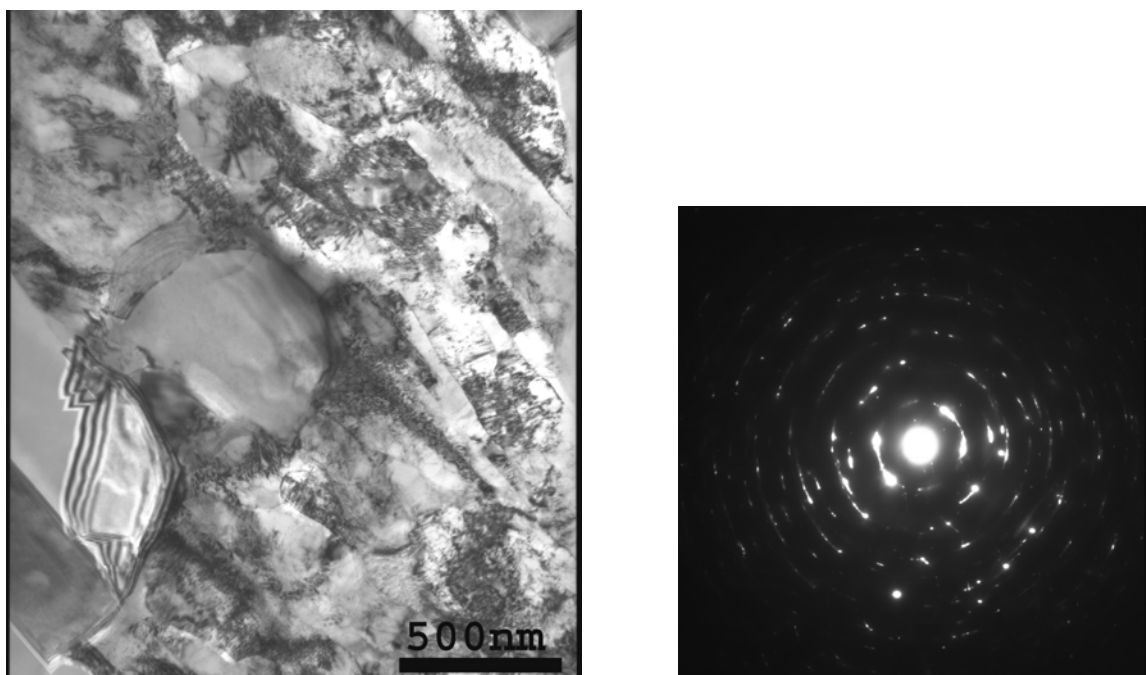


Fig. 95. TEM of CDA 101 Cu processed through route 4E and heat treated at 180°C for 60 minutes.

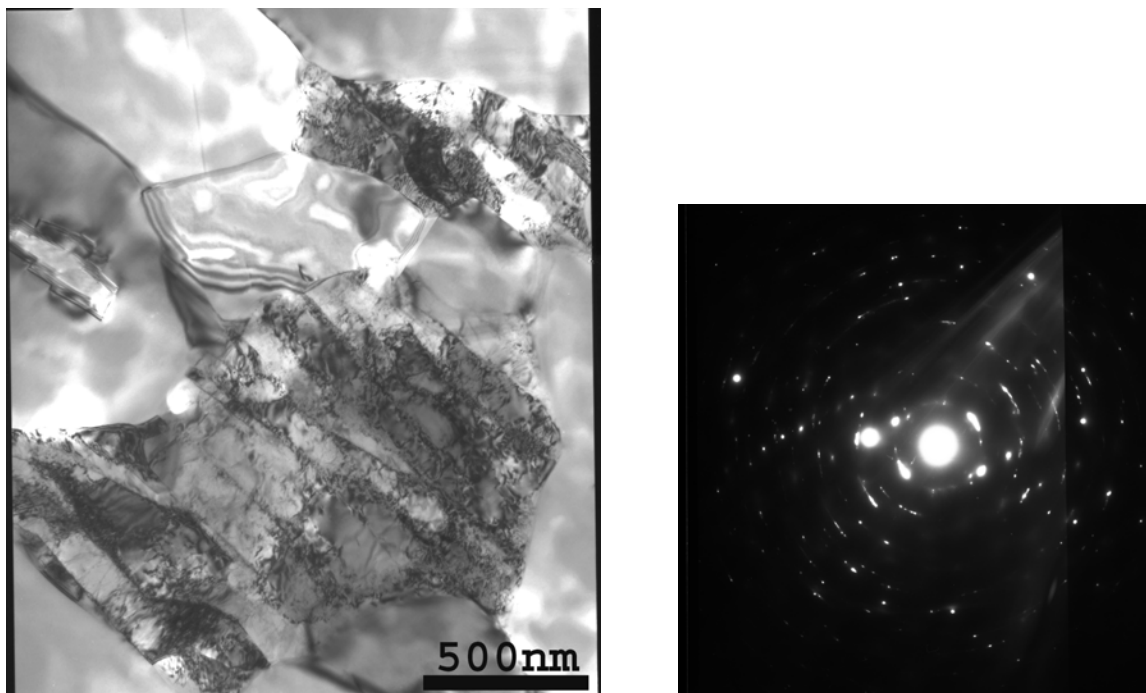


Fig. 96. TEM of CDA 101 Cu processed through route 4E and heat treated at 190°C for 60 minutes.

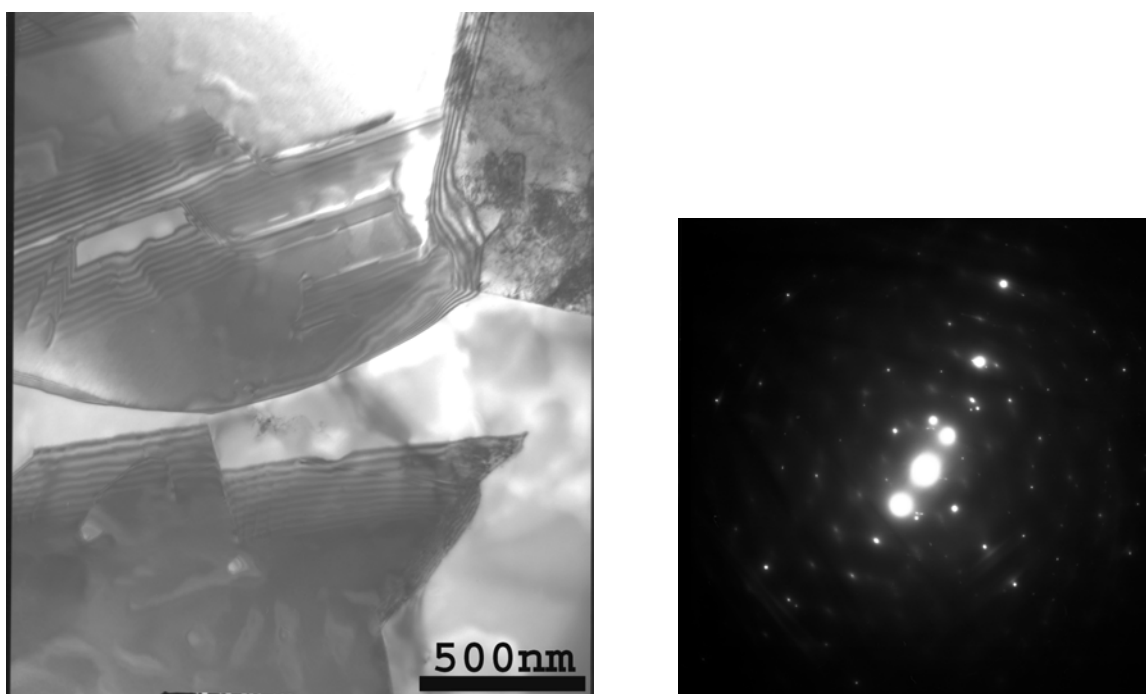


Fig. 97. TEM of CDA 101 Cu processed through route 4E and heat treated at 190°C for 60 minutes.

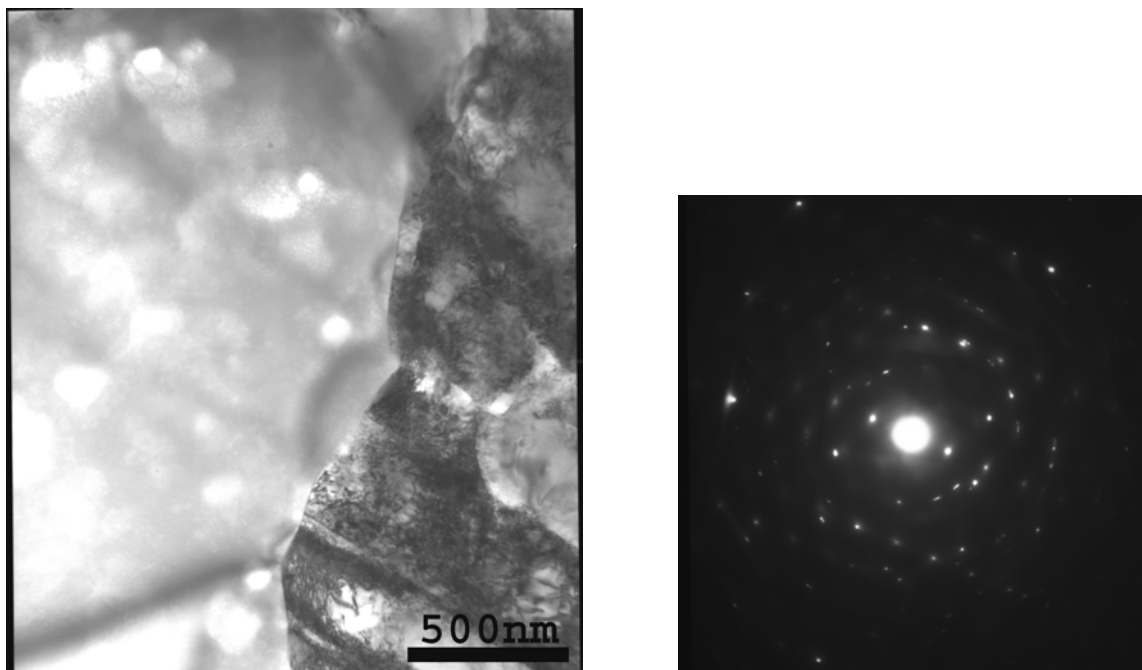
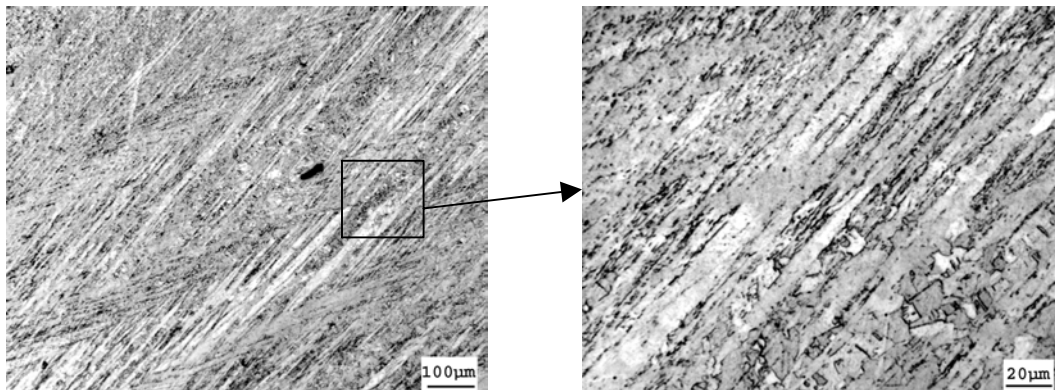


Fig. 98. TEM of CDA 101 Cu processed through route 4E and heat treated at 200°C for 60 minutes.

4.7. Optical microscopy

Optical microscopy forms a very important part of this research, especially for the second part of the project which deals with grain refinement of as-cast Cu. Optical micrographs were obtained and analyzed for all the recrystallized material.

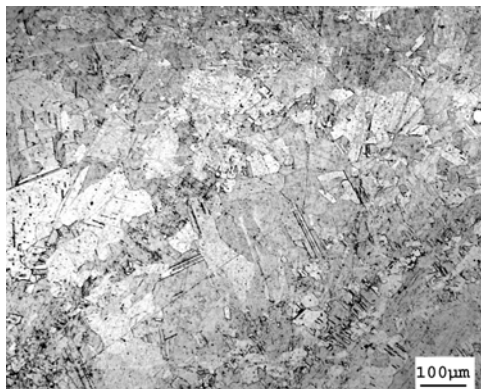
4.7.1. Scale-up project. The partially recrystallized microstructure of as-cast CDA 101 Cu processed to 1A extrusion pass is shown in Fig. 99. The microstructure is characterized by shear bands which are inclined to the flow plane at an angle of 45°. Notice that recrystallization in some regions has already started and some recrystallized grains are visible within the shear bands. The fully recrystallized microstructure for Cu processed through route 1A is shown in Fig. 100. The microstructure is characterized by a very inhomogeneous grain structure, some grains which may have originated from the shear bands are much smaller in size compared to others. The grain size histogram confirms this. Notice that ~ 40% of the analyzed microstructure is occupied by grains having sizes greater than 50 μm .



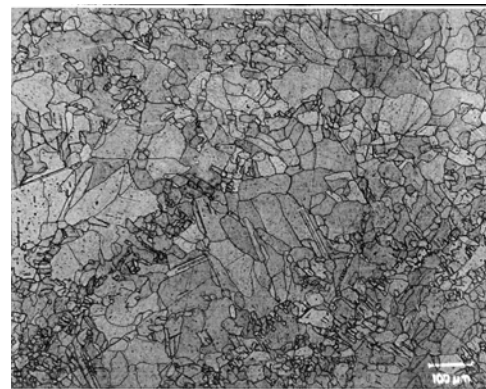
(a)

(b)

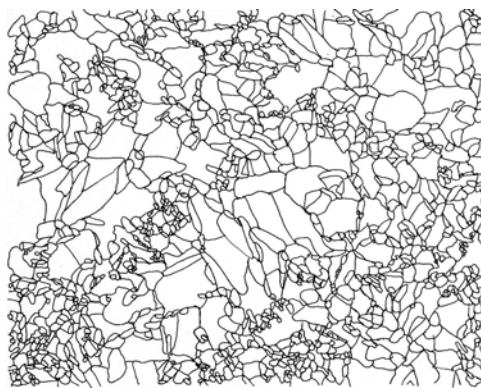
Fig 99. Optical micrograph of CDA 101 Cu processed through 1A extrusion route and annealed at 175°C for 60 min. (a) 20X and (b) 100X.



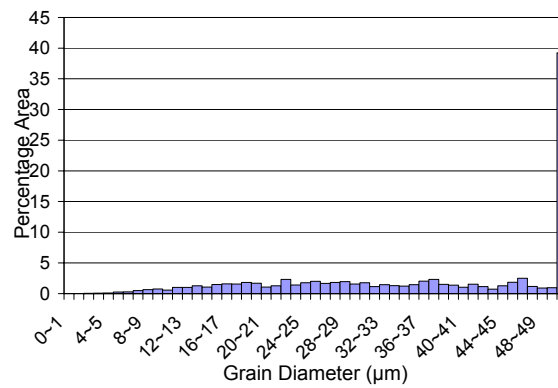
(a)



(b)



(c)



(d)

Fig. 100. (a) Optical micrograph of CDA 101 Cu processed through 1A extrusion route in fully recrystallized condition, (b) Scanned image of (a) with grain boundaries delineated, (c) trace of grain boundaries for micrograph (a), (d) grain size histogram for micrograph (a).

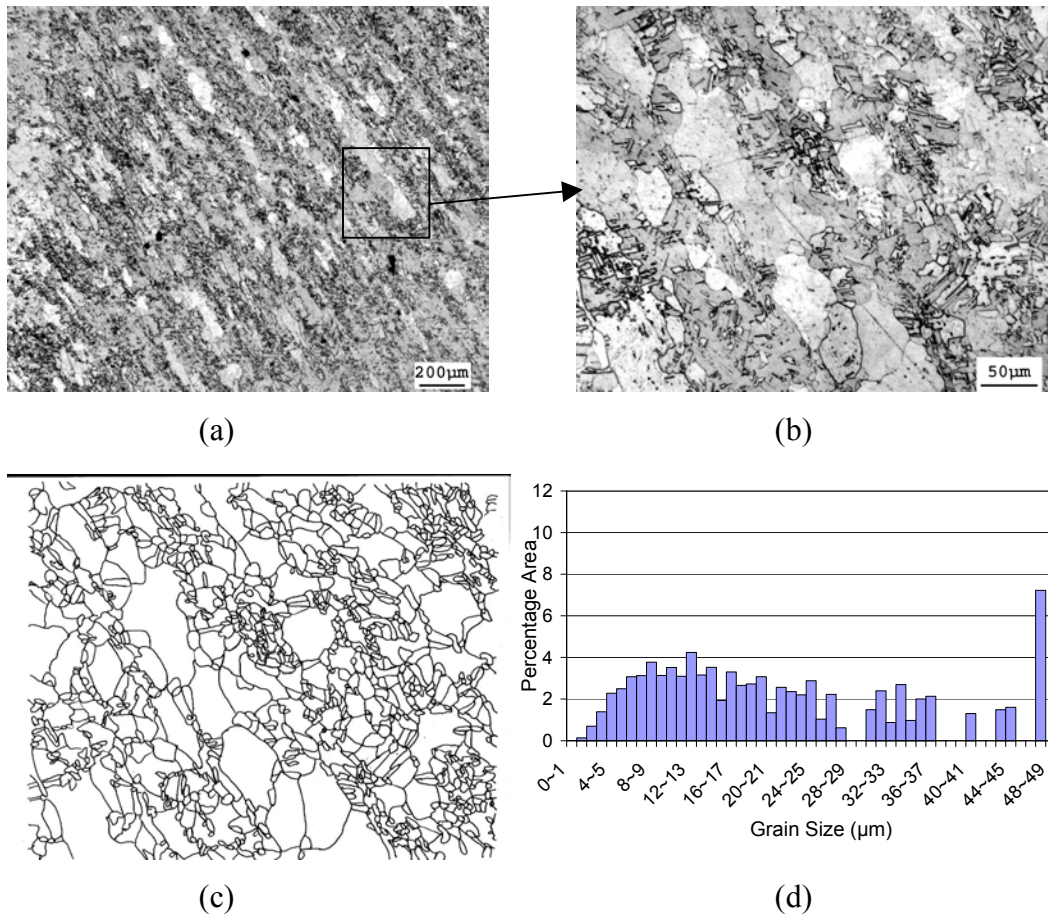


Fig. 101. (a) Optical micrograph of CDA 101 Cu processed through 2C extrusion route in fully recrystallized condition, (b) Scanned image of (a) with grain boundaries delineated, (c) Trace of grain boundaries for micrograph (a), (d) grain size histogram for (a).

Fig. 101 shows the microstructure of a 25 mm square cross section Cu billet processed through 2C extrusion route and annealed to complete recrystallization. Notice the formation of alternate bands of large and small grains in the fully recrystallized condition. These bands are the effects of macroscopic shear bands generated during deformation in the material. The fully recrystallized microstructure generated in a 50 mm square billet after being deformed through route 2C is shown in Fig. 102.

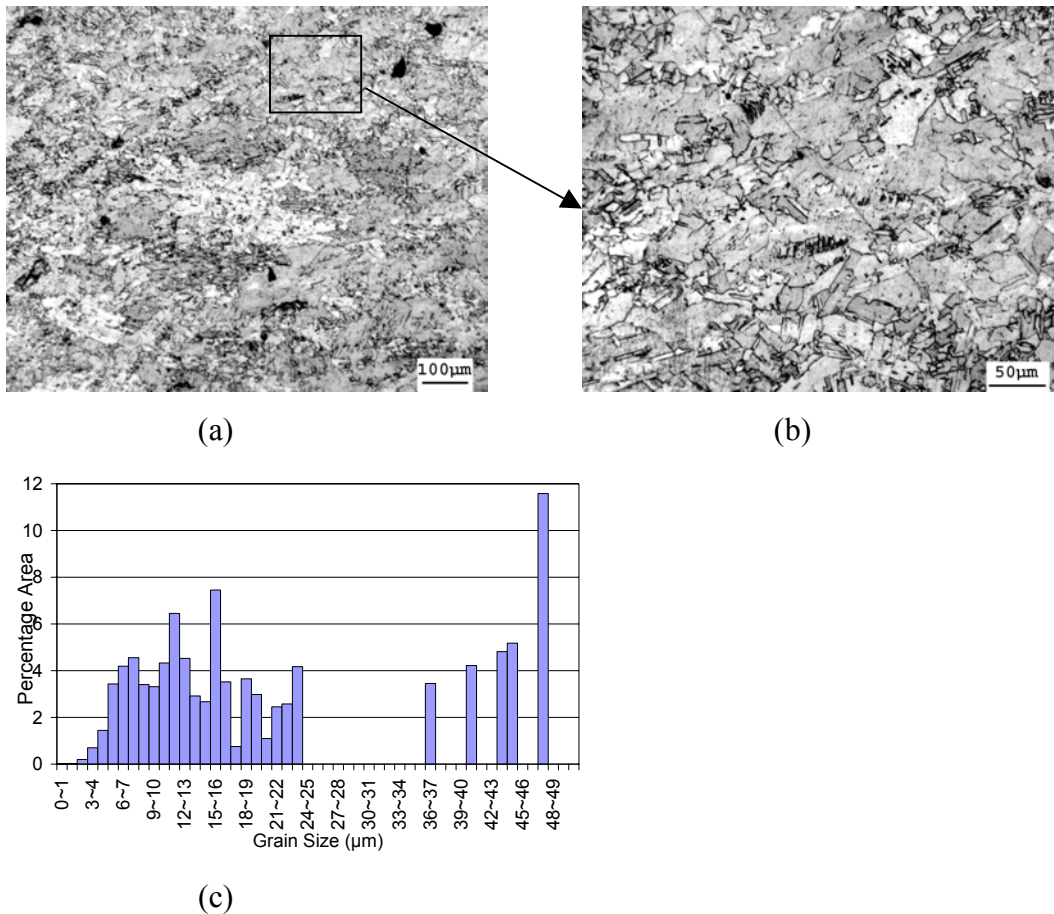
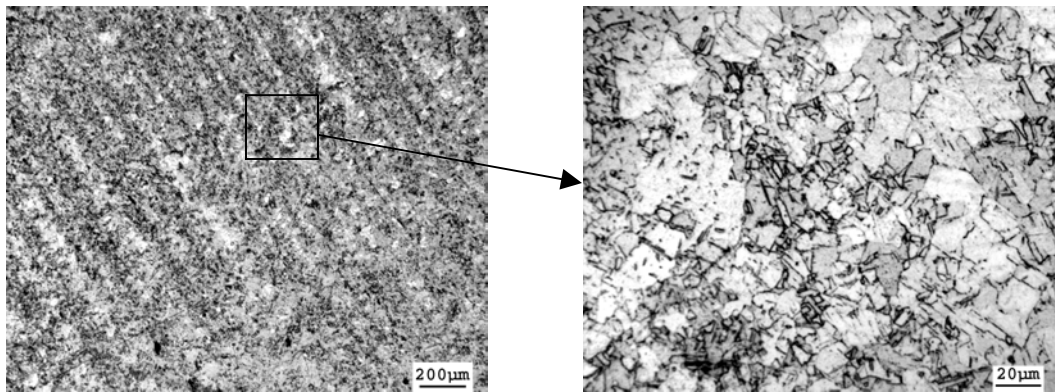


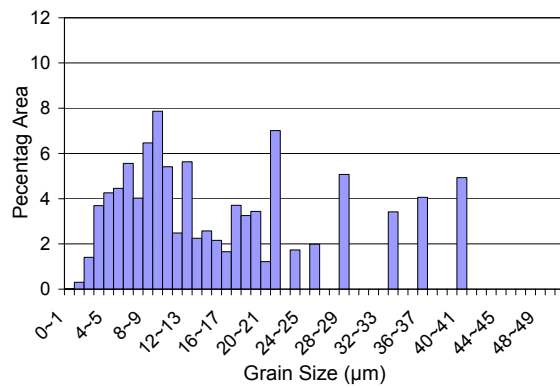
Fig. 102. Optical micrograph of CDA 101 Cu processed through 2C extrusion route in fully recrystallized condition, billet has 50 mm square cross-section. (a) 20X magnification, (b) 50X magnification, (c) typical grain size histogram.

Microstructures obtained after an extrusion through route 4A are shown in Figs. 103-105. Again notice the formation of macroscopic shear bands along the flow plane. Fig. 104 is a partially recrystallized microstructure obtained in billet with 50 mm square cross-section. Notice the inclination of the shear bands along the flow plane.



(a)

(b)



(c)

Fig. 103. Optical micrograph of CDA 101 Cu processed through 4A extrusion route in fully recrystallized condition, billet has 25 mm square cross-section. (a) 10X magnification, (b) 100X magnification, (c) typical grain size histogram.

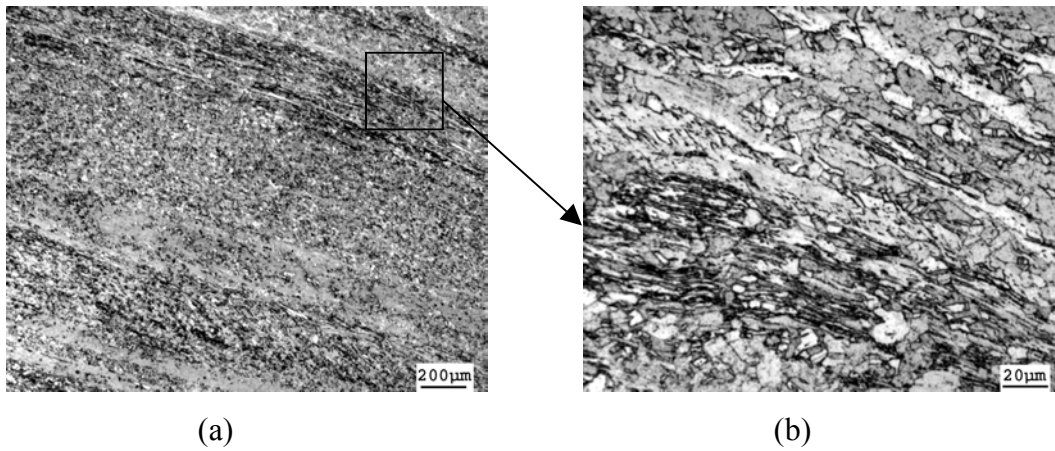


Fig. 104. Optical micrograph of CDA 101 Cu processed through 4A extrusion route in partially recrystallized condition, billet has 50 mm square cross-section. (a) 20X magnification, (b) 100X magnification.

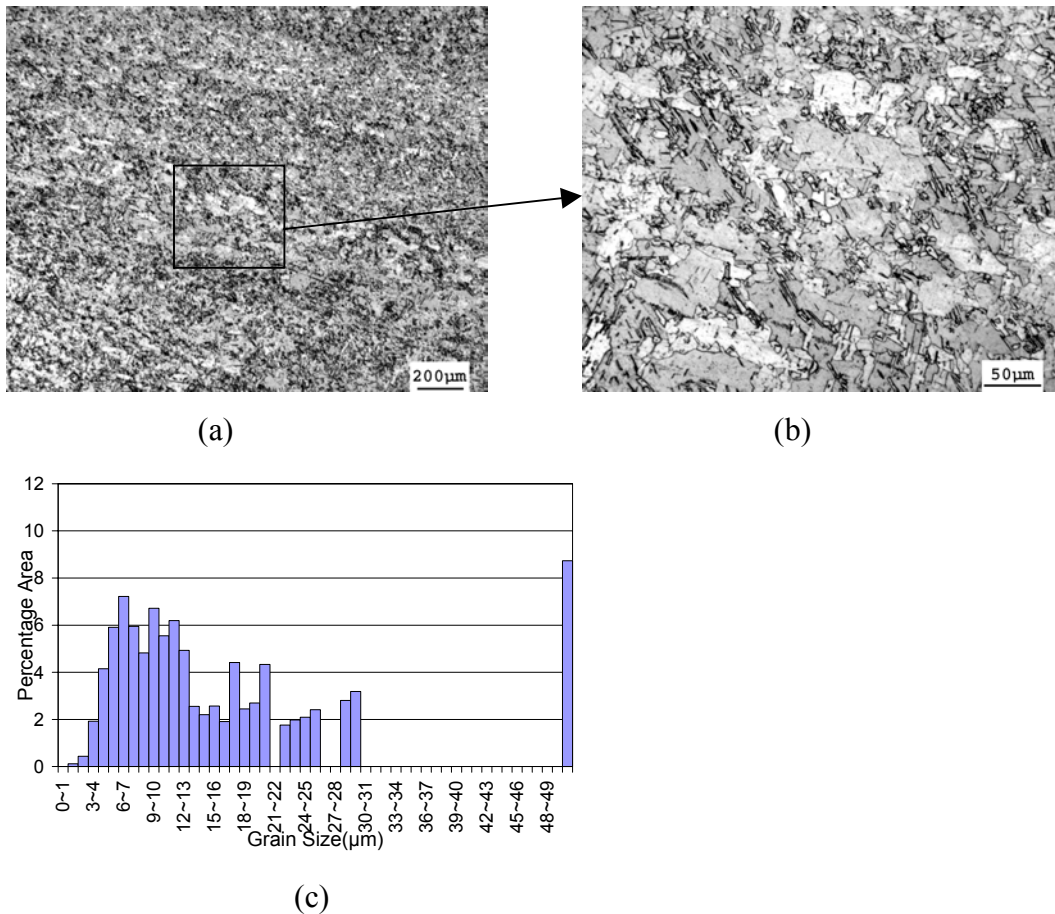


Fig. 105. Optical micrograph of CDA 101 Cu processed through 4A extrusion route in fully recrystallized condition, billet has 50 mm square cross-section. (a) 10X magnification, (b) 50X magnification, (c) typical grain size histogram.

The completely recrystallized microstructure obtained after 4B extrusion route is shown in Fig. 106. The billet size for this material is 25 mm. The microstructure shows bands of large and small grains which are a consequence of macroscopic shear banding in the material.

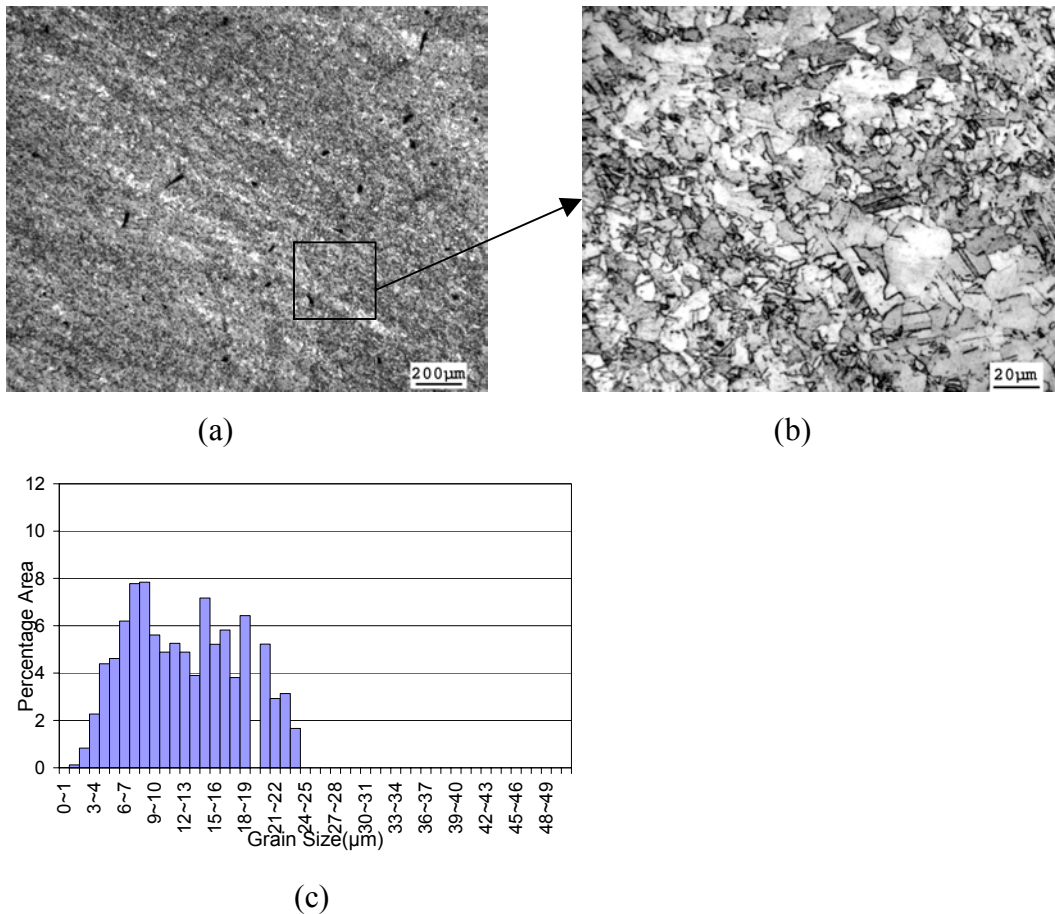
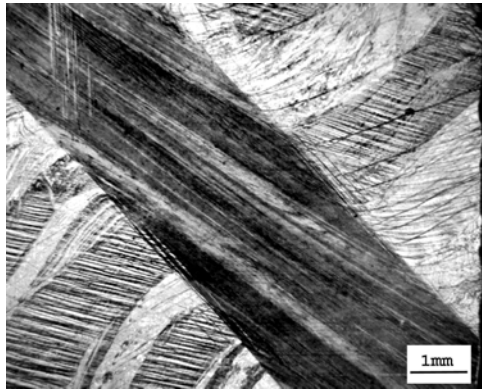


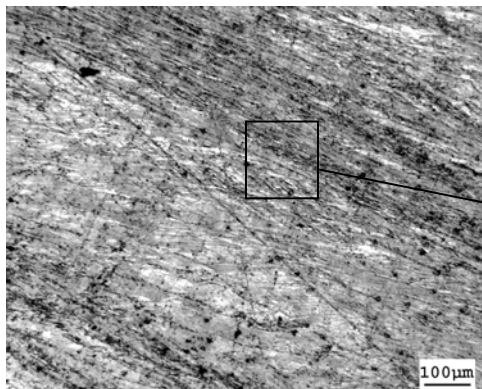
Fig. 106. Optical micrograph of CDA 101 Cu processed through 4B extrusion route in partially recrystallized condition, billet has 25 mm square cross-section. (a) 10X magnification, (b) 100X magnification, (c) typical grain size histogram.

Fig. 107 shows the as-worked and partially recrystallized microstructures for the 50 mm square billet processed through route 4B. This billet showed shear localization in the last extrusion pass. The gigantic shear band region is clearly visible in the as-worked condition. The fully recrystallized microstructure and grain size histogram are shown in Fig. 108. Figs. 109-112 show micrographs for billets having 19 mm, 25 mm and 50 mm square cross-section and processed through route 4E. It is interesting to notice the effects of shear banding in the fully recrystallized material. It was not expected that route 4E, with its strain path will produce shear banding in a ductile and workable material like CDA 101 Cu. The histograms indicate that the grain sizes and grain size distributions are

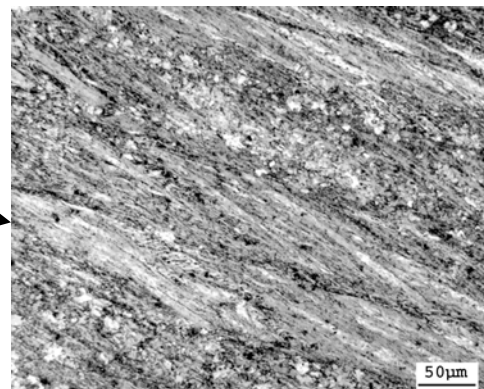
very similar for the three billets, adding evidence to the fact that induced shear in ECAE independent of billet size.



(a)



(b)



(c)

Fig. 107. Optical micrograph of 50 mm square cross-section billet of CDA 101 Cu processed through 4B. (a) as-worked condition; (b) and (c) partially recrystallized by heat treatment at 160°C for one hour.

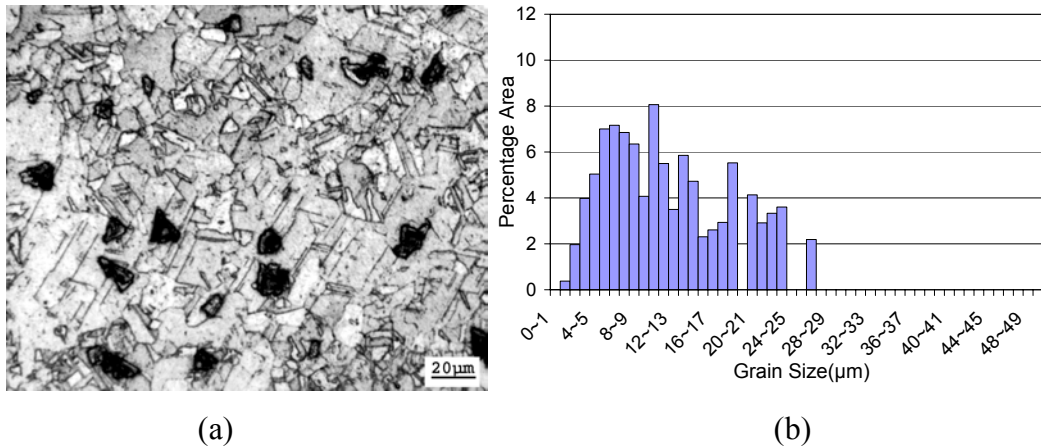


Fig. 108. Optical micrograph of CDA 101 Cu processed through 4B extrusion route in fully recrystallized condition, billet has 50 mm square cross-section. (a) 100X magnification, (b) typical grain size histogram.

Figs. 113-115 show the micrographs obtained after a processing through route 8E and fully recrystallized after a heat treatment of 250°C. The grain size histograms indicate a small average grain size and very small grain size range compared to other routes. No shear banding was observed in the fully recrystallized material.

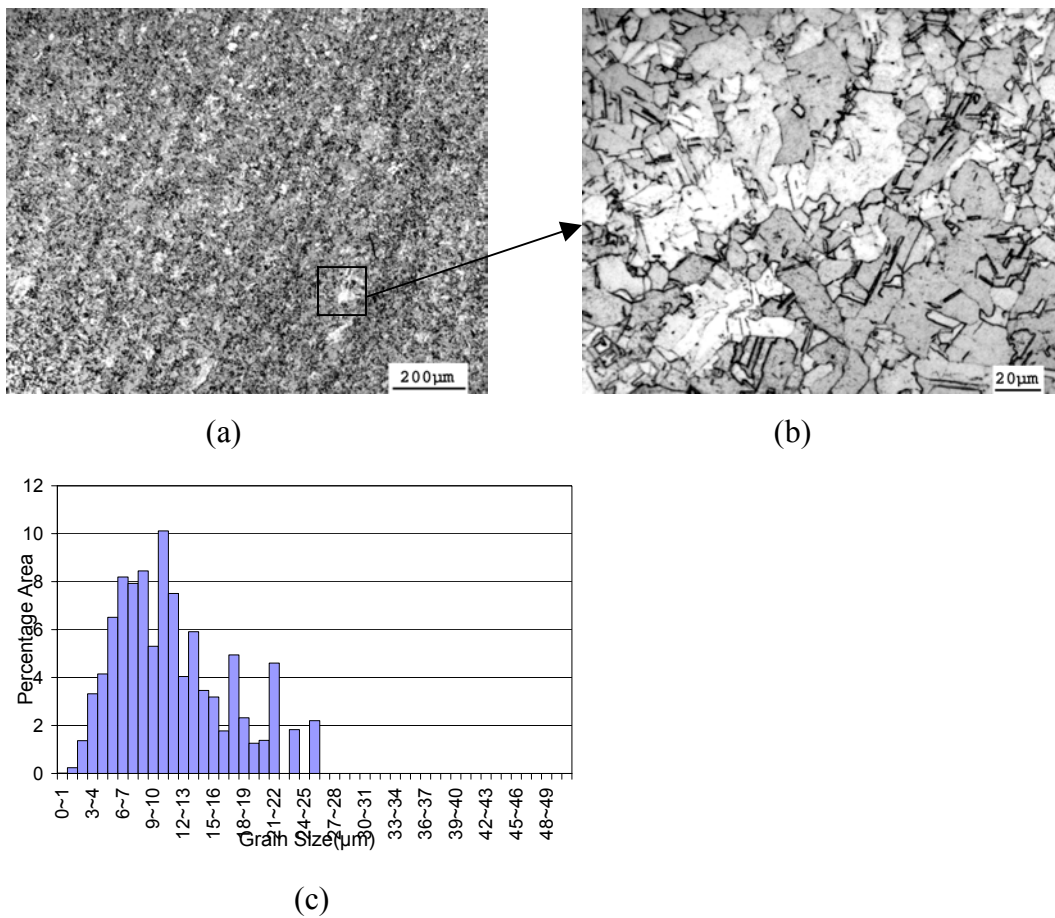


Fig. 109. Optical micrograph of CDA 101 Cu processed through 4E extrusion route in fully recrystallized condition, billet has 50 mm square cross-section. (a) 10X magnification, (b) 100X magnification, (c) typical grain size histogram.

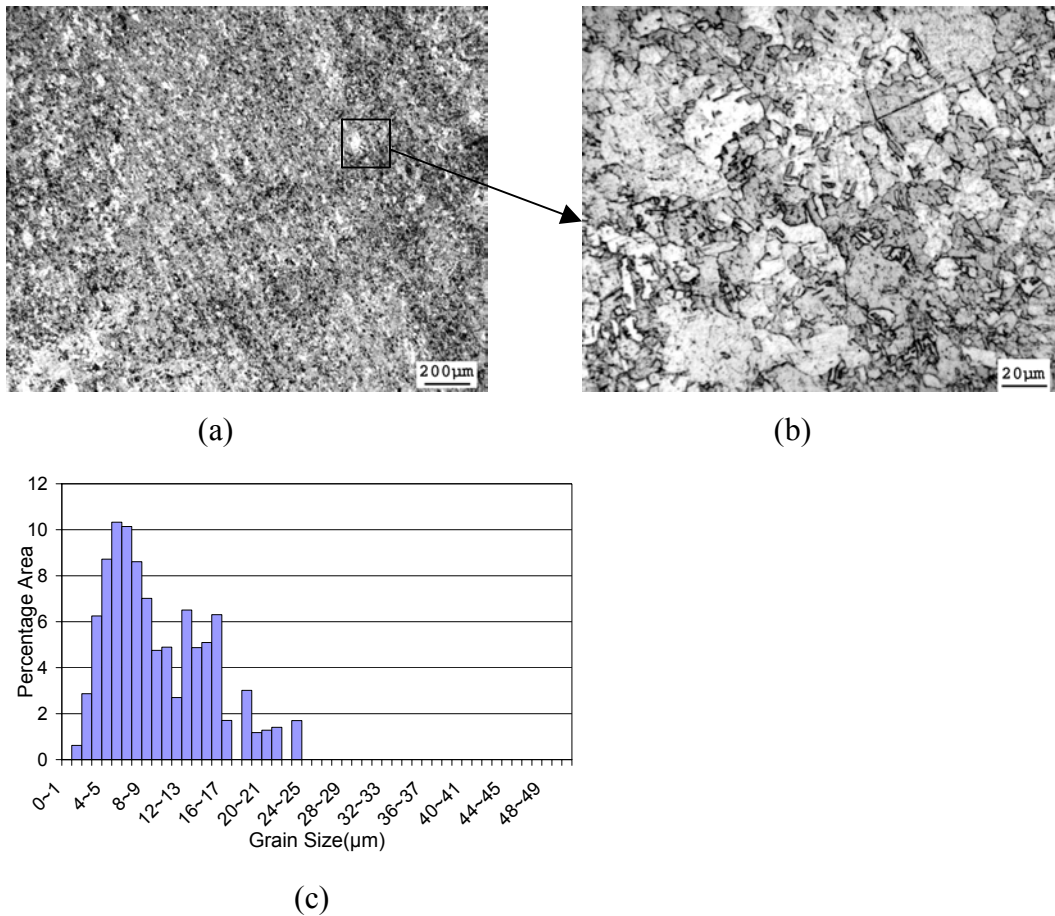


Fig. 110. Optical micrograph of CDA 101 Cu processed through 4E extrusion route in fully recrystallized condition, billet has 25 mm square cross-section. (a) 10X magnification, (b) 100X magnification, (c) typical grain size histogram.

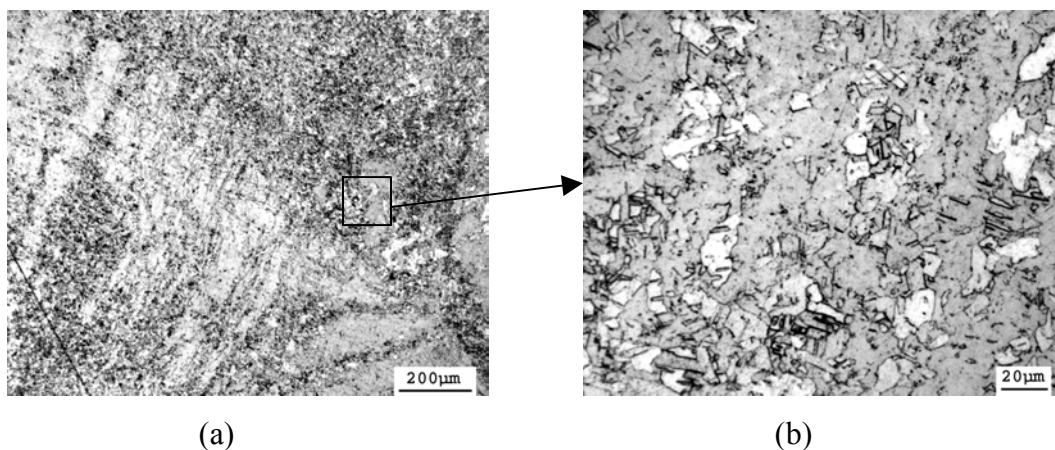


Fig. 111. Optical micrograph of CDA 101 Cu processed through 4E extrusion route in partially recrystallized condition, billet has 19 mm square cross-section. (a) 10X magnification, (b) 100X magnification.

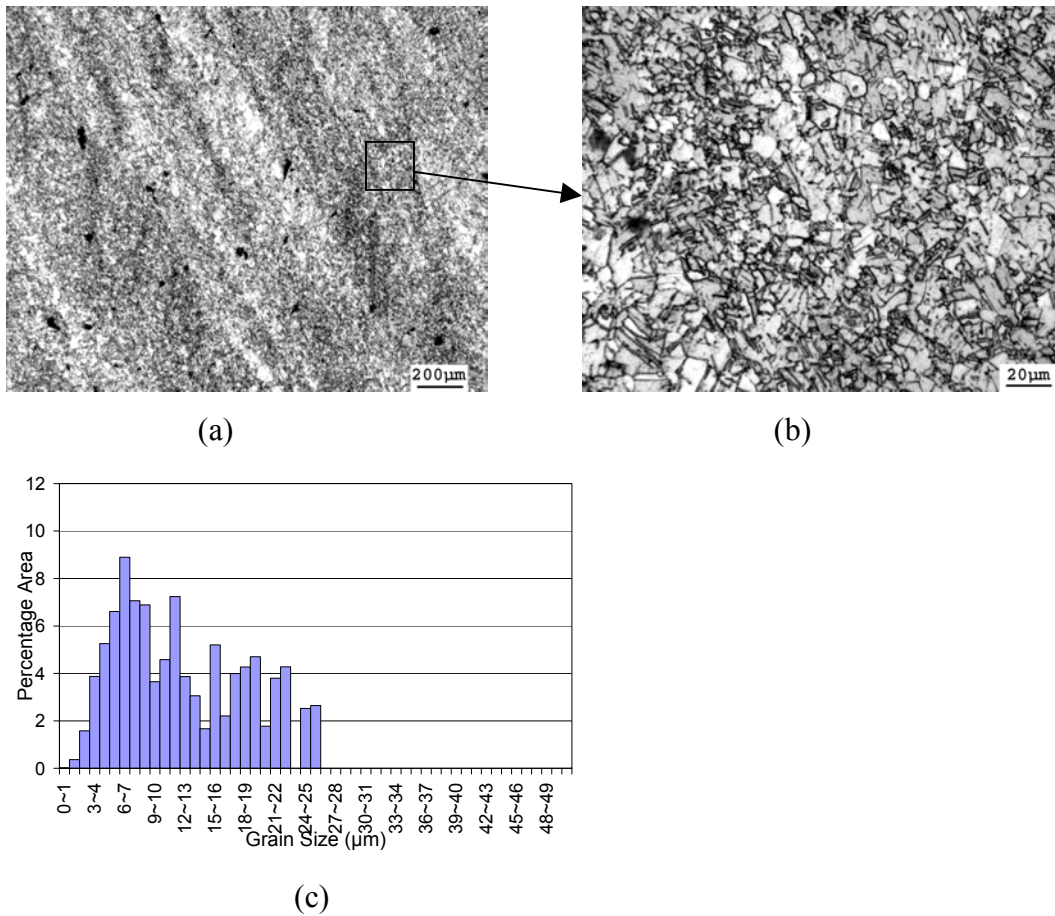


Fig. 112. Optical micrograph of CDA 101 Cu processed through 4E extrusion route in fully recrystallized condition, billet has 19 mm square cross-section. (a) 10X magnification, (b) 100X magnification, (c) typical grain size histogram.

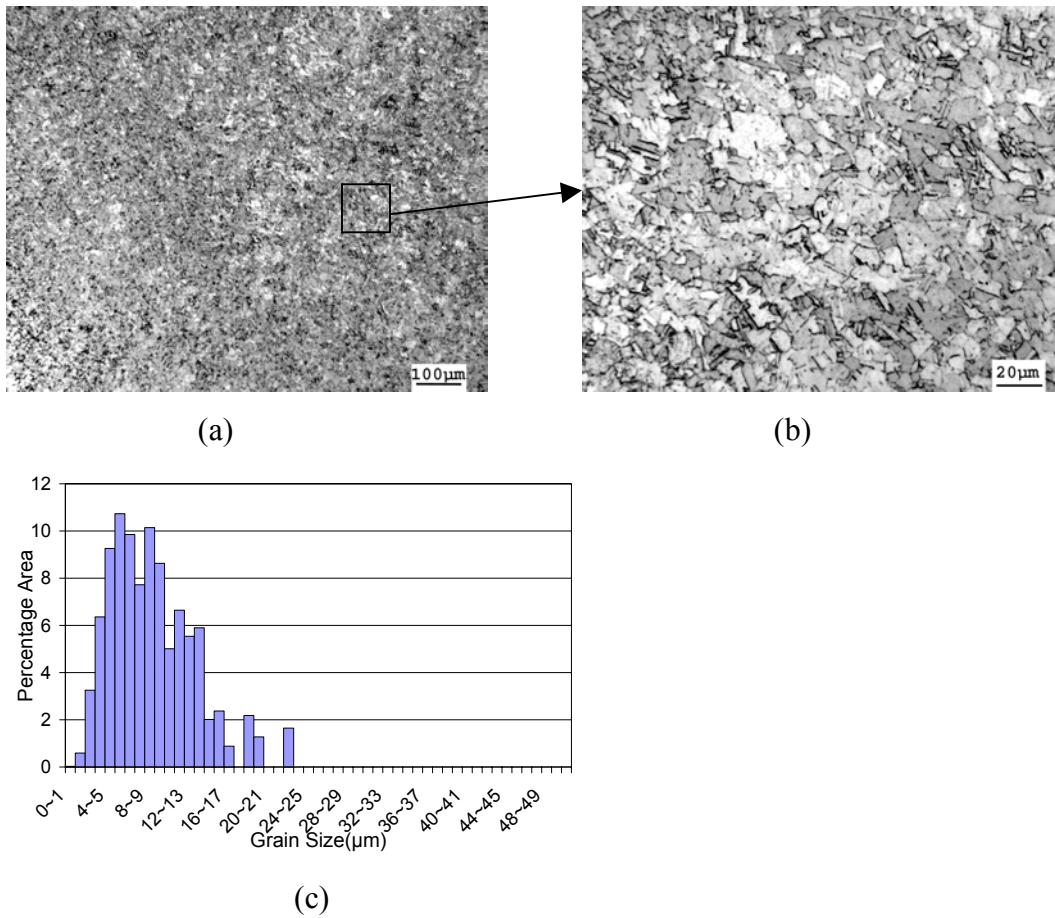


Fig. 113. Optical micrograph of CDA 101 Cu processed through 8E extrusion route in fully recrystallized condition, billet has 50 mm square cross-section. (a) 20X magnification, (b) 100X magnification, (c) typical grain size histogram.

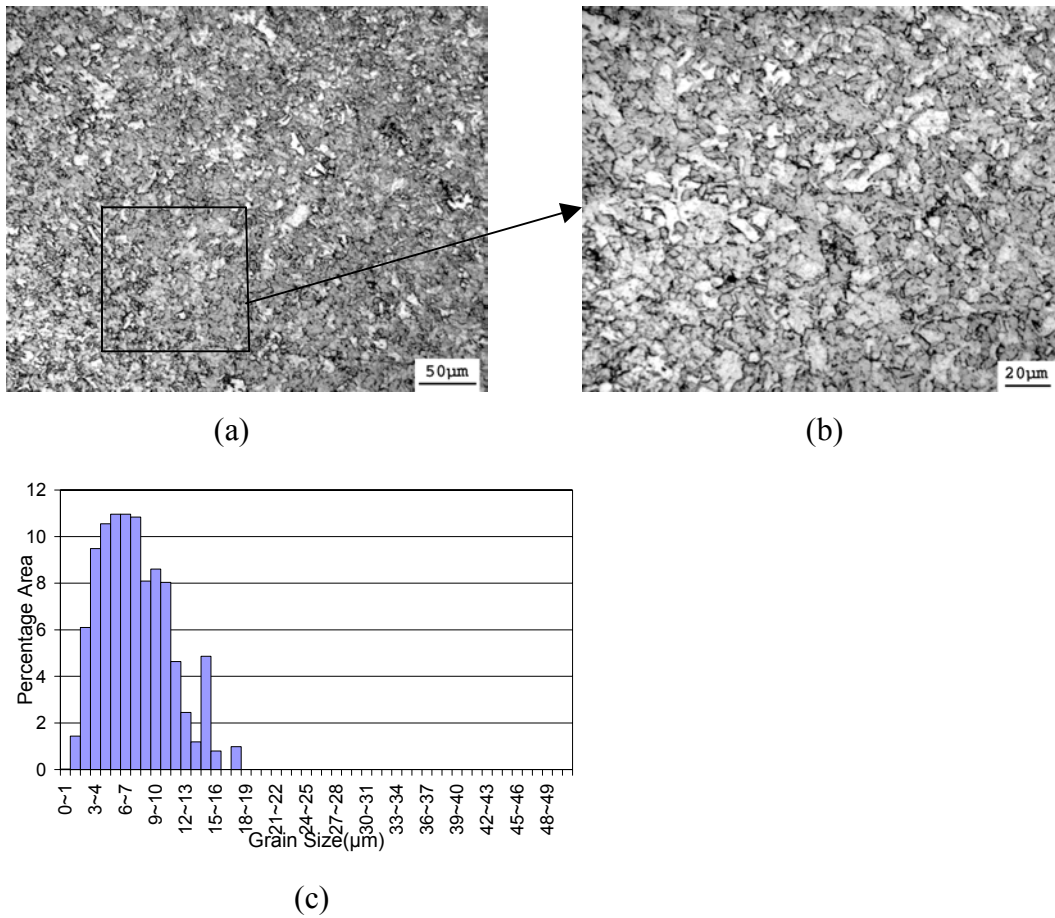


Fig. 114. Optical micrograph of CDA 101 Cu processed through 8E extrusion route in fully recrystallized condition, billet has 25 mm square cross-section. (a) 50X magnification, (b) 100X magnification, (c) typical grain size histogram.

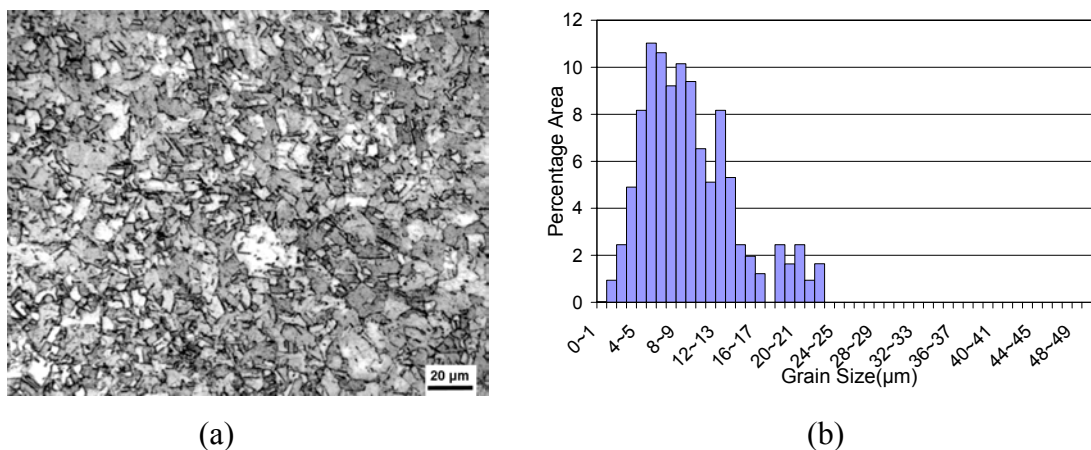


Fig. 115. Optical micrograph of CDA 101 Cu processed through 8E extrusion route in fully recrystallized condition, billet has 19 mm square cross-section. (a) 100X magnification, (b) typical grain size histogram.

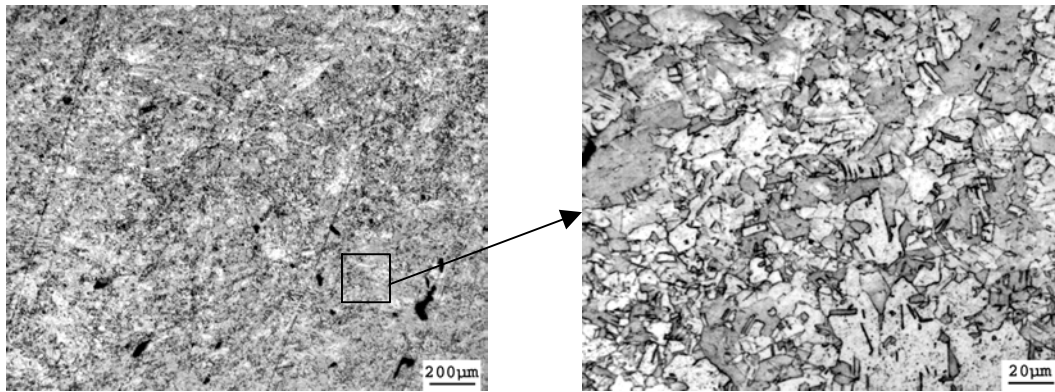
4.7.2. Microstructural breakdown project. The aim of this study was to determine the effectiveness of ECAE in breaking down the as-cast microstructure of CDA 101 Cu and to find the best thermo-mechanical schedule (from the set of schedules analyzed) for grain refinement of CDA 101 Cu. For these reasons, optical microscopy of recrystallized grains is extremely important for this research.

Figs. 116-117 show the recrystallized microstructure and grain size distributions for processing routes 2C and 2E. Routes 2C and 2E induce the same deformation as route E is 2C*2C and we notice that there is little difference in the recrystallized microstructures obtained after these routes.

The recrystallized microstructure obtained after a TMP schedule of 2E-400°C-2E is given in Fig. 118. The microstructure is free from shear banding, but an inhomogeneous microstructure is observed. There are a few very large grains embedded in a matrix of fine grains. Also notice that ~9% of the micrograph area is covered by grains having size of greater than 50 μm. The microstructure obtained for a TMP schedule of 2E- 350°C- 2E does not show such gigantic grains, but the microstructure is still highly inhomogeneous.

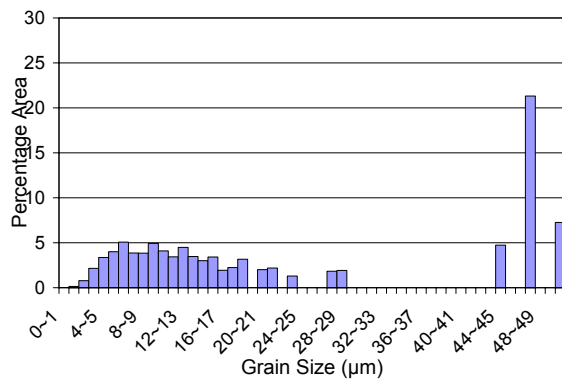
The fully recrystallized microstructures obtained for routes C, Bc and F up to four passes are shown in Figs. 119 – 125. It is generally noticed that TMP schedules not

involving intermediate heat treatments give better grain size uniformity compared to those that incorporate intermediate heat treatments.



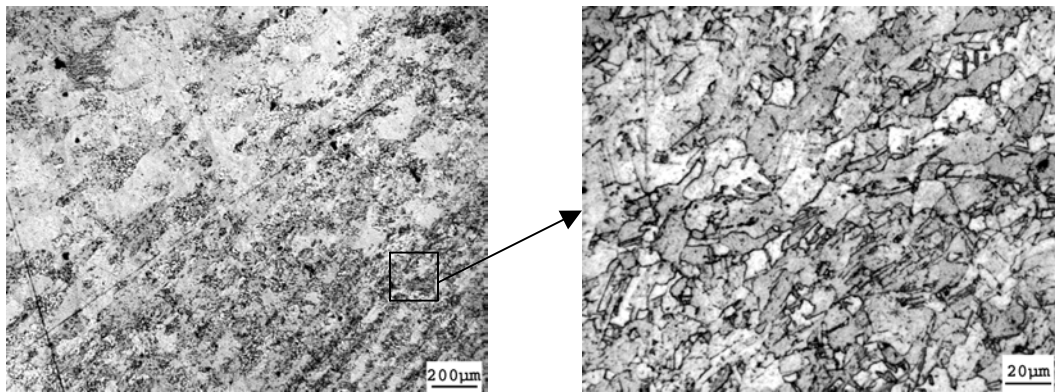
(a)

(b)



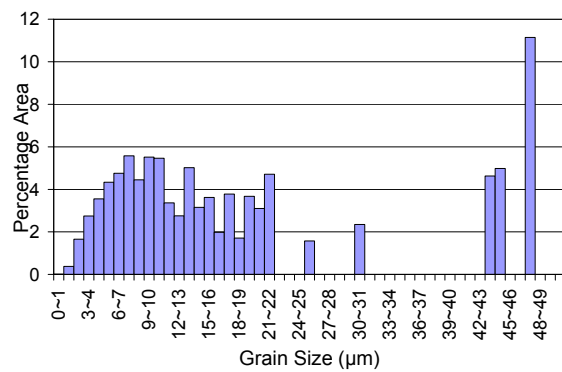
(c)

Fig. 116. Optical micrograph of CDA 101 Cu processed through 2E extrusion route in fully recrystallized condition. (a) 10X magnification, (b) 100X magnification, (c) typical grain size histogram.



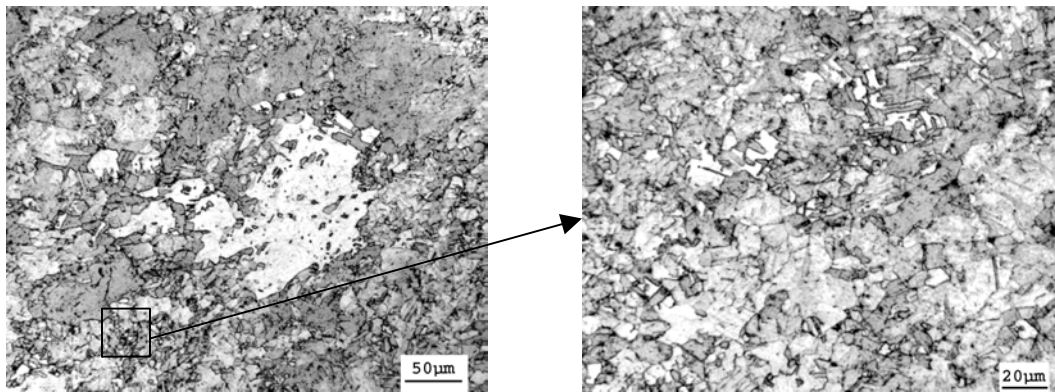
(a)

(b)



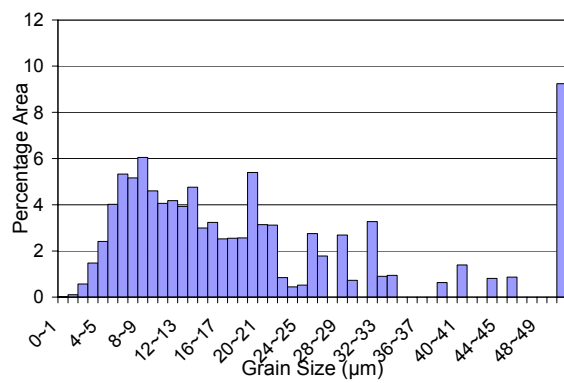
(c)

Fig. 117. Optical micrograph of CDA 101 Cu processed through 2C extrusion route in fully recrystallized condition. (a) 10X magnification, (b) 100X magnification, (c) typical grain size histogram.



(a)

(b)



(c)

Fig. 118. Optical micrograph of CDA 101 Cu processed through 2E-400°C-2E thermomechanical schedule in fully recrystallized condition. (a) 50X magnification, (b) 100X magnification, (c) typical grain size histogram.

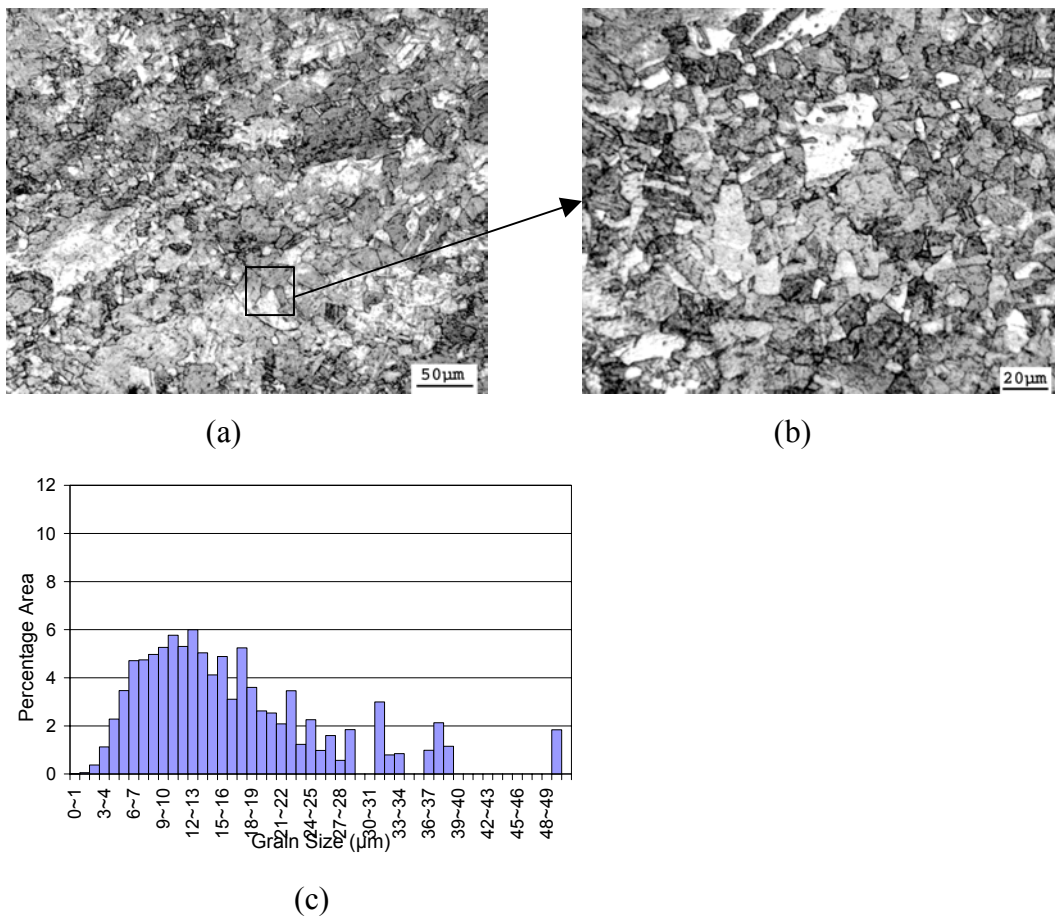


Fig. 119. Optical micrograph of CDA 101 Cu processed through 2E-350°C-2E thermomechanical schedule in fully recrystallized condition. (a) 50X magnification, (b) 100X magnification, (c) typical grain size histogram.

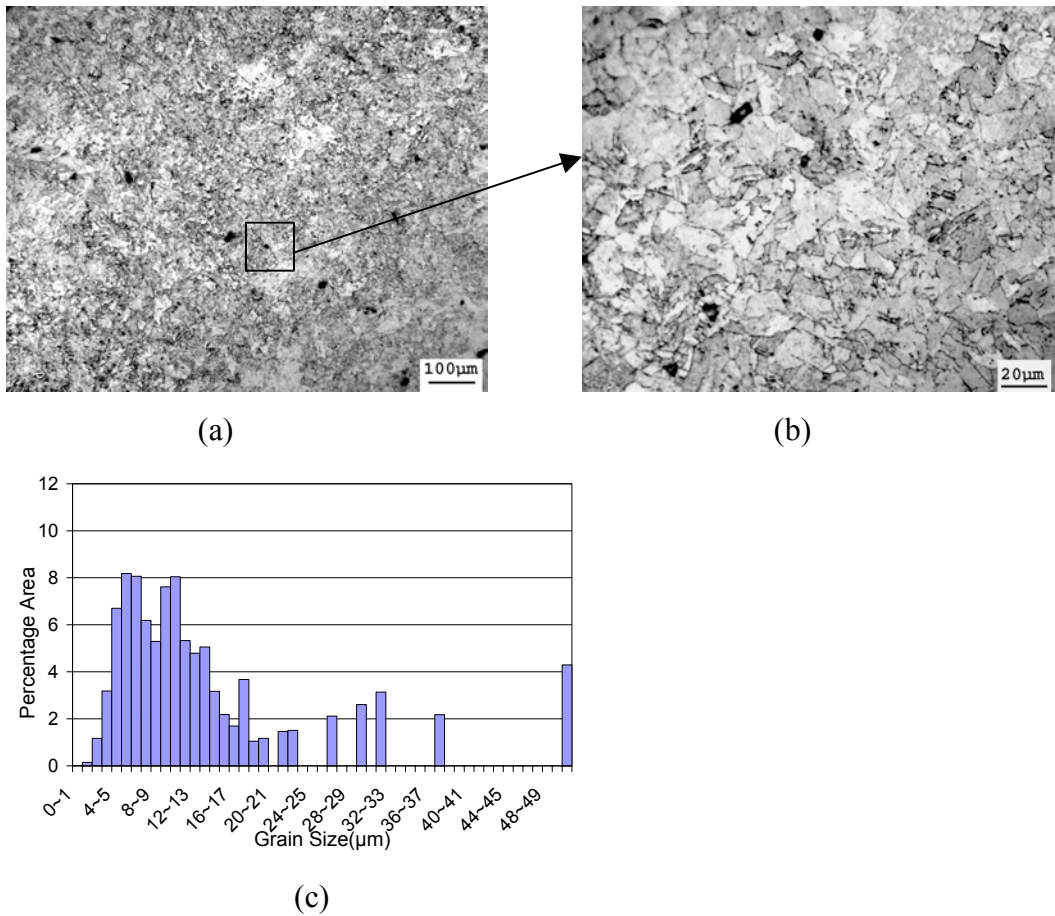
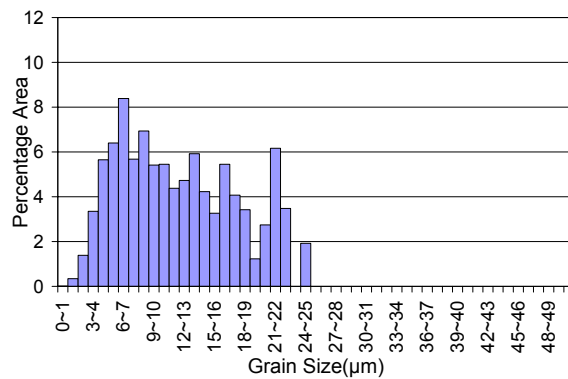
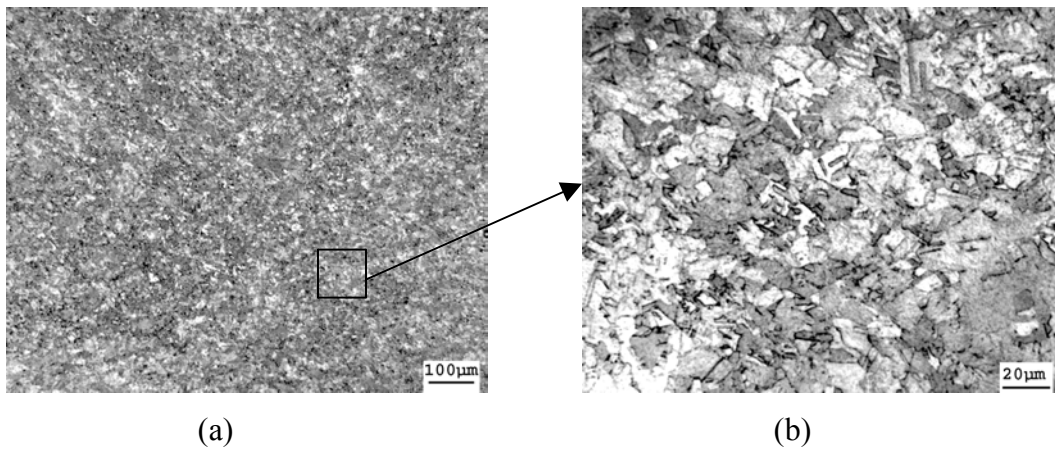
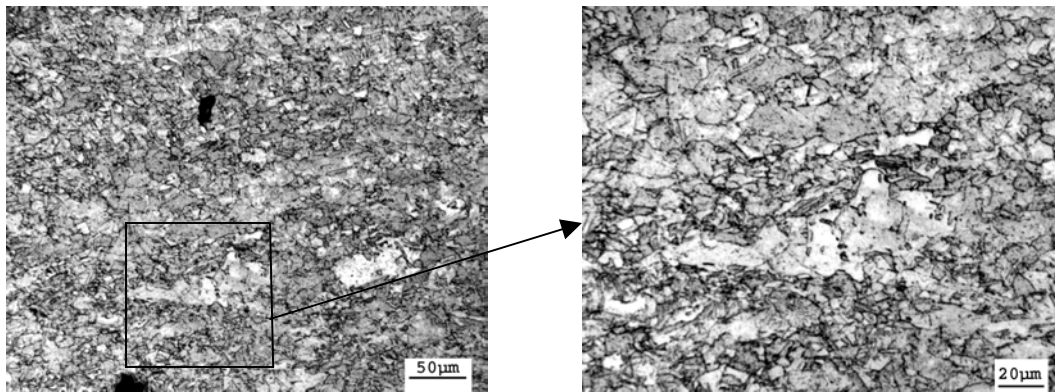


Fig. 120. Optical micrograph of CDA 101 Cu processed through 2C-400°C-2C thermomechanical schedule in fully recrystallized condition. (a) 20X magnification, (b) 50X magnification, (c) typical grain size histogram.



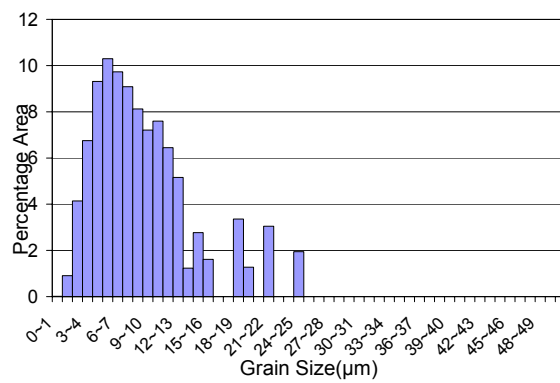
(c)

Fig. 121. Optical micrograph of CDA 101 Cu processed through 4C extrusion route in fully recrystallized condition. (a) 20X magnification, (b) 100X magnification, (c) typical grain size histogram.



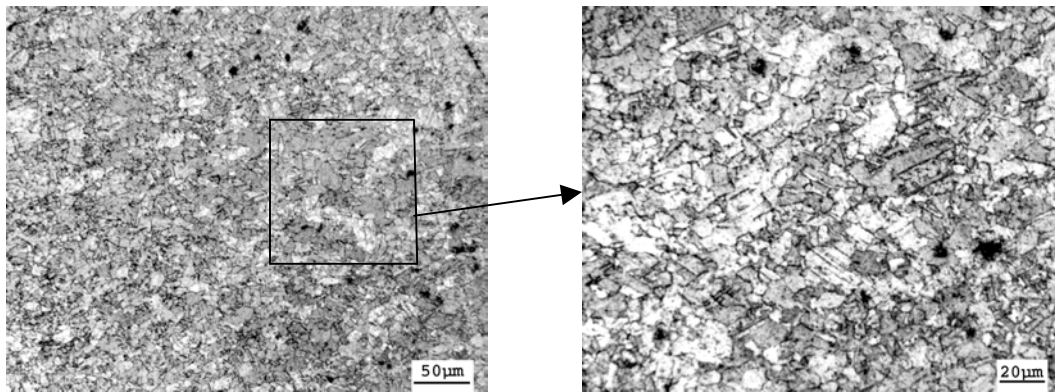
(a)

(b)



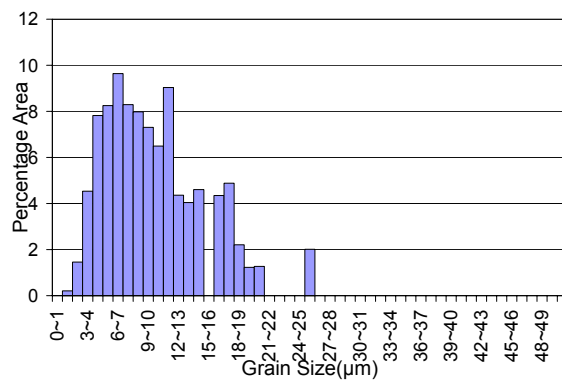
(c)

Fig. 122. Optical micrograph of CDA 101 Cu processed through 2F-400°C-2F thermomechanical schedule in fully recrystallized condition. (a) 50X magnification, (b) 100X magnification, (c) typical grain size histogram.



(a)

(b)



(c)

Fig. 123. Optical micrograph of CDA 101 Cu processed through 4F extrusion route, in fully recrystallized condition. (a) 50X magnification, (b) 100X magnification, (c) typical grain size histogram.

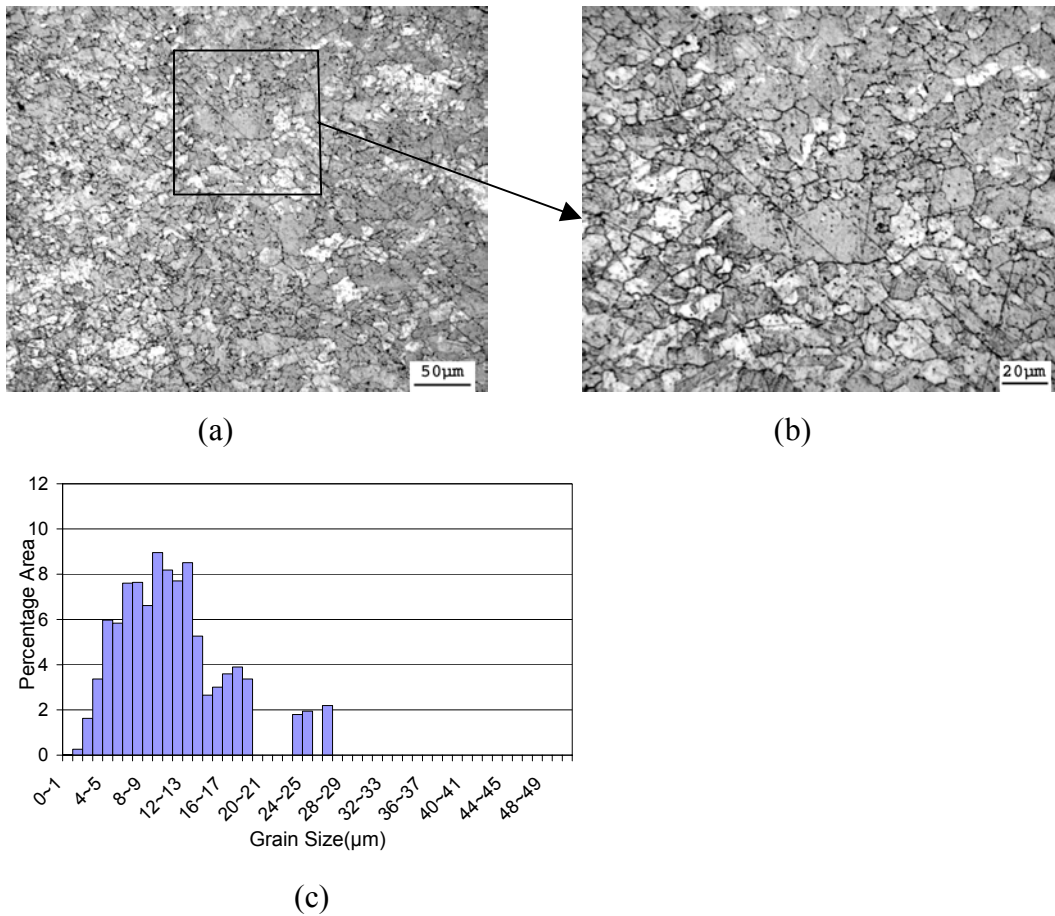


Fig. 124. Optical micrograph of CDA 101 Cu processed through 2Bc-400°C-2Bc thermomechanical schedule, in fully recrystallized condition. (a) 50X magnification, (b) 100X magnification, (c) typical grain size histogram.

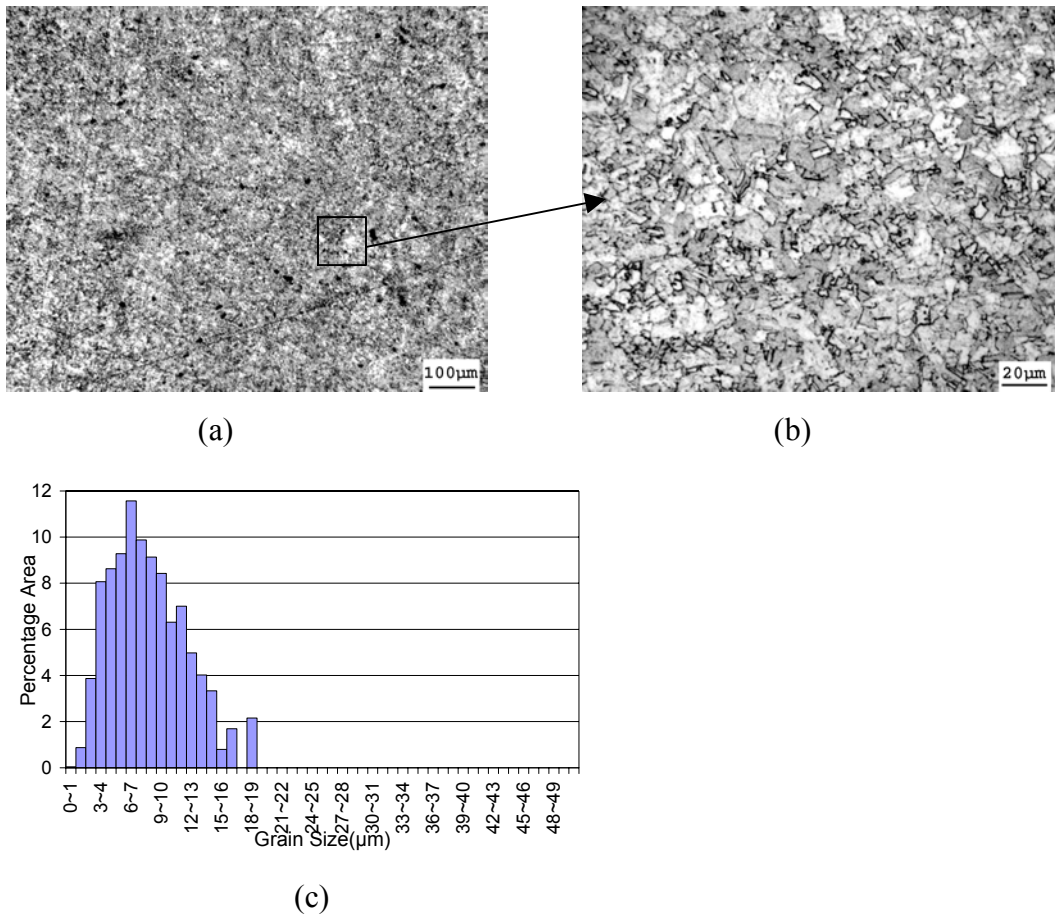


Fig. 125. Optical micrograph of CDA 101 Cu processed through 4Bc extrusion route, in fully recrystallized condition. (a) 20X magnification, (b) 100X magnification, (c) typical grain size histogram.

Fully recrystallized microstructure for TMP schedule 2E-400°C-2E-300°C-2E is shown in Fig. 126. The microstructure obtained is better than those obtained after four passes, but still contains some large grains. Observe the microstructure for a TMP schedule 2C-400°C-2C-300°C-2C in Fig. 127.

Fully recrystallized microstructures obtained after eight passes, with different routes and TMP schedules are shown in Figs. 128-136. It is observed that there is a great improvement in the homogeneity of the microstructure. The spread of the grain size is narrow compared to four pass extrusions. There is not a substantial change in the average grain size of the microstructure. Route C gives the most inhomogeneous microstructure for all eight pass extrusions. The best microstructure is obtained in the case of route Bc.

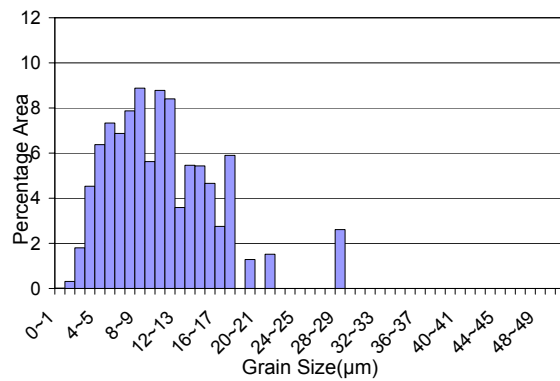
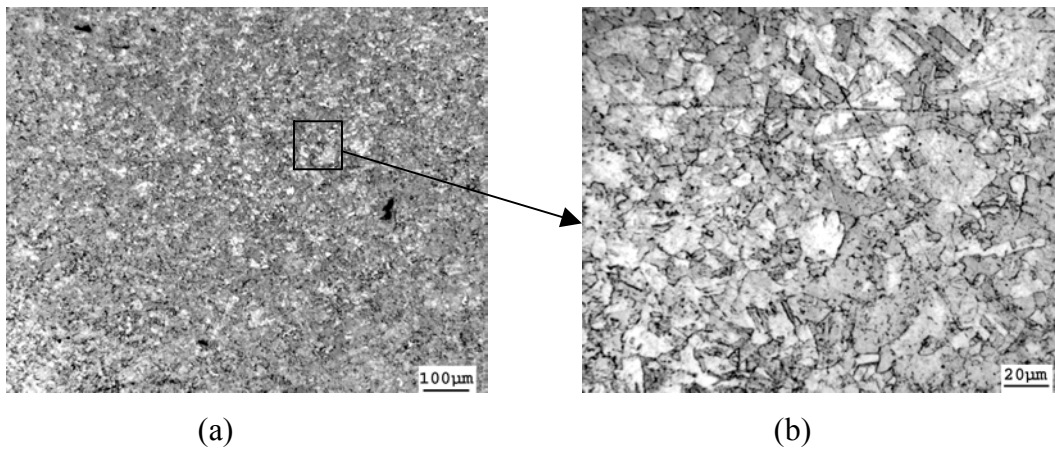


Fig. 126. Optical micrograph of CDA 101 Cu processed through 2E-400°C-2E-300°C-2E thermomechanical schedule, in fully recrystallized condition. (a) 20X magnification, (b) 100X magnification, (c) typical grain size histogram.

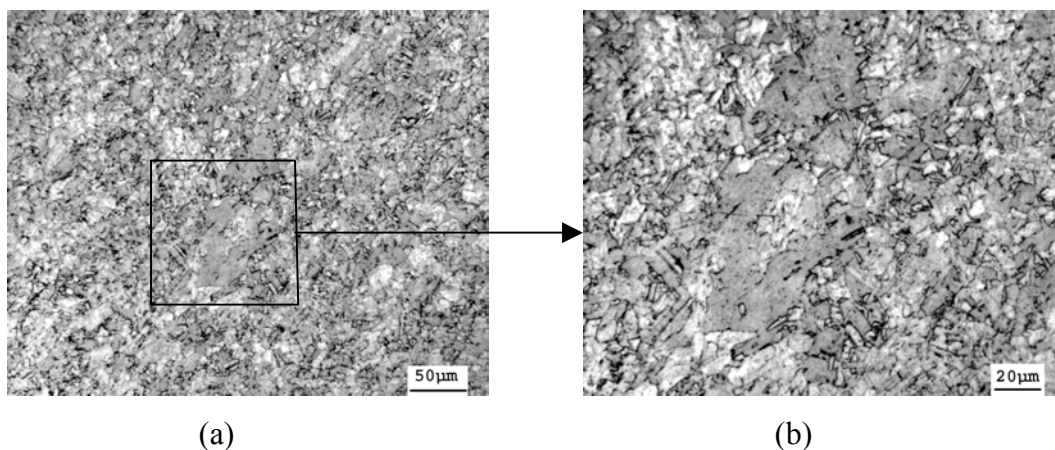


Fig. 127. Optical micrograph of CDA 101 Cu processed through 2C-400°C-2C-300°C-2C thermomechanical schedule, in fully recrystallized condition. (a) 50X magnification, (b) 100X magnification.

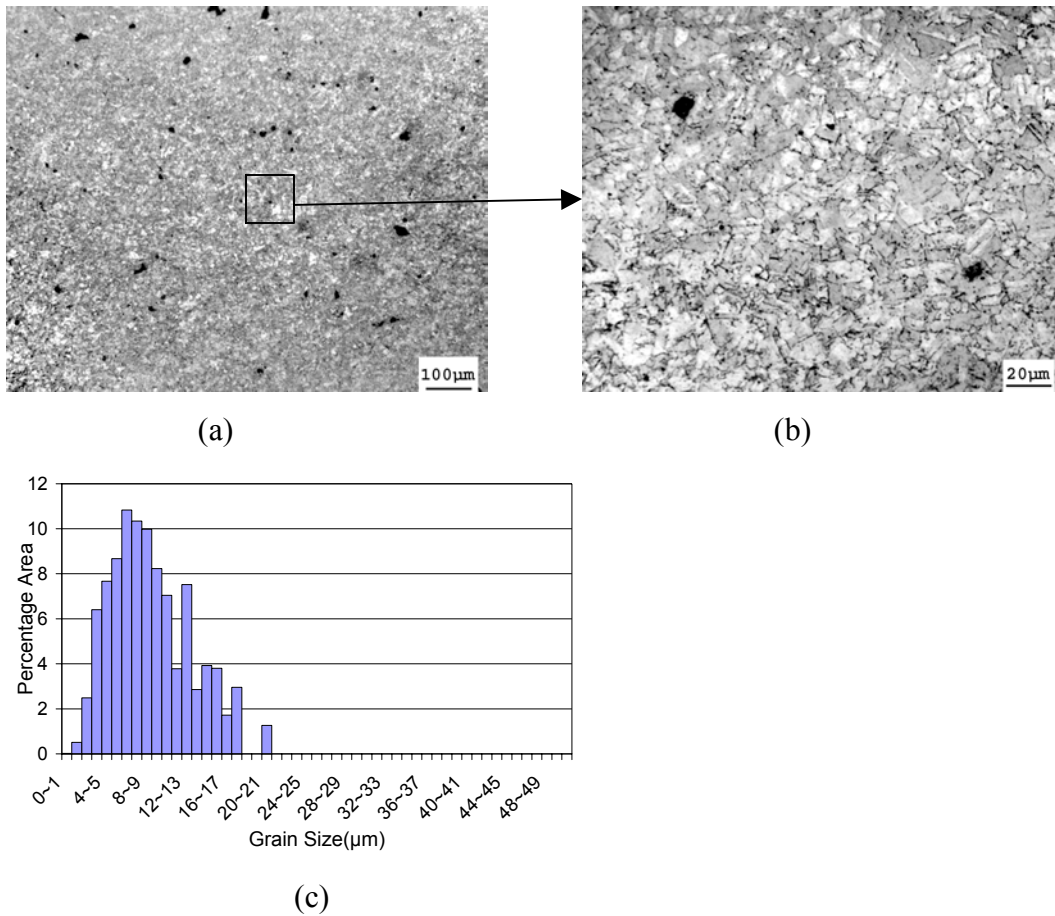


Fig. 128. Optical micrograph of CDA 101 Cu processed through 2E-400°C-2E-300°C-2E-200°C-2E thermomechanical schedule, in fully recrystallized condition. (a) 20X magnification, (b) 100X magnification, (c) typical grain size histogram.

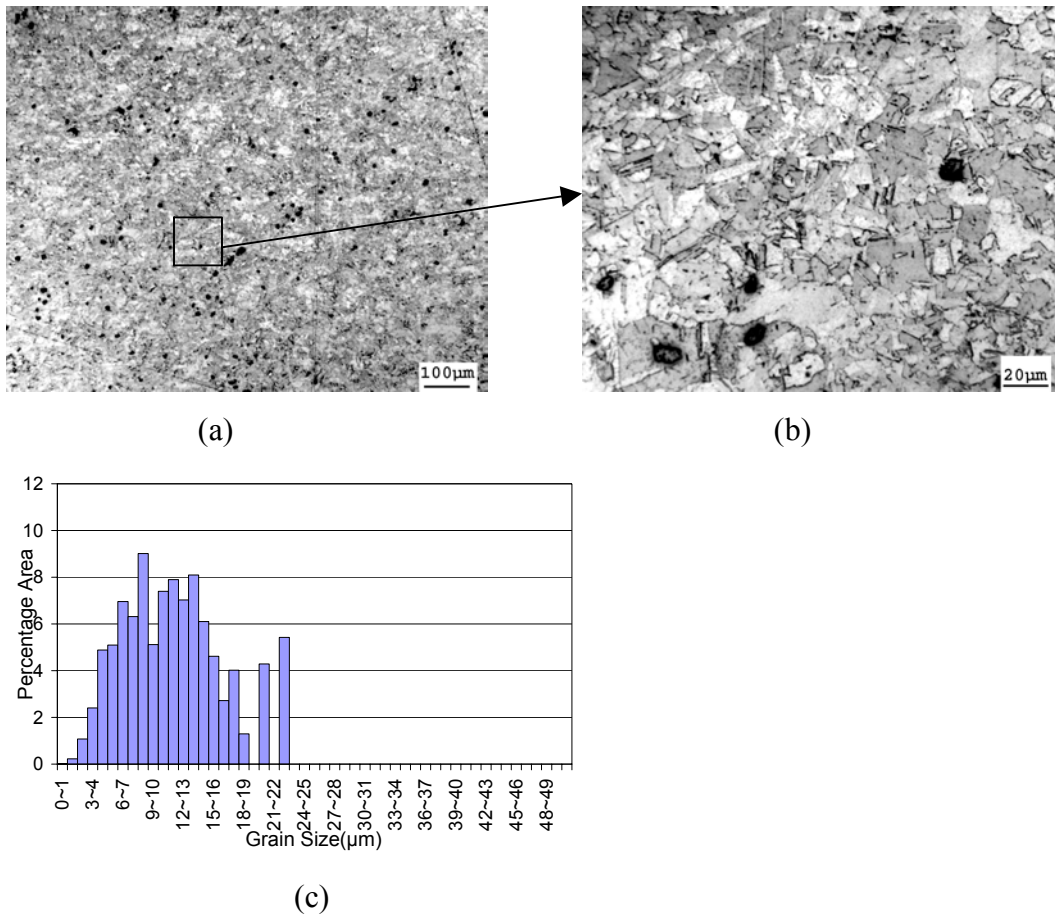


Fig. 129. Optical micrograph of CDA 101 Cu processed through 2E-350°C-2E-350°C-2E-350°C-2E thermomechanical schedule, in fully recrystallized condition. (a) 20X magnification, (b) 100X magnification, (c) typical grain size histogram.

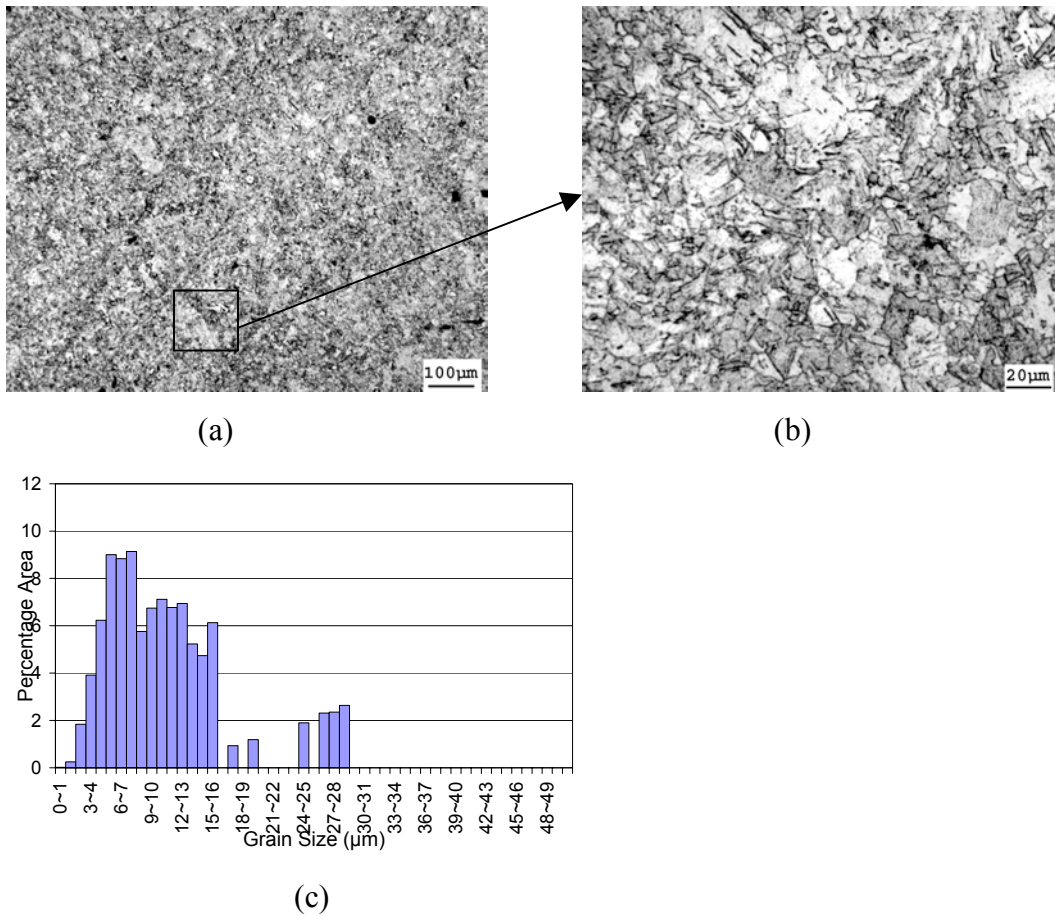


Fig. 130. Optical micrograph of CDA 101 Cu processed through 2C-400°C-2C-300°C-2C-200°C-2C thermomechanical schedule, in fully recrystallized condition. (a) 20X magnification, (b) 100X magnification, (c) typical grain size histogram.

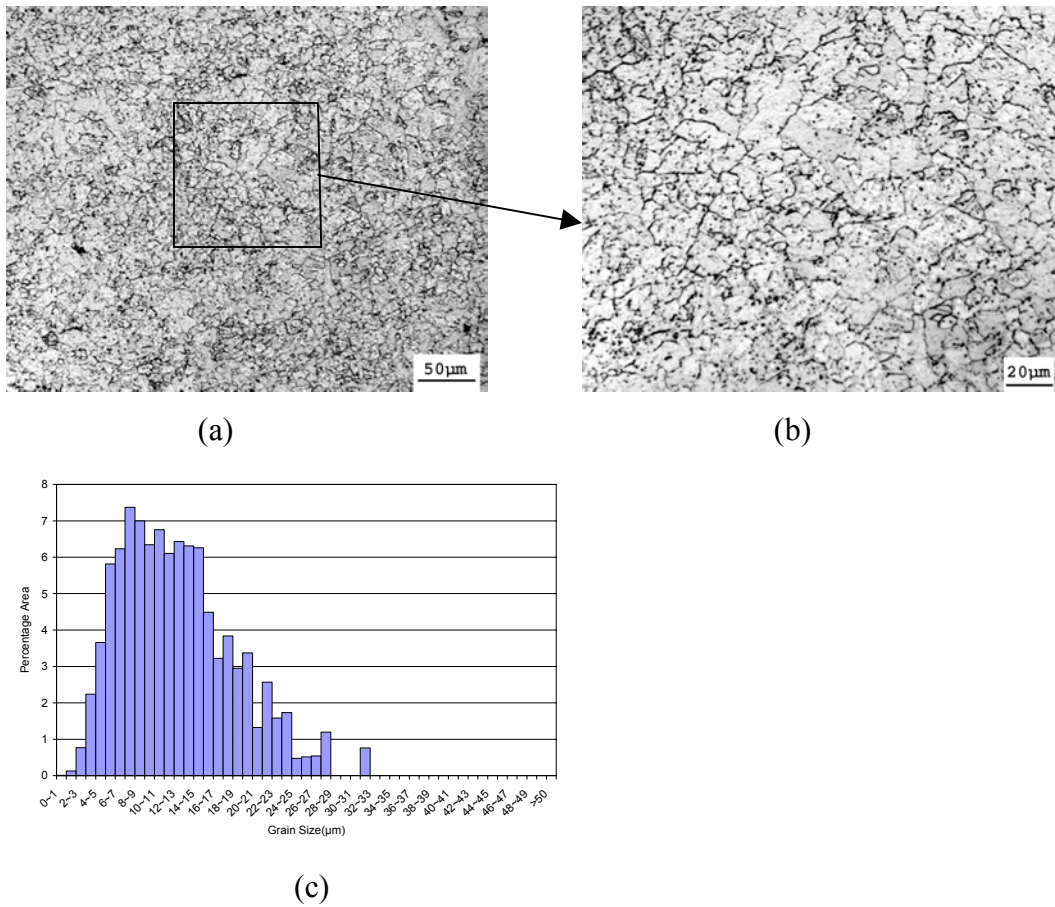


Fig. 131. Optical micrograph of CDA 101 Cu processed through 8C extrusion passes, in fully recrystallized condition. (a) 50X magnification, (b) 100X magnification, (c) typical grain size histogram.

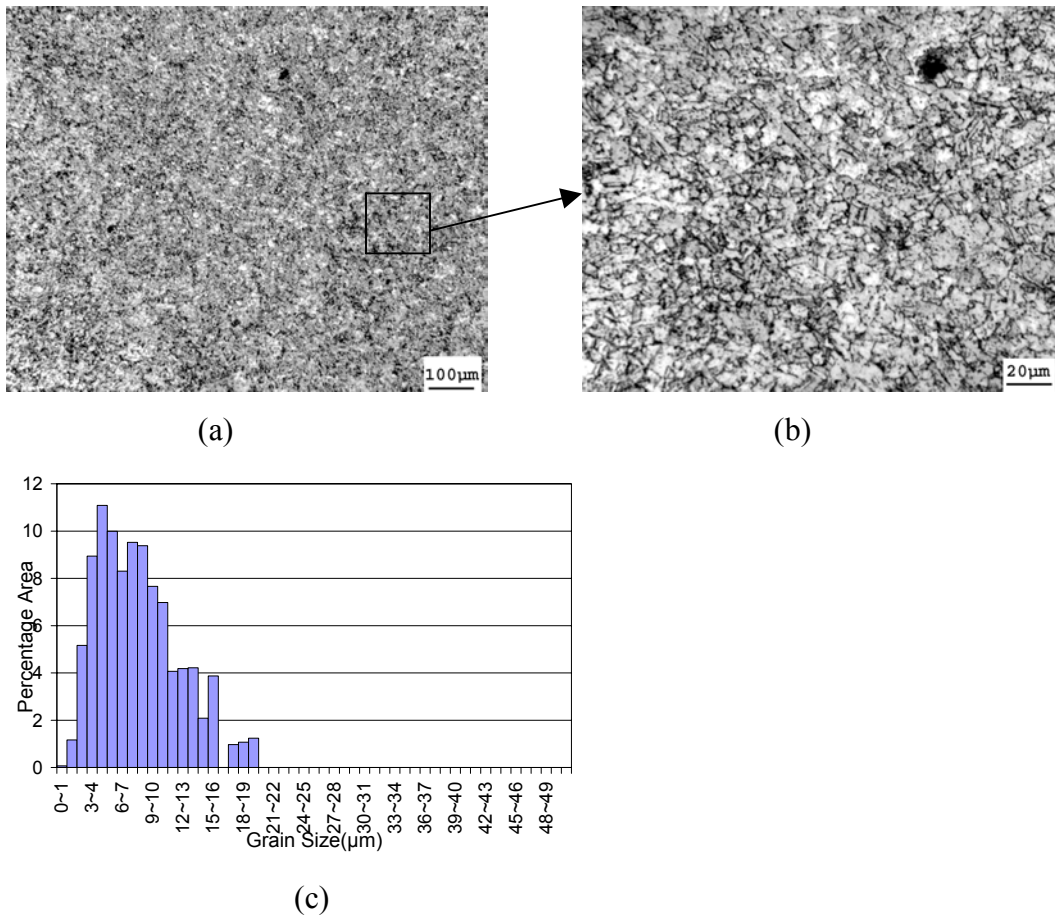


Fig. 132. Optical micrograph of CDA 101 Cu processed through 2F-400°C-2F-300°C-2F-200°C-2F thermomechanical schedule, in fully recrystallized condition. (a) 20X magnification, (b) 100X magnification, (c) typical grain size histogram.

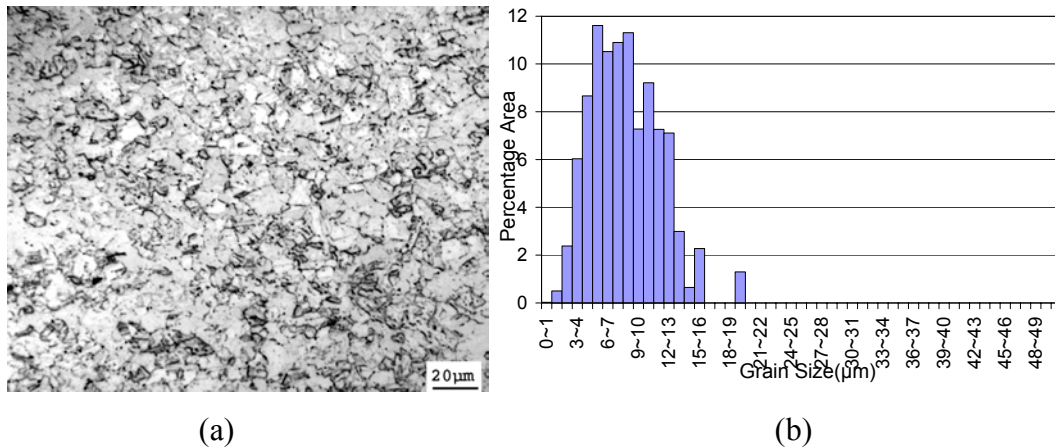


Fig. 133. Optical micrograph of CDA 101 Cu processed through 8F extrusion passes in fully recrystallized condition. (a) 100X magnification, (b) typical grain size histogram.

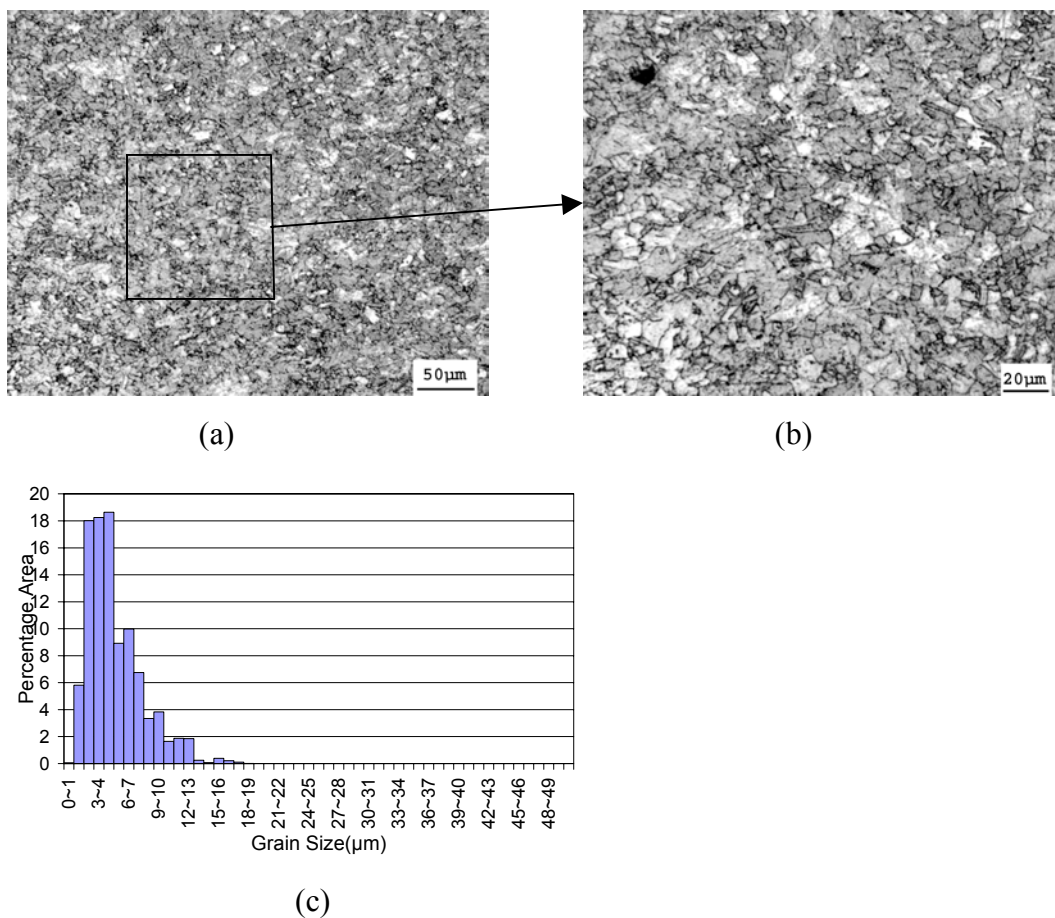


Fig. 134. Optical micrograph of CDA 101 Cu processed through 2Bc-400°C-2Bc-300°C-2Bc-200°C-2Bc thermomechanical schedule, in fully recrystallized condition. (a) 20X magnification, (b) 100X magnification, (c) typical grain size histogram.

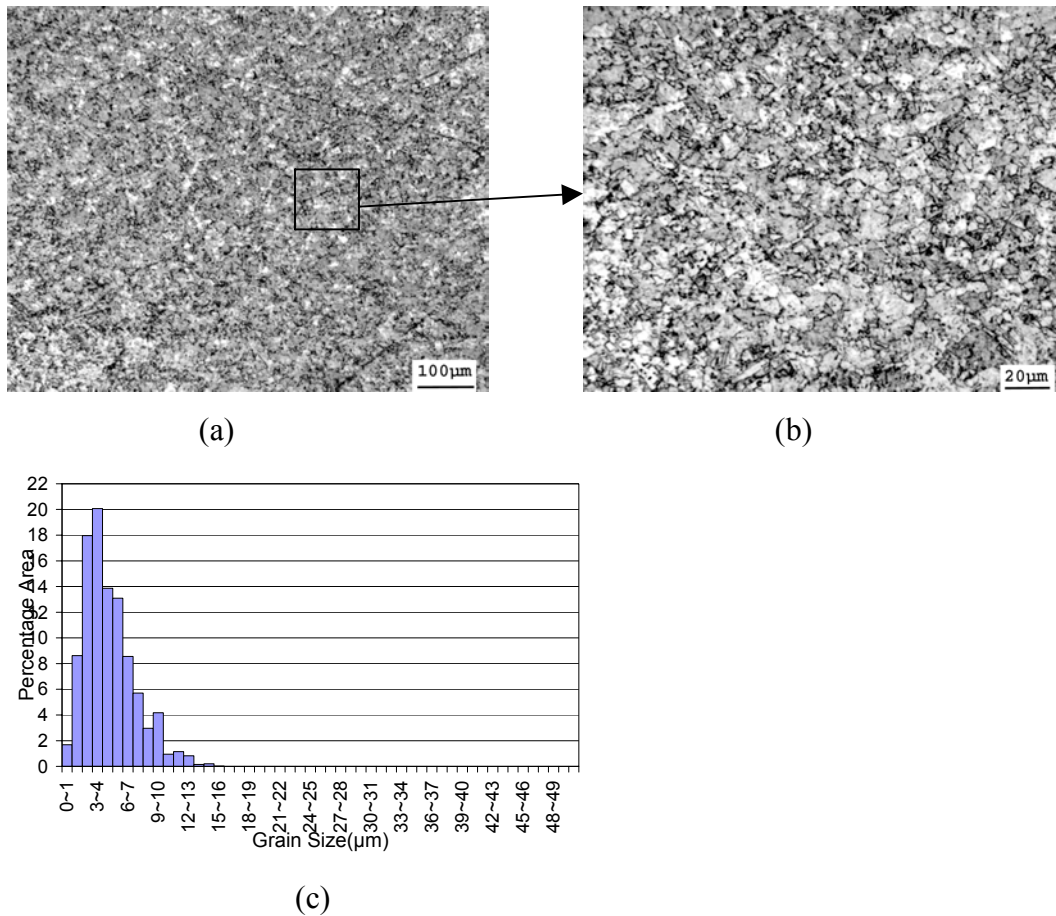


Fig. 135. Optical micrograph of CDA 101 Cu processed through 8Bc extrusion passes in fully recrystallized condition. (a) 20X magnification, (b) 100X magnification, (c) typical grain size histogram.

Figs. 136 - 141 and Table 13 summarize the data obtained in the above micrographs. It is observed that there is little change in the average grain size obtained after two extrusions for different routes and TMP schedules. But a decrease in the values of error bars is observed. This indicates a decrease in the standard deviation values of grain size obtained as CDA 101 Cu is processed to higher passes.

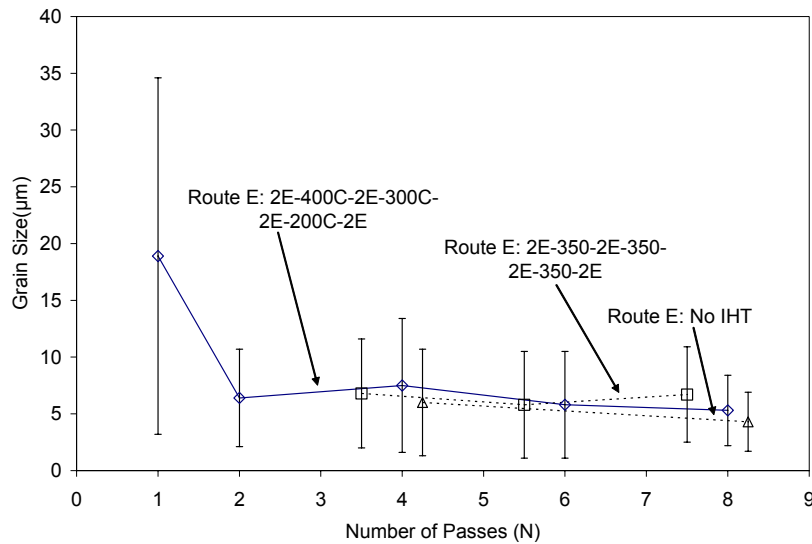


Fig. 136. Grain size as a function of thermo-mechanical processing schedule for route E. IHT: Intermediate heat treatment. Error bars indicate standard deviation values.

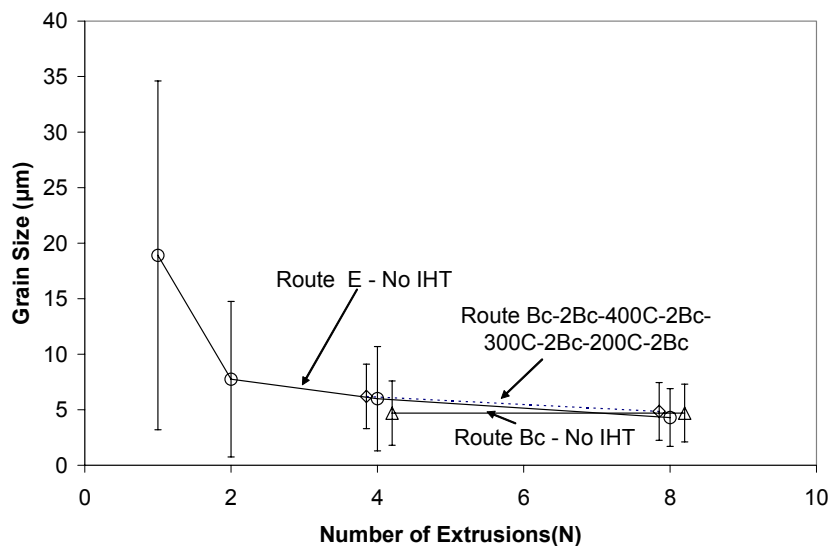


Fig. 137. Grain size as a function of thermo-mechanical processing schedule for route Bc. IHT: Intermediate heat treatment. Error bars indicate standard deviation values.

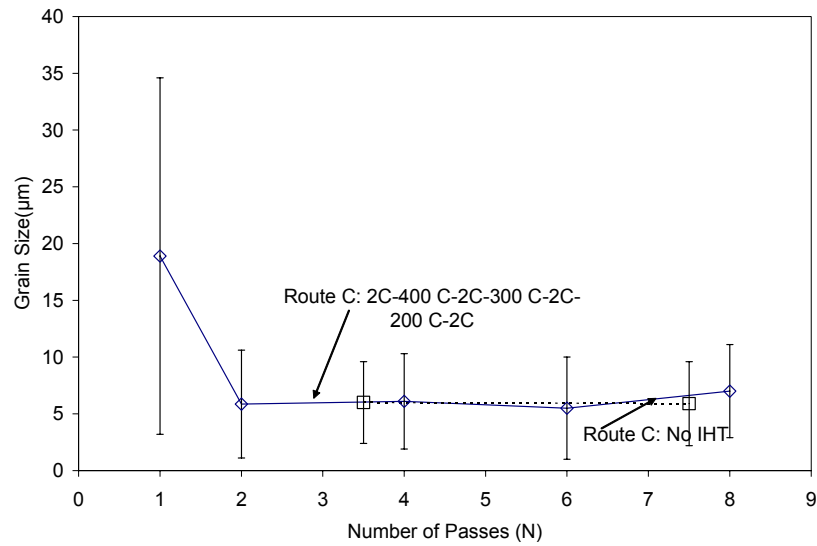


Fig. 138. Grain size as a function of thermo-mechanical processing schedule for route C. IHT: Intermediate heat treatment. Error bars indicate standard deviation values.

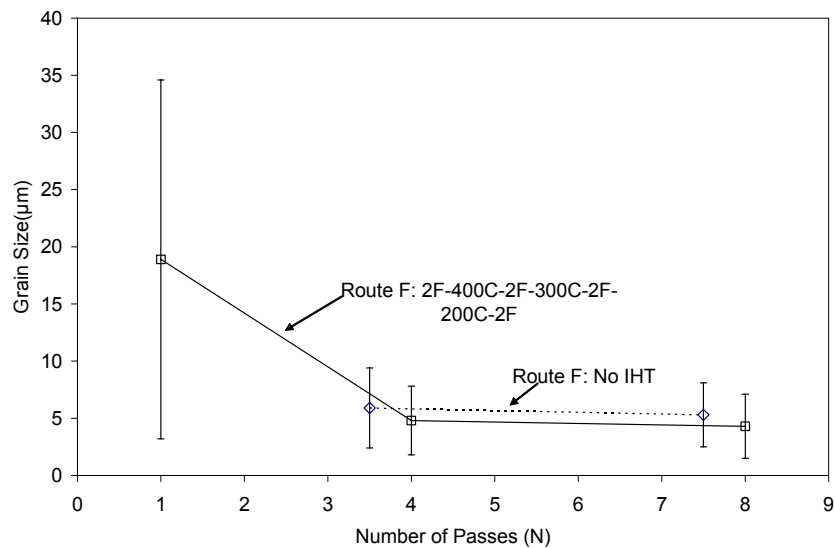


Fig. 139. Grain size as a function of thermo-mechanical processing schedule for route F. IHT: Intermediate heat treatment. Error bars indicate standard deviation values.

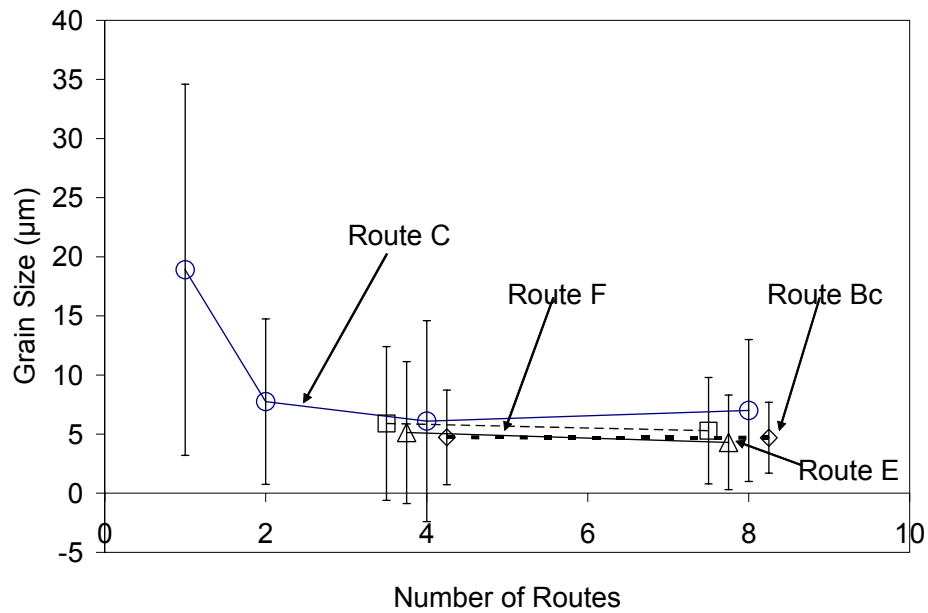


Fig. 140. Grain size as a function of different routes. No intermediate heat treatment was carried out. Error bars indicate full width at half maximum values.

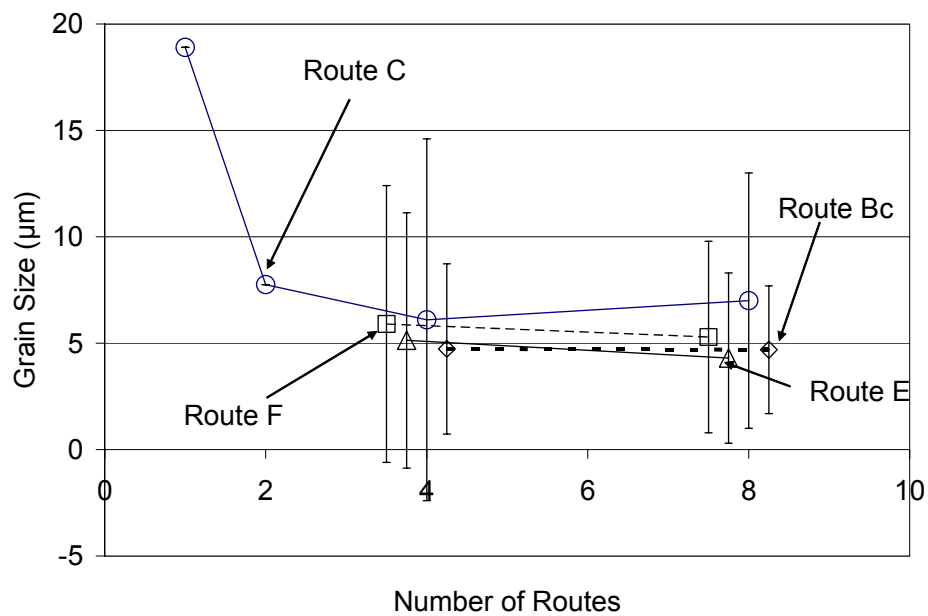


Fig. 141. Grain size as a function of different thermo-mechanical processing schedules. Error bars indicate full width at half maximum values.

Table 13. Recrystallized grain size after processing with different thermo-mechanical processing schedules

TMP Conditions		IHT Condition	Recrystallization Temperature	Average Grain Size (μm)	G.S. Distribution (μm)	FWHM of Range (μm)
# of Passes	Route					
1	A	1A	350	18.9	39	2-110
2	C	2C	250	7.75	41	1-72
4	A	4A	250	6.2	36	1-40
4	B	4B	250	7	16	1-23
4	C	4C	250	6.1	17	0.7-29
4	E	4E	250	5.13	12	1-24
4	F	4F	250	5.9	13	0.6-25.3
4	Bc	4Bc	250	4.73	8	0.6-18.7
4	C	2C+A1+2C	250	6.24	9	0.5-121
4	E	2E+A1+2E	250	7.56	16	0.5-121
4	E	2E+A+2E	250	8.32	17	0.2-33
4	F	2F+A1+2F	250	4.8	9	0.8-24.4
4	Bc	2Bc+A1+2Bc	250	6.2	9	0.5-38
6	E	2E+A1+2E+A2+2E	250	5.8	14	0.5-28.2
6	C	2C+A1+2C+A2+2C	250	5.52	11	0.9-58.9
8	C	8C	250	7	12	1.7-22
8	E	8E	200	4.3	8	0.7-17.5
8	F	8F	250	5.29	9	0.8-20
8	Bc	8Bc	250	4.69	6	0.7-15
8	C	2C+A1+2C+A2+2C+A3+2C	250	5.86	11	0.7-28.6
8	E	2E+A1+2E+A2+2E+A3+2E	250	5.27	9	0.6-20
8	E	2E+A+2E+A+2E+A+2E	250	6.73	11	0.75-26.2
8	F	2F+A1+2F+A2+2F+A3+2F	250	4.31	7	0.2-19.4
8	Bc	2Bc+A1+2Bc+A2+2Bc+A3+2Bc	250	4.86	4	0.9-19.5

5. DISCUSSION

5.1. Increase in load with higher extrusions

As seen in Figs. 28-29, there is an increase in the required punch load with each subsequent extrusion. The largest increase in extrusion load is observed for the second extrusion pass, this large increase is similar in nature to the increase in as-worked hardness with extrusion passes. The main reason for this large increase is the increase in dislocation density of the material. The distance between dislocations decreases, making it difficult for dislocations to pass through one another, which ultimately reflects in the work hardening of the material. After two passes, i.e. a strain of $\sim 2-3$, the dislocation density nears saturation and dynamic recovery processes initiate in the material. Substantial work hardening is not observed with increasing passes, leading to a plateauing of required extrusion loads.

It is interesting to observe a large increase in extrusion loads when a billet is rotated 90° from the previous extrusion direction (Figs. 28-32). One reason for this increase could be related to activation of slip systems during extrusion. The slip systems that are favorable to the shear plane are usually activated during extrusion, leading to generation and interaction of dislocations along these slip systems. Upon rotation of the billet by 90° , new slip systems which are favorable to this new shear plane (which intersects the previous one) get activated. The interactions of dislocations along these new slip systems and the ones generated by the previous extrusion lead to a drastic increase in hardness and strength of the material. In the case of a 180° rotation the shear plane is not changed during subsequent extrusions and dislocations interact along the already activated slip systems. This does lead to increase in strength and hardness, but not as large as compared to the case involving a 90° rotation.

5.2. Shear localization in billet

The shear localization (Figs. 23-24) observed in billet processed through route 4B can be attributed to a combination of initial grain morphology and texture, strain path, higher speed and lower temperature of extrusion (in this case the extrusions were done at room temperature). Although all the extrusions were done at the same strain rate and

temperature, route B showed a greater tendency towards shear localization than other routes. As described by Segal [39] shear localization is seen in the form of large shear bands within the microstructure of the material. There are bands of intensive shear separated by regions of lower strains. The load-displacement curve clearly indicates this localization. There is a build-up of load followed by a sudden drop in it (Fig. 25). The increase of load could be associated with a region in the billet not undergoing extensive shear, when the load exceeds a particular value there is extensive flow of the material along with a drop in the load. This region of extensive flow will be the region containing excessive shear bands. One condition of shear localization is the exhaustion of work hardening capacity coupled with high extrusion speed. It is interesting to observe that this condition is met only for one particular billet; billets extruded through other routes and even to higher passes do not show shear localization. This indicates that initial grain morphology and orientation play an important role in determining the behavior of the material during ECAE.

5.3. Increase in hardness with number of extrusions

The Brinell hardness increases from ~ 42 BHN for the as-cast condition to ~ 130 BHN in the as-worked condition after eight passes (Fig. 32). The largest increase in hardness is recorded during the first pass, where the hardness increases from ~ 42 BHN to ~ 100 BHN. This large increase can be again attributed to the generation of new dislocations due to the shear plastic strain, the formation of dense dislocation forests and the difficulty experienced by other dislocations in passing through these dislocation forests.

The Vickers microhardness values follow the same trend as seen in Brinell hardness measurements (Fig. 33). The Vickers microhardness for as-cast CDA 101 Cu is ~ 55 VHN, which increases to $\sim 115 \pm 6$ VHN after the first pass. It is interesting to observe the trends in hardness increase for routes C and E. For route C the as-worked hardness plateaus after two passes, increasing from 125 ± 5 HV₃₀₀ to 126 ± 3 HV₃₀₀ after two and four passes respectively. Route E processing, on the other hand, leads to an average as-worked hardness of 121 ± 3 HV₃₀₀ after two passes which increases appreciably to 132 ± 2 HV₃₀₀ after four passes. Although the hardness difference between

2C and 2E is statistical, a higher increase in hardness for 4E compared to 4C is consistently observed. This higher hardness increase can again be attributed to the activation of new slip systems and their increased interaction following the 90° after the second pass.

It is also interesting to observe the decrease in values of standard deviation with increasing number of passes, the standard deviation in as-worked Vickers microhardness after one pass is ~ 5 VHN which decreases to ~ 2 VHN after four passes. The initial large standard deviation can be explained by the different orientations of grains in the initial microstructure. As described by Kalidindi et al [37] and Sandim et al [38] the amount of deformation undergone by a grain depends upon whether it has a favorable slip system or not. The grains having favorable orientations with respect to the shear plane deform to a greater extent and contain a higher dislocation density, leading to a greater degree of work hardening. The hardness values reflect the variations seen due to these different orientations. But, as the number of passes increases and as the billet is rotated between passes, the slip systems activated by these extrusions interact more, leading to the breakdown and homogenization of the microstructure. Although the shear plane does not change for route C, the increase in stored strain energy is still sufficient to activate slip systems in grains having unfavorable orientations, leading to the above mentioned phenomenon.

It is interesting to observe that saturation in hardness occurs after four passes irrespective of the processing route. This shows that after four passes, a state of equilibrium in terms of dislocation density and arrangement is achieved. A further increase in passes, at least up to eight, does not lead to a significant change in the same, which is reflected in the saturation of hardness values.

5.4. Hardness scans

The hardness scan along the flow plane of 25 mm square billet processed through one extrusion pass is shown in Fig. 34. As can be seen from the plot, the hardness varies from a minimum of 105 VHN to a maximum of 124 VHN. A major reason for this large variation could be the initial grain orientation and texture within the billet, leading to the same phenomenon as mentioned previously. The hardness within each grain depends

upon the amount of dislocations generated and the arrangement of these dislocations within the grain. Those grains having favorable slip systems break up easily and tend to show higher hardness compared to others.

In case of hardness scans for route 2C (Fig. 35), observe that there is a trend of increase in as-worked hardness in going from the top surface of the billet to the bottom surface. It is difficult to explain this general increase in hardness, but it may be attributed to the initial grain morphology and orientation.

Looking at the hardness scan for 50 mm square cross-section billet (Fig. 35), it is observed that a large variation in the hardness occurs, the hardness ranges from a minimum of ~ 114 VHN to a maximum of ~ 136 VHN for the 2C route. Such a large range could again be attributed to different initial grain orientations. A 180° rotation in the billet creates redundant shear strain and does not sufficiently break up the initial microstructure to cause uniform straining and hardness increase in all the grains.

The hardness scans for the 25 mm and 50 mm square cross-section billets processed up to four passes via route A (Figs. 36-38) do not show any difference due to size of the billets. The as-worked hardness values are more uniform compared to routes 1A and 2C. There is some variation observed in the hardness values, the hardness value varies from 120 VHN to 143 VHN for 25 mm square billet, while for the 50 mm square billet it varies from 123 VHN to 140.6 VHN. This variation could be attributed to microscopic shear banding in the material. There can be another reason for the variation in hardness observed in the as-worked material. Route A deforms the material in two orthogonal planes; this deformation is not effective in breaking down the as-cast microstructure of the billet, leading to preferential working in grains based on their orientation with respect to the shear plane. The hardness scans for other planes and other routes also show some variation, which could be due to initial grain orientation and texture, or could just be statistical.

In case of hardness scans done for the 25 mm and 50 mm square billets deformed through route 4B (Figs. 40-42), observe that the hardness in the fully worked region shows the influence of shear localization and shear banding, giving regions of high and low hardness. Observe that the same trend is observed in case of route 4E and 8E (Figs. 44-47), where a periodic change in hardness is observed, indicating the presence of

microscopic shear bands in the as-worked material. As described by Segal, this lower hardness occurs due to dynamic recrystallization because of significant adiabatic heating in the shear bands [39].

5.5. Recrystallization curves

The Vickers microhardness measurement is a very effective method of plotting recrystallization curves. The recrystallization curve for CDA 101 Cu processed through one extrusion is shown in Fig. 51. It is observed that there is no significant variation in the hardness of the material after heat treatment up to a heat treatment temperature of 150°C. As a matter of fact, the hardness slightly increases after heat treatment up to 150°C. It is interesting to observe that there is a significant drop in average hardness upon annealing at 50°C. This hardness drop is difficult to explain, and has not been observed for materials processed to higher passes. One possible explanation can be the preferential working and subsequent work hardening of grains depending upon their orientation to the shear plane. The average size of as-cast grains for the material used in this study is ~ 15-20 mm in length and ~ 2-5 mm in diameter. The samples for recrystallization study were cubes having nominal dimensions of 8 mm x 8 mm x 8 mm. It is quite possible that the majority of hardness measurements taken for the 50°C heat treatment were on a few grains that did not effectively break up during extrusion, leading to a lower average hardness value. Full recrystallization for 1A material appears to occur after a heat treatment at 350°C for 60 minutes.

The recrystallization curve for material processed through route 4B gives some interesting information (Fig. 54). The hardness measurements show drastic variations with relatively small changes in annealing temperature, especially for the 50 mm square billet. One reason can be the shear localization of this billet during the final extrusion pass. This shear localization led to the formation of large alternating bands of material having undergone heavy plastic deformation compared to material between these alternating bands. Due to such high deformation, there is adiabatic heating within these regions, leading to possible dynamic recrystallization of the material in these bands. A shear localized region can cover a large portion of a sample examined for recrystallization study; when hardness measurements are taken, a substantially lower

hardness value is obtained compared to the rest of the material. Optical microscopy results clearly support this argument about the early commencement of recrystallization within these shear bands [40].

The large “undulations” in the recrystallization curve are absent for extrusions 4E and 8E (Figs. 55-56). Optical microscopy results indicate that there is microscopic shear banding for the 19 mm square billet processed to 4E extrusion passes. This shear banding can be at a smaller scale and not manifested in hardness measurements.

There are some important points worthy of observation in the recrystallization curves for the microstructural breakdown study. With an increasing amount of plastic strain, the recrystallization curves clearly shift to a lower temperature, indicating a decrease in the temperature required for commencement of recrystallization. There is an absence of the so-called “undulations” observed in the recrystallization curves in the case of scale-up study, and the error-bars for these curves are small compared to those for scale-up study. The main reason for the uniform curves could be intermediate heat treatments. Intermediate heat treatments were done at four different temperatures, at 400°C, 300°C, 200°C and 350°C. These heat treatments lead to recrystallization and some grain growth in the as-worked material. The recrystallized grains are much more uniform in size, shape and texture compared to the initial as-cast grains. Due to a uniform starting microstructure, any further plastic deformation leads to a more uniform deformation in these grains and a very similar recrystallization behavior during subsequent heat treatments. Due to homogenization of the microstructure, there is less tendency of the material to shear band, so shear banding and subsequently non-uniform recrystallized grain sizes are absent in such material.

The recrystallization curves for route C indicate that the recrystallization commences at a temperature of ~ 175°C as indicated by a drop in the Vickers hardness measurements (Fig. 60). The recrystallization process is completed at a temperature of ~250-300°C. Route C involves redundant shear: the grains in the billet being plastically deformed in one pass are returned to their original shape and morphology during the next pass. Routes Bc, E and F show commencement of recrystallization at ~125 – 150°C.

Routes like Bc, E and F involve rotation of the billet by 90° between passes, leading to a change in the shear plane during deformation, and a three dimensional

network of intersecting shear bands is created in the material. The intersection points of these shear bands are points of high strain energy and high lattice distortion. During heat treatments, these points act as nucleation sites for recrystallization (Figs. 58-62). Compared to this, route C may lack these intersecting networks of shear bands and points of high strain energy, leading to delayed commencement of recrystallization.

5.6. Recrystallization range

Figs. 64-66 show recrystallization ranges calculated from the recrystallization curves of different routes and thermomechanical schedules. These curves indicate the temperature range required for recrystallization from 10% recrystallization to 90% recrystallization. It is again observed that route C needs a higher temperature for recrystallization compared to routes that involve billet rotation by 90° between extrusions. As can be seen from Fig. 64, the recrystallization processes commences in routes B and E before routes C and A. One possible reason again could be the generation of the three dimensional network of dislocations and shear bands in the material due to rotation of the billet by 90°. Route A does not involve rotation of billet between extrusions, but there is a change in the orientation of the shear plane with each extrusion pass. This mechanism may not be as effective in the formation of three dimensional networks of shear bands and dislocations compared to route E, but is better than route C which leads to redundant strain. Thus, recrystallization in route A commences before recrystallization in route C.

The plots for different thermo-mechanical schedules also indicate a similar trend, with route C having a very high temperature for commencement of recrystallization, while routes Bc and F have the lowest temperature required for the commencement of recrystallization.

Another interesting point is the temperature range required to reach 90% recrystallization from an initial condition of 10% recrystallization. It is observed that this temperature range is small for the case of material processed to two extrusions (Figs. 65-66). It is also low for 4C extrusion route and for 2E-400°C-2E TMP schedule. This can again be due to the mechanism of dislocation interaction and formation of shear band networks. As there are fewer points of heavy lattice distortion and of high stored strain

energy in the above mentioned cases, there is a delay in the commencement of recrystallization. Along with this, nucleation for recrystallization originates on a much larger scale compared to other cases having points of high strain energy. As the commencement of recrystallization occurs at numerous locations and the strained material has similar levels of strain energy, recrystallization progresses very quickly compared to the case of materials having points of high strain energy while majority of the microstructure is having relatively low strain energy [40]. Route 2E-400°C-2E is similar to route C, as an intermediate heat treatment is carried out after the second pass, negating the influence of the 90° rotation of the billet. Compared to this, routes F and Bc show a wider range of recrystallization temperature even with intermediate heat treatments as these heat treatments do not coincide with the 90° rotation of the billets.

It is also observed that TMP schedules involving intermediate heat treatments achieve 90% recrystallization temperature at a lower temperature range compared to their counterparts without intermediate heat treatments. One reason for this can be that the material which has not been processed through intermediate heat treatments may show heterogeneity in the as-worked structure. Some heterogeneity in the microstructure originates in the grain size and grain orientation of the starting microstructure. Due to the different orientations of the grains in the original microstructure, they have different plastic strains after been processed via ECAE. These grains recover/recrystallize to different degrees during recrystallization heat treatments and consequently give a broad temperature range for full recrystallization. The large standard deviation values also indicate the variation of micro-structure in the as-worked material.

Another reason for the above phenomenon could be the amount of stored strain energy. We know that copper has relatively low stacking fault energy (SFE), about 40 erg/cm² (~75mJ/m²) [41, 42]. This low stacking fault energy promotes the formation of stacking faults which complicate the process of dislocation interaction. There is little dynamic recovery of the as-worked material up to ~2-3 passes. The high stored energy provides a greater driving force to the process of recrystallization which leads to the abrupt annihilation of the dislocation structures within the sub-grains. At higher temperatures there is a destruction of as-worked microstructure and we see the formation of new strain free grains. The above mentioned process happens in a very narrow range

of temperature. Compared to the material processed to these fewer passes, when the material is processed to four or more passes, dynamic recovery starts to occur. The rate of dislocation annihilation equals the rate of dislocation generation and the dislocations are arranged in low energy dislocation structures (LEDS). The amount of dynamic recovery is initially low for the four pass material, but increases as the number of passes goes up. Due to this reduction of stored driving energy, the process of recrystallization happens slowly over a wider temperature range.

Recrystallization behavior of OFHC Cu having different initial grain sizes and cold rolled to a reduction of 93% has indicated that material with finer initial grains recrystallizes earlier and in a narrow temperature range compared to material having coarse initial grains [43]. One reason has been attributed to the profuse formation of shear bands in the large grained material, leading to the cutting up of the cube-bands and formation of a very inhomogeneous as-worked microstructure [44]. Thus large initial grains may lead to a variation in the stored energy between different microscopic regions, leading to slow kinetics of recrystallization.

5.7. Transmission electron microscopy

Figs. 67–69 show the as-worked microstructure in the flow plane for CDA 101 Cu processed up to four extrusion passes via route E. It can be seen that the microstructure does not depend upon the size of the processed billet.

The samples for TEM were taken from similar locations for the three billets. The microstructures indicate identical sub-grain size and morphology obtained for these different sized billets. It may be concluded that the sub-grains obtained after four passes via route E are independent of the size of the processed billet. But these results could be just fortuitous, the region observed through transmission electron microscopy is very small, and the similarity may be just localized to that particular small region. Other researchers, especially Ferrasse [24] have obtained similar results after four passes through different routes which seem to confirm the claim that the sub-grain structure obtained is independent of the billet size, even independent of the strain path and depends more upon the level of strain.

The transmission electron micrographs for the three different sized billets processed up to eight passes via route E are shown in Figs.70-72. From the figures, it is concluded that the strain induced in the billets, and hence the microstructural evolution of the material is independent of the billet size.

It is interesting to observe the TEM micrograph of as-cast CDA 101 Cu (starting material, Fig. 73). Some dislocations in the form of small tangles are observed in the microstructure. It is possible that these dislocations are solidification dislocations, created during the solidification of Cu from the molten metal. It is also possible that these dislocations may have been created in the material during sample preparation. Looking at the proportion of these dislocations it is concluded that if these dislocations are created during sample preparation, they do not influence the results drastically.

Two different types of dislocation structures are observed for the material processed for one extrusion pass. As shown in Fig. 74, small and refined sub-grains having aspect ratios close to one are observed in some portions of the microstructure. The same sample contains irregular dislocation structures and sub-grains having diffuse dislocation walls (Fig. 75). The non-uniformity observed in the microstructure can be attributed to the initial grain orientation and texture. Some grains have favorable orientations and during shear deformation easily break-up into refined sub-grains. Compared to these, some grains are not oriented favorably and lead to the formation of sub-grains and dislocation structures as shown in Fig. 75. It can thus be concluded that one extrusion pass, corresponding to a plastic shear strain of 1.16 is not sufficient to completely break-up the microstructure and produce a uniform sub-grain structure.

Hatherly and Malin [45] have reviewed the development of substructure during deformation of copper and its alloys via rolling. It has been observed that at very low levels of deformation ($\epsilon < 0.05$), the dislocation configuration consists of bundles of primary dislocations lying on the $\{111\}$ planes and predominantly in the $\langle 121 \rangle$ directions. These are soon replaced by a nearly equiaxed cell structure in which the cell size decreases with further strain. In this structure, the cell walls are rather diffuse regions of high dislocation density parallel to the simple crystallographic planes but subsequently this crystallographic association is lost. In rolled copper, the cell structure is well developed after $\sim 10\%$ reduction. It has been suggested that the equiaxed cell structure is

incapable of supporting extensive homogeneous deformation and this leads to the formation of instability in the form of a microbands. These microbands are usually parallel to the direction of macroscopic shear and develop on the $\{111\}$ orthographic plane.

It is worth mentioning that stacking fault energy plays a key role in the sub-structure formation in FCC metals. For medium to high SFE metals, during rolling, the microbands form along the $\{111\}$ plane and are separated by regions of equiaxed cells. The low SFE materials like 70:30 brass do not show the development of microbands and cell regions, but the deformation is supported by microscopic twinning. The twins are rotated during deformation until they are aligned parallel to the direction of maximum strain. Further deformation by microband formation or twinning is difficult and plastic instabilities develop lead to the formation of shear bands.

Malin et al [46] deformed OFHC Cu single crystals in simple shear by rolling. The single crystals had three different orientations, (110) $[1\bar{1}2]$, (100) $[001]$ and (111) $[1\bar{1}0]$. Rolling was carried out at room temperature and at 77 K. It was concluded that at low temperatures, twinning was a major deformation mode. Twinning was not observed after room temperature deformation for any of the above mentioned materials. Neither slip nor twinning can be regarded as the unique deformation process for any FCC material except one with extremely high or extremely low stacking fault energy. Twinning was observed for the (100) $[001]$ and (111) $[1\bar{1}0]$ cases during deformation at either 77 K or at room temperature. While in the case of (110) $[1\bar{1}2]$ twinning was not observed in either case. In this orientation two slip systems are symmetrically oriented with respect to the transverse direction and favorably oriented for both elongation and thinning. This provides an opportunity for extension without transverse strain and without change of orientation.

The TEM micrograph for pure Cu processed to two extrusion passes via route C indicates the formation of elongated lamellar sub-grains having some dense sub-grain boundaries (Fig. 76). Some dislocation tangles are still visible, but majority of the dislocations have moved to low energy dislocation structures (LEDS), i.e. sub-grain boundaries. The sub-grain size reaches a saturation level after two passes, without any further refinement in terms of minimum size achieved for higher extrusion passes.

Further deformation to four and eight extrusions leads to the generation of lamellar sub-grains free from dislocations. The microstructure shows signs of dynamic recovery with the reduction of stored strain energy as the dislocations move from high energy configurations to low energy ones.

Fig. 77 indicates the formation of a mixture of equiaxed and elongated sub-grains after four passes through route C. The redundant shear helps in retaining the shape of the sub-grains even after a strain of ~ 4.64 . The sub-grain boundaries generated after processing up to eight passes through different routes and with IHTs are diffuse and the sub-grains contain internal dislocations (Figs. 78-91). Similar results are obtained for all routes. The as-worked microstructures after equivalent strains with and without IHT consist of sub-grains having similar shapes. The microstructure generated in case of processing with IHTs is similar to the one produced after two ECAE passes. The IHTs lead to complete annihilation of the sub-grain structure and newer subgrains are formed during subsequent ECAE processing. The sub-grains show a lamellar structure typically associated with ECAE processing. The average length is ~ 400 nm and width ~ 250 nm after four extrusions. After eight extrusions the dimensions decrease to ~ 350 - 400 nm in length and ~ 150 - 200 nm in width. Some equiaxed sub-grains are observed for all extrusion routes. The microstructure obtained after equivalent strains but without IHTs contain cleaner sub-grains, dense and thin boundaries, indicating a recovered microstructure. A drastic change in size or morphology compared to TMP schedules incorporating IHTs is not observed. The selected area diffraction (SAD) patterns confirm that most sub-grains after processing with IHTs have low angle boundaries (LABs) while most sub-grains produced after processing without IHTs have a majority of high angle boundaries (HABs). The sub-grain size and morphology obtained in this study agree well with those obtained by other researchers.

Fig. 90 illustrates the sub-grain structure obtained on the flow plane after route 8Bc. It is very interesting to observe the formation of a recrystallized grain in the fully worked material. No such recrystallization was observed in other cases. Some researchers have observed this phenomenon after similar strains. Wang et al [47] processed pure Cu single crystals through a 90° tooling through route E up to five passes. After two months of storage at room temperature some samples extruded to three passes and all the samples

extruded to five passes showed the formation of new strain free grains at the intersection points of microscopic shear bands. It is concluded that with eight passes, a large portion of the grain boundaries in the material are high angle grain boundaries with a random orientation. This provided a large amount of driving force for sub-grain nucleation and growth. The activation energy for diffusion in nanocrystalline Cu is much smaller compared to that of coarse grained copper, making the process of diffusion controlled grain boundary migration and consequently recrystallization process much easier [48]. It is also possible that the heating of the thin slice of Cu during sample preparation for TEM may lead to the formation of these recrystallized nuclei. Other routes did not produce such recrystallized grains. This process needs further investigation.

Chang and Shan have carried out intermediate heat treatments during ECAE of pure Al [31]. 99.9 % pure Al bars were extruded through route A up to four passes in a 90° die. It was observed that IHT lead to a decrease in the sub-grain size but increased the aspect ratio of these sub-grains. Elongated sub-grains were formed after two passes, but upon further processing these sub-grains broke up into equi-axed ones. The heat treatment at 200°C for two hours after two passes lead to the formation of equiaxed grains. This equi-axed microstructure, upon processing formed a substructure containing elongated sub-grains. It was also observed that annealing at the same temperature after four extrusions created a very large fraction of high angle grain boundaries in the microstructure.

As described by Dalla Torre et al [23], with increasing number of passes, the cells rotate to reach higher misorientation angles. With further deformation, these cells are transformed to sub-grains, which are confined by dislocation walls, and well developed sub-grain boundaries with higher misorientation angles. The dynamic recovery occurring at these higher passes leads to the formation of sub-grains relatively free of dislocations and dense sub-grain boundaries.

The sub-grain size obtained in this research agrees well with the sub-grain sizes obtained by other researchers. Ferrasse et al [21] performed ECAE on conventionally extruded and annealed CDA 101 Cu and reported the formation of long and parallel subgrains right after the first pass. The average width of these sub-grains was 300 nm. After four passes through route A, a reduction in the size of the sub-grains was observed.

The sub-grains become more dislocation-free and the misorientation between the subgrains increased. Dalla Torre [23] performed ECAE up to 16 passes via route Bc on annealed copper and reported observation of elongated subgrains having an average width of ~400 nm. The width of these subgrains decreases with the number of passes to ~200 nm after two passes and remains fairly constant to 16 passes. Both Ferrasse and Dalla Torre observed the formation of equi-axed subgrains with an increase in the number of passes. Ferrasse reports the formation of equi-axed subgrains after four passes through routes A, B and C. Dalla Torre reports formation of equi-axed subgrains after a 360° rotation of the billet (four passes through route Bc). It is worth noting that Dalla Torre observed the transverse plane of the billets, while Ferrasse observed the flow plane of the billet. In our study some equiaxed subgrains were observed for the material processed to eight passes via all the routes. These results agree well with those obtained by Huang et al [22] who report the observation of equiaxed subgrains along the transverse plane and a mixture of elongated and equiaxed subgrains along the flow plane in Cu extruded to eight passes via route Bc and C. We can conclude that eight passes are not enough to generate equiaxed subgrains in copper, if generation of equi-axed subgrains is at all possible through ECAE.

The sub-grain size obtained after high plastic strain levels in this research agrees well with that obtained for different starting grain size and even for different materials. The starting material in most of the above mentioned cases was annealed CDA 101 Cu having a much smaller initial grain size compared to the as-cast Cu used in this research. Harris et al [49] carried out ECAE on commercial purity aluminum having two different starting grain sizes. Al samples having 1500 μm and 150 μm grain sizes were extruded, and it was concluded that the deformed states became identical after a strain level of ~ 6 (Fig. 142). In a large initial grain size material, a large portion of the grains are less constrained by their neighbors and are more likely to behave like single crystals, possibly resulting in a greater degree of grain subdivision into different textural components.

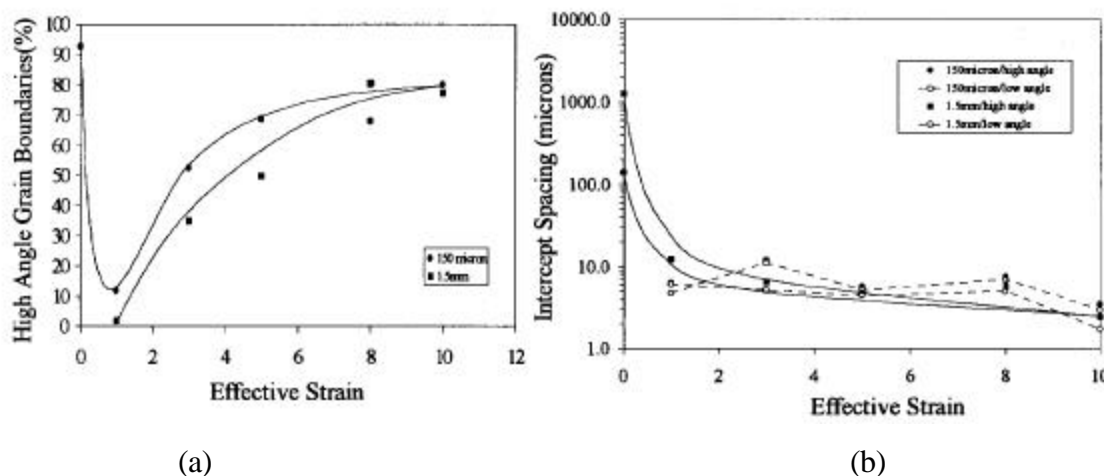


Fig. 142. (a) Percentage of low (<15%) and high (>15%) angle boundaries, as a function of strain, for commercial purity Al having an initial grain size of 1500 μm and 150 μm . (b) low and high angle boundary mean linear intercept spacing of the samples with initial grain sizes of 1500 μm or 150 μm as a function of strain [49].

When a metal is plastically deformed, there are significant changes in the microstructure, especially in terms of the dislocation density, arrangement of dislocations, and generation of low and high angle grain boundaries. At intermediate strains when a polycrystalline material is deformed by simple shear (through rolling) the following changes occur in its microstructure [50]:

- (1) The original grains are deformed to a shape determined by the applied strain and strain path, and the area of the high angle grain boundaries is increased.
- (2) A cell and sub-grain structure develops within the grains, and with increasing strain, the sub-grain size decreases and the misorientation angle between these sub-grains increases until a steady state is reached after a strain level of 1-2. It is thought that the steady state sub-grain structures are the result of the sub-grain boundaries being constantly altered, formed and removed by the passage of dislocations during deformation. Such sub-grain boundaries are termed as incidental dislocation boundaries
- (3) Some medium and high-angle boundaries may be created within the old grains by grain subdivisions. Such boundaries may separate regions within a grain that are deforming on different set of slip systems, such that their orientations diverge

until stable end-orientations are reached. High-angle boundaries may also be formed as a result of coarse slip associated with shear banding.

As discussed by Hughes and Hansen [51] the sub-grains are formed due to the sub-division of the grains by the geometrically necessary boundaries (GNBs) and the incidental dislocation boundaries (IDBs). At higher strains the dislocation boundaries show a tendency of reorienting themselves from the typical cell-block structure to the more lamellar structure. As the strain increases, the dislocations start amassing in these boundaries leading to a further increase in the orientation spread. Even within the individual crystallites there are different slip systems which are active leading to the formation of complex dislocation boundaries. This results in different parts of the grain rotating towards different end orientations which in turn leads to the formation of HABs. Segal [39] has suggested that a large portion of the HABs are laid out in shear bands, which are parallel to the shear plane of the ECAE pass, and during subsequent ECAE passes the new shear bands intersect with the old ones and produce a well dispersed network of shear bands in the material.

5.8. Recrystallization TEM

We see that the microstructure after four passes is made up of sub-grains which still contain some dislocations in their interiors but have densely packed boundaries (Fig.67-69). The stacking fault energy (SFE) of Cu is relatively low, which leads to slower dislocation movement and there is an accumulation of dislocations in the sub-grain interiors. Other FCC metals like Al and Ni which have much higher stacking fault energies, show sub-grains which are relatively free of dislocations and have larger sub-grain sizes at the given plastic strains. This happens because of easy dynamic recovery. Due to the low SFE, there is little recovery in Cu, but there is a lot of stored strain energy in the microstructure which leads to a rapid grain growth even at low recrystallization temperatures [41]. Ferrasse reports the formation of strain free grains from the highly strained sub-structure at an annealing temperature of 160°C for OFHC Cu. This material was processed for eight passes via route A. We observed the formation of strain-free grains at an annealing temperature of 180°C. Komura et al [41] carried out recrystallization studies on as-worked commercial purity Cu and 99.99% Al. Both Cu and

Al were extruded in a 90° tooling for up to six and four extrusion passes via route Bc. TEM was carried out on the transverse plane of the as-worked and recrystallized samples, and it was observed that in the case of Cu, a uniform sub-structure is not obtained even after a plastic strain of ~ 10 (~10 passes), but in case of Al, a uniform substructure was obtained after four passes. The main reason for the microstructural evolution in the case of Cu is the low stacking fault energy (SFE); ~ 40 erg/cm² compared to ~ 200 erg/cm² for Al. This low SFE retards dislocation motion leading to a slower microstructural evolution in Cu compared to Al, and this leads to the formation of a non-uniform substructure in the case of Cu. Upon static recrystallization, new and strain free grains start to evolve from the microstructure after a heat treatment of ~ 150°C where the microstructure has a duplex nature, containing both sub-micron scale sub-grains and large micron-scale recrystallized grains at this level. Upon annealing at 200°C, the small strained sub-grains are totally consumed by the newly developing recrystallized grains. In the present research, at an annealing temperature of 200°C, a duplex microstructure is visible (Fig. 98). One reason for this could be the lower level of plastic strain (~4.6) imparted to the material.

It is noted that there is a continuous drop in the Vicker's hardness with an increase in the annealing temperature, even though the TEM micrographs show little change in the microstructure up to 180°C. No clear explanation can be provided for this behavior. One reason can be the area of observation in the TEM. The size of regions observed during TEM is of the order of 2-3 μm, compared to this, a micro-hardness indentation is spread over a much larger area, around 250 μm². Although more than one TEM specimen was observed for recrystallization microstructure, it is possible that the small area under observation did not contain any recrystallized grains.

5.9. Optical microscopy

For pure Cu processed up to one extrusion pass, optical microscopy of partially recrystallized material reveals a network of shear bands inclined at 45° to the extrusion axis along the flow plane (Fig. 99). These shear bands are regions of severe plastic strain and consequently contain high dislocation concentrations, severe lattice distortion and strain energy. The heat treatment at 175° C leads to the formation of some recrystallized

grains in these shear bands, while the rest of the microstructure does not show any clear sign of recrystallization. The fully recrystallized microstructure is obtained after a heat treatment at 350°C. As expected, the recrystallized microstructure is banded, showing smaller grains in regions containing shear bands, and large grains in regions free from these shear bands (Fig. 100). Shear bands due to their high strain energy, contain numerous nucleation sites. The other regions contain fewer nucleation sites and consequently the formation of very large grains is observed. The high recrystallization temperature may lead to some grain growth in regions containing shear bands; but even with this grain growth, the grain size remains small and uniform compared to the remaining microstructure.

Optical microscopy can be correlated with the large error bars of the recrystallization curves. The recrystallization in shear bands initiates at $\sim 175^\circ\text{C}$, leading to the formation of recrystallized grains in these bands. These recrystallized grains have much lower hardness compared to the grains in the as-worked condition, leading to the large error bars. With an increase in the temperature, the microstructure is fully recrystallized, giving smaller error bar values obtained for temperatures of 300°C and 350°C. It is observed that $\sim 40\%$ of the analyzed area is occupied by grains having size greater than 50 μm after annealing at 350°C for one hour.

Image analysis was performed on the fully recrystallized microstructure to determine parameters like average grain size, standard deviation and spread in the grain size. In studies done by other researchers, grain size histograms are plotted with percentage number of grains along the ordinate [52]. In this research, it was observed that some microstructures contain few gigantic grains in a matrix of smaller grains. If a histogram is plotted with percentage number of grains as the ordinate, these large grains are not properly represented. So, it was decided to plot the histograms with percentage of area as the ordinate. In general, it is observed that even in a uniform microstructure, plotting a histogram with percentage area as the ordinate leads to a shift in the curve towards the right, i.e. we get a larger average grain size.

Route C involves shear deformation of the material along a single shear plane, the direction of the shear being reversed in every alternative extrusion which leads to the generation of shear bands along one plane. Upon recrystallization, route 2C leads to the

formation of alternate bands of small and large grains. It is interesting to observe the different microstructures obtained for 25 mm and 50 mm square billets processed through route 2C (Figs. 101-102). The 50 mm square billet upon recrystallization leads to a non-uniform microstructure, but we do not observe the banded grain structure obtained in the 25 mm square billet. One reason for this can be the different initial orientation and texture of grains in these billets. The grains in the 25 mm square billet could be oriented in a manner that favors the formation of macroscopic shear bands during extrusion.

It is observed that there is little difference in terms of average grain size and grain size range for fully recrystallized microstructures for the 25 mm and 50 mm square billets processed through 2C route. There is a drastic improvement in the uniformity of the grains in the microstructure compared to route 1A. Route 2C leads to ~10% of the area being occupied by grains with size $> 50 \mu\text{m}$. A small peak is starting to appear at an average grain size of 12-13 μm .

Cu processed through route 4A also shows the formation of microscopic shear bands when viewed along the flow plane (Fig. 103). The recrystallized grains start to form along these shear bands and at a temperature of 250°C, complete recrystallization is achieved. The histogram for 25 mm square billet shows an average grain size of 6 μm while the histogram for 50 mm square billet shows an average grain size of 7 μm . In case of the 50 mm square billet, some large grains having equivalent diameters of $>50 \mu\text{m}$ are observed, and occupy ~ 8% of the analyzed area (Fig.105). Non-uniformity is clearly observed in the microstructures for material processed through 4A route. One reason can be the deformation path for route 4A. Route A leads to deformation in multiple directions. But the deformation is restricted to two orthogonal planes and as there is no billet rotation, we do not observe the creation of a dense three dimensional network of shear bands which would lead to the formation of a more uniform microstructure during recrystallization.

The micrographs for 25 mm and 50 mm square billets processed through route 4B are shown in Figs. 106-108. As mentioned earlier, the 50 mm square billet shear localized at the last extrusion pass. This lead to the formation of gigantic masses of shear bands containing regions of intense shear deformation, the material between these masses did not undergo such severe deformation and hence it is expected that a duplex grain size will

be obtained for this billet. We do observe the formation of small grains in the location of these large shear bands and large grains in the regions free for these shear bands, but the difference is not as drastic compared to route 2C and 4A. One reason for this can be the rotation of the billet between subsequent extrusions in route B. It is also possible that the shear localization in the final pass did not create a very big difference in the levels of plastic strains induced in the shear localization bands and material between them.

Before the start of this study, it was assumed that route E would not lead to the formation of shear bands after four extrusion passes because it involves rotation of the billet by 90° between passes. But the optical micrographs for fully recrystallized Cu processed through route 4E show evidence of shear banding (Figs. 109-112). Alternating bands of large and small grains are observed in the microstructure. The shear banding is prominent in the 19 mm square cross-section billet compared to the other two sizes. This could again be attributed to the initial grain orientation and texture.

The billets processed through eight passes via route E lead to a uniform microstructure free from any evidence of shear banding (Figs.113-115). The standard deviation and range for the grain size is also small compared to the other extrusion schedules. The grain size data obtained for the three billet sizes is very similar indicating the effectiveness of ECAE in processing larger sized billets just as effectively as smaller billets.

The microstructures obtained for the microstructural breakdown project reveal some interesting information. Fully recrystallized microstructures were observed after annealing at 250°C in the case of billets processed for 2C and 2E extrusion passes. As expected, the microstructure is non-uniform with some very large grains embedded in a matrix of medium and small grains (Figs. 116-117).

Figs. 118-119 show microstructures for billets processed up to four extrusion passes via route E, with intermediate heat treatments, at 400°C and 350°C . It is observed that the microstructure is free from shear bands compared to the microstructure obtained after route 4E without intermediate heat treatment. This indicates that intermediate heat treatments reduce the tendency to form shear bands. Another point worth noting is the overall uniformity of the microstructure. We observe that although the microstructure is

free of shear bands, it is not as uniform compared to the microstructure obtained after 4E extrusions without intermediate heat treatment.

The microstructure obtained after four extrusion passes via routes E and C with intermediate heat treatments are very similar (Figs. 118-120). It is not surprising as route E is 2C*2C, with a rotation of 90° between the second and third extrusions. The intermediate heat treatment at 400°C led to recrystallization and some grain growth, and all the shear bands developed during the first two passes were eliminated due to the heat treatment. As a result, the effect of 90° rotation was nullified; giving results similar to route 4C which does not involve any 90° rotation between passes. The fully recrystallized microstructure obtained after 4C extrusions without intermediate heat treatment did not show effects of prominent shear banding (Fig. 121). But the microstructure is not uniform and is inferior in terms of grain size and uniformity compared to route 4E without intermediate heat treatment. Thus we can conclude that a rotation of 90° between passes leads to better breakdown and homogenization of the microstructure.

The microstructures obtained after route 4F with and without intermediate heat treatments are similar in terms of grain size and homogeneity (Figs. 122-123). Similarly, the microstructure obtained after route 4Bc without intermediate heat treatment is not appreciably better than the one obtained after route 4Bc with intermediate heat treatment (Figs. 124-125). But it is interesting to note that the microstructures obtained for routes 4F and 4Bc are more uniform compared to those obtained for routes C and E. Route E is 2C*2C and the microstructure is returned to the original shape before a 90° rotation is given to the billet. So the generation of a network of shear bands may not be as effective as in the case of route F. In route F, the billet is given a 90° rotation prior to a 180° rotation, so there is shear deformation in three orthogonal planes during the second extrusion path. The generation of a three dimensional network of shear bands early in the extrusion route appears to lead to better breakdown of the microstructure. Route Bc involves a 90° rotation between each extrusion pass and should be the most efficient method of generating a 3-D network of shear bands.

The fully recrystallized microstructures obtained after eight extrusion passes with and without intermediate heat treatments do not show any unexpected results. The grain

size histograms obtained for route 8C with and without intermediate heat treatments are not very different (Fig. 130-131). The average grain size for 8C with a TMP schedule of 2C-400°C-2C-300°C-2C-200°C-2C is 5.8µm while without intermediate heat treatment the grain size is 7 µm.

Processing via route E with and without intermediate heat treatments gives us different microstructures. Route 8E without intermediate heat treatment results in a fine and homogenous microstructure with an average grain size of 4.3 µm and a spread of 0.7-17.5 µm (Fig.114). A TMP schedule of 2E-400°C-2E-300°C-2E-200°C-2E leads to a slightly more homogeneous microstructure with a smaller average grain size compared to a TMP schedule of 2E-350°C-2E-350°C-2E-350°C-2E (Figs. 128-129). The average grain size and grain size spread for the former TMP schedule is 5.3 µm and 0.6-20 µm. For the latter TMP schedule these values are 6.7 µm and 0.7-26 µm. One reason for this difference in microstructures even after equal amounts of plastic deformation through an identical strain path could be the different IHT temperatures. For the first case, the heat treatment temperature is reduced with increasing strain. This would lead to lesser grain growth, especially in the case of 300°C, and at a temperature of 200°C it is not expected that the microstructure is even fully recrystallized. Thus shear bands generated during pervious processing are carried over after the heat treatment, and during subsequent processing these old shear bands interact with the newly created ones to produce a three dimensional array of nucleation sites for recrystallization. Compared to this schedule, when heat treatments at temperature of 350°C are carried out, it is expected that there is full recrystallization and some grain growth. Subsequent processing just leads to formation of dislocations arrays in one plane, which upon recrystallization lead to the formation of a non-uniform microstructure.

Processing to eight extrusion passes via routes F and Bc also indicates a similar trend (Figs. 132-135). The grain size and uniformity of the microstructures obtained with and without intermediate heat treatments are similar. The processed material even without an intermediate heat treatment does not show any affect of macroscopic shear banding. Table 13 indicates the average recrystallized grain size obtained for different processing schedules; note that 8Bc produces the best results. Full width at half

maximum value has been used to indicate the uniformity of grain size distribution in a more representative manner.

6. CONCLUSIONS

There were two main objectives of this research project. The first was to determine if plastic strain induced during ECAE is dependent upon the work-piece size. The second was to determine the effectiveness of ECAE in breaking down the as-cast microstructure of CDA 101 Cu and to devise an effective and efficient thermo-mechanical schedule for grain refinement of both as-worked and recrystallized CDA 101 Cu.

The following is a list of conclusions and findings from the work done for the first research project (examination of size effects).

1. Hardness scans, transmission electron microscopy and optical microscopy indicate uniformity in strain induced in the billet, irrespective of the billet size. Thus severe plastic strain induced in the material is independent of work-piece cross-sectional dimensions.
2. However, the punch loads required for extrusions generally increase with increasing number of passes due to work hardening in the material. The extrusion loads required during first extrusion pass of as-cast CDA 101 Cu are found to depend upon the initial grain orientation and texture with respect to the extrusion direction. A corollary to this is that high loads are required for extrusion when a billet is rotated by 90° from the previous extrusion pass.
3. Extrusion loads required for a 50 mm square cross-section billet are ~ 3 times the load required for extrusion of a 25 mm square cross-section billet. This indicates that a larger billet gives better load efficiency during extrusion.

The following conclusions and findings are obtained from work done during the second project which was aimed at the determination of effectiveness of ECAE in grain refinement of as-cast CDA 101 Cu.

4. ECAE leads to rapid microstructural breakdown of as-cast CDA 101 Cu. A uniform recrystallized microstructure can be obtained after eight extrusion passes (strain ~ 9.6).
5. Route C, with and without intermediate heat treatments produces the most inhomogeneous recrystallized microstructure. Route Bc, with and without

- intermediate heat treatments produces the most homogeneous recrystallized microstructure.
6. Intermediate heat treatments for the cases examined (after every two extrusion passes) did not lead to any improvement in the recrystallized microstructure.
 7. TEM on the flow plane indicates that the microstructure obtained after eight extrusion passes contains regions of lamellar and highly recovered sub-grains with large misorientations across sub-grain boundaries. There are some regions containing equi-axed sub-grains. Thus eight passes are not sufficient to produce equi-axed sub-grains in cast CDA 101 Cu.
 8. There is a shift towards the left (lower temperature) in the recrystallization curve with an increasing number of extrusion passes indicating a decrease in recrystallization temperature with increase in plastic strain
 9. Recrystallization for multi-pass routes which involve a 90° rotation of the billet between passes commences early due to the presence of nucleation sites having high stored strain energy, compared to route C.
 10. Some regions in the fully recrystallized microstructure obtained after two extrusion passes via route C contain very small grains. These grains are equal in size to the smallest grains produced after eight passes. Thus, some regions after route 2C achieve maximum refinement possible for up to eight extrusions. However, the microstructure obtained after two extrusion passes is inhomogeneous.

7. RECOMMENDATIONS FOR FUTURE STUDIES

A more detailed load analysis for billets of different sizes and under different tooling conditions will give a better understanding of the factors influencing the load requirements during extrusion. Load requirements for billets extracted from different locations in an ingot are different. A detailed analysis relating these load requirements with the initial grain morphology and texture will help in understanding the extrusion process. A detailed TEM and optical microscopy analysis of the transition regions obtained in some routes like A and B would help in understanding the process of shear deformation during ECAE. Thermo-mechanical testing of materials obtained for different sized billets can also provide good supplementary information to the work already done in this research.

For future work that can be done in determining the effectiveness of ECAE in grain refinement of Cu, electron back scattered diffraction (EBSD) analysis is strongly recommended. EBSD analysis on as-worked and heat treated material will give extensive information about grain size and grain size distributions, the orientation and texture in the material. With the current TEM facilities available at Texas A&M University, it is possible to carry out in situ heat treatments. Such TEM examinations while the specimen is being heat treated will give a better understanding of recrystallization behavior in severely deformed Cu. For this particular project, intermediate heat treatments were carried out after every two extrusions; these heat treatments negated some of the benefits achieved by the 90° rotation of the billet after every even numbered pass. Heat treatments done after every four extrusions in case of routes like E and F may give some more information regarding their effectiveness in grain refinement of as-cast CDA 101 Cu. A hardness increase before recrystallization was observed during heat treatment of Cu. This increase has been attributed to polygonization of the microstructure and to the formation of Cottrell atmospheres; a detailed high resolution TEM (HRTEM) study will reveal the importance of these two mechanisms on this hardness increase in Cu.

REFERENCES

- 1) Mitchell, B.S., *An Introduction to Materials Engineering and Science for Chemical and Materials Engineers*, Wiley Interscience, Hoboken, NJ, 2004, p. 41.
- 2) Reed-Hill, R. E. and Abbaschian, R., *Physical Metallurgy Principles*, PWS Publishing Company, Boston, MA, 1998, p. 352.
- 3) Joseph, G., in *Copper – Its Trade, Manufacture, Use, and Environmental Status*, ed. K. J. A. Kundig, ASM International, Materials Park, OH, 1999, p. 331.
- 4) Granger, D. A. and Liu, J., *J. Metals*, 1983, **35**, 54.
- 5) Colengelo, V. J. and Thornton, P. A., in *Metals Handbook, Failure Analysis and Prevention*, ed. G. W. Powell and S. E. Mahmoud, Metals Park, OH, 1986, p. 316.
- 6) Taha, M. A., El-Mahallawy, N. and Hamuda, R., *Mater. Des.*, 2002, **23**, 86.
- 7) Easton, M. and StJohn, D., in *Solidification of Aluminum Alloys*, ed. M. G. Chu, D. A. Granger and Q. Han. TMS, Warrendale, PA, 2004, p. 147.
- 8) Greer, A.L., in *Solidification of Aluminum Alloys*, ed. M. G. Chu, D. A. Granger and Q. Han. TMS, Warrendale, PA, 2004, p. 131.
- 9) Bustos O., Mannheim, R., Rivera, A. and Carvajal, L, in *Copper 95 – International Conference*, ed. C. Diaz, O. Bokovay, O. Lagos, H. Larravide and M. Sahoo, TMS, Warrendale, PA, 1995, p. 491.
- 10) McKenzie, P. W. J., Lapovok, R., Wells, P. and Raviprasad K, in *Thermec 2003 - International Conference on Processing and Manufacturing of Advanced Materials*, ed. T. Chandra, J. Maria Torralba and T. Sakai, Leganes, Spain, 2003, p.322.
- 11) Lee, E. W., Garg, A. and McNeeley, T. R., *Mater. Sci. Tech.*, 1993, **9**, 995.
- 12) Park, J. J., Lee and S. J., *J. Mater. Process. Tech.*, 2003, **140**, 454.
- 13) Cui, Q. and Ohori, K., *Mater. Sci. Tech.*, 2002, **16**, 1095.
- 14) Mabuchi, M., Kubota, K. and Higashi, K., *Mater. Lett.*, 1994, **19**, 247.
- 15) Saqib, M., Apgar, L. S., Eylon, D. and Weiss, I., *Mat. Sci. Eng. A*, 1995, **201A**, 169.

- 16) Song, J. W., Kim, K. W., Han, J. W., Kim, M. S. and Hwang, S. K., *Mater. Sci. Forum*, 2003, **439**, 65.
- 17) Segal, V. M., Reznikov, V. I., Drobyshvskly, A. E. and Kopylov V. I., *Russian Metallurgy*, 1981, **1**, 564.
- 18) Bier, D. W., M.S. Thesis, Texas A&M University, 1997.
- 19) Luis-Pérez, C. J., Luri-Irigoyen, R. and Gastón-Ochoa, D., *J. Mater. Process. Tech.*, 2004, **153-154**, 846.
- 20) Yu, C.Y., Sun, P. L., Kao, P. W. and Chang, C. P., *Mater. Sci. Eng. A*, 2004, **366A**, 310.
- 21) Ferrasse, S., Segal, V. M., Hartwig, K. T. and Goforth, R. E., *Metall. Mater. Trans. A*, 1997, **28A**, 1047.
- 22) Huang, W. H., Yu, C. Y., Kao, W. and Chang, C. P., *Mater. Sci. Eng. A*, 2004, **366A**, 221.
- 23) Dalla Torre, F., Lapovok, R., Sandlin, J., Thomson, P. F., Davies, C. H. J. and Pereloma, E. V., *Acta Mater.*, 2004, **52**, 4819.
- 24) Haouaoui, M., Hartwig, K. T. and Payzant, A., *Acta Mater.*, 2005, **53**, 801.
- 25) Luo, P., Wu, X. and Xia, K. J., *Mater. Sci. Tech.*, 2003, **19**, 513.
- 26) Golobordko, A., Sidtikov, O., Sakai, I., Kaibeshev, H. and Miura, H., *Mater. Trans.*, 2004, **381**, 121.
- 27) Mathaudhu, S. N., M.S. Thesis, Texas A&M University, 2001.
- 28) Mathaudhu, S. N., Blum, S., Barber, R. E. and Hartwig, K. T., in *Proc. of the NATO Workshop on Nanomaterials by High-Pressure Severe Plastic Deformation*, Donetsk, Ukraine, 2004, p. 219.
- 29) Jahazi, M. and Goudarzi, M., *J. Mater. Process. Tech.*, 1997, **63**, 610.
- 30) Jin, H. and Saimoto, S., *Mater. Sci. Tech.*, 2003, **19**, 1197.
- 31) Chang, J. Y. and Shan, Y., *J. Mater. Sci.*, 2003, **38**, 2613.
- 32) Raab, G. J., Valiev, R. Z., Lowe, T. C. and Zhu, Y. T., *Mat. Sci. Eng. A*, 2004, **382A**, 30.
- 33) Stolyarov, V. V., Zhu, Y. T., Raab, G. I., Zharikov, A.I. and Valiev, R. Z., *Mat. Sci. Eng. A*, 2004, **385A**, 309.
- 34) Horita, Z., Fujinami, T. and Langdon, T., *Mat. Sci. Eng. A*, 2001, **318A**, 34.

- 35) Blum, S., Semester project at the Institute for Metal Forming and Casting, Technical University of Munich, 2004.
- 36) Barber, R. E., Dudo, T., Yasskin, P. B. and Hartwig, K. T., *Scripta Mater.*, 2004, **51**, 373.
- 37) Kalidindi, S. R., Bhattacharya, A. and Doherty, R. D., *Adv. Mater.*, 2003, **15**, 1345.
- 38) Sandim, H. R. Z., Lins, J. F. C., Pinto, A. L. and Padilha, A. F., *Mat. Sci. Eng. A*, 2003, **354A**, 217.
- 39) Segal, V. M., *Mat. Sci. Eng. A*, 1999, **271A**, 322.
- 40) Haouaoui, M., M.S. Thesis, Texas A&M University, 2001.
- 41) Komura, S., Horita, Z., Nemoto, M. and Langdon, T. G., *J. Mat. Res.*, 1999, **14**, 4044.
- 42) Neishi, K., Horita, Z. and Langdon, T. G., *Mater. Sci. Eng. A*, 2002, **325A**, 54.
- 43) Hutchinson, B., Jonsson, S. and Ryde, L., *Scripta Metall.*, 1989, **23**, 671.
- 44) Huh, M. Y., Cho, Y. S. and Engler, O., *Mat. Sci. Eng. A*, 1998, **247A**, 152.
- 45) Hatherly, M. and Malin, A. S., *Metals Technology*, 1979, **6**, 308.
- 46) Malin, A., Huber, J. and Hatherly, M., *Z. Metallkde.*, 1981, **72**, 310.
- 47) Wang, G., Wu, S. D., Esling, C., Zue, L., Wang, Z.G. and Li, G.Y., *Mater. Sci. Forum*, 2002, **408**, 709.
- 48) Valiev, R. Z., Kozlov, E.V., Ivanov, Y.F., Lian, J., Nazarov, A.A. and Baudalet, B., *Acta Metall. Mater.*, 1994, **42**, 2467.
- 49) Harris, C., Prangnell, P. B. and Duan, X., in *Proceedings of the 6th Annual Conference on Aluminum Alloys ICAA-6*, Vol. 1, ed. Sato, T., Kumai, S., Kobayashi, T. and Murakami, Y. Toyohashi, Japan, The Japan Institute of Light Metals, Tokyo, 1998, p. 583.
- 50) Humphreys, F.J., Prangnell, P.B., Bowen, J.R., Gholinia, A. and Harris, C., *Phil. Tran. R. Soc. Lond.*, 1999, **357**, 583.
- 51) Hughes, D.A. and Hansen, N., *Acta Mater.*, 1997, **45**, 3871.
- 52) Chuvil'deev, V. N., Kopylov, V. I., Nokhrin, A. V., Makarov, I. M., Malashenko, L. M. and Kokareko, V. A., *Phys. Metals Metallogr.*, 2003, **96**, 486.

VITA

Shabib Jehangir Kadri was born on Sunday, January 20, 1980, in Ahmedabad, India, the youngest child of Mr. Jehangir Kadri and Mrs. Rashida Kadri. He received his entire education in Ahmedabad, a city where his family has been living for over 500 years.

He pursued a degree in mechanical engineering at Gujarat University, Ahmedabad, India and obtained a B.S. degree in 2001.

In order to pursue a Master of Science degree, he enrolled at Texas A&M University in fall of 2002 and earned his Master of Science degree in mechanical engineering in August 2005. He intends to work in the industry for a couple of years before coming back to the ECAE research group at Texas A&M University for a Ph.D. degree.

His permanent address is:

Shabib Kadri
"Sardar Manzil"
Kadri Road, Raikhad
Ahmedabad
Gujarat- 380 001
India